FUNCTIONAL ANALYSIS OF CHLOROPLAST FTSZ1 AND FTSZ2

By

Allan David TerBush

A DISSERTATION

Submitted to
Michigan State University
In partial fulfillment of the requirements
For the degree of

Biochemistry and Molecular Biology – Doctor of Philosophy

2015

ABSTRACT

FUNCTIONAL ANALYSIS OF CHLOROPLAST FTSZ1 AND FTSZ2

By

Allan David TerBush

Chloroplasts arose from the endosymbiosis of an ancient cyanobacterium by a primitive heterotrophic eukaryote. Among their diverse functions, they are best known for the capture and conversion of light energy into chemical energy through the process of photosynthesis. Therefore, their propagation as plant cells grow and divide is critical. Chloroplasts cannot be made *de novo* but maintain normal accumulation through the process of binary fission, where a constriction forms at the mid-point and squeezes until separation of two daughter chloroplasts. As chloroplasts are descended from bacteria, many of their division proteins are homologs of bacterial cell division factors.

Chloroplast division is driven by the assembly and constriction of multiple ring structures at the chloroplast midpoint. The central structure is the FtsZ ring (Z ring), which likely provides at least some of the constrictive force driving division. Unlike bacterial Z rings, which are homopolymers composed of a single FtsZ, those of plants and green algae are composed of two FtsZ isoforms, FtsZ1 and FtsZ2. FtsZ1 and FtsZ2 are each critical for division and perform distinct functions. However, the functional relationship between the FtsZ families prior to this study was poorly understood. In this work, I present my research analyzing the distinct behaviors and functionality of FtsZ1 and FtsZ2 using *Schizosaccharomyces pombe* as a heterologous expression system for analyzing the inherent assembly and dynamic properties of chloroplast FtsZs.

FtsZ1 and FtsZ2 from Arabidopsis assembled filaments with differing morphologies when expressed alone, and coassembled into FtsZ2-like filaments when coexpressed. FRAP experiments showed that FtsZ1 filaments are more dynamic than FtsZ2 filaments, and that FtsZ1 enhances FtsZ2 turnover in coassembled hetero-polymers. Additionally, GTPase activity is essential for FtsZ2 filament turnover but is not solely responsible for turnover of FtsZ1 filaments. These data suggest that FtsZ2 is the structural determinant of the Z ring while FtsZ1 facilitates Z-ring remodeling.

In subsequent studies, I analyzed the conservation of distinct assembly and dynamic properties of FtsZ pairs from phylogenetically diverse photosynthetic organisms and the effect the FtsZ N- and C-termini have on FtsZ1 and FtsZ2 filament assembly and dynamics. FtsZ1/FtsZB and FtsZ2/FtsZA proteins from diverse photosynthetic eukaryotes displayed filament assembly and dynamic properties consistent with those of Arabidopsis FtsZ1 and FtsZ2, respectively, while FtsZ from a cyanobacterium showed filament properties more consistent with those of FtsZ2. In other experiments, FtsZ1 and FtsZ2 proteins lacking their N- and/or C-termini assembled filaments with reduced bundling and turnover properties. These data suggest that the distinct properties of the FtsZ1 and FtsZ2 families are well conserved across the various photosynthetic lineages and that FtsZ2 is likely the direct homolog of the ancient cyanobacterial FtsZ. They also show that the N- and C-termini of FtsZ1 and FtsZ2 promote filament bundling and turnover and also contribute to the distinct behaviors of the chloroplast FtsZ families, while not being solely responsible for them. This work has substantially improved our understanding of FtsZ functionality and provides many hypotheses for testing in future analyses.

Dedication

I dedicate this work to my loving wife, Carissa, who supported and encouraged me throughout my studies. I also dedicate this work to my son, Luke, and all of our future children. You can accomplish your goals. It only takes time, consistency, and perseverance.

ACKNOWLEDGMENTS

I wish to firstly thank my advisor, Katherine W. Osteryoung, for the years of mentoring and support that she has poured into me throughout my graduate schooling.

I wish to also thank the members of my guidance committee for their encouragement and council:

Dr. Harold Erickson

Dr. Beronda Montgomery

Dr. Curtis Wilkerson

Dr. Michael Feig

Thanks to Deena Kadirjan-Kalbach, Aaron Schmitz, Yue Yang, Min Zhang, Charles Chen, Siddhartha Dutta, Yamato Yoshida, Katie Porter, and John Froehlich for insightful discussions, encouragement, and friendship.

This work was supported by the National Science Foundation under grant MCB-1121943 to Katherine Osteryoung.

TABLE OF CONTENTS

LIST OF TABLES

LIST OF FIGURES

KEY TO ABBREVIATIONS

ARC	Accumulation and Replication of Chloroplasts
BiFC	Bimolecular fluorescence complementation
CLSM	Confocal Laser Scanning Microscope
CTL	C-terminal linker
CTV	C-terminal variable region
eCFP	enhanced Cyan Fluorescent Protein
eYFP	enhanced Yellow Fluorescent Protein
FtsZ	Filamentous Temperature Sensitive Z
IDP	Intrinsically disordered peptide
IEM	Inner envelope membrane
ITC	Isothermal titration calorimetry
KO	Knockout
MORN	Membrane Occupation and Recognition Nexus
OEM	Outer envelope membrane
PARC6	Paralog of ARC6
PCC	Pearson's Correlation Coefficient
PMT	Photomultiplier tube
SIM	Structured illumination microscopy
$t_{1/2}$	Half-time of fluorescence recovery
TEM	Transmission Electron Microscopy
TP	Transit peptide
WT	Wild-type
Y2H	Yeast-2-hybrid
Z ring	FtsZ ring

Chapter 1

FtsZ in Chloroplast Division: Structure, Function and Evolution

This chapter was originally published in *Curr Opin Cell Biol*.

TerBush, A.D, Y. Yoshida, and K.W. Osteryoung. 2013. FtsZ in Chloroplast division: structure, function and evolution. *Curr Opin Cell Biol*. 25:461-470

Minor edits have been made to the original manuscript to conform to dissertation formatting requirements and Figure callouts.

The section on FtsZ in the division of primitive mitochondria was written by co-author Yamato Yoshida, Department of Plant Biology at Michigan State University.

Abstract

FtsZ is a key cytoskeletal component of the chloroplast division machinery that arose from the related cell division FtsZ in the cyanobacterial ancestor of chloroplasts. FtsZ is widely conserved in photosynthetic eukaryotes, where it forms a ring inside the organelle at the chloroplast division site. A distinctive feature of chloroplast division systems is the evolution of two phylogenetically and structurally distinct *FtsZ* families by independent gene duplications in different photosynthetic lineages. While many functional aspects of these proteins remain unknown, recent studies on the biochemical and dynamic properties of FtsZs from land plants, in combination with ongoing research on bacterial FtsZs, have begun to suggest mechanisms by which two functionally distinct FtsZ proteins may cooperate to drive chloroplast division.

Introduction

Plastids arose by endosymbiosis of an ancient cyanobacterium and comprise a metabolically diverse group of organelles. The most familiar and best-studied type of plastid is the chlorophyll-containing chloroplast, which carries out photosynthetic CO_2 fixation in plants and algae. In land plants, chloroplasts proliferate during leaf cell growth, often to more than 100 chloroplasts per cell, to attain maximum photosynthetic capacity (Leech and Baker, 1983). In addition, chloroplasts in all photosynthetic eukaryotes and various non-photosynthetic plastids in land plants, such as those in root cells, also perform other vital metabolic functions. These include fatty acid synthesis, amino acid synthesis, nitrogen metabolism and sulfur metabolism. Consequently, plastids are essential organelles in all plant cells. All plastids are surrounded by two membranes, called the inner envelope membrane (IEM) and outer envelope membrane (OEM), both of which are of cyanobacterial origin (Gould et al., 2008). Chloroplasts also contain thylakoids, a network of internal membranes in which photosynthetic pigments and protein complexes are embedded. The thylakoids are surrounded by the stroma, the dense fluid matrix of the chloroplast.

As descendants of a once free-living bacterium, plastids cannot be made *de novo*. Instead, plastid proliferation within individual cells, which promotes their proper partitioning to daughter cells during cell division, is accomplished by division of preexisting organelles (Falconet, 2012; Gould et al., 2008; Miyagishima, 2011). Although all plastid types presumably undergo division, the molecular details of this process have been studied mostly in chloroplasts. The chloroplast division machinery contains at least three contractile components (summarized in Fig. 1.1). The first to

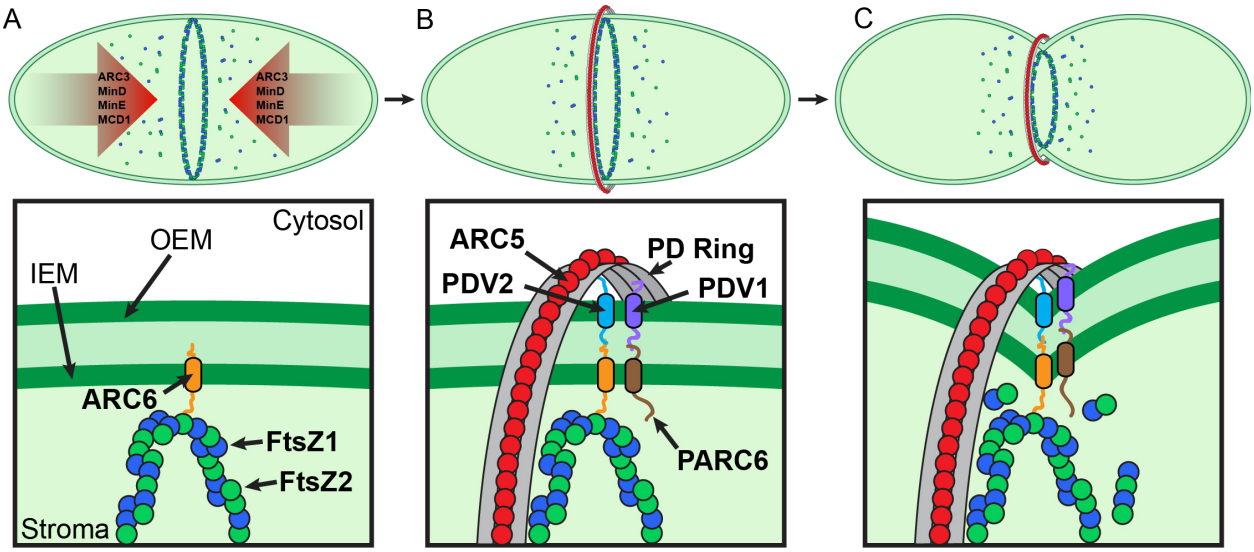

Figure 1.1: Partial working model depicting formation of the chloroplast division complex in plants. A) The first step in formation of the division complex is Z-ring assembly, which is restricted to the mid-plastid by ARC3, MinD, MinE and MCD1. The Z ring is tethered to the inner envelope membrane (IEM) through interaction between FtsZ2 and ARC6. B) Z-ring assembly is followed by recruitment of additional division components to the mid-plastid, including PARC6, PDV1 and PDV2 and the contractile ARC5/DRP5B and PD rings. C) Once the complex has fully assembled, the coordinated activities of the FtsZ, ARC5/DRP5B and PD rings constrict the IEM and outer envelope membrane (OEM) the chloroplast. The recently identified protein CLMP1 may play a role in final separation of the daughter chloroplasts (Yang et al., 2011) (not shown). The division-site positioning factors ARC3, MinD, MinE and MCD1 also localize partly to the division site, but their functions there are unclear and they are omitted from the diagram here. For details and relevant references, see (Miyagishima, 2011).

assemble is the FtsZ ring (Z ring), which is cyanobacterial in origin and localized inside the chloroplast on the stromal surface of the IEM. Following Z-ring formation, the ARC5/DRP5B ring, composed of a dynamin-related protein that originated from the eukaryotic host (Osteryoung and Nunnari, 2003), and the plastid-diving (PD) ring, an electron-dense structure widely observed in plants and algae, assemble on the cytosolic surface of the OEM. The PD ring was recently shown to be composed of polyglucan fibrils in a primitive red alga (Yoshida et al., 2010), but its composition in other organisms is not known. The internal and external machineries are linked by transmembrane proteins that span the IEM and OEM (Fig. 1.1). During division, these ring structures constrict the two membranes at the mid-plastid until final scission occurs, producing two daughter chloroplasts. However, the details of the membrane-remodeling events associated with fission of the envelope membranes are still unclear, and how the thylakoid membranes divide is completely unknown.

As the first component of the chloroplast division complex to assemble (Miyagishima, 2011), the Z ring establishes the placement of the external division components (Nakanishi et al., 2009) and is a central driver of chloroplast division. The Z ring is composed of FtsZ, a cytoskeletal GTPase with structural similarity to tubulins. Plastidic FtsZ was originally derived from the cell division FtsZ in the cyanobacterial ancestor of chloroplasts. In addition to being critical for chloroplast division, FtsZ has also been shown to mediate the division of other plastid types, such as the starch-storing amyloplasts (de Pater et al., 2006; Yun and Kawagoe, 2009). FtsZ also drives cell division in modern-day bacteria, where it forms homopolymers that assemble into a cytoplasmic Z ring that is tethered to the membrane via interactions with other division

proteins. The bacterial Z ring generates a bending force on the membrane as a result of fixed curvature, producing contractile activity, and recruits additional division proteins to the division site (Adams and Errington, 2009; Erickson et al., 2010; Osawa et al., 2008; Osawa et al., 2009). However, unlike in bacteria in which a single FtsZ is sufficient for cell division, many photosynthetic eukaryotes possess two phylogenetically distinct, plastid-localized FtsZ families (Miyagishima et al., 2004; Osteryoung and McAndrew, 2001; Osteryoung et al., 1998). Though cyanobacterial in origin, chloroplast FtsZs are now nuclear-encoded and imported into the stroma, where, in higher plants, they colocalize to the Z ring and are both required for chloroplast division (Fujiwara and Yoshida, 2001; McAndrew et al., 2001; Osteryoung and Vierling, 1995; Vitha et al., 2001) (Fig. 1.2). In this review, we discuss recent evolutionary, biochemical, and genetic data that suggest how two FtsZ families may cooperate to drive chloroplast division. We also touch on the role of FtsZ in the division of mitochondria. We refer readers to recent reviews for discussion of the spatial regulation of Z-ring assembly and other components of the chloroplast division complex (Falconet, 2012; Miyagishima, 2011) and, other than in the summary of Fig. 1.1, restrict this review to consideration of FtsZ.

FtsZ duplication during chloroplast evolution

The primary endosymbiotic event from which chloroplasts arose led to the evolution of three eukaryotic lineages bearing primary chloroplasts: the basal glaucophytes (Glaucophyta), red algae (Rhodophyta), and green algae and plants (Viridiplantae) (Falconet, 2012; Gould et al., 2008). Later, secondary endosymbioses in which one red alga and two different green algae were independently engulfed by heterotrophic eukaryotes created the Chlorarachniophyta, Euglenophyta (both green-

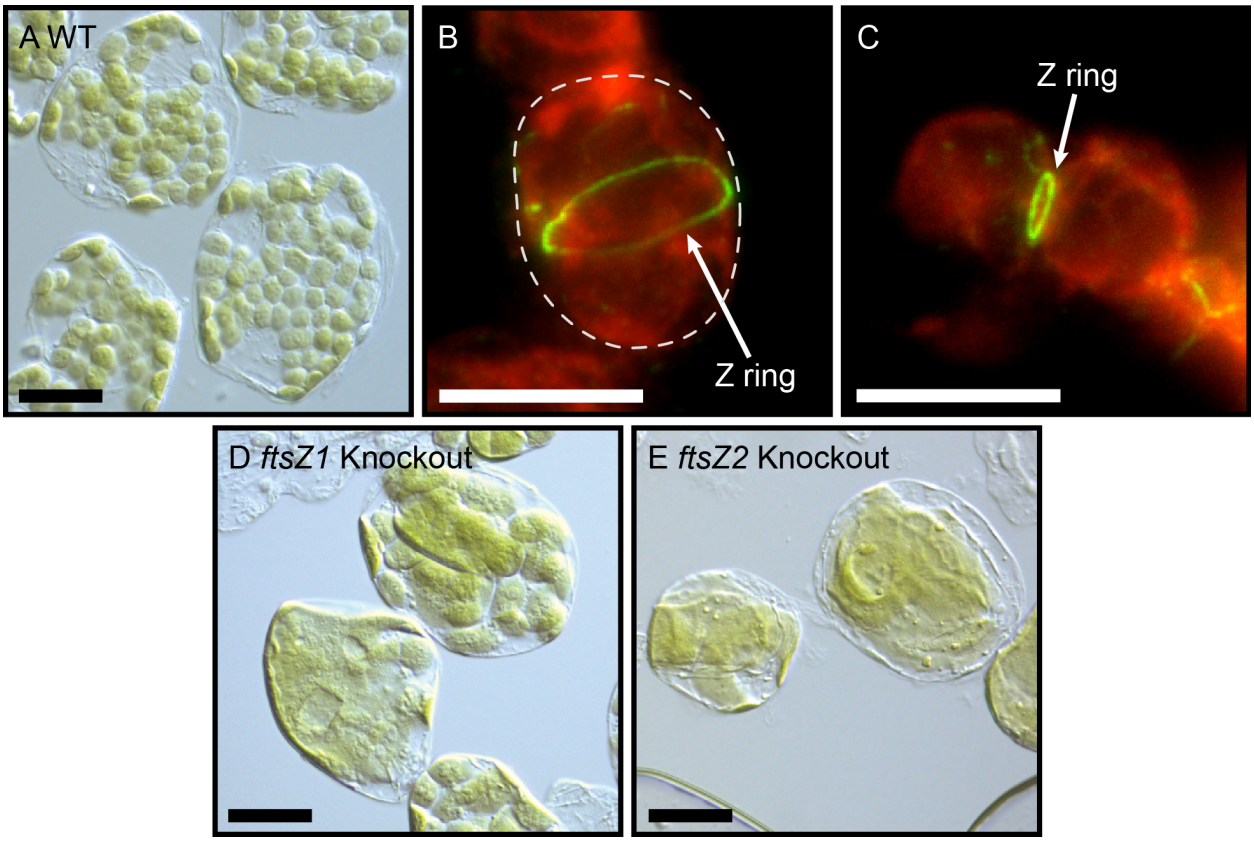

Figure 1.2: Chloroplast morphology and Z-ring localization in *Arabidopsis* leaf cells and phenotypes of *ftsZ1 and ftsZ2* knockout mutants. (A, D-E) Nomarski differential interference contrast micrographs of individual mesophyll cells isolated from leaves of the indicated genotype. Leaf samples were fixed and squashed to separate individual cells for imaging. (B-C) Immunofluorescence micrographs showing (B) unconstricted and (C) highly constricted Z rings in chloroplasts of mesophyll cells from WT *Arabidopsis* plants. Z rings were detected with an antibody raised against *At*FtsZ1. Images represent a merger of the FtsZ signal (green) and chlorophyll autofluorescence (red). Arrows indicate the Z rings, while the dashed line represents the chloroplast outline. Black bars, 20 μm. White bars, 5 μm.

lineage) and very diverse Chromalveolata (red-lineage). In addition to bearing the IEM and OEM common to all plastids, secondary plastids in these organisms are surrounded by at least one membrane derived from the endomembrane system of the phagocytic host (Gould et al., 2008). *FtsZ* genes encoding presumed plastidic proteins have been identified in at least some members of all these taxa except the Euglenophyta (Hopkins et al., 2012; Miyagishima et al., 2011). Two or more such *FtsZ* genes are evident in numerous species of Viridiplantae, including all plants and green algae with fully sequenced genomes, where they cluster into two distinct families called FtsZ1 and FtsZ2 (Miyagishima, 2011; Osteryoung and McAndrew, 2001; Osteryoung et al., 1998). Two plastidic FtsZ families called FtsZA and FtsZB also occur in Rhodophyta. *FtsZ2* and *FtsZA* are more ancestral in character and probably evolved from a single *FtsZ* in the common ancestor of Viridiplantae and Rhodophyta after these two lineages split. *FtsZ1* and *FtsZB* arose subsequently by duplication of *FtsZ2* and *FtsZA*, respectively (Miyagishima et al., 2004). FtsZA and FtsZC are found in members of the Chromalveolata, the latter having arisen from duplication of *FtsZA* after acquisition of the ancestral red alga (Miyagishima et al., 2004). Thus, independent gene duplications yielding two plastidic FtsZ families with distinct structural features (discussed below) have occurred at least three times during chloroplast evolution, suggesting that FtsZ functional divergence may have accompanied chloroplast evolution in these lineages (Miyagishima et al., 2004). However, as described below, distinct functions have only been established thus far for FtsZ1 and FtsZ2.

Recent genome information also revealed two plastidic FtsZs encoded in the chlorarachniophyte *Bigelowiella natans*, but these cluster together and are very similar

in sequence (Hopkins et al., 2012), suggesting they may not be functionally divergent. Only a single chloroplast *FtsZ* has been identified in the glaucophyte *Cyanophora paradoxa* (Sato et al., 2007). Glaucophytes contain primitive chloroplasts that, like cyanobacteria, still require peptidoglycan synthesis for division. The peptidoglycan wall has been lost from chloroplasts in other lineages (Takano and Takechi, 2010), but whether there is any relationship between this and *FtsZ* duplication or other aspects of chloroplast division is unknown.

Plastidic FtsZ has not been retained in all plastid-bearing organisms. For example, members of the Apicomplexa, a non-photosynthetic subgroup within the Chromalveolata that includes *Plasmodium* malaria pathogens, contain vastly reduced secondary plastids and have lost FtsZ, implying a different mechanism for plastid division (Webster and McFadden, 2009). However, the widespread duplication, divergence and maintenance of two FtsZ families in diverse photosynthetic eukaryotes suggests they have evolved distinct and critical functions in chloroplast division in many photosynthetic organisms.

Chloroplast FtsZ domain architecture

Bacterial FtsZ contains two conserved domains (Fig. 1.3). The GTP-binding domain adopts a Rossmann fold common to many GTPases, including tubulins, and contains all residues required for binding GTP (Lowe and Amos, 1998). The C-terminal domain contains the T7 or synergy loop that, upon polymerization, makes key contacts in the GTP-binding pocket of the subunit below to catalyze GTP hydrolysis (Oliva et al., 2004) (Fig. 1.4). Bacterial FtsZs also contain a conserved C-terminal peptide (Fig. 1.3),

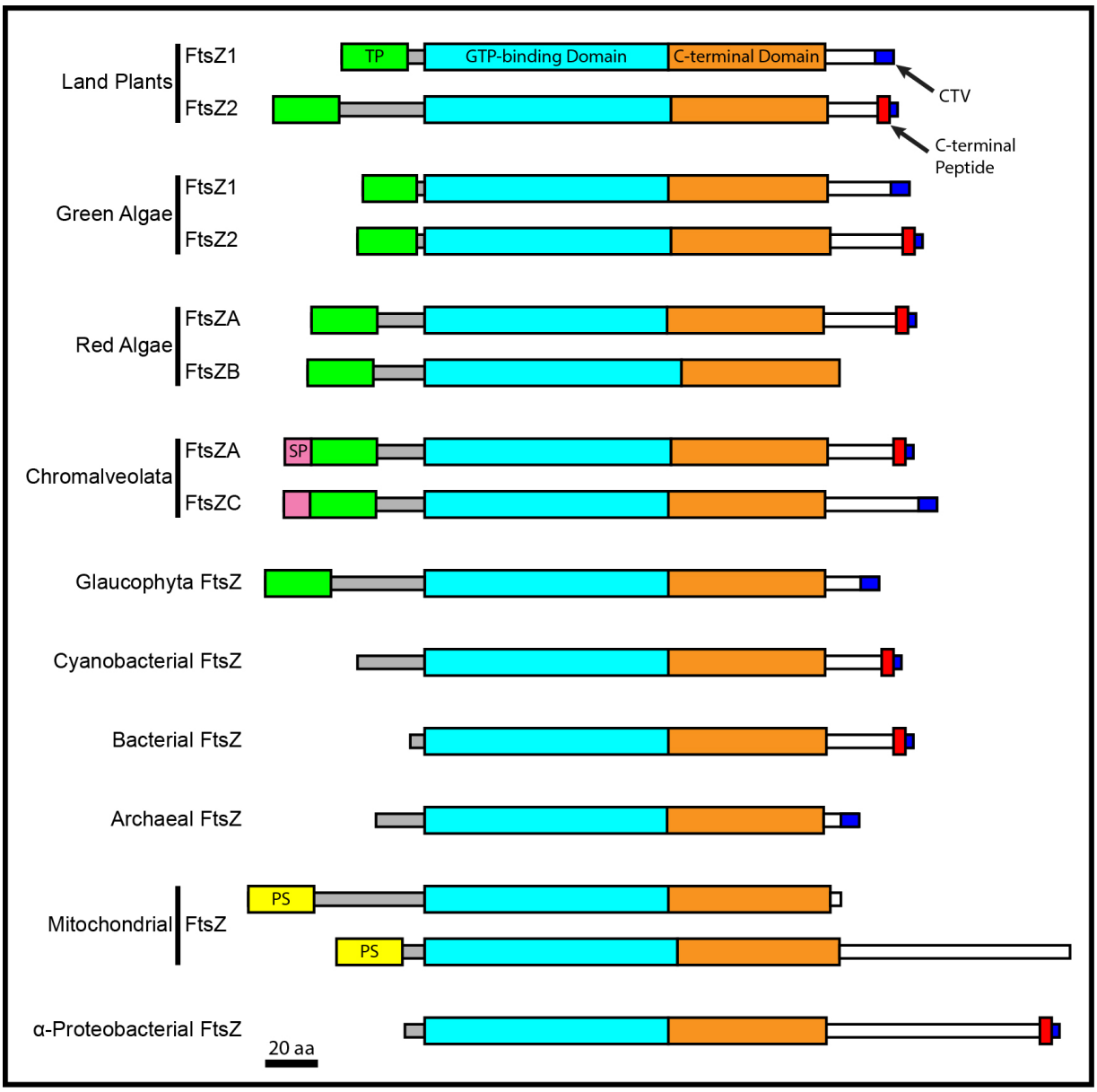

Figure 1.3: Domain architectures of chloroplast, mitochondrial, and prokaryotic FtsZs. Diagrams are drawn to scale, with each region representing the average length for its corresponding group of FtsZs. Colors represent the chloroplast transit peptide (green, TP), ER signal peptide (pink, SP), mitochondrial presequence (yellow, PS), N-terminal extension (gray), GTP-binding domain (cyan), C-terminal domain (orange), C-terminal spacer region (white), C-terminal variable region (CTV, blue), and C-terminal

Figure 1.3 (cont'd): peptide (red). The indicated FtsZ groups are represented by 19 (plant FtsZ1), 23 (plant FtsZ2), 6 (green algal FtsZ1), 6 (green algal FtsZ2), 5 (red algal FtsZA), 2 (red algal FtsZB), 7 (Chromalveolata FtsZA), 7 (Chromalveolata FtsZC), 1 (Glaucophyta), 14 (cyanobacterial), 17 (bacterial), 11 (archaeal), 10 (mitochondrial), and 8 (alpha-proteobacterial) sequences. Black bar, 20 residues.

which is required for interaction with membrane-associated assembly regulators that probably anchor the Z ring to the membrane (Ma and Margolin, 1999).

The GTP-binding and C-terminal domains of chloroplast FtsZs are well-conserved with those in bacteria, but other regions have diverged (Fig. 1.3, Fig. 1.4A).

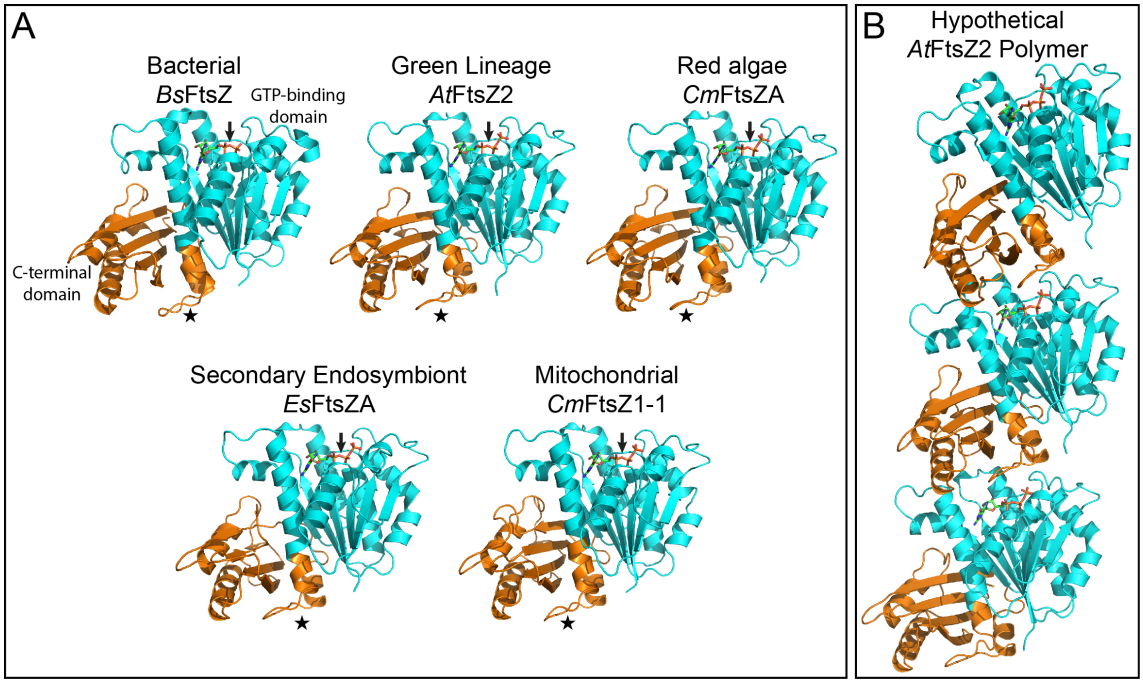

Figure 1.4: Comparison of eukaryotic FtsZ models with a bacterial FtsZ crystal structure. (A) A *Bacillus subtilis* FtsZ (*Bs*FtsZ)crystal structure (pdb entry 2RHL)

Figure 1.4 (cont'd): depicting the GTP-binding (cyan) and C-terminal (orange) domains is compared to predicted tertiary structures of *A. thaliana* FtsZ2-1 (NP_565839.1), *C. merolae* FtsZA (BAC87807.1), *Ectocarpus siliculosus* FtsZA (CBN79234.1), and *C. merolae* FtsZ1-1 (BAC87805.1). (B) The predicted *At*FtsZ2-1 structure was modeled onto an FtsZ dimer crystal structure from *Methanococcus jannaschii* (pdb entry 1W5A) (Oliva et al., 2004) to generate a hypothetical *At*FtsZ2-1 polymer. Eukaryotic FtsZ models were generated using the Phrye2 prediction server in intensive mode (Kelley and Sternberg, 2009) (http://www.sbg.bio.ic.ac.uk/phyre2/html/page.cgi?id=index), and ligand binding predictions were computed by the 3DLigandSite prediction server (Wass et al., 2010) (http://www.sbg.bio.ic.ac.uk/~3dligandsite/). Eukaryotic FtsZ models and the *Bs*FtsZ crystal structure were rendered in Pymol (http://www.pymol.org), depicting GTP or GDP, respectively, in the nucleotide-binding site. Stars indicate the T7 loop. Arrows indicate GDP and GTP in the nucleotide-binding pocket of the *Bs*FtsZ crystal structure and eukaryotic FtsZ models, respectively.

The N-terminal extensions are longer, owing partly to predicted transit peptides that direct protein import into chloroplasts and are subsequently cleaved (McAndrew et al., 2001; Osteryoung and Vierling, 1995). Interestingly, this region has diverged between plant FtsZs as well. Excluding the transit peptides, plant FtsZ1 N-terminal extensions are shorter (~13 residues) than those of FtsZ2 (~65 residues). However, the N-terminal extensions are similar in length in FtsZ pairs from other organisms, such as green and red algae. As no functions aside from protein targeting have yet been shown for the N-terminal extensions, the significance of these differences is unknown.

In organisms with secondary chloroplasts, the transit peptide is preceded by a predicted N-terminal signal peptide that directs cotranslational import of the protein into the endoplasmic reticulum, where the signal peptide is cleaved. This exposes the transit peptide, which subsequently targets the protein to the plastid (Gould et al., 2008). Consistent with this import mechanism, FtsZs containing predicted bipartite targeting peptides have been identified in various organisms with secondary chloroplasts (Nishikawa et al., 2010; Nishikawa et al., 2012; Vieler et al., 2012) (Fig. 1.3). Recent studies show that the N-terminal signal and transit peptides of such FtsZs can direct protein import to the ER and chloroplast, respectively (Nishikawa et al., 2010; Nishikawa et al., 2012). These results indicate that FtsZ, like other chloroplast-targeted proteins in organisms with secondary plastids, enter the endomembrane system before chloroplast import.

Like bacterial FtsZs, green-lineage FtsZ2 and red-lineage FtsZA have retained the C-terminal peptide (Miyagishima et al., 2004; Osteryoung and McAndrew, 2001) (Fig. 1.3). The *Arabidopsis* FtsZ2 C-terminal peptide mediates a specific interaction with the transmembrane protein ARC6. ARC6 is a positive regulator of FtsZ assembly that probably tethers the Z ring to the IEM (Fig. 1.1) and is conserved throughout plants and green algae (Maple et al., 2005; Vitha et al., 2003). However, green-lineage FtsZ1, which is not known to interact directly with any IEM protein, as well as red-lineage FtsZB and FtsZC, have lost the C-terminal peptide during evolution (Miyagishima et al., 2004; Osteryoung and McAndrew, 2001) (Fig. 1.3). This observation suggests that divergence of the C-terminus to generate a second FtsZ that may not mediate

membrane tethering is a functionally significant aspect of the evolution of chloroplast FtsZ pairs in different lineages.

Plastidic FtsZ functional properties and behavior: clues from FtsZ1 and FtsZ2

Functional studies suggesting how FtsZ pairs might cooperate in plastid division have thus far been performed only with land-plant FtsZ1 and FtsZ2. In *Arabidopsis*, both depletion and overexpression of FtsZ1 or FtsZ2 caused dose-dependent defects in chloroplast division, as indicated by a reduction in chloroplast number and increase in chloroplast size (Osteryoung et al., 1998; Stokes et al., 2000). These data suggest their absolute levels and/or stoichiometry may be critical for their *in vivo* functions. Consistent with this possibility, quantitative immunoblotting showed that FtsZ1 and FtsZ2 maintain a constant 1:2 ratio in whole leaves over development (McAndrew et al., 2008). However, their ratio in the Z ring and whether it changes during constriction or with development is not yet known. Recent studies in *Arabidopsis* demonstrated conclusively that these families have non-redundant functions in chloroplast division (Schmitz et al., 2009). The FtsZ2-specific interaction with ARC6 described above partly explains their functional divergence (Maple et al., 2005). FtsZ1 was reported to interact uniquely with the division-site positioning factor ARC3 (Maple et al., 2007), but we recently determined that FtsZ2 does so as well (Zhang et al., 2013). Therefore, interaction with ARC3 probably does not represent a functional distinction between FtsZ1 and FtsZ2 as proposed earlier, though unique interactions with other proteins, perhaps through their divergent regions (Fig. 1.3), may be discovered. However, differences in their biochemical properties and dynamic behavior may also contribute to their distinct functionalities, as discussed below.

Bacterial FtsZs undergo *in vitro* GTP-dependent assembly into homopolymers. Because the GTPase active site is formed by interaction between FtsZ subunits, polymerization stimulates GTP hydrolysis. This destabilizes subunit interfaces and promotes polymer turnover (subunit exchange), which is essential for sustained Z-ring constriction and remodeling (Erickson et al., 2010; Osawa and Erickson, 2011). Similarly, plant FtsZs are capable of *in vitro* GTP-dependent homopolymerization and assembly-stimulated GTPase activity (El-Kafafi et al., 2005; Lohse et al., 2006; Olson et al., 2010; Smith et al., 2010). Comparative analyses showed that *Arabidopsis* FtsZ1 has higher GTPase activity than FtsZ2 (Olson et al., 2010; Smith et al., 2010). Because the rate of GTP hydrolysis appears to correlate with the rate of filament turnover in bacteria (Erickson et al., 2010), this suggested that FtsZ1 filaments may turn over more rapidly than FtsZ2 filaments. However, FtsZ1 and FtsZ2 colocalize *in vivo* (Vitha et al., 2001) where they may not normally assemble as homopolymers. One study convincingly demonstrated that FtsZ1 and FtsZ2 interact to form the GTPase active site *in vitro*, showing they are capable of coassembling as heteropolymers (Olson et al., 2010). Coassembly occurred at variable FtsZ1:FtsZ2 ratios, but displayed maximum kinetics at 1:1 (Olson et al., 2010). The assembly subunits for homopolymer formation have recently been explored (Smith et al., 2011), but the pathway for heteropolymer formation has not been studied.

Recent work begins to hint at the functional significance of coassembly (TerBush and Osteryoung, 2012). *Arabidopsis* FtsZ1 and FtsZ2 fused to fluorescent tags were expressed separately and together in fission yeast to investigate their inherent filament morphology and dynamics in the absence of their native assembly regulators. Each

assembled homopolymers with differing morphologies, but heteropolymers always exhibited FtsZ2-like morphologies. FRAP experiments revealed that FtsZ1 homopolymers were more dynamic than FtsZ2 homopolymers and that FtsZ2 turnover was increased in heteropolymers. Surprisingly, in contrast with GTPase-deficient FtsZ2 and bacterial FtsZ mutants, which assemble filaments that are completely static (Osawa and Erickson, 2011), GTPase-deficient FtsZ1 remained dynamic, suggesting that the higher turnover of FtsZ1 may not be due solely to its higher GTPase activity. These findings also suggested the possibility that FtsZ2 plays a more structural role in Z-ring assembly while FtsZ1 facilitates Z-ring remodeling during constriction (TerBush and Osteryoung, 2012).

In the *in vitro* assembly study described above (Olson et al., 2010), FtsZ1/FtsZ2 coassembly (but not separate assembly) was accompanied by extensive polymer bundling, indicating lateral interactions between heteropolymers. In bacterial cells, FtsZ bundles are thought to consist of loosely associated polymers held together by electrostatic interactions, and bundling is thought to impart Z-ring stability (Erickson et al., 2010). Recently, the C-terminal variable region (CTV) of bacterial FtsZ (Fig. 1.3) was shown to promote *in vitro* bundling of bacterial polymers depending on its overall charge. The positively charged *Bacillus subtilis* CTV induced bundling whereas the neutral *E. coli* CTV and negatively charged variants did not (Buske and Levin, 2012). The CTV is at the end of a flexible linker that extends out from the negatively charged polymer core. Bundling was proposed to result from sandwiching of the positively charged *B. subtilis* CTV between negatively charged polymers. Interestingly, the FtsZ1 and FtsZ2 CTVs (Fig. 1.3) are both overall positively charged but the FtsZ2 CTV is

more so. This may suggest that bundling of coassembled heteropolymers is enhanced by FtsZ2 or by the additive effect of CTV positive charges in both proteins. A charge difference is also evident in red-lineage FtsZs. The FtsZA CTV is positively charged while FtsZB lacks this region altogether (Fig. 1.3) and the FtsZC CTV contains few positively charged residues.

The studies above have implications for understanding plastidic Z-ring structure and dynamics. It has been noted that FtsZ2 assembles into long filaments and occasional rings and supports some degree of chloroplast division in *Arabidopsis ftsZ1* null mutants. These data suggest that FtsZ2 rings are partly functional *in vivo* but that constriction is inefficient without FtsZ1. In contrast, FtsZ1 only forms short disorganized filaments in mutants lacking FtsZ2 (Schmitz et al., 2009; Yoder et al., 2007). These observations suggest greater stability of FtsZ2 filaments *in vivo*, consistent with the hypothesis that FtsZ2 plays a larger structural role while FtsZ1 promotes turnover. FtsZ2-specific membrane tethering and perhaps a greater capacity for bundling may also contribute to the ability of FtsZ2 to independently form filaments and rings *in vivo*. The finding that FtsZ1 and FtsZ2 coassemble at variable ratios *in vitro* (Olson et al., 2010) speculatively suggests that changes in the FtsZ1:FtsZ2 ratio could represent a mechanism for regulating Z-ring dynamics and constriction during chloroplast division. Such regulation may be important for effective Z-ring activity in chloroplasts with large diameters or for allowing the division complex to become fully assembled before Z-ring constriction ensues. *In vivo* studies of Z-ring structure and dynamics will be important for expanding on these ideas.

Other functions and regulation of chloroplast FtsZs

Sub-plastidal localization experiments in *Arabidopsis* showed that both FtsZ1 and FtsZ2 localize partly to thylakoid membranes as well as to the stroma in young tissues, suggesting a possible role in thylakoid development (El-Kafafi et al., 2008; Karamoko et al., 2011). Studies in rice showed that FtsZ plays a significant role in the formation of compound starch granules within individual amyloplasts (Yun and Kawagoe, 2010). Additionally, the non-vascular moss *Physcomitrella patens* contains a third FtsZ family not present in seed plants that dually localizes to the stroma and cytosol, and initial studies suggest it might function in cell as well as chloroplast division (Kiessling et al., 2004; Martin et al., 2009). Moss FtsZs have also been proposed to play a structural role in chloroplasts as components of a filamentous network termed the “plastoskeleton,” but such networks have not been observed in higher plants (Martin et al., 2009).

Though little is known about plastidic FtsZ regulation, a few studies have begun to suggest potential mechanisms. Expression profiling in unicellular algae with single primary chloroplasts indicated that restricting FtsZ expression to the S phase potentially helps coordinate cell and chloroplast division in these organisms (Miyagishima et al., 2012). Proteomics approaches in *Arabidopsis* showed that FtsZ2 is specifically phosphorylated (Gargano et al., 2012), and FtsZ1 was found to interact with thioredoxin (Balmer et al., 2003), perhaps suggesting redox regulation. These data suggest that posttranslational modifications could mediate independent regulation of the two families. Future studies should continue to explore other functions and regulation of chloroplast FtsZs.

FtsZ in the division of primitive mitochondria

The alpha-proteobacterial ancestor of mitochondria, like other bacteria, presumably used FtsZ for cell division. Although no mitochondrial FtsZ sequences are found in yeast, animals or plants, FtsZ-based mitochondrial division appears to have been retained in diverse protists (Beech et al., 2000; Gilson et al., 2003; Kiefel et al., 2004; Vieler et al., 2012). FtsZ was shown to form a matrix-localized ring at the division site, and mitochondrial division is impaired in *ftsZ* null mutants of the slime mold *Dictyostelium discoideum* (Beech et al., 2000; Gilson et al., 2003; Nishida et al., 2003), suggesting mitochondrial FtsZs function similarly to those in chloroplasts. Interestingly, in organisms with two identified mitochondrial FtsZs, the N-terminal extensions and C-terminal spacers have diverged (Fig. 1.3), though the functional significance is unknown. Another bacterially-derived protein is required for mitochondrial Z-ring localization and division in the red alga *Cyanidioschyzon merolae* (Yoshida et al., 2009), but little else is known about FtsZ-based mitochondrial division.

Conclusions

We are just beginning to uncover clues about how FtsZ1 and FtsZ2 act in a coordinated manner during chloroplast division in *Arabidopsis*, but much additional work on FtsZ pairs from both higher plants and other organisms is needed to fully understand the mechanistic implications of *FtsZ* gene duplication and divergence for chloroplast division and evolution. *In vitro* approaches, recently including reconstitution of Z rings on liposomes, have yielded critical insights into mechanisms of bacterial FtsZ function, such as the importance of polymer curvature for generating constriction force on the

membrane, the link between GTPase activity, Z-ring turnover and sustained Z-ring constriction, and the effect of C-terminal charge on FtsZ polymer bundling (Buske and Levin, 2012; Huecas et al., 2007; Osawa et al., 2008; Osawa et al., 2009; Osawa and Erickson, 2011). Related approaches could prove equally valuable for deciphering how FtsZ pairs function together in chloroplasts. Cryo-electron and super-resolution microscopy may be useful in probing chloroplast Z-ring organization, as they have provided insight into bacterial Z-ring substructure and mechanisms of constriction (Fu et al., 2010; Li et al., 2007; Strauss et al., 2012). Genetic analysis and *in vivo* studies will no doubt also continue to inform these issues.

In conclusion, recent studies have begun to suggest specialized functions for FtsZ pairs resulting from gene duplication and divergence that may be critical for Z-ring structure and dynamics in chloroplast division. While many aspects of FtsZ function await discovery, recent advances provide exciting new avenues for future research into chloroplast FtsZ activity across the photosynthetic lineages.

Addendum

The original article that constituted Chapter 1 was submitted for publication nearly two and a half years ago. Since that time, there have been additional research articles published studying bacterial and chloroplast FtsZs that have expanded our understanding of FtsZ structure and function. Therefore, I will present these studies in this addendum following the same sections as the main introduction to update and improve this chapter of my dissertation.

Chloroplast FtsZ domain architecture

The C-terminal linker (CTL) is positioned downstream of the C-terminal domain (Fig. 1.3, white bars) and terminates at the border to the C-terminal peptide for FtsZ2 proteins and the CTV for FtsZ1 proteins in plants. This region shows very little sequence conservation and ranges from 2-330 residues among bacterial and eukaryotic FtsZs, but is commonly ~50 residues in length (Vaughan et al., 2004). The CTL is not resolved in crystal structures of bacterial FtsZs, suggesting that it is an intrinsically disordered peptide (IDP) (Oliva et al., 2007; Raymond et al., 2009). Recent work on bacterial FtsZs has shown that this region is in fact an IDP (Buske and Levin, 2013; Gardner et al., 2013). The authors demonstrated that CTL functionality was insensitive to its particular amino acid composition but sensitive to its overall length and disordered nature, suggesting that the CTL serves as a flexible tether linking FtsZ polymers to the membrane. Interestingly, as stated in the main section of this chapter, FtsZB proteins from Rhodophytes do not possess this region, as those proteins terminate at the end of

the C-terminal domain (Fig. 1.3). Future studies will be needed to show that the CTL is in fact an IDP for eukaryotic FtsZs and elucidate its functional significance *in planta*.

As discussed in the main text of this chapter, the FtsZ2 C-terminal peptide mediates the specific interaction of FtsZ2 with ARC6 (Maple et al., 2005). As a result of this interaction, ARC6 likely tethers Z rings to the chloroplast IEM. Recently, FtsZ mobility was explored by single particle tracking analysis in chloroplasts of WT and *arc6* mutant backgrounds expressing FtsZ1-GFP or FtsZ2-GFP proteins (Johnson et al., 2013). Consistent with a role for ARC6 in tethering FtsZ assemblies to the IEM, all results in the WT background showed FtsZ binding to the IEM. However, only 30% of individual FtsZ particles tracked in the *arc6* background showed free diffusion, while the remaining showed properties of either confined diffusion or intermittent binding, suggesting that an ARC6-independent mechanism of FtsZ-tethering to the IEM is present within chloroplasts. Recently, we found that FtsZ2 also interacts with the IEM-associated protein Paralog of ARC6 (PARC6) through its C-terminal peptide, which may represent such an alternative mechanism of FtsZ-binding to the chloroplast membrane (Zhang, Chen et al., 2015).

Plastidic FtsZ functional properties and behavior: clues from FtsZ1 and FtsZ2

In planta FtsZ1 and FtsZ2 turnover has recently been investigated in live chloroplasts in Arabidopsis epidermal cells (Johnson et al., 2015b). Both FtsZ1-GFP and FtsZ2-GFP expressed in the WT background showed subunit exchange from Z rings that was much slower than I previously reported in the *S. pombe* system. These data suggest that FtsZ-interacting regulatory proteins may greatly influence FtsZ

dynamics *in planta*, such as tethering Z rings to the IEM via the interaction between FtsZ2 and ARC6. However, FtsZ1-GFP had a faster rate of turnover than FtsZ2-GFP, suggesting that FtsZ behavioral trends in *S. pombe* are physiologically relevant. Additionally, the authors investigated the effect of ARC3 on FtsZ1-GFP turnover by performing FRAP analysis on FtsZ1-GFP overexpressed in the WT and *arc3* knockout (KO) backgrounds. FtsZ1-GFP in the *arc3* KO background showed a significant reduction in subunit exchange compared to FtsZ1-GFP in the WT background, suggesting that ARC3 acts on FtsZ assemblies as a destabilizing factor and not by inhibiting FtsZ assembly.

Another recent *in planta* study analyzed the assembly of FtsZ into mini-rings in various Arabidopsis mutant and transgenic backgrounds (Johnson et al., 2015a). In this study, the authors used structured illumination microscopy (SIM) to show that FtsZs assembled mini-rings with a mean diameter of 208 ± 68 nm (n = 248) in chloroplasts overexpressing FtsZ2-GFP in the WT background. The authors analyzed the filament organization of such mini-rings by transmission electron microscopy (TEM) of serial sections and performed 3D reconstructions. They found using TEM analysis that the mini-rings assembled with a mean diameter of 183 ± 50 nm (n = 21), which was consistent with their SIM data. Interestingly, FtsZ mini-rings displayed a bipartite organization, with one-half of the ring being highly organized into parallel protofilaments with repeats of 4.2 nm along the axis and with 3 nm protofilament strand thickness. The other half was highly disordered, with greater degrees of protofilament unraveling and adoption of higher-order structures. Taken together, these data represent the first

evidence of *in planta* FtsZ protofilament organization into higher-ordered structures and suggest that FtsZs actively assemble and reorganize within Z rings.

Chapter 2

Distinct Functions of Chloroplast FtsZ1 and FtsZ2 in Z-ring Structure and Remodeling

This research was originally published in *J Cell Biol*.

TerBush, A.D., and K.W. Osteryoung. 2012. Distinct functions of chloroplast FtsZ1 and FtsZ2 in Z-ring structure and remodeling. *J Cell Biol*. 199:623-637

Minor edits have been made to this manuscript to conform to dissertation formatting requirements and Figure callouts.

Abstract

FtsZ, a cytoskeletal GTPase, forms a contractile ring for cell division in bacteria and chloroplast division in plants. Whereas bacterial Z rings are composed of a single FtsZ, those in chloroplasts contain two distinct FtsZ proteins, FtsZ1 and FtsZ2, whose functional relationship is poorly understood. We expressed fluorescently tagged FtsZ1 and FtsZ2 in fission yeast to investigate their intrinsic assembly and dynamic properties. FtsZ1 and FtsZ2 formed filaments with differing morphologies when expressed separately. FRAP showed that FtsZ2 filaments were less dynamic than FtsZ1 filaments and that GTPase activity was essential for FtsZ2 filament turnover but may not be solely responsible for FtsZ1 turnover. When coexpressed, the proteins colocalized, consistent with coassembly, but exhibited an FtsZ2-like morphology. However, FtsZ1 increased FtsZ2 exchange into coassembled filaments. Our findings suggest that FtsZ2 is the primary determinant of chloroplast Z-ring structure, whereas FtsZ1 facilitates Z-ring remodeling. We also demonstrate that ARC3, a regulator of chloroplast Z-ring positioning, functions as an FtsZ1 assembly inhibitor.

Introduction

FtsZ is a self-assembling GTPase related to tubulins that facilitates cell division in bacteria and chloroplast division in photosynthetic eukaryotes (Adams and Errington, 2009; Erickson et al., 2010; Falconet, 2012; Miyagishima, 2011). Bacterial FtsZ, a soluble protein, assembles at the midcell into a dynamic "Z ring," which is tethered to the membrane at the division site by interaction with membrane proteins. The Z ring acts as a scaffold for recruitment of other cell division proteins to the division site and generates at least some contractile force for membrane constriction (Adams and Errington, 2009; Bi and Lutkenhaus, 1991; Lowe and Amos, 1998; Osawa et al., 2008).

In vitro, *E. coli* FtsZ typically polymerizes into single-stranded protofilaments in a GTP-dependent manner, but also assembles into bundles, helices, and sheets under various assembly conditions (Erickson et al., 2010; Mingorance et al., 2010). Polymerization stimulates GTPase activity, which destabilizes protofilaments and promotes their fragmentation (Huecas et al., 2007). These activities do not require accessory proteins, though a number of such proteins regulate protofilament and Z-ring dynamics *in vivo*. Although the mechanism of Z-ring constriction remains uncertain, a current model suggests that tethered protofilaments generate a bending force on bacterial membranes as a consequence of their fixed direction of curvature (Osawa et al., 2009). Protofilament turnover, which may include fragmentation and dissociation of subunits from protofilament ends, facilitates nucleotide exchange and recycling of subunits back into the Z ring (Chen and Erickson, 2009; Huecas et al., 2007; Mingorance et al., 2005; Mukherjee and Lutkenhaus, 1998). Continuous turnover of protofilaments has recently been shown to be required for the sustained contractile

activity of Z rings reconstituted on liposomes (Osawa and Erickson, 2011). The rates of Z-ring turnover *in vivo* and of protofilament turnover *in vitro* correlate with GTPase activity, which varies among FtsZs from different bacteria (Chen et al., 2007; Chen and Erickson, 2009; Huecas et al., 2007; Mukherjee and Lutkenhaus, 1998; Srinivasan et al., 2008).

In contrast to bacteria in which the Z ring is composed of only a single FtsZ protein, plants have two FtsZ families, FtsZ1 and FtsZ2, which both function in chloroplast division (Osteryoung and McAndrew, 2001; Osteryoung et al., 1998; Strepp et al., 1998). Both proteins are nuclear-encoded and imported to the chloroplast stroma by N-terminal transit peptides that are cleaved upon import (Fujiwara and Yoshida, 2001; McAndrew et al., 2001; Mori et al., 2001; Osteryoung and Vierling, 1995. Inside the chloroplast, the mature FtsZ1 and FtsZ2 proteins colocalize to form the mid-plastid Z ring {McAndrew, 2001 #4; Vitha et al., 2001) . Overexpression or depletion of FtsZ1 or FtsZ2 *in vivo* results in fewer and larger chloroplasts per cell than in wild type, suggesting their stoichiometry may be critical for chloroplast division (Osteryoung et al., 1998; Stokes et al., 2000). Recent genetic analysis in *Arabidopsis thaliana* has established conclusively that FtsZ1 and FtsZ2 are not interchangeable, and therefore have distinct functions *in vivo* (Schmitz et al., 2009).

Except for their transit peptides, FtsZ1 and FtsZ2 are well conserved with their bacterial counterparts. They both bear a core region common to all FtsZs that is required for GTP binding and hydrolysis (Margolin, 2005; Osteryoung and McAndrew, 2001; Vaughan et al., 2004) and are each capable of GTP-dependent assembly into protofilaments *in vitro* and of assembly-stimulated GTP hydrolysis (El-Kafafi et al., 2005;

Lohse et al., 2006; Olson et al., 2010; Smith et al., 2010). Importantly, however, they also coassemble and hydrolyze GTP as heteropolymers, apparently with variable stoichiometry (Olson et al., 2010). In the only two comparative *in vitro* studies, the GTPase activity of Arabidopsis FtsZ1 was slightly higher than that of FtsZ2, though both hydrolyze GTP more slowly than *E. coli* FtsZ (Olson et al., 2010; Smith et al., 2010). FtsZ1 and FtsZ2 differ primarily downstream of the core region in their C-termini, within which only FtsZ2 has retained a short peptide conserved in most bacterial FtsZs (Ma and Margolin, 1999; Osteryoung and McAndrew, 2001). In chloroplasts, this C-terminal peptide mediates a specific interaction between FtsZ2 and a transmembrane protein localized at the chloroplast division site, presumably to tether the Z ring to the inner envelope membrane (Maple et al., 2005). However, the equivalent region in bacterial FtsZ is not required for protofilament assembly *in vitro* (Margolin, 2005; Wang et al., 1997) and other functional differences between FtsZ1 and FtsZ2 remain elusive.

Recently, Srinivasan et *al.* (2008) used the fission yeast *Schizosaccharomyces pombe* to study bacterial FtsZ in an *in vivo*-like environment. They showed that bacterial FtsZ expressed as a GFP fusion protein in *S. pombe* robustly reproduced behavior observed earlier in both *in vivo* and *in vitro* experiments, including the ability to self-assemble into filaments and rings without membrane-tethering or other accessory proteins, and similar rates of subunit exchange. They also showed that coexpression of FtsZ with SulA, an inhibitor of FtsZ polymerization, disrupted FtsZ assembly in *S. pombe* (Srinivasan et al., 2007). Thus, *S. pombe* is a valuable system in which to analyze the intrinsic self-assembly behavior of FtsZ proteins and the effects of assembly regulators.

In this study, we exploit *S. pombe* to investigate the self-assembly and dynamic properties of fluorescently tagged *Arabidopsis* FtsZ1 and FtsZ2 expressed separately and together. We show that both proteins assemble into filaments in the *S. pombe* cytosol, but with different morphologies and subunit exchange dynamics. Coassembly experiments provide evidence that FtsZ2 controls filament morphology and FtsZ1 promotes protofilament turnover. The data suggest that, *in vivo*, FtsZ2 forms the chloroplast Z-ring backbone while FtsZ1 facilitates Z-ring remodeling. In addition, we show that the chloroplast Z-ring positioning factor ARC3 inhibits FtsZ1 assembly, consistent with its hypothesized role as a functional analogue of the bacterial Z-ring positioning factor MinC (Maple et al., 2007).

Results

Functionality of FtsZ1 and FtsZ2 C-terminal fusion proteins

In their experiments, Srinivasan et al. (2008) used C-terminal GFP fusions to study bacterial FtsZ in *S. pombe*. Although FtsZ-GFP cannot fully complement bacterial *ftsZ* mutants (Ma et al., 1996), at least partly because the tag blocks membrane-tethering through the conserved C-terminal peptide (Ma and Margolin, 1999), they are nevertheless competent for assembly in bacteria, *in vitro* and in *S. pombe* (Fu et al., 2010; Ma et al., 1996; Osawa et al., 2009; Srinivasan et al., 2008). Further, as indicated above, the behavior of the bacterial fusion proteins in *S. pombe* mirrors their behavior *in vitro* and *in vivo* (Chen et al., 2007; Chen and Erickson, 2005; Srinivasan et al., 2008), indicating the tags do not interfere with their intrinsic cytoskeletal behavior. Therefore, we likewise generated C-terminal FtsZ1-eYFP and FtsZ2-eCFP fusion proteins for expression in *S. pombe*. A nearly identical FtsZ1-mCerulean fusion localized to the chloroplast division site and fully complemented the chloroplast division defect in an Arabidopsis *ftsZ1* knockout mutant (Fig. 2.1 A-C), showing it is functional *in vivo*. In contrast, FtsZ2-GFP or FtsZ2-His fusions do not complement *ftsZ2* mutants, probably because the C-terminal peptide involved in inner envelope tethering is blocked. However, FtsZ2 fluorescent fusions assemble into filaments in chloroplasts (Fig. 2.1 D) (Suppanz et al., 2007) and in *E. coli* (Fig. 2.1 E). Further, FtsZ1 and FtsZ2 bearing C-terminal His tags assemble into protofilaments *in vitro* (Olson et al., 2010; Smith et al., 2010). These data indicate that C-terminally tagged chloroplast FtsZs, like bacterial FtsZs, are assembly-competent and valuable for investigating their intrinsic behavior. Therefore, we expressed FtsZ1-eYFP and FtsZ2-eCFP in *S. pombe* and studied their

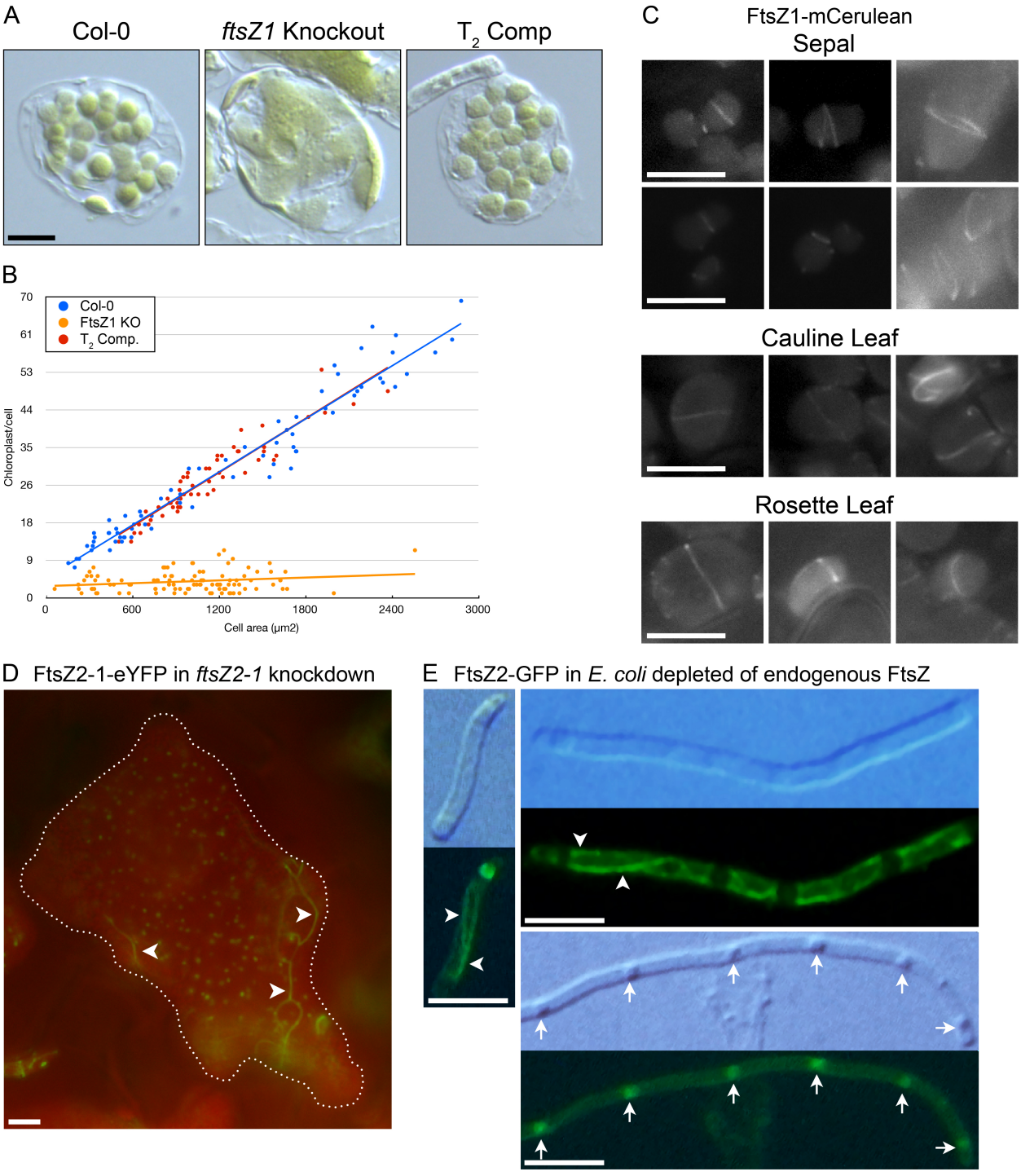

Figure 2.1: Functional analysis of FtsZ C-terminal fluorescent fusion proteins. (A) Differential interference contrast micrographs of mesophyll chloroplast phenotypes for WT Col-0, *ftsZ1* knockout, and T_2 *ftsZ1* knockout/P_{FtsZ1}*::FtsZ1-mCerulean* (T_2 Comp.).

Figure 2.1 (cont'd): (B) Graph of chloroplast numbers per cell relative to cell area. A single plant from each genotype was analyzed. The best-fit lines have slopes of .0206 (R^2 = 0.95), 0.0011 (R^2 = 0.04), and 0.0208 (R^2 = 0.88) for WT Col-0, *ftsZ1* knockout, and T_2 Comp., respectively. The number of mesophyll cells quantified were 73,104, and 55 for the Col-0, *ftsZ1* knockout, and T_2 Comp. lines, respectively. (C) Epifluorescence micrographs of FtsZ1-mCerulean signal in mesophyll cells from various leaf types from T_2 Comp. (D) Fluorescence microscopy images depicting FtsZ2-eYFP (green) assembly in an *Arabidopsis* chloroplast (red). Dotted line represents chloroplast outline. (E) Differential interference contrast and fluorescence micrographs depicting FtsZ2-GFP assembly in an *E. coli* mutant depleted of endogenous FtsZ (*E. coli* strain WM746; Ma and Margolin, 1999). In the absence of bacterial FtsZ, FtsZ2-GFP assembles filaments (arrowheads) and spots (arrows) in the bacterial. Black bar, 10 μm. White bars, 5 μm.

assembly and dynamic properties. All experiments were performed 36-40 h after fusion protein induction.

FtsZ1 and FtsZ2 expressed separately in S. pombe *assemble into filaments with distinct morphologies*

FtsZ1-eYFP and FtsZ2-eCFP (FtsZ1 and FtsZ2 hereafter) both formed filamentous structures (filaments) in the cytosol, as visualized by epifluorescence microscopy (Fig. 2.2). FtsZ1 typically formed long, gently curved cable-like filaments that looped around the cell, and also large closed rings (Fig. 2.2 A-B). Both structures appeared to follow the interior contours of the cell and the fluorescence distribution appeared even, suggesting uniform filament thickness. In contrast, FtsZ2 consistently

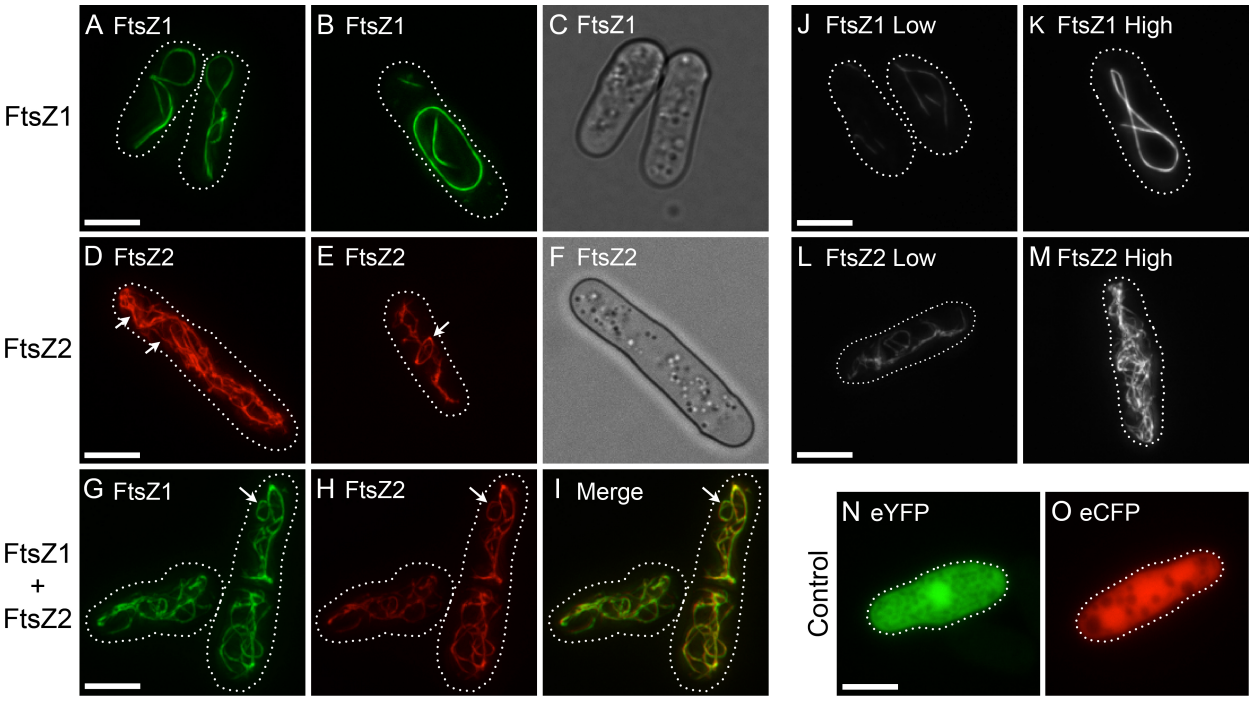

Figure 2.2: FtsZ1 and FtsZ2 filament morphologies in *S. pombe* single- and co-expression strains. (A-B, D-E, G-M) Epifluorescence micrographs of cells expressing (A-B, J-K) FtsZ1-eYFP (green), (D-E, L-M) FtsZ2-eCFP (red), (G-I) FtsZ1-eYFP and FtsZ2-eCFP, (N) eYFP or (O) eCFP. Because the eYFP signals in panels J and K or eCFP signals in panels L and M are from the same identically processed images, respectively, the differences in fluorescence intensity reflect differences in protein level. Dotted lines show cell outlines. (C and F) Differential interference contrast micrographs of cells in panels A and D, respectively. Bars, 5 μm.

formed elaborate networks (Fig. 2.2 D-E). Filaments within these networks were of variable thickness (fluorescence distribution) (Fig. 2.2 D, arrows). Similar to FtsZ1, FtsZ2 formed closed rings (Fig. 2.2 E, arrow). This is the first evidence that FtsZ1 and

FtsZ2 are capable of assembling into rings without the aid of accessory proteins or membrane attachment. However, FtsZ2 rings were observed less frequently than FtsZ1 rings, perhaps because the intricate FtsZ2 network obscured some of them. Similar FtsZ1 and FtsZ2 filament morphologies (i.e., FtsZ1 cables and FtsZ2 filamentous networks) were observed in cells with different levels of expression (Fig. 2.2 J-M, Fig. 2.3 A-B), indicating the distinct morphologies were not due to differences in protein level.

FtsZ1 and FtsZ2 expressed together colocalize in FtsZ2-like filament networks

Arabidopsis FtsZ1 and FtsZ2 colocalize *in vivo*, not only to chloroplast Z rings in wild-type (WT) plants, but also to filaments with aberrant morphologies in various mutants and transgenic plants (McAndrew et al., 2001; Vitha et al., 2003; Vitha et al., 2001) They also coassemble in bundled heteropolymers *in vitro* (Olson et al., 2010). To assess if these proteins colocalize in *S. pombe*, FtsZ1 and FtsZ2 were coexpressed and visualized by epifluorescence microscopy. Imaging was performed on a strain that displayed minimum cell-to-cell variability in coexpression of FtsZ1 and FtsZ2. Immunoblots of soluble culture extracts from this strain showed FtsZ1 and FtsZ2 to be at near-equal levels (Fig. 2.4).

In the coexpression strain, FtsZ1 and FtsZ2 colocalized to an intricate network of filaments (Fig. 2.2 G-I) that closely resembled the networks observed in the strain expressing only FtsZ2 (Fig. 2.2 D-E). They also colocalized to closed rings (Fig. 2.2 G-I, arrow). The extent of colocalization was quantified using the Pearson's correlation coefficient (PCC), which gives a measure of both the overlap between the two fluorescence signals and of how closely the signal intensities are correlated (Bolte and

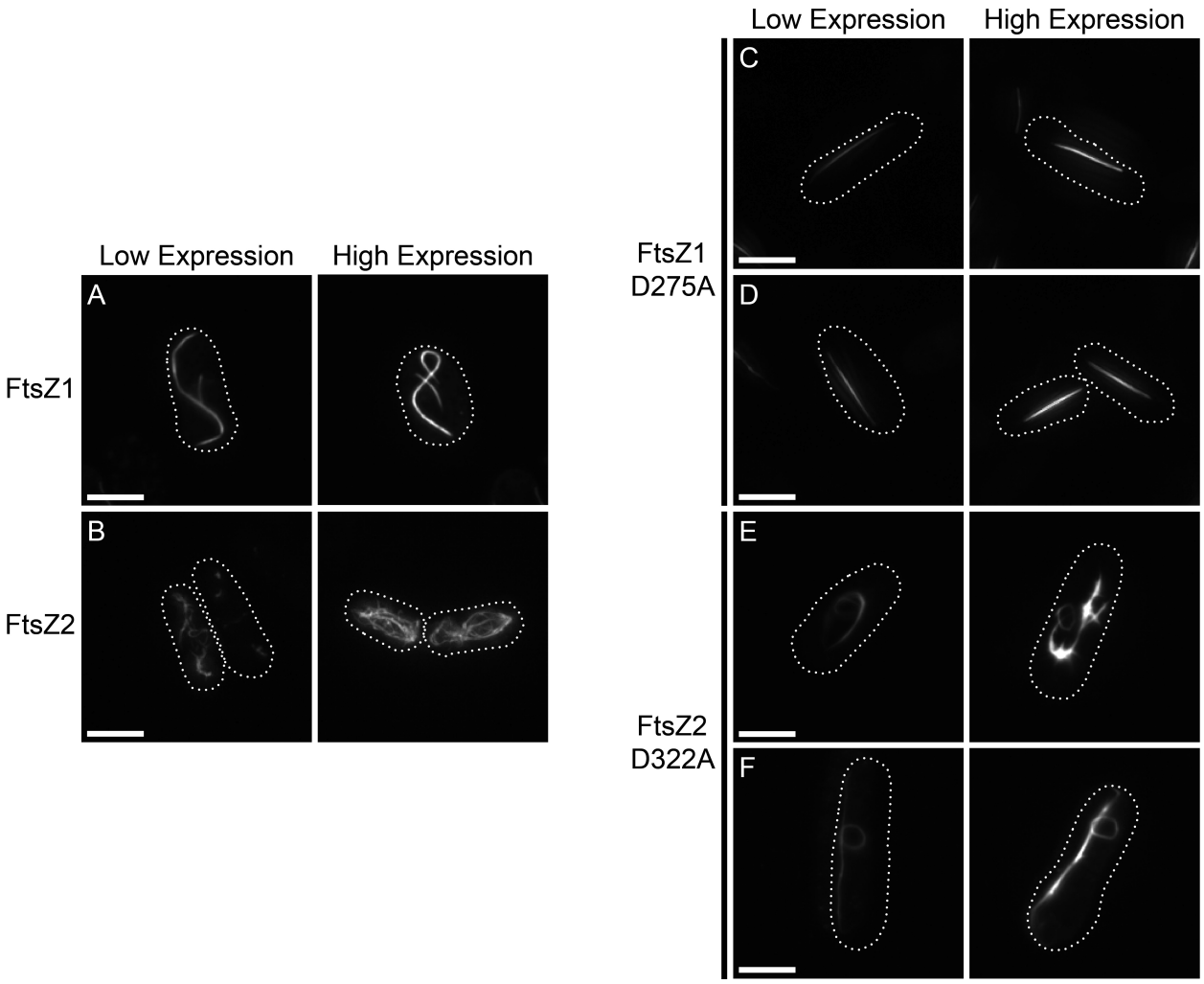

Figure 2.3: FtsZ1 and FtsZ2 distinct filament morphologies are independent of protein expression level. Epifluorescence micrographs of *S. pombe* cells expressing (A) FtsZ1-eYFP, (B) FtsZ2-eCFP, (C-D) FtsZ1-eYFP D275A, and (E-F) FtsZ2-eCFP D322A at variable expression levels. Because the two panels shown in each row were taken from the same image and processed identically, the difference in fluorescence intensity reflects a difference in protein level. Cell cultures were grown in inducing conditions for 36-40 h and imaged for eYFP (FtsZ1) and eCFP (FtsZ2). Dotted lines represent cell outlines. Bars, 5 μm**.**

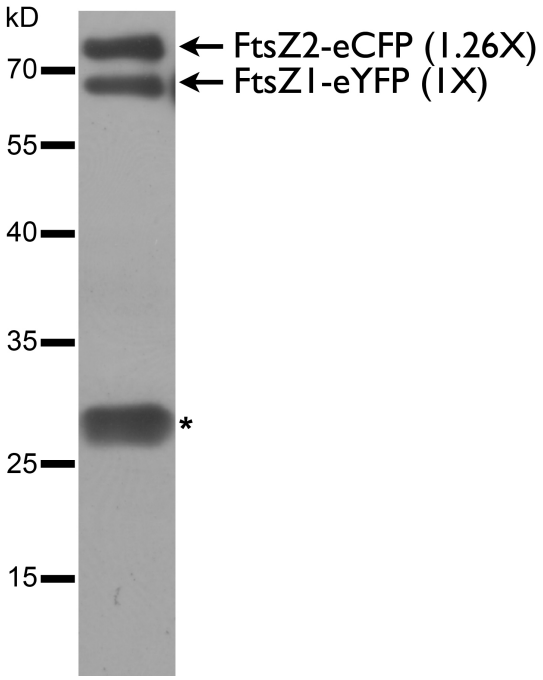

Figure 2.4: Relative FtsZ1 and FtsZ2 protein levels from bulk culture extracts. Immunoblot analysis of FtsZ1-eYFP and FtsZ2-eCFP protein levels from a soluble bulk culture extract from a yeast strain coexpressing these two proteins. The blot was probed with a monoclonal αGFP. The resulting band intensities, corresponding to FtsZ1-eYFP (bottom arrow, ~66 kD) and FtsZ2-eCFP (top arrow, ~72 kD), were quantified, the FtsZ1-eYFP signal was normalized to 1, and the FtsZ2-eCFP signal was normalized relative to the FtsZ1-eYFP signal. The bottom band (asterisk) likely represents a breakdown product formed during extraction, as diffuse fluorescence signal was not evident during imaging. Approximate molecular masses in kD are shown to the left.

Cordelières, 2006). FtsZ1 and FtsZ2 fluorescence signals had an average PCC of 0.77 ± 0.08 (*n*=10 for all measurements), which indicates that FtsZ1 and FtsZ2 colocalize

within filament networks. It also indicates that the FtsZ1 and FtsZ2 signals are directly proportional, i.e., as one signal increases, so does the other.

GTPase-deficient mutants exhibit altered filament morphology

The effect of GTPase activity on chloroplast FtsZ filament morphology is not yet known. To test for this, the GTPase-deficient mutants FtsZ1 D275A and FtsZ2 D322A, which retain less than 10% of their wild-type activity (Olson et al., 2010), were expressed in *S. pombe.* The mutations alter a conserved aspartate required for GTP hydrolysis in presumably all FtsZ proteins, but do not prevent GTP binding (Oliva et al., 2004; Olson et al., 2010; Scheffers et al., 2001). Consistent with our previous findings that FtsZ1 D275A and FtsZ2 D322A are capable of assembling separately *in vitro*, the mutant proteins formed filaments when expressed individually in *S. pombe.* However, the filament morphologies differed from those of the WT proteins (Fig. 2.5). FtsZ1 D275A formed straight filaments of variable length (Fig. 2.5 A). Like the looping cables and rings formed by FtsZ1 (Fig. 2.2 A-B), the straight filaments formed by FtsZ1 D275A showed even fluorescence distribution. In contrast to FtsZ2 filament networks (Fig. 2.2 D-E), FtsZ2 D322A formed irregular filaments that appeared to be split and frayed (Fig. 2.5 B). However, similar to FtsZ2 filaments, FtsZ2 D322A filaments displayed regions of variable thickness (Fig. 2.5 B, arrows), and occasionally formed closed rings (Fig. 2.5 B, arrowhead). FtsZ2 D322A also formed aster-shaped structures and amorphous assemblies (Fig. 2.5 B, inset). Similar structures were observed in cells with different levels of expression (Fig. 2.3 C-F), indicating the distinct FtsZ1 D275A and FtsZ2 D322A morphologies were not due to differences in protein level. While we cannot completely rule out that the structures formed by the mutant proteins result from

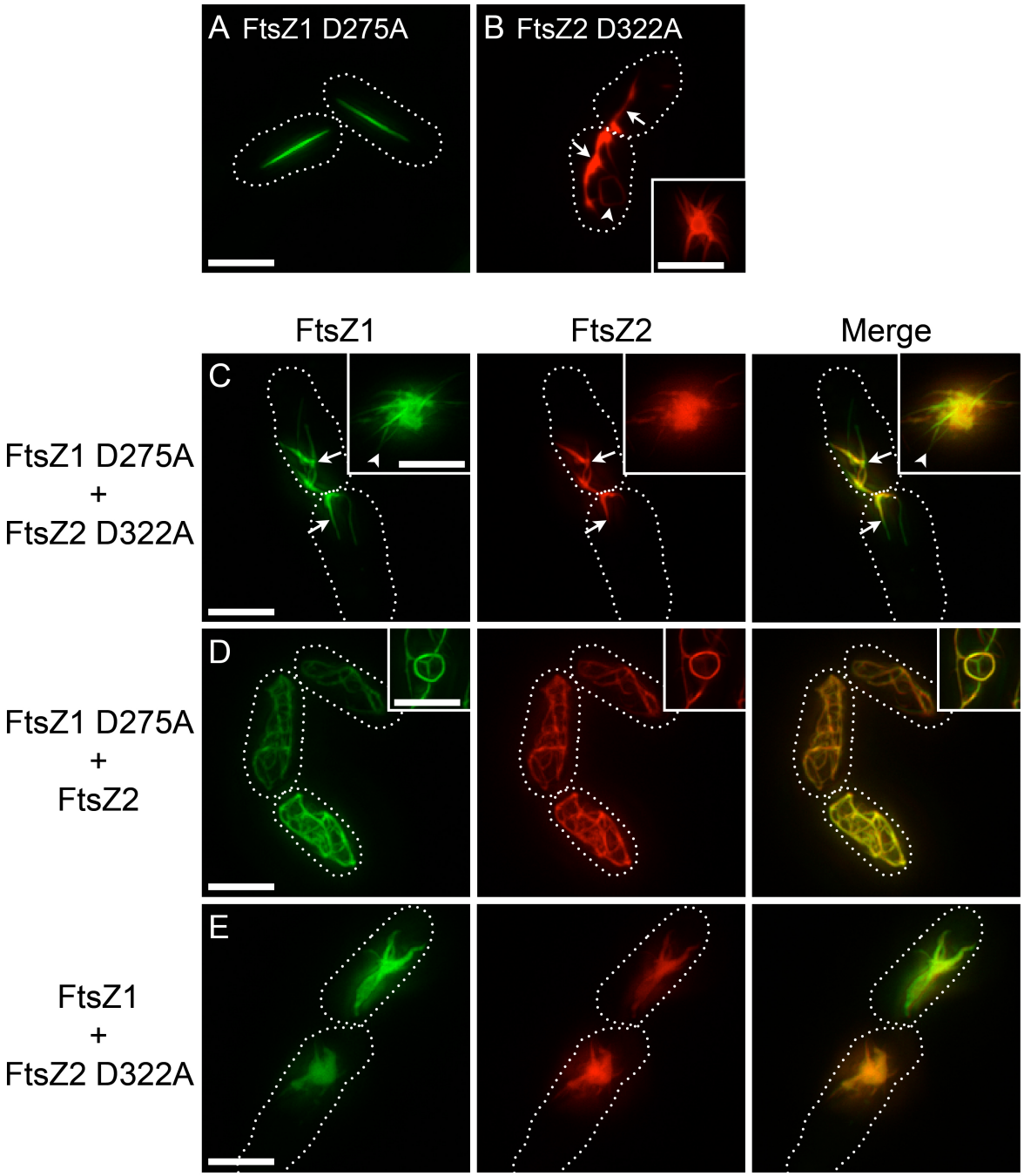

Figure 2.5: Filament morphologies in strains expressing GTPase-deficient FtsZ1 and FtsZ2. Epifluorescence micrographs of cells expressing (A) FtsZ1 D275A (B) FtsZ2 D322A, (C) FtsZ1 D275A and FtsZ2 D322A, (D) FtsZ1 D275A and FtsZ2, or (E) FtsZ1

Figure 2.5 (cont'd): and FtsZ2 D322A. WT and mutant FtsZ1 and FtsZ2 proteins were fused to eYFP (green) and eCFP (red), respectively. Insets show regions in different cells from the same cultures as in larger panels. Dotted lines show cell outlines. Bars, 5 μm.

misfolding in the *S. pombe* cytosol, we have shown that recombinant FtsZ1 D275A and FtsZ2 D322A, like the WT proteins, undergo GTP-dependent assembly into homopolymers and thick heteropolymer bundles *in vitro* (Olson et al., 2010) indicating they are capable of adopting their native structures. An FtsZ2 D322A-GFP fusion protein also assembles in *E. coli* (Olson, 2008) with the same localization pattern as FtsZ2-GFP (Fig. 2.1 E), suggesting proper folding in bacterial cells as well. Further, in the *S. pombe* coexpression strains described below, both FtsZ1 and FtsZ1 D275A colocalize tightly with FtsZ2 D322A and undergo active turnover, including in the amorphous assemblies. These latter observations suggest the mutant proteins coassemble in heteropolymers in *S. pombe* as *in vitro*, consistent with proper folding, and argue that the amorphous assemblies and other structures formed by the mutants represent thick filament bundles rather than protein aggregates. Finally, the equivalent *E. coli* FtsZ mutant (D212A) assembles on its own, coassembles with WT FtsZ, supports some degree of cell division in bacteria and assembles reconstituted Z rings on liposomes (Osawa and Erickson, 2011; Redick et al., 2005; Stricker and Erickson, 2003). Collectively, these findings provide evidence that FtsZ1 D275A and FtsZ2 D322A fold similarly to the WT proteins in *S. pombe*.

FtsZ1 D275A and FtsZ2 D322A were coexpressed to test how they would influence one another. In these strains and the mixed strains described below, coexpression levels were variable. For imaging, we chose cells that displayed fluorescence intensities equivalent to those in the WT coexpression strain described above in which FtsZ1 and FtsZ2 were at near-equal levels. FtsZ1 D275A and FtsZ2 D322A colocalized to irregular filaments, asters, and amorphous assemblies (Fig. 2.5 C). Similar to the FtsZ2 D322A filaments, irregular filaments in the coexpression strain had regions of variable thickness (Fig. 2.5 C, arrows). Rarely, amorphous assemblies displayed some variable composition. In the core of such structures, FtsZ1 D275A and FtsZ2 D322A were strongly colocalized whereas at the periphery, filaments more similar to those formed by FtsZ1 D275A were observed (Fig. 2.5 C, inset arrowhead). The latter regions were enriched in FtsZ1 D275A. However, overall FtsZ1 D275A and FtsZ2 D322A were highly colocalized (PCC 0.86 ± 0.07).

We also coexpressed WT FtsZ1 with GTPase-deficient FtsZ2 and vice versa. FtsZ1 D275A and FtsZ2 colocalized (PCC 0.85 ± 0.07) to an intricate filament network and occasionally to closed rings (Fig. 2.5 D). This morphology was visually indistinguishable from that observed when FtsZ2 was expressed alone (Fig. 2.2 D-E) or with WT FtsZ1 (Fig. 2.2 G-I). FtsZ1 coexpressed with FtsZ2 D322A colocalized (PCC 0.91 ± 0.06) in asters and amorphous assemblies (Fig. 2.5 E) closely resembling those formed when FtsZ2 D322A was expressed alone (Fig. 2.5 B) or with FtsZ1 D275A (Fig. 2.5 C).

A consistent result of the above experiments was that filament morphologies in all coexpression strains were very similar to those in the corresponding single FtsZ2

strain (FtsZ2 or FtsZ2 D322A), regardless of which form of FtsZ1 was present. These data suggest that FtsZ2 has structural dominance over FtsZ1 and controls filament morphology in the coexpression strains.

Dynamics of chloroplast FtsZ filaments

We studied the dynamics of subunit exchange within FtsZ1 and FtsZ2 filaments using FRAP. We measured the rate at which the proteins can diffuse into preexisting filaments, and also assessed the mobile and immobile fractions by calculating the extent of recovery following photobleaching. Cells selected for FRAP varied visibly in fluorescence intensity and hence in protein expression level. Photobleached regions were selected to represent the range of filament morphologies observed in a given strain.

When expressed separately, FtsZ1 and FtsZ2 fluorescence signals showed recovery back into bleached regions (Fig. 2.6), indicating that filaments composed of either protein undergo subunit exchange. FtsZ1 recovered with a half-time ($t_{½}$) of 33.10 ± 7.83 s (*n*=10 for all FRAP experiments) (Fig. 2.6 A), while FtsZ2 had a slower $t_{½}$ of 86.96 ± 22.08 s (Fig. 2.6 B). FtsZ1 fluorescence recovered to 71.32 ± 11.51% of the pre-bleach intensity (Fig. 2.6 A), whereas FtsZ2 fluorescence only recovered to 31.07 ± 7.70% (Fig. 2.6 B). These differences were statistically significant ($P < 0.01$). No consistent correlation between the maximum fluorescence intensity in the photobleached cells and either $t_{½}$ or % recovery could be discerned (Fig. 2.7 A-B), suggesting that protein level did not influence FRAP measurements over the expression ranges represented in our experiments. FRAP data are summarized in Table 2.1.

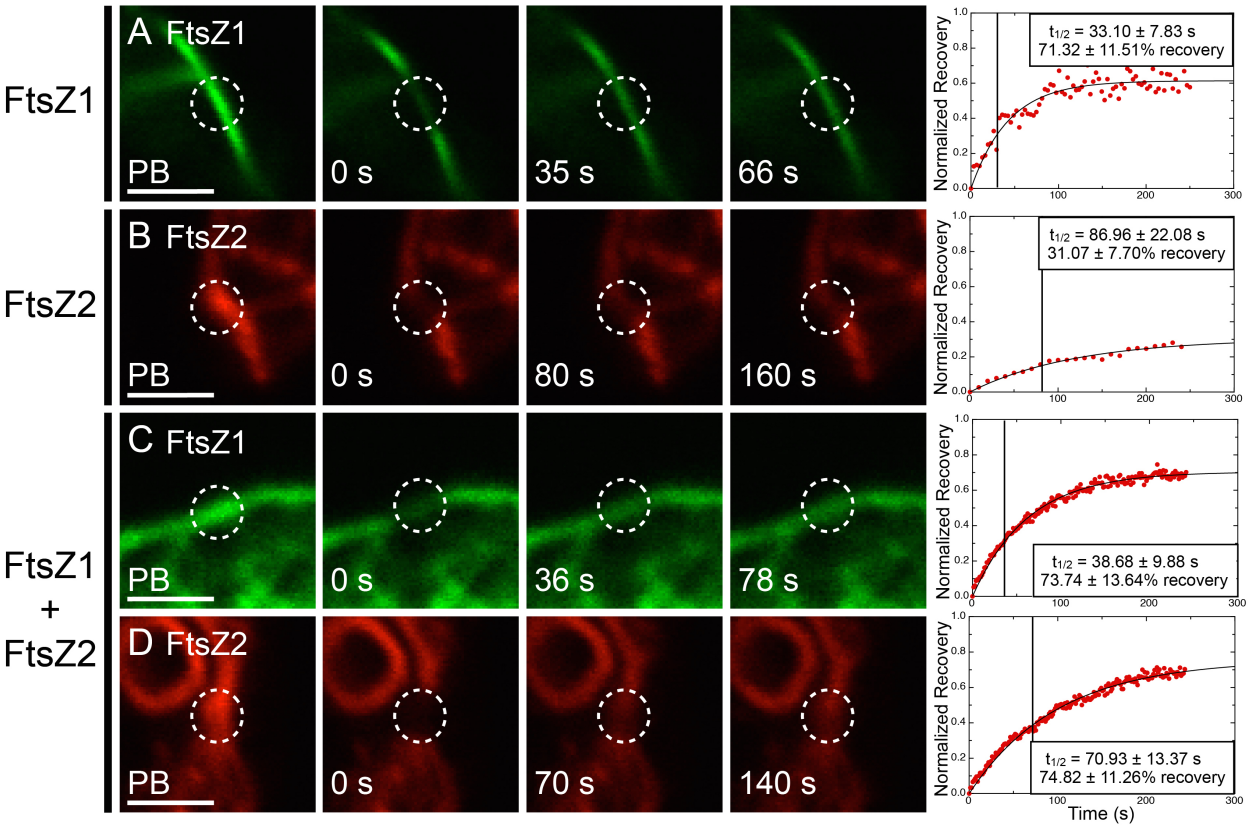

Figure 2.6: Dynamics of FtsZ1 and FtsZ2 expressed singly or together. *S. pombe* cells expressing (A) FtsZ1-eYFP (green), (B) FtsZ2-eCFP (red), or (C and D) FtsZ1-eYFP and FtsZ2-eCFP were analyzed by FRAP. Images from left to right represent fluorescence signals in photobleached regions (circled) just prior to bleaching (PB), at the time of bleaching (0 s), at the time closest to $t_{½}$, and at twice $t_{½}$. Representative plots of fluorescence recovery vs time are shown at right. Data in each plot were normalized to the PB fluorescence signal (1 on the y-axis) and the signal intensity at the time of bleaching (0 on the y-axis). Boxes in the plots show the average $t_{1/2}$ (also indicated by vertical lines) and average % recovery ± SD for 10 independent FRAP datasets obtained for each strain. Bars, 2 µm.

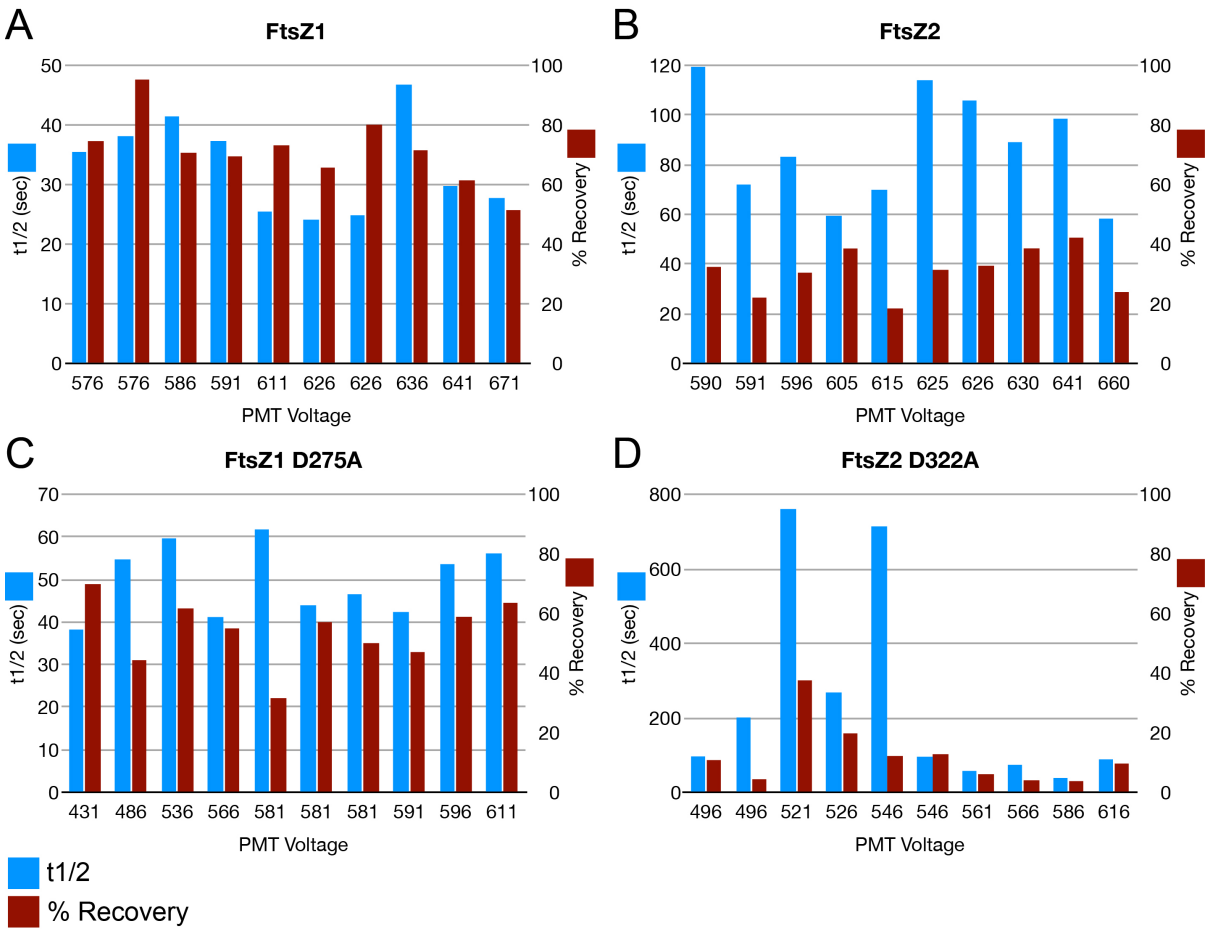

Figure 2.7: FtsZ1 and FtsZ2 dynamics were not altered over the range of protein levels analyzed during FRAP analysis. Graphs show individual half-time and % recovery values versus photomultiplier tube (PMT) voltage settings for each of the ten cells analyzed by FRAP in all four single-expression stains. With all other microscope acquisition settings remaining constant for all experiments, PMT voltage inversely correlates to fluorescence intensity (http://www.olympusmicro.com/primer/techniques/confocal/pmtintro.html) and therefore with protein content (high voltage = lower protein and vice versa), though the relationship is not necessarily linear. Left y-axis represents recovery half-time (blue

Figure 2.7 (cont'd): bars); right y-axis represents percent recovery (red bars). (A) FtsZ1, (B) FtsZ2, (C) FtsZ1 D275A, and (D) FtsZ2 D322A expressed alone.

We also assessed how coexpression of FtsZ1 and FtsZ2 affected each of their dynamics. When coexpressed, FtsZ1 and FtsZ2 recovered with $t_{½}$'s of 38.68 ± 9.88 s and 70.93 ± 13.37 s, respectively (Fig. 2.6 C-D). These values were not statistically different from those measured when FtsZ1 and FtsZ2 were expressed alone (Fig. 2.6 A-B). FtsZ1 recovered to 73.74 ± 13.64% of the pre-bleach (Fig. 2.6 C), equivalent to the recovery when FtsZ1 was expressed by itself (Fig. 2.6 A). However, FtsZ2 recovered to 74.82 ± 11.26% (Fig. 2.6 D; Table 2.1), nearly 2.5-fold greater than when expressed on its own (Fig. 2.6 B), indicating an FtsZ1-dependent increase in FtsZ2 dissociation from filaments. This effect suggests that FtsZ1 destabilizes FtsZ2-containing protofilaments, consistent with the formation of heteropolymers.

GTPase-deficient proteins show altered turnover

To assess whether GTPase activity affects FtsZ1 and FtsZ2 dynamics, FtsZ1 D275A and FtsZ2 D322A were analyzed for rate and extent of subunit turnover in *S. pombe* using FRAP (Fig. 2.8). The straight FtsZ1 D275A filaments recovered with a $t_{½}$ of 49.79 ± 8.35 s and displayed a maximum recovery of 53.91 ± 11.03% (Fig. 2.8 A; Table 2.1). Both values were significantly reduced compared to those of FtsZ1 (Fig. 2.6 A). Surprisingly, however, even with its severely inhibited GTPase activity (Olson et al., 2010), FtsZ1 D275A filaments displayed a significant amount of subunit exchange. In contrast, turnover of FtsZ2 D322A was almost completely abolished. FtsZ2 D322A

Yeast Expression Strain	$t_{1/2}$ (s)	% Recovery
FtsZ1	33.10 ± 7.83	71.32 ± 11.51
FtsZ1 D275A	49.79 ± 8.35[a]	53.91 ± 11.03[a]
FtsZ2	86.96 ± 22.08[a]	31.07 ± 7.70[a]
FtsZ2 D322A	239.21 ± 271.60	12.09 ± 10.25[b]
FtsZ1 + FtsZ2	38.68 ± 9.88	73.74 ± 13.64
	70.93 ± 13.37	74.82 ± 11.26[b]
FtsZ1 D275A + FtsZ2 D322A	46.93 ± 9.37	56.66 ± 10.31
	123.21 ± 69.66	19.27 ± 12.47
FtsZ1 + FtsZ2 D322A	38.00 ± 11.01	46.83 ± 10.44[a]
	72.11 ± 106.96	7.57 ± 8.53
FtsZ1 D275A + FtsZ2	41.22 ± 11.10	50.37 ± 12.85
	112.06 ± 49.74	30.74 ± 20.44

Table 2.1: FRAP data for all single and coexpression strains. Time for one-half recovery ($t_{1/2}$, s) and maximum percent recovery for each protein in each expression/coexpression strain. Data represent an average of ten FRAP measurements ± standard deviation.

[a]Statistically significant difference from the corresponding value in FtsZ1 single expression strain ($P < 0.01$).

[b]Statistically significant difference from the corresponding value in FtsZ2 single expression strain ($P < 0.01$).

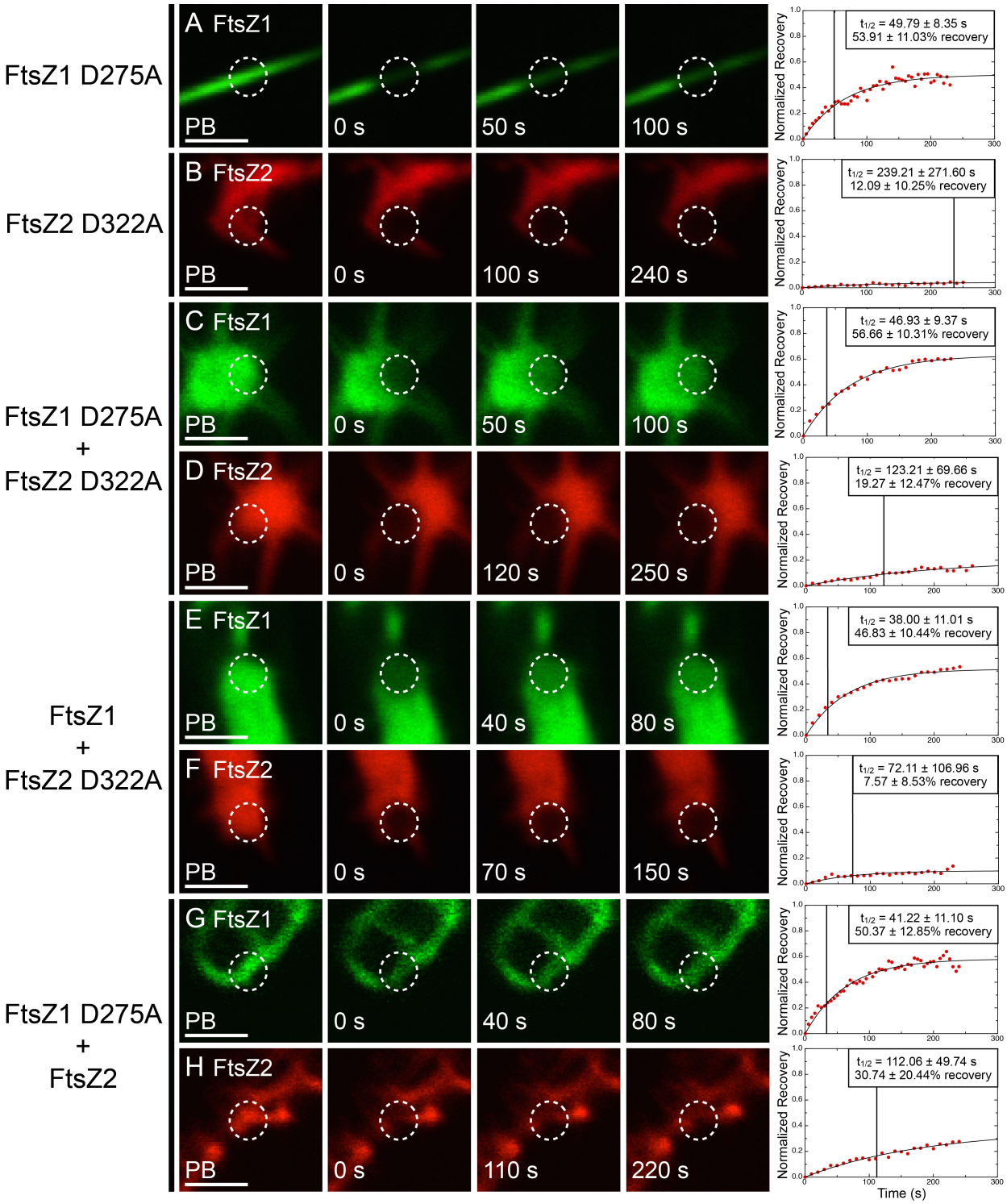

Figure 2.8: Dynamics of GTPase-deficient FtsZ1 and FtsZ2 expressed in various combinations. *S. pombe* cells expressing (A) FtsZ1 D275A, (B) FtsZ2 D322A (panel 3

Figure 2.8 (cont'd): is 100 s recovery, panel 4 is the image acquired closest to $t_{½}$), (C and D) FtsZ1 D275A and FtsZ2 D322A, (E and F) FtsZ1 and FtsZ2 D322A, and (G and H) FtsZ1 D275A and FtsZ2. WT and mutant FtsZ1 and FtsZ2 proteins were fused to eYFP (green) and eCFP (red), respectively. Images from left to right (except in B) represent fluorescence signals in photobleached regions (circled) just prior to bleaching (PB), at the time of bleaching (0 s), at the time closest to $t_{½}$, and at twice $t_{½}$. Representative plots of fluorescence recovery vs time are shown at right. Data in each plot were normalized to the PB fluorescence signal (1 on the y-axis) and the signal intensity at the time of bleaching (0 on the y-axis). Boxes in the plots show the average $t_{1/2}$ (also indicated by the vertical lines) and average % recovery ± SD for 10 independent FRAP datasets obtained for each strain. Bars, 2 µm.

filaments had a $t_{½}$ of 239.21 ± 271.60 s and recovered to a maximum of 12.09 ± 10.25% (Fig. 2.8 B). As observed for FtsZ1 and FtsZ2, turnover of FtsZ1 D275A and FtsZ2 D322A filaments did not appear to be affected by protein expression level over the range of levels measured (Fig. 2.7 C-D). The reduced turnover of GTPase-deficient FtsZ filaments indicates that GTP hydrolysis is an important factor in promoting subunit exchange. However, in the case of FtsZ1, it may not be solely responsible, as filaments consisting of only FtsZ1 D275A still undergo significant turnover.

When FtsZ1 D275A and FtsZ2 D322A were coexpressed, $t_{½}$'s were 46.93 ± 9.37 s and 123.21 ± 69.66 s, while maximum recoveries were 56.66 ± 10.31% and 19.27 ± 12.47%, respectively (Fig. 2.8 C-D). These values were statistically similar to those observed when FtsZ1 D275A and FtsZ2 D322A were expressed alone.

To extend our analysis, mutant and WT FtsZ proteins were assayed in different combinations. When coexpressed, FtsZ1 and FtsZ2 D322A recovered with $t_{½}$'s of 38.00 ± 11.01 s and 72.11 ± 106.96 s, and had maximum recoveries of 46.83 ± 10.44% and 7.57 ± 8.53%, respectively (Fig. 2.8 E-F; Table 2.1). These were similar to values obtained when each protein was expressed individually, except that the percent recovery for FtsZ1 was statistically lower than when FtsZ1 was expressed alone (Fig. 2.6 A), indicating decreased FtsZ1 dissociation from the filaments. Conversely, when FtsZ1 D275A and FtsZ2 were coexpressed, $t_{½}$'s were 41.22 ± 11.10 s and 112.06 ± 49.74 s, while maximum recoveries were 50.37 ± 12.85% and 30.74 ± 20.44%, respectively (Fig. 2.8 H). In this combination, all values were similar to those observed when FtsZ1 D275A and FtsZ2 are expressed alone.

Based on the FRAP data, we conclude that FtsZ1 is more dynamic than FtsZ2 in *S. pombe*, that FtsZ2 but not FtsZ1 turnover is abolished by loss of GTPase activity, and that FtsZ1 enhances turnover of FtsZ2 in heteropolymers.

Effect of ARC3 on FtsZ1 assembly

The chloroplast division protein ARC3 (Pyke and Leech, 1992; Shimada et al., 2004) regulates placement of the division site by restricting Z-ring assembly to the mid-plastid, as shown by the formation of multiple constrictions and Z rings in chloroplasts of Arabidopsis *arc3* mutants (Glynn et al., 2007; Maple et al., 2007). ARC3 was reported to interact specifically with FtsZ1 in yeast two-hybrid assays and has been proposed to function similarly to bacterial MinC (Maple et al., 2007), suggesting it may be a direct inhibitor of FtsZ assembly (Hu et al., 1999; Lutkenhaus, 2007). To begin testing this hypothesis, we fused eCFP to a truncated form of ARC3, $ARC3_{41\text{-}598}$, that lacks the N-

terminal chloroplast transit peptide and the C-terminal MORN domain. The MORN domain was shown to inhibit ARC3-FtsZ1 interaction in yeast (Maple et al., 2007), possibly because another Z-ring assembly regulator not present in yeast normally sequesters the MORN domain *in vivo* (Glynn et al., 2009).

$ARC3_{41\text{-}598}$ was coexpressed with FtsZ1 in *S. pombe* and FtsZ1 morphology was examined. In cells with strong $ARC3_{41\text{-}598}$ fluorescence, FtsZ1 adopted a diffuse localization pattern and did not produce any filaments (Fig. 2.9 A). In cells with weaker $ARC3_{41\text{-}598}$ fluorescence, some FtsZ1 filaments could be observed (Fig. 2.9 B). These filaments varied in length and displayed a straight or bent morphology, but were never as long as those observed when FtsZ1 was expressed alone (Fig. 2.2 A-B). $ARC3_{41\text{-}598}$ colocalized with FtsZ1 filaments in cells where filaments were visible (Fig. 2.9 B, arrow), consistent with the $ARC3_{41\text{-}598}$-FtsZ1 interaction in yeast (Maple et al., 2007). In contrast, when coexpressed with only eCFP as a control, FtsZ1 assembled into cable-like filaments and rings similar to those seen when FtsZ1 was expressed alone, regardless of eCFP protein level (Fig. 2.9 C-D). These results provide evidence that $ARC3_{41\text{-}598}$ functions as an inhibitor of FtsZ1 assembly, possibly in a dose-dependent manner, and support the hypothesis that ARC3 regulates division-site placement *in vivo* by interfering with protofilament formation away from the chloroplast midpoint.

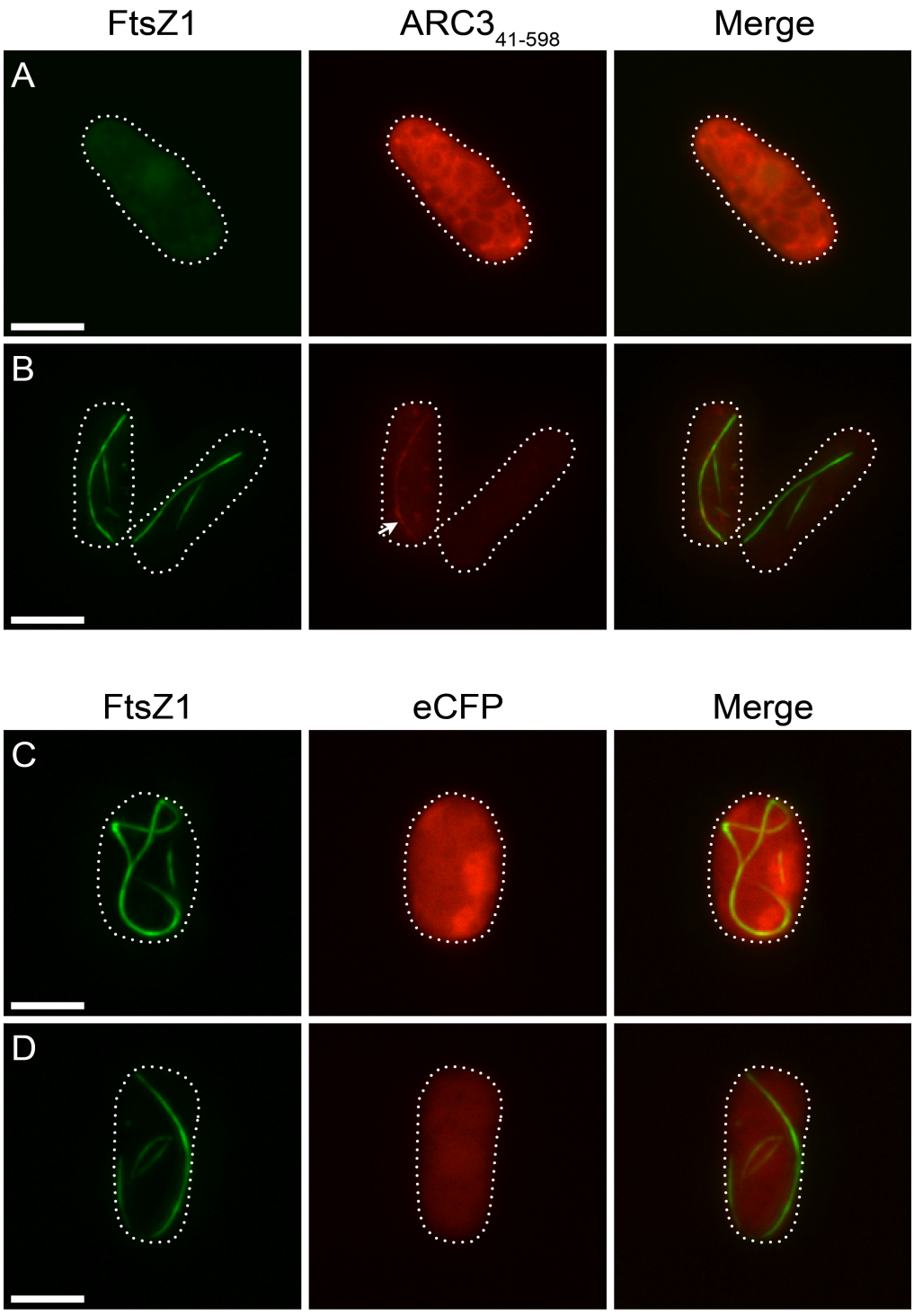

Figure 2.9: Effect of ARC3$_{41-598}$ on FtsZ1 assembly. Epifluorescence micrographs of *S. pombe* cells expressing FtsZ1-eYFP (green) and (A) higher levels of ARC3$_{41-598}$-

Figure 2.9 (cont'd): eCFP (red), (B) lower levels of $ARC3_{41\text{-}598}$-eCFP, (C) higher levels of eCFP, or (D) lower levels of eCFP. Exposure times and image processing for cells in panels A and B were identical. Cells in panels C and D were taken from the same identically processed image; hence differences in fluorescence intensity reflect differences in protein level. Dotted lines show cell outlines. Bars, 5 μm.

Discussion

Bacterial FtsZs, which function as homopolymers, have been studied extensively and, though questions remain, much has been learned about their assembly and dynamic properties (Adams and Errington, 2009; Aylett et al., 2011; Erickson et al., 2010; Mazouni et al., 2004). In contrast, the assembly properties of chloroplast FtsZ1 and FtsZ2 are poorly understood. Expression of fluorescent FtsZ1 and FtsZ2 fusions in fission yeast, which lacks the native assembly regulators present in chloroplasts, has allowed us to begin exploring their intrinsic self-assembly properties in an *in vivo*-like system. As observed by Srinivasan et al. (2008) for bacterial FtsZ, the behavior of FtsZ1 and FtsZ2 in *S. pombe* is consistent with findings from previous studies. For example, FtsZ1 and FtsZ2 are independently capable of forming filaments in *S. pombe* as they are *in vitro* and in plants (El-Kafafi et al., 2005; Lohse et al., 2006; Olson et al., 2010; Schmitz et al., 2009; Smith et al., 2010; Yoder et al., 2007). Further, the colocalization of FtsZ1 and FtsZ2 in *S. pombe* agrees with their tight colocalization *in vivo* and with recent work showing that they preferentially coassemble as heteropolymers *in vitro* (McAndrew et al., 2001; Olson et al., 2010; Vitha et al., 2001). Thus, *S. pombe* accurately reproduces key features of FtsZ1 and FtsZ2 behavior.

FtsZ filament morphology

We suggest that the distinct morphologies displayed by FtsZ1 and FtsZ2 in *S. pombe* represent protofilament bundles based on observations that *E. coli* FtsZ protofilaments, which are typically single-stranded when polymerized in dilute solution *in vitro*, undergo bundling when assembled in crowding reagents more closely resembling the *S. pombe* cytosol (Erickson et al., 2010; Mukherjee and Lutkenhaus, 1999; Popp et

al., 2009). The width and intensity of the fluorescence signals also suggest bundling, as assumed by Srinivasan et al. (2008) for the linear cables formed by bacterial FtsZ in *S. pombe*. Several studies suggest that bacterial FtsZ bundles and Z rings consist of loosely packed, overlapping protofilaments held together by weak lateral interactions, probably involving electrostatic forces (Buske and Levin, 2012; Fu et al., 2010; Li et al., 2007; Popp et al., 2009), though membrane tethering may enhance lateral interactions and packing between protofilaments (Milam et al., 2012). The split and frayed appearance and variable thickness of FtsZ2 and FtsZ2 D322A filaments (Fig. 2.2 D-E; Fig. 2.5 B) and more uniform appearance of FtsZ1 and FtsZ1 D275A filaments (Fig. 2.2 A-B; Fig. 2.5 A) could indicate that lateral interactions are stronger between FtsZ1 than FtsZ2 protofilaments. *In vitro* assembly experiments that mimic molecular crowding conditions in *S. pombe* and in chloroplasts will be important for understanding these differences.

Our finding that FtsZ1 and FtsZ2 are each capable of forming closed ring structures in *S. pombe* (Fig. 2.2 B, E), similar to bacterial FtsZ (Srinivasan et al., 2008), suggests that the ability to form closed rings, perhaps by annealing of protofilaments (Chen and Erickson, 2009; Erickson et al., 2010; Mingorance et al., 2005) is an inherent characteristic of FtsZ1 and FtsZ2 and does not require membrane-tethering or accessory proteins. The fact that GTPase-deficient FtsZ2 D322A homopolymers could also form closed rings (Fig. 2.5 B) indicates that this property, at least for FtsZ2, does not depend on active protofilament turnover. This is consistent with recent reports showing that *E. coli* FtsZ forms closed rings on the surface of liposomes and on a mica

surface even when GTPase activity and subunit exchange are severely inhibited (Mateos-Gil et al., 2012; Osawa and Erickson, 2011).

We presume that the consistent colocalization of FtsZ1 and FtsZ2 in *S. pombe*, also observed in chloroplasts (McAndrew et al., 2001; Vitha et al., 2001), represents coassembly in heteropolymers based on *in vitro* assembly experiments (Olson et al., 2010). The predominant structures in the *S. pombe* coexpression strains invariably resembled those assembled by whichever form of FtsZ2 was present (WT or FtsZ2 D322A) irrespective of the form of FtsZ1 present. This suggests that FtsZ2 exerts a significant degree of dominance over FtsZ1 in determining heteropolymer morphology, at least when unrestrained by membrane tethering or the action of assembly regulators. The reason for FtsZ2's morphological dominance over FtsZ1 is not yet clear. A possibility is that the interface geometry between FtsZ1 and FtsZ2 subunits in heteropolymers is more similar to the geometry between subunits in FtsZ2 homopolymers. Structural approaches would be required to assess this. Whatever the explanation, morphological dominance by FtsZ2 may depend on the ratio between FtsZ1 and FtsZ2 in heteropolymers, as suggested by the enrichment of FtsZ1 D275A in straight filaments protruding from the amorphous assemblies of colocalized FtsZ1 D275A and FtsZ2 D322A (Fig. 2.5 C, inset arrowhead). We suggest these filaments arise from the ability of FtsZ1 D275A but not FtsZ2 D322A to dissociate from filaments, leading over time to the formation of the FtsZ1 D275A-enriched protrusions. Future studies in which the FtsZ1-FtsZ2 ratio in individual *S. pombe* cells is quantified and manipulated should provide insight into how the interplay between FtsZ1 and FtsZ2 influences filament morphology.

FtsZ filament dynamics

Studies on bacterial FtsZ have shown that GTPase activity correlates with the rate of subunit exchange from protofilaments and Z rings and is probably essential for Z-ring remodeling (Chen et al., 2007; Chen and Erickson, 2009; Huecas et al., 2007; Mukherjee and Lutkenhaus, 1998; Osawa and Erickson, 2011). Because FtsZ1 has higher GTPase activity than FtsZ2 *in vitro* (Olson et al., 2010; Smith et al., 2010), the higher turnover of FtsZ1 than FtsZ2 filaments in *S. pombe* (Fig. 2.6 A-B) may partly reflect this difference, though the difference in GTPase activity is fairly small. As these are the first comparative analyses of chloroplast FtsZ dynamics, it remains to be seen whether other methods yield similar data. However, turnover rates for *E. coli* and *M. tuberculosis* FtsZ in *S. pombe* were very close to those measured in bacterial cells and *in vitro* (Anderson et al., 2004; Chen et al., 2007; Chen and Erickson, 2005; Srinivasan et al., 2008), suggesting that our measurements in this system reflect the intrinsic dynamics of the chloroplast proteins as well. Recovery half-times for FtsZ1 and FtsZ2 in homopolymers as well as in coassembled filaments were well below those reported for *E. coli* FtsZ, consistent with their lower GTPase activities (Lu et al., 1998; Olson et al., 2010; Redick et al., 2005; Smith et al., 2010). However, turnover of FtsZ1 in *S. pombe* was comparable to that of *M. tuberculosis* FtsZ (Srinivasan et al., 2008), which has a similar GTP hydrolysis rate (Chen et al., 2007).

The reduced recovery half-times and altered filament morphologies of GTPase-deficient FtsZ1 D275A and FtsZ2 D322A mutants demonstrate that GTPase activity is important for maintaining FtsZ1 and FtsZ2 protofilament structure and dynamics. However, in contrast with the static FtsZ2 D322A filaments, FtsZ1 D275A filaments still

exhibited significant though reduced turnover compared to WT FtsZ1 filaments. Given the high degree of similarity between the conserved GTP-binding and hydrolysis domains of FtsZ1 and FtsZ2 (Osteryoung and McAndrew, 2001), it is not clear why equivalent mutations inhibit dynamics severely in FtsZ2 D322A and only moderately in FtsZ1 D275A, even though the GTPase activities in both cases are reduced below background (Olson et al., 2010). These findings suggest that some other factor facilitates turnover of FtsZ1 homopolymers and heteropolymers. One such factor could be the strength of their subunit interfaces. FtsZ1-FtsZ1 interfaces may be inherently weaker than FtsZ2-FtsZ2 interfaces, perhaps making FtsZ1 homopolymers, both WT and mutant, more prone to fragmentation and subunit dissociation than FtsZ2 homopolymers, resulting in higher turnover. As described below, this conjecture could also explain the behavior of heteropolymers.

Our finding that FtsZ2 displays a 2.5-fold increase in fluorescence recovery when coexpressed with FtsZ1 suggests that more FtsZ2 dissociates from heteropolymers than from homopolymers (Fig. 2.6). A preliminary model consistent with these findings and with recent models of bacterial FtsZ behavior is depicted in Fig. 2.10. The model is meant to represent the intrinsic steady-state dynamic behavior of FtsZ1 and FtsZ2 in *S pombe*. In chloroplasts, self-assembly and turnover would be modulated by numerous assembly regulators (Maple and Moller, 2010; Pyke, 2010; Yang et al., 2008). 1) We suggest that, in *S. pombe*, FtsZ1 and FtsZ2 homopolymers and heteropolymers assemble in loosely bundled filaments. This conjecture is based in part on *in vivo* data suggesting loose protofilament bundling through weak lateral interactions in bacteria (Buske and Levin, 2012; Fu et al., 2010; Li et al., 2007) and on our observation that

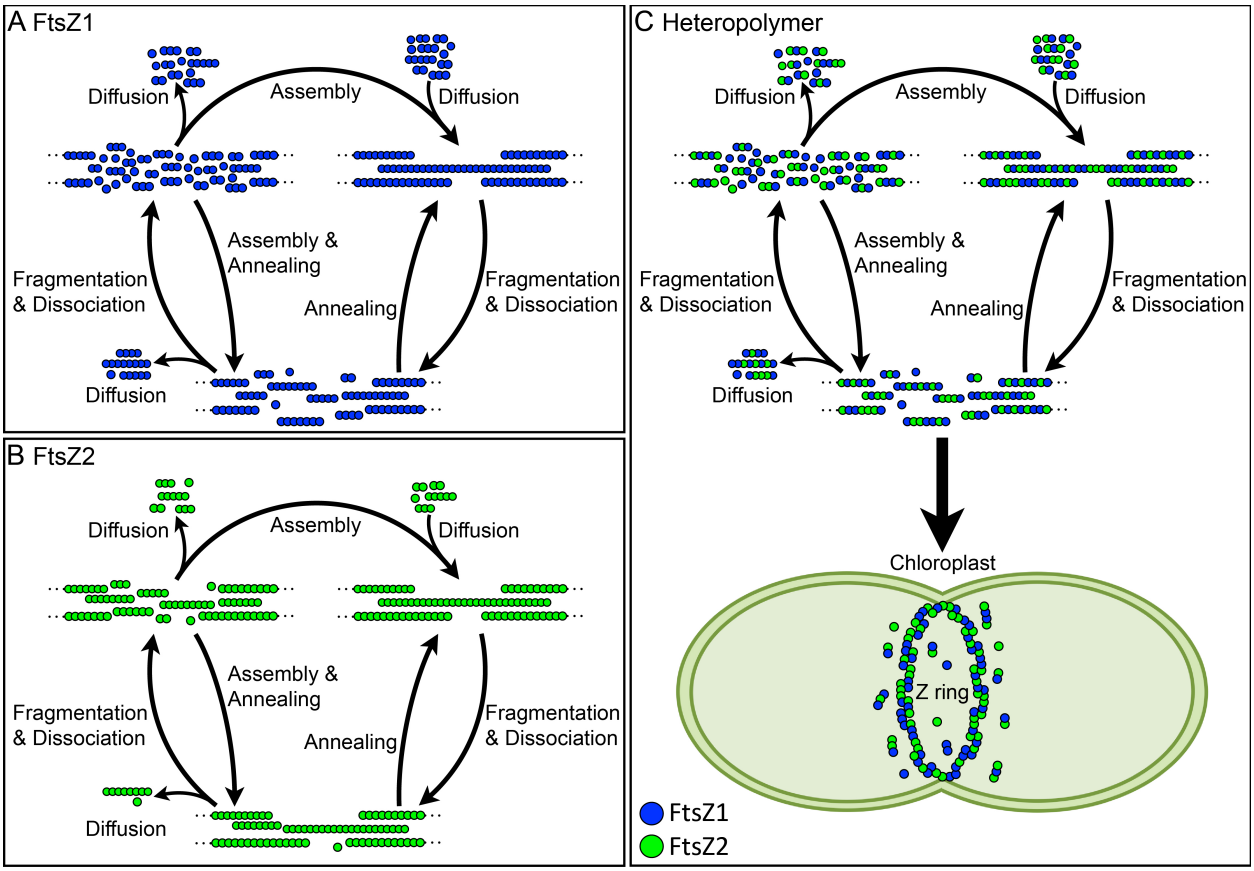

Figure 2.10: Working model of the intrinsic steady-state turnover of FtsZ1 and FtsZ2 homopolymers and heteropolymers in *S. pombe* based on FRAP analysis and models of bacterial FtsZ dynamics. (A and B) FtsZ1 homopolymers have higher rates of fragmentation and loss of subunits from protofilament ends than FtsZ2 homopolymers. The diffusible pool of small oligomers and subunits that can be recycled back into protofilaments is therefore larger for FtsZ1 than FtsZ2, resulting in higher FtsZ1 turnover. (C) FtsZ1 incorporation into heteropolymers enhances fragmentation and loss of subunits from protofilament ends. The diffusible pool of small FtsZ2-containing oligomers and FtsZ2 subunits that can be recycled back into protofilaments is therefore larger for heteropolymers than for FtsZ2 homopolymers, resulting in higher FtsZ2 turnover from heteropolymers. We hypothesize that heteropolymers represent the

Figure 2.10 (cont'd): predominant protofilament form in the chloroplast Z ring *in vivo* (wide arrow). Annealing of protofilaments and addition of subunits onto protofilament ends may both contribute to turnover in all cases. Blue circles, FtsZ1; green circles, FtsZ2. Dotted lines represent continuation of FtsZ protofilaments. Important details are elaborated in the Discussion.

changes in FtsZ1 and FtsZ2 expression levels do not appear to affect turnover dynamics under our experimental conditions (Fig. 2.7). If protofilaments were tightly packed, diffusion out of protofilament bundles might be reduced at higher expression levels, though additional experiments, perhaps coupled with new super-resolution imaging techniques (Fu et al., 2010; Jennings et al., 2010; Li et al., 2007), will be necessary to rigorously explore the arrangement of chloroplast FtsZ protofilaments. 2) The faster turnover and higher maximum recovery of FtsZ1 than FtsZ2 in the single-expression strains suggest that FtsZ1 homopolymers may be less stable and more likely to fragment and lose subunits from protofilament ends than FtsZ2 homopolymers (Fig. 2.10 A-B). Fragmentation of FtsZ1 filaments would therefore produce a larger pool of diffusible subunits and small oligomers that could be recycled back onto FtsZ1 protofilaments than fragmentation of FtsZ2 filaments, making FtsZ1 filaments more dynamic. Further disassembly of small FtsZ1 oligomers would contribute to FtsZ1 turnover. 3) Coassembly of FtsZ1 and FtsZ2 in heteropolymers would increase fragmentation and subunit dissociation (Fig. 2.10 C), producing a larger pool of diffusible FtsZ2-containing oligomers than would occur for FtsZ2 homopolymers (Fig. 2.10 B). Small oligomers containing FtsZ2 and/or FtsZ1 could further depolymerize,

increasing the overall assembly-ready pool of FtsZ2 available for reassembly onto free protofilament ends. Additionally, as proposed for bacterial FtsZ (Osawa and Erickson, 2011), annealing of protofilament fragments could also contribute to recycling of both FtsZ1 and FtsZ2 subunits and short oligomers back into larger filaments, leading to the increased turnover of FtsZ2 observed in the coexpression strains (Fig. 2.6). Because FtsZ1 and FtsZ2 tightly colocalize to the chloroplast division site *in vivo* and form heteropolymers *in vitro* (McAndrew et al., 2001; Olson et al., 2010; Vitha et al., 2001), we suggest that this situation may be more representative of the dynamic behavior of FtsZ1 and FtsZ2 in dividing chloroplasts (Fig. 2.10 C, bottom). We also note that the assembly subunit is not yet known, but if it is a dimer or tetramer as proposed by Smith et al. for FtsZ1 and FtsZ2 homopolymers (Smith et al., 2011), or a hetero-oligomer of FtsZ1 and FtsZ2, then the minimal protofilament could be two or more subunits thick instead of a single subunit thick as depicted in Fig. 2.10. This would not necessarily alter the effect of FtsZ1 on heteropolymer dynamics, however.

The mechanistic explanation for the increased turnover of FtsZ2 from heteropolymers is not yet clear. As FtsZ1 has somewhat higher GTPase activity than FtsZ2 and GTPase is correlated with turnover of bacterial FtsZ protofilaments, one potential explanation could be that heteropolymers hydrolyze GTP more rapidly than homopolymers, leading to increased turnover. However, coassembly of FtsZ1 and FtsZ2 *in vitro* only slightly increased (Olson et al., 2010) or decreased (Smith et al., 2010) GTPase activity, suggesting that GTP hydrolysis may not occur much more rapidly in FtsZ1-FtsZ2 than FtsZ1-FtsZ1 subunit interfaces. Another possibility, suggested by our finding that GTPase-deficient FtsZ1 D275A filaments are still dynamic

(Fig. 2.8 A), is that weaker FtsZ1-FtsZ1 interfaces in heteropolymers stimulate fragmentation, enhancing turnover. Based on our previous *in vitro* work suggesting that FtsZ1 and FtsZ2 heteropolymers assemble with variable stoichiometry (Olson et al., 2010), in Fig. 2.10 C we have represented the arrangement of FtsZ1 and FtsZ2 subunits in heteropolymers as variable rather than as strictly alternating. Where FtsZ1-FtsZ1 interfaces are present, heteropolymers would fragment more readily if these interfaces are indeed weaker. This model would predict that increasing the FtsZ1-to-FtsZ2 ratio in heteropolymers would destabilize and promote turnover of heteropolymers. A combination of *in vitro* and *in vivo* approaches will be necessary to address these speculations. However, even if FtsZ1-FtsZ1 (or potentially FtsZ1-FtsZ2) interfaces are inherently weaker than FtsZ2-FtsZ2 interfaces, GTPase activity still appears to be necessary for the enhancement of FtsZ2 turnover by FtsZ1,as FtsZ1 D275A does not result in a statistically significant increase FtsZ2 turnover from heteropolymers as does FtsZ1 (Fig. 2.6 B; Fig. 2.8 H).

Function of ARC3

In *E. coli*, MinC antagonizes FtsZ polymerization by direct interaction near the cell poles. MinC is spatially regulated by MinD and MinE through a complex set of interactions, resulting in Z-ring formation and cell division only at the midcell (de Boer, 2010; Lutkenhaus, 2007). Green-lineage chloroplasts inherited homologues of MinD and MinE through endosymbiosis, and these proteins likewise function to restrict Z-ring formation to the mid-plastid (de Boer, 2010; Glynn et al., 2007; Itoh et al., 2001; Maple et al., 2002; Vitha et al., 2003). However, although MinC also occurs in the cyanobacterial relatives of chloroplasts (Mazouni et al., 2004; Miyagishima, 2005),

higher plants lack MinC. Instead, the plant-specific FtsZ1-interacting protein ARC3 has been postulated as a functional replacement for MinC (Maple et al., 2007; Shimada et al., 2004). Our finding that ARC3 inhibits FtsZ1 assembly in *S. pombe* supports this hypothesis. Because ARC3 also interacts with MinD and MinE (Maple et al., 2007), these results also suggest that ARC3, like MinC, functions as a direct assembly inhibitor whose activity is controlled by MinD, MinE and possibly several other plant-specific proteins (Miyagishima, 2011) to regulate Z-ring assembly and positioning. However, since ARC3 bears no obvious structural similarity to MinC, its mechanism of action may be different. MinC is thought to inhibit bacterial Z-ring formation by inhibiting bundling of protofilaments (Dajkovic et al., 2008; de Boer, 2010; Hu et al., 1999). ARC3 bears an FtsZ-like domain that interacts with FtsZ1, though it probably is not a functional GTPase (Maple et al., 2007; Shimada et al., 2004). We speculate that the FtsZ-like region of ARC3 might assemble directly into protofilaments and destabilize them, perhaps by promoting fragmentation. Further experimentation will be needed to understand the mechanism of ARC3 action.

Potential roles of FtsZ1 and FtsZ2 in chloroplast Z rings

Our analysis of the intrinsic assembly properties of FtsZ1 and FtsZ2 in *S. pombe,* suggests potential specialized functions for these proteins. Our finding that coassembled filaments invariably adopt an FtsZ2-like morphology suggests that FtsZ2 may be the primary structural determinant of the chloroplast Z ring. This function may be enhanced *in vivo* by membrane tethering of FtsZ2 through its interaction with the transmembrane chloroplast division protein ARC6 (Maple et al., 2005; Vitha et al., 2003). The higher turnover of FtsZ1 than FtsZ2 homopolymers and the FtsZ1-

dependent increase in FtsZ2 turnover from heteropolymers suggest that FtsZ1 may facilitate Z-ring constriction by enhancing Z-ring turnover. Consistent with these ideas, FtsZ2 occasionally forms mid-plastid Z rings and supports some degree of chloroplast division in an Arabidopsis *ftsZ1* null mutant, but only in very small chloroplasts (Yoder et al., 2007). By promoting turnover, FtsZ1 may sustain Z-ring constriction during leaf growth, when chloroplasts are expanding and dividing. FtsZ1 and FtsZ2 maintain a constant 1:2 ratio in whole rosettes of Arabidopsis throughout plant development (McAndrew et al., 2008), but the ratio in individual chloroplasts, and more importantly in Z rings, remains unknown. The possibility that FtsZ1 and FtsZ2 assemble at variable ratios *in vivo* as observed *in vitro* (Olson et al., 2010) potentially represents a novel mechanism for regulating Z-ring constriction during plant growth and/or over a single chloroplast contractile cycle. Quantitative *in vivo* studies of FtsZ1 and FtsZ2 behavior and protein levels during plant development and in chloroplast Z rings will be important for further addressing the functional interplay between FtsZ1 and FtsZ2 and establishing how Z-ring assembly, positioning and contractile activity are regulated in chloroplasts.

Materials and Methods

Cloning and S. pombe *Transformation*

Sequences encoding WT or GTPase-deficient *Arabidopsis thaliana* FtsZ1 (AtFtsZ1-1, At5g55280) and FtsZ2 (AtFtsZ2-1, At2g36250) lacking the predicted transit peptides (the first 57 and 48 amino acids, respectively), were amplified by PCR from the corresponding cDNA bacterial expression plasmids (Olson et al., 2010). The primers used were: 5'-TTT TTT CTC GAG ACC ATG AGG TCT AAG TCG ATG CGA TTG AGG-3' (forward) and 5'-GCC CTT GCT CAC CAT CTG CAT GAA GAA AAG TCT ACG GGG AGA AGA-3' (reverse) for *FtsZ1* and 5'-TTT TTT CTC GAG ACC ATG GCC GCT CAG AAA TCT GAA TCT TCT-3' (forward) and 5'-GCC CTT GCT CAC CAT CTG CAT GAC TCG GGG ATA ACG AGA GCT-3' (reverse) for *FtsZ2*. The *FtsZ1* and *FtsZ2* PCR products were then fused to *enhanced Yellow Fluorescent Protein* (*eYFP)* or *enhanced Cyan Fluorescent Protein* (*eCFP)* (Clontech), respectively, at their C-termini by Splicing by Overlap Extension (SOE) and asymmetric PCR (Warrens et al., 1997). The primers used to amplify *eYFP* and *eCFP* were 5'-ATG GTG AGC AAG GGC GAG GAG CTG-3' (forward) and 5'-TTT TTT GGA TCC TTA CTT GTA CAG CTC GTC CAT GC-3' (reverse). *FtsZ1-eYFP* and *FtsZ2-eCFP* fusion products were subcloned into *pREP41X* and *pREP42X,* under control of the medium strength *nmt1** promoter (Basi et al., 1993; Forsburg, 1993), using standard molecular biology techniques and Xho1 and BamH1 restriction sites.

Control constructs were generated for the expression of eYFP and eCFP only. The primers used to amplify *eYFP* and *eCFP* were: 5'-TTT TTT CTC GAG ACC ATG GTG AGC AAG GGC GAG GAG CTG-3' (forward) and the same reverse primer as

described above for creation of the FtsZ fusion constructs. The *eYFP* and *eCFP* PCR products were subcloned into *pREP41X* and *pREP42X* as described above, but using the Xho1 and BamH1 HF restriction sites.

A truncated *ARC3* (*AtARC3*, At1g75010) construct consisting of the FtsZ-like domain and the middle region ($ARC3_{41\text{-}598}$, amino acids 41-598) (Maple et al., 2007; Shimada et al., 2004) was amplified from a cDNA clone by PCR. The primers used were: 5'-TTT TTT CAT ATG GCC AAC TGT ACA TCT CGA AAG GCG CGT CG-3' (forward) and 5'-GCC CTT GCT CAC CAT CTG CAT ATC TCC GGC GTC CAC TTG TTT CC-3' (reverse). *eCFP* was fused to the 3' end of the $ARC3_{41\text{-}598}$ PCR product by SOE and asymmetric PCR (Warrens et al., 1997). The primers used to amplify *eCFP* were the same as described above. The $ARC3_{41\text{-}598}$-*eCFP* fusion product was subcloned into *pREP42*, under control of the *nmt1** promoter (Basi et al., 1993; Forsburg, 1993), using the Nde1 and BamH1 restriction sites.

FtsZ constructs were transformed into *S. pombe* using a modified lithium acetate procedure (http://www.sanfordburnham.org/labs/wolf/Protocols/Protocols/Fission%20Yeast/Nurse%20Lab%20Manual.htm). *S. pombe* (strain MBY192 (h^- leu1-32 ura4-D18)) cultures were grown in 50 mL of Pombe Glutamate medium (PMG) at 32°C with shaking at 250 rpm to an OD = 0.5 ($1x10^7$ cells/mL) and pelleted at 4,000x*g* at room temperature. The pellet was washed with ½ culture volume of TE (10 mM Tris-HCl, 1 mM EDTA, pH 7.5). The cells were pelleted again, resuspended in 1 mL of TE and LiAc (100 mM lithium acetate, pH 7.5) and allowed to incubate at 30°C for 30 min. 200 µL of cells were aliquoted into microfuge tubes containing 20 µL of 10 µg/µL carrier sperm

DNA (Stratagene) and 1 µg of plasmid DNA (~2-3 µL in 2 mM Tris-HCl pH 8.5) and mixed by vortexing. 1.2 mL of PEG solution (40% PEG, TE pH 7.5, and LiAc) was added and each tube was vortexed for 10 s to mix. Tubes were incubated at 30°C with 200 rpm shaking for 30 min and then heated for 15 min at 42°C. The cells were pelleted at 7,000x*g* for 30 s and the supernatant was discarded. The cells were resuspended in 300 µL of TE, plated on solid PMG with selection for the plasmids (-uracil for pREP41X or -leucine for pREP42 or pREP42X), and allowed to grow at 28°C until colonies formed. Coexpression lines were generated by taking a culture in which cells had approximately uniform fluorescence of FtsZ1-eYFP, transforming the *FtsZ2-eCFP*, *ARC3*$_{41\text{-}598}$*-eCFP*, or *eCFP* construct into that cell line by the same protocol described above, and plating on solid PMG with both selection markers (-uracil and -leucine). The *FtsZ2-eCFP*, *ARC3*$_{41\text{-}598}$*-eCFP*, and *eCFP* constructs were under the control of the same promoter but a different selection marker (*ura4*+) than the *FtsZ1-eYFP* construct (*LEU2*).

Growth and Expression of Transformed Cell Lines

*The nmt1** promoter is repressible with 15 µM thiamine (Maundrell, 1990). Yeast strains were streaked for isolation and grown on solid PMG containing 15 µM thiamine in the absence of leucine and/or uracil to select for the *FtsZ1-eYFP* and/or *FtsZ2-eCFP/ARC3*$_{41\text{-}598}$*-eCFP* constructs, respectively, at 28°C until colonies formed. Colonies were used to inoculate liquid cultures without thiamine to activate expression of the fusion proteins, and allowed to grow at 32°C with 250 rpm shaking for 36-40 hrs.

A culture coexpressing FtsZ1-eYFP and FtsZ2-eCFP was identified, in which cells displayed strong fluorescence signal for each protein and minimal cell-to-cell

variation in expression. This strain was used to make a glycerol stock on which subsequent analyses were performed. Cultures grown from this stock were also used to determine the relative levels of FtsZ1-eYFP and FtsZ2-eCFP by immunoblotting using a monoclonal αGFP (Clontech, http://www.clontech.com/). The resulting band intensities were quantified, FtsZ1-eYFP signal was normalized to 1, and FtsZ2-eCFP signal was normalized relative to FtsZ1-eYFP signal.

Fluorescence Microscopy and FRAP Analysis

Aliquots (2 μL) of the liquid culture were pipetted onto glass or poly-lysine coated slides and covered with a cover slip. Samples were imaged by differential interference contrast and epifluorescence microscopy, using a Leica DMRA2 microscope with a Leica HCX PL apochromat 63X (1.32 NA) oil-immersion objective and a QImaging Retiga Exi camera at room temperature. Z-stacks were taken, 0.5 μm increment, and the images were de-blurred by performing Nearest Neighbor deconvolution with 70% haze removal using Image-Pro 7.0 software (Media Cybernetics (http://www.mediacy.com/)). Further image manipulations were performed using ImageJ software (http://rsbweb.nih.gov/ij/). Projections were made from Z-stacks using the max-intensity algorithm, and the images were falsely colored, green for FtsZ1-eYFP and red for FtsZ2-CFP and $ARC3_{41\text{-}598}$-eCFP. Coexpression overlays were generated with the merge channels option. Colocalization of FtsZ proteins in each coexpresion strain was quantified by averaging the PCCs calculated in 10 cells using the Colocalization finder plugin for ImageJ ± standard deviation.

FRAP was performed at room temperature on an Olympus FluoView 1000 Laser Scanning Confocal Microscope, with a Plan FLN 60X (1.42 NA) oil-immersion objective

with a 3.4X zoom. Immediately prior to collecting FRAP data, the photomultiplier tube (PMT) voltage was adjusted so that the maximum fluorescence signal in each cell imaged was just below saturation. Data were collected with Olympus FV1000 ASW software. 2 µL of cell culture was mounted on poly-lysine coated slides. FtsZ1-eYFP filaments were photobleached for 20 msec with a 515 nm laser at 50%. FtsZ2-eCFP filaments were photobleached for 20 msec with a 458 nm laser at 50%. Fluorescence intensity measurements were taken over a time-course of 250 s after photobleaching for each photobleached region of interest, a background sample, and an area of fluorescence signal that was away from the bleached location. The FRAP raw data were processed to produce the normalized recovery curves (Rabut and Ellenberg, 2005). FRAP analysis was performed for yeast strains coexpressing all combinations of FtsZ1-eYFP and FtsZ2-eCFP (WT and GTPase-deficient mutant). Coexpressing cells chosen for FRAP analysis displayed strong fluorescence signals from both fluorescent proteins present. FRAP measurements for the strains coexpressing WT FtsZ1-eYFP and FtsZ2-eCFP were performed by taking ten FtsZ1-eYFP datasets followed by ten FtsZ2-eCFP datasets from different cells in the same culture. For the remainder of the coexpression strains, FRAP data for each FtsZ construct were obtained sequentially in the same cell. Recovery of FtsZ1-eYFP (WT or mutant) was measured first, as the eYFP emission spectrum does not overlap with the excitation spectrum of eCFP. Curve-fitting of FRAP data was performed using pro Fit software (http://www.quansoft.com/), where the data were fit to the single exponential equation $f(t) = A(1-e^{-kt})$. The time for one-half recovery of the fluorescence signal ($t_{1/2}$) was calculated as $t_{1/2}= \ln(½)/-k$. Analysis of statistically

significant differences between average recovery half-time and % recovery in different strains were performed using a two-tailed Student's t test ($P < 0.01$).

To assess the effect of protein expression level on filament dynamics, individual half-time and % recovery values were plotted against the PMT voltage setting for each of the ten cells analyzed by FRAP in all four single-expression stains. PMT voltage inversely correlates with fluorescence intensity (http://www.olympusmicro.com/primer/techniques/confocal/pmtintro.html).

Functional Analysis of FtsZ1 and FtsZ2 C-Terminal Fusion Proteins

An *FtsZ1-mCerulean* construct was made as in Schmitz et al. (2009), except that the 3' piece was fused to *mCerulean* (Addgene) at the 3' end of *FtsZ1* by splicing by overlap extension and asymmetric PCR (Warrens et al., 1997). The Multisite Gateway® recombinations were performed using Gateway® LR+ ClonaseTM (Invitrogen), pMDC204 (http://botserv1.uzh.ch/home/grossnik/curtisvector/index_2.html) modified with a Gateway® R4-R3 cassette, and 5', middle, and 3'-*mCerulean* pENTR vectors to create the P_{FtsZ1}*::FtsZ1-mCerulean* genomic clone.

ftsZ1 knockout plants were transformed using a standard floral dipping protocol (Clough and Bent, 1998) with *Agrobacterium tumefaciens* strain GV3101 containing P_{FtsZ1}*::FtsZ1-mCerulean*. Transformants were selected on plates containing 20 µg/L hygromycin B based on hypocotyl length following germination in the dark (Kadirjan-Kalbach et al., 2012). Positive transformants were transplanted to soil and grown in environmentally controlled growth chambers under white fluorescent light (100 µmol m^{-2} s^{-1}, 16/8 h light/dark) at 21°C and relative humidity of 60%. T_2 seeds harvested from T_1 plants that showed partial complementation of the chloroplast division phenotype were

grown and analyzed for chloroplast division complementation and fluorescence signal. Rosette leaf samples for phenotypic analysis were harvested on the same day from Col-0, *ftsZ1* knockout, and T_2 transgenic plants sown and grown together. Leaf samples were fixed with 3.5% glutaraldehyde for 3 h followed by 1.5 h at 50°C in 0.1 M Na_2-EDTA (Pyke and Leech, 1991). Leaf samples were imaged by differential interference contrast microscopy using a Leica DMI 300B microscope with a Leica HCX PL FLUOTAR 40X (0.75 NA) dry objective at room temperature and Leica Application Suite (Media Cybernetics (http://www.mediacy.com/)). Images were acquired with a Leica DFC320 camera. Mesophyll cell area was determined using ImageJ software and the chloroplast number per cell was manually counted for each cell. Various leaf types from a T_2 transgenic plant that was fully complemented were analyzed for FtsZ1-mCerulean fluorescence signal by epifluorescence microscopy as described above but with a Leica HCX PL FLUOTAR 100X (1.30 NA) oil-immersion objective.

An *FtsZ2-GFP* fusion construct was generated by subcloning an *FtsZ2-GFP* fusion product (FtsZ2 beginning at residue 89, with a QGDIT linker) into pUC19. The *FtsZ2-GFP* construct was transformed into *E. coli* strain WM746 (Ma and Margolin, 1999), an *ftsZ* null strain carrying a low copy number plasmid that displayed temperature-sensitive replication and contained an *E. coli FtsZ* gene. Bacterial cells were grown at 33°C until the exponential growth phase, then used to inoculate fresh medium. Fresh cultures were grown at 42°C with 500 μM IPTG to induce expression of FtsZ2-GFP, while depleting the bacterial FtsZ protein, for 5 hrs. Bright-field images were obtained with differential interference contrast optics and fluorescence microscopy using an Olympus BH2 microscope with a 100X (1.25 NA) oil-immersion objective at room

temperature; GFP epifluorescence images were captured with an Optronics (Goleta, CA) DEI 750 color video camera and Scion Image 1.62 software (Scion Corporation, Frederick, MD). Noise in the fluorescence images was reduced by applying a median filter (radius = 2). Images were assembled using Adobe Photoshop 5.0 (Adobe Systems Inc., San Jose, CA) and Canvas 6.0 (Deneba Software, Miami, FL) software.

An *FtsZ2-eYFP* fusion construct was generated by subcloning the *FtsZ2-1* full length coding sequence into a derivative of pCambia-1302 (Cambia, Canberra, Australia) in which GFP was replaced by eYFP using standard molecular biology techniques. The *FtsZ2-eYFP* construct was transformed into an Arabidopsis *ftsZ2-1* knockdown mutant (Schmitz et al., 2009) as described above. Positive transformants were selected for by growth on plates containing hygromycin, as described above. T_1 plants were analyzed for FtsZ2-eYFP signal by epifluorescence microscopy.

Chapter 3

Conservation of FtsZ Functionality Across the Photosynthetic Lineages

The *pREP41-SeFtsZ-msfGFP* and *pREP41-msfGFP* expression constructs were generated and initially imaged by co-author Joshua S. MacCready, Microbiology and Molecular Genetics Graduate Program, Department of Plant Biology, and Plant Research Laboratory at Michigan State University.

Abstract

FtsZ, a cytoskeletal GTPase, self-assembles into a ring that is responsible for providing force for membrane constriction during cell division in bacteria and chloroplast division in photosynthetic eukaryotes. While bacteria accomplish cell division with a single FtsZ, chloroplast division requires the coordinated action of two functionally distinct FtsZ isoforms, FtsZ1 and FtsZ2 in plants and green algae and FtsZA and FtsZB in red algae with primary chloroplasts. Recent functional studies have begun to elucidate the properties of FtsZ1 and FtsZ2 from Arabidopsis, yet very little functional data for FtsZ pairs from other photosynthetic organisms exist. In this study, we expressed fluorescent fusions of FtsZs from a monocot and dicot plant, green alga, red alga, and cyanobacterium in the heterologous *Schizosaccharomyces pombe* system to study their inherent filament morphology and turnover characteristics. We found that the distinct filament morphologies for the FtsZ1/FtsZB and FtsZ2/FtsZA families are highly conserved across a broad evolutionary distance. When coexpressed, FtsZs from plants coassembled into FtsZ2-like rings, while FtsZs from a red alga coassembled in filaments with characteristics of both FtsZ families. Additionally, FRAP experiments demonstrated that FtsZ1s have greater filament turnover properties than FtsZ2s and that the GTPase activity of FtsZ2/FtsZA, but not FtsZ1/FtsZB, is critical for promoting filament turnover. Interestingly, a cyanobacterial FtsZ displayed filament morphology characteristics of both FtsZ families, but turnover properties highly similar to those of FtsZ2 and FtsZA. Taken together, our data suggest that the distinct properties previously described for Arabidopsis FtsZ1 and FtsZ2 extend to FtsZs from both green

and red photosynthetic lineages and support the theory that FtsZ2 and FtsZA are the direct homologs of cyanobacterial FtsZ.

Introduction

FtsZ is a cytoskeletal GTPase that self-assembles into a ring-like structure that is responsible for driving cytokinesis in bacteria and chloroplast division in photosynthetic eukaryotes (Adams and Errington, 2009; Erickson et al., 2010; Mingorance et al., 2010; Osteryoung and Pyke, 2014). In bacteria, a single FtsZ protein assembles at the midcell to form the FtsZ ring (Z ring), which is attached to the cytoplasmic membrane via interaction with peripheral and integral membrane proteins (Addinall and Lutkenhaus, 1996; Bi and Lutkenhaus, 1991; Liu et al., 1999). Once assembled, the Z ring acts as a scaffold for the recruitment of additional downstream division-related proteins to the midcell before constriction occurs (Adams and Errington, 2009).

When assembled *in vitro*, purified *E. coli* FtsZ normally assembles single-stranded protofilaments, but also assembles into helices, sheets, and large bundles depending on assembly conditions (Adams and Errington, 2009; Erickson et al., 2010). FtsZ assembly stimulates its GTPase activity, which destabilizes the subunit interface and induces filament fragmentation and eventually polymer turnover (Huecas et al., 2007). Once assembled, FtsZ filaments alone are able to exert contractile force on membranes, which may be a result of a hinge-opening mechanism induced by GTP hydrolysis and a fixed direction of curvature (Li et al., 2013; Osawa et al., 2008; Osawa et al., 2009). GTPase activity is correlated with both rates of polymer turnover and protofilament length and extent of bundling (Chen et al., 2007; Chen and Erickson, 2009; Mukherjee and Lutkenhaus, 1998; Srinivasan et al., 2008). Additionally, it has been shown that GTPase activity is critical for sustaining Z-ring constriction, as *E. coli*

FtsZ assembled with a non-hydrolysable GTP analog formed Z rings on tubular liposomes that began to constrict but the process is quickly halted (Osawa and Erickson, 2011).

In contrast to bacteria, the division of chloroplasts in plants and green algae requires the cooperation of two FtsZ families, FtsZ1 and FtsZ2 (Osteryoung et al., 1998; Osteryoung and Vierling, 1995). FtsZ1 and FtsZ2 are highly conserved across all plants and green algae with sequenced genomes. Additionally, two FtsZ families, FtsZA and FtsZB, are highly conserved among red algae (Miyagishima and Kabeya, 2010; TerBush et al., 2013). FtsZ2 and FtsZA are believed to be more ancestral, as they have retained a C-terminal peptide, also present in bacterial FtsZs, that has been shown to anchor plant Z rings to the inner chloroplast membrane via interaction with the trans-membrane protein ARC6 (Maple et al., 2005; TerBush et al., 2013; Vaughan et al., 2004; Vitha et al., 2003). Therefore, both FtsZ2 and FtsZA likely evolved from a single FtsZ in the cyanobacterial ancestor of modern day chloroplasts, while FtsZ1 and FtsZB are thought to have evolved by duplication of the more ancestral FtsZ2 in the green lineage and FtsZA in the red lineage, respectively (Miyagishima et al., 2004). FtsZ1 and FtsZ2 are nuclear-encoded and translocated into the chloroplast stroma via an N-terminal transit peptide, which is subsequently cleaved, where they coassemble into the mid-plastid Z ring (El-Kafafi et al., 2005; McAndrew et al., 2001; Vitha et al., 2001). Both FtsZ1 and FtsZ2 are critical for chloroplast division, as mutant plants lacking either FtsZ show severe defects in chloroplast morphology, indicated by larger and fewer chloroplasts per cell (Osteryoung et al., 1998). Other genetic evidence has shown that

FtsZ1 and FtsZ2 from Arabidopsis are incapable of rescuing the other's *null* mutant phenotype, indicating that they are not functionally redundant and possess distinct functions (Schmitz et al., 2009).

In vitro, FtsZ1 and FtsZ2 assemble homopolymers and coassemble into thick bundles (El-Kafafi et al., 2005; Lohse et al., 2006; Olson et al., 2010; Smith et al., 2010). FtsZ1 and FtsZ2 both possess GTPase activity, with FtsZ1 activity being slightly greater than that of FtsZ2 (Olson et al., 2010; Smith et al., 2010). Recently, we expressed FtsZ1 and FtsZ2 fluorescent fusion proteins in the fission yeast *Schizosaccharomyces pombe* to analyze their inherent assembly properties in a model cellular environment (TerBush and Osteryoung, 2012). We found that FtsZ1 and FtsZ2 have distinct filament morphology and dynamic properties. FtsZ1 filaments are more dynamic, with greater rates and extents of subunit exchange (turnover), and are able to increase the turnover of FtsZ2 in presumed heteropolymers, suggesting that FtsZ1 facilitates Z-ring remodeling. FtsZ2 determines the morphology of coassembled filaments, suggesting that FtsZ2 has structural dominance over FtsZ1 in mixed heteropolymers and therefore is the structural determinant of Z rings. Recent *in vivo* analysis of FtsZ1 and FtsZ2 turnover in live chloroplast Z rings found that FtsZ1 has greater dynamic properties than FtsZ2 (Johnson et al., 2015b), indicating that results in *S. pombe* accurately reflect behavioral trends *in vivo*.

Until now, the vast majority of functional work on eukaryotic FtsZs has been performed on those from Arabidopsis. Due to the high conservation of two FtsZ families across both the green and red photosynthetic lineages, it is of great interest to study the

properties of FtsZs from different species to better understand the functional significance of the FtsZ duplication events and whether both families of FtsZ possess conserved features across a broad evolutionary distance. Therefore, in this study, we continue to utilize *S. pombe* to investigate the assembly and dynamic properties of FtsZ proteins from species representing dicot and monocot plants, green algae, red algae, and cyanobacteria. We show that distinct assembly and dynamic properties for the FtsZ1 and FtsZ2 families are maintained across all species analyzed, including structural dominance of FtsZ2 and the higher turnover characteristics of FtsZ1. Additionally, we show that cyanobacterial FtsZ behavior is consistent with that of the eukaryotic FtsZ2 proteins, giving support to the theory that FtsZ2 is more ancestral and FtsZ1 arose from gene duplication and then diverged in functional properties.

Results

Conservation of distinct filament morphologies across the evolutionary lineages

In our previous publication (TerBush and Osteryoung, 2012), we expressed FtsZ1 and FtsZ2 from Arabidopsis as fluorescent fusions to eYFP and eCFP, respectively. However, these fluorescent fusion proteins have a tendency to dimerize at high concentrations (Zacharias et al., 2002), potentially skewing the results away from the true inherent characteristics of FtsZ proteins. Therefore, in this study we express FtsZ1 and FtsZ2 representatives as C-terminal fusions to a monomeric variant of the yellow fluorescent protein Venus (mVenus) and to the monomeric cyan fluorescent protein mCerulean, respectively. Both mVenus and mCerulean harbor the A206K mutation, which has been shown to eliminate the dimerization potential of GFP-derived fluorescent proteins (Zacharias et al., 2002), which should eliminate the possibility that fluorescent protein-induced dimerization might affect the analyzed properties of FtsZs in *S. pombe*.

To begin our analysis, we expressed each FtsZ1 and FtsZ2 protein separately in *S. pombe* to analyze their intrinsic filament morphologies (Fig. 3.1). *Arabidopsis thaliana* FtsZ1 (AtFtsZ1), representing dicot plants, assembled into long filaments that followed the interior contours of the cell and annealed end-to-end to form large rings that split into thinner filaments with a less intense fluorescence signal (Fig. 3.1 A), as seen previously when AtFtsZ1-eYFP was expressed in *S. pombe* (TerBush and Osteryoung, 2012). FtsZ1 from the monocot plant *Oryza sativa* (OsFtsZ1), or rice, assembled into long cables that possessed flared ends (Fig. 3.1 B) and did not anneal into large rings to

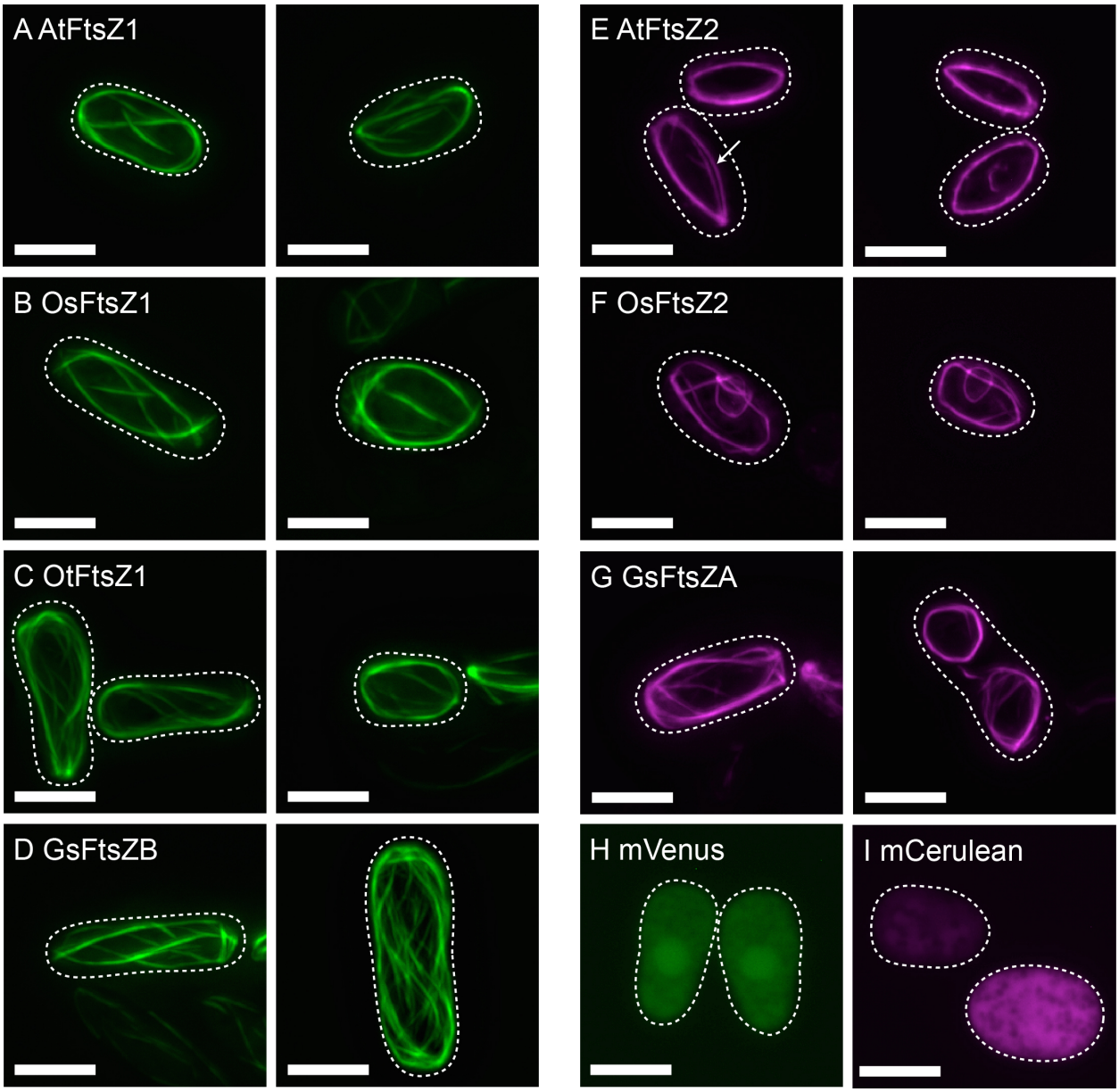

Figure 3.1: Distinct FtsZ1 and FtsZ2 filament morphologies are conserved across FtsZs from various plants and algae. Epifluorescence micrographs of *S. pombe* cells expressing (A) AtFtsZ1-mVenus, (B) OsFtsZ1-mVenus, (C) OtFtsZ1-mVenus, (D) GsFtsZB-mVenus, (E) AtFtsZ2-mCerulean, (F) OsFtsZ2-mCerulean, (G) OtFtsZ2-mCerulean, (H) GsFtsZA-mCerulean, (I) mVenus, and (J) mCerulean. AtFtsZ1-mVenus, OsFtsZ1-mVenus, OtFtsZ1-mVenus, GsFtsZB-mVenus, and mVenus fluorescence

Figure 3.1 (cont'd): signals are falsely colored green. AtFtsZ2-mCerulean, OsFtsZ2-mCerulean, OtFtsZ2-mCerulean, GsFtsZA-mCerulean, and mCerulean fluorescence signals are falsely colored magenta. Dashed lines represent the cell outlines. Bars, 5 μm.

the same degree as AtFtsZ1. FtsZ1 from *Ostreococcus tauri* (OtFtsZ1), a green alga, assembled into long filaments that annealed to rings and laterally associated into bundles that commonly split and frayed into loosely associated filaments (Fig. 3.1 C). FtsZB from *Galdieria sulphuraria* (GsFtsZB), a red alga, also assembled into long filaments and loosely associated bundled structures (Fig. 3.1 D) similar to those of OtFtsZ1. However, due to lower sequence similarity and poor transit peptide prediction tools, GsFtsZB and GsFtsZA, described below, expressed here were constructed without the N-terminal region.

AtFtsZ2 assembled into large ring-shaped structures with smaller filaments breaking from the main ring (Fig. 3.1 E, arrow left panel). This is in contrast to the elaborate networks assembled by AtFtsZ2-eCFP (TerBush and Osteryoung, 2012), which is likely due to the fusion to monomeric mCerulean used here. OsFtsZ2 assembled into large rings with cross-linking filaments protruding from the main ring structures, and into rings roughly 2 μm in diameter (Fig. 3.1 F). OtFtsZ2 expressed in *S. pombe* failed to assemble any filamentous structures. Instead it adopted either a diffuse localization pattern or seemed to aggregate into spot-like structures whether expressed alone or coexpressed with OtFtsZ1 (Fig. 3.2 A & B). Western blot analysis with a

monoclonal antibody recognizing GFP derivatives showed single bands for OtFtsZ1-mVenus and OtFtsZ2-mCerulean at their predicted molecular masses (Fig. 3.2 C),

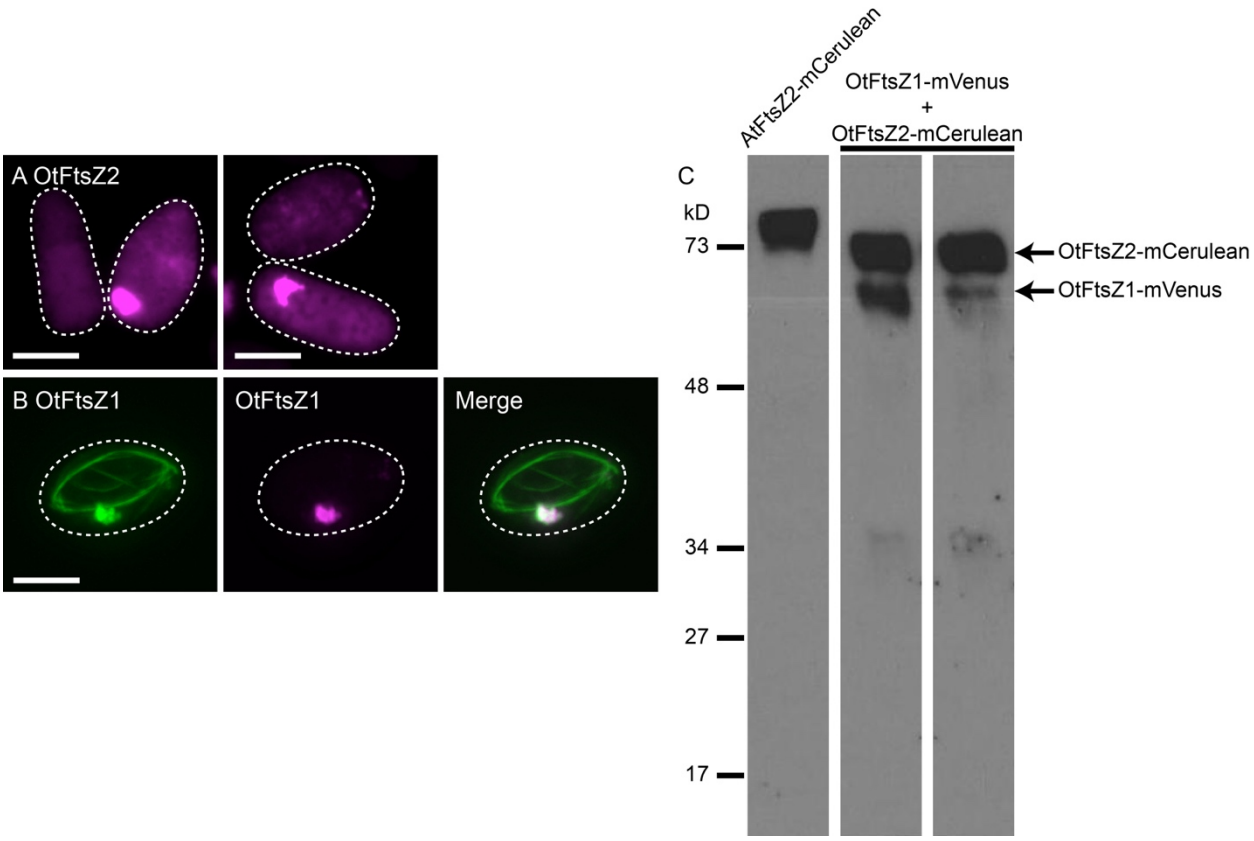

Figure 3.2: Expression of *Ostreococcus tauri* FtsZ2 in *S. pombe*. (A-B) Epifluorescence micrographs of *S. pombe* cells expressing (A) OtFtsZ2-mCerulean or (B) OtFtsZ1-mVenus coexpressed with OtFtsZ2-mCerulean. OtFtsZ1-mVenus and OtFtsZ2-mCerulean were falsely colored green and magenta, respectively. The white color in the merged image indicates regions where the fluorescence signals colocalize. Dashed lines represent the cell outline. Bars, 5 μm. (C) Immunoblot analysis of soluble bulk culture extracts to determine the molecular masses of AtFtsZ2-mCerulean singly expressed (left) and OtFtsZ1-mVenus and OtFtsZ2-mCerulean coexpressed (middle and right) in *S. pombe*. Each lane represents an independently grown culture. The blot

Figure 3.2 (cont'd): was probed with a monoclonal αGFP. The bands representing OtFtsZ1-mVenus (~65 kD, bottom arrow) and OtFtsZ2-mCerulean (~69 kD, top arrow) ran slightly lower on the blot than that of AtFtsZ2-mCerulean (~72 kD, positive control). Approximate molecular masses in kD are shown to the left.

indicating the fluorescence signals represent full-length OtFtsZ2-mCerulean. The OtFtsZ2 morphology is radically different from that of any FtsZ that has been previously visualized *in vivo* (Fu et al., 2010; Kiessling et al., 2004; Li et al., 2007; Mingorance et al., 2005; Miyagishima et al., 2012; Strauss et al., 2012; Vitha et al., 2001) or in *S. pombe* (Srinivasan et al., 2007; Srinivasan et al., 2008; TerBush and Osteryoung, 2012). Therefore, we will not pursue OtFtsZ2 in further analysis, due to the unknown cause of its peculiar assembly characteristics. Finally, GsFtsZA assembled into large rings with filament splitting and cross-linking (Fig. 3.1 G). In control experiments, unfused mVenus and mCerulean adopted completely diffuse localization patterns (Fig. 3.1 H-I). Taken together, the single expression data indicate that, while there are slight differences in morphology from one species to the next, the distinct long cables for FtsZ1/FtsZB and rings of FtsZ2/FtsZA are well conserved from plants to green, and red algae.

Colocalization of FtsZ pairs

FtsZ pairs invariably colocalize to mid-plastid Z rings in wild type plants and to abnormal filaments in various chloroplast division mutants (McAndrew et al., 2001; Vitha et al., 2001). Additionally, FtsZ1 and FtsZ2 from Arabidopsis coassembled into bundled

heteropolymers *in vitro* and colocalized when previously coexpressed as FtsZ1-eYFP and FtsZ2-eCFP fusions in *S. pombe* (Olson et al., 2010; TerBush and Osteryoung, 2012). To assess if this behavior is consistent with Arabidopsis FtsZ1-mVenus and FtsZ2-mCerulean, and conserved among the additional FtsZ pairs being analyzed here, we coexpressed each FtsZ pair in *S. pombe* to analyze their coassembled filament morphology characteristics and degree of colocalization.

When coexpressed, AtFtsZ1 and AtFtsZ2 coassembled into ring structures that had cross-linking filaments and regions where the ring split into smaller filaments (Fig. 3.3 A). We used the Pearson's correlation coefficient to quantify the degree of fluorescence signal overlap and how well the signal intensities were correlated (Bolte and Cordelières, 2006). AtFtsZ1 and AtFtsZ2 displayed a high PCC of 0.92 ± 0.01 (mean ± SEM, n = 23), which indicates that the fluorescence signals were extensively colocalized and that the signal intensities were directly correlated to each other. Similarly, OsFtsZ1 and OsFtsZ2 also colocalized to large and small rings that were highly similar to those assembled when OsFtsZ2 was expressed alone (Fig. 3.3 B). OsFtsZ1 and OsFtsZ2 also displayed a very high PCC value of 0.92 ± 0.01 (n = 9). In contrast, GsFtsZA and GsFtsZB colocalized to large loosely bundled rings (Fig. 3.3 C, arrow) and a network of interconnected filaments. The overall morphology of the colocalized filaments resembled a hybrid of between GsFtsZA and GsFtsZB expressed alone (Fig. 3.1 D & G). However, consistent with the other FtsZ pairs, GsFtsZA and GsFtsZB displayed a very high PCC value of 0.91 ± 0.01 (n = 17).

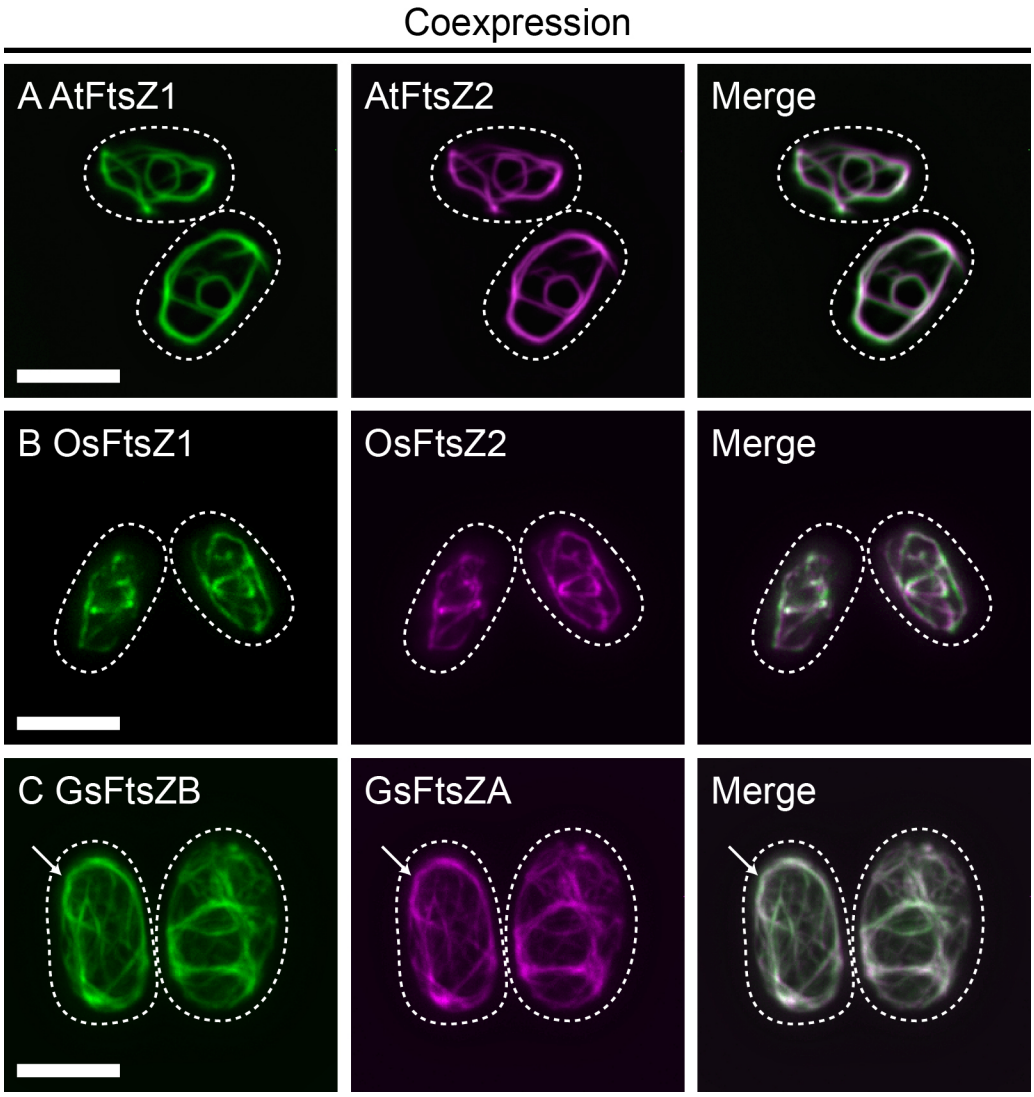

Figure 3.3: FtsZ1 and FtsZ2 proteins from plants colocalize into FtsZ2-like rings while FtsZA and FtsZB coassemble into a hybrid filament network. Epifluorescence micrographs of *S. pombe* cells coexpressing (A) AtFtsZ1-mVenus and AtFtsZ2-mCerulean, (B) OsFtsZ1-mVenus and OsFtsZ2-mCerulean, and (C) GsFtsZB-mVenus and GsFtsZA-mCerulean. AtFtsZ1-mVenus, OsFtsZ1-mVenus, and GsFtsZB-mVenus were falsely colored green. AtFtsZ2-mCerulean, OsFtsZ2-mCerulean, and GsFtsZA-mCerulean were falsely colored magenta. The white color in merged images indicates

Figure 3.3 (cont'd): regions where the fluorescence signals colocalize. Dashed lines represent the cell outline. Bars, 5 μm.

Our coexpression data indicate that, at least in plant FtsZ pairs, FtsZ2 maintains structural dominance over FtsZ1 when these proteins coassemble into presumed heteropolymers. The data also suggest that the FtsZ2 structural dominance may be lost in red algal FtsZA. However, due to the lack of the N-terminal region in the GsFtsZ constructs analyzed here, the possibility remains that this region is required for GsFtsZA to exhibit structural dominance over GsFtsZB.

Conservation of distinct FtsZ1 and FtsZ2 polymer turnover characteristics

We also analyzed the subunit exchange properties of FtsZ filaments using fluorescence recovery after photobleaching (FRAP) experiments. When expressed individually, all FtsZ proteins displayed fluorescence recovery back into the bleached region (Fig. 3.4). AtFtsZ1 recovered with a half-time, the time it takes for the fluorescence signal to recover to one half of its total recovery ($t_{1/2}$), of 51 s and to 53% of the pre-bleach prebleach intensity (n = 16, Fig. 3.4 A). OsFtsZ1 fluorescence signal recovered with a $t_{1/2}$ of 74 s and to 45% of the pre-bleach intensity (n = 13, Fig. 3.4 B). OtFtsZ1 recovered with a $t_{1/2}$ of 101 s and to a maximum recovery of 45% (n = 16, Fig. 3.4 C). GsFtsZB recovered with a $t_{1/2}$ of 54 s and to a maximum recovery of 61% (n = 14, Fig. 3.4 D). AtFtsZ2 filaments displayed much less turnover than those composed of AtFtsZ1 with a $t_{1/2}$ of 67 s and to 13% of the pre-bleach intensity (n = 16, Fig. 3.4 E). OsFtsZ2 filaments recovered with a $t_{1/2}$ of 95 s and with a total recovery of 35 % (n = 12,

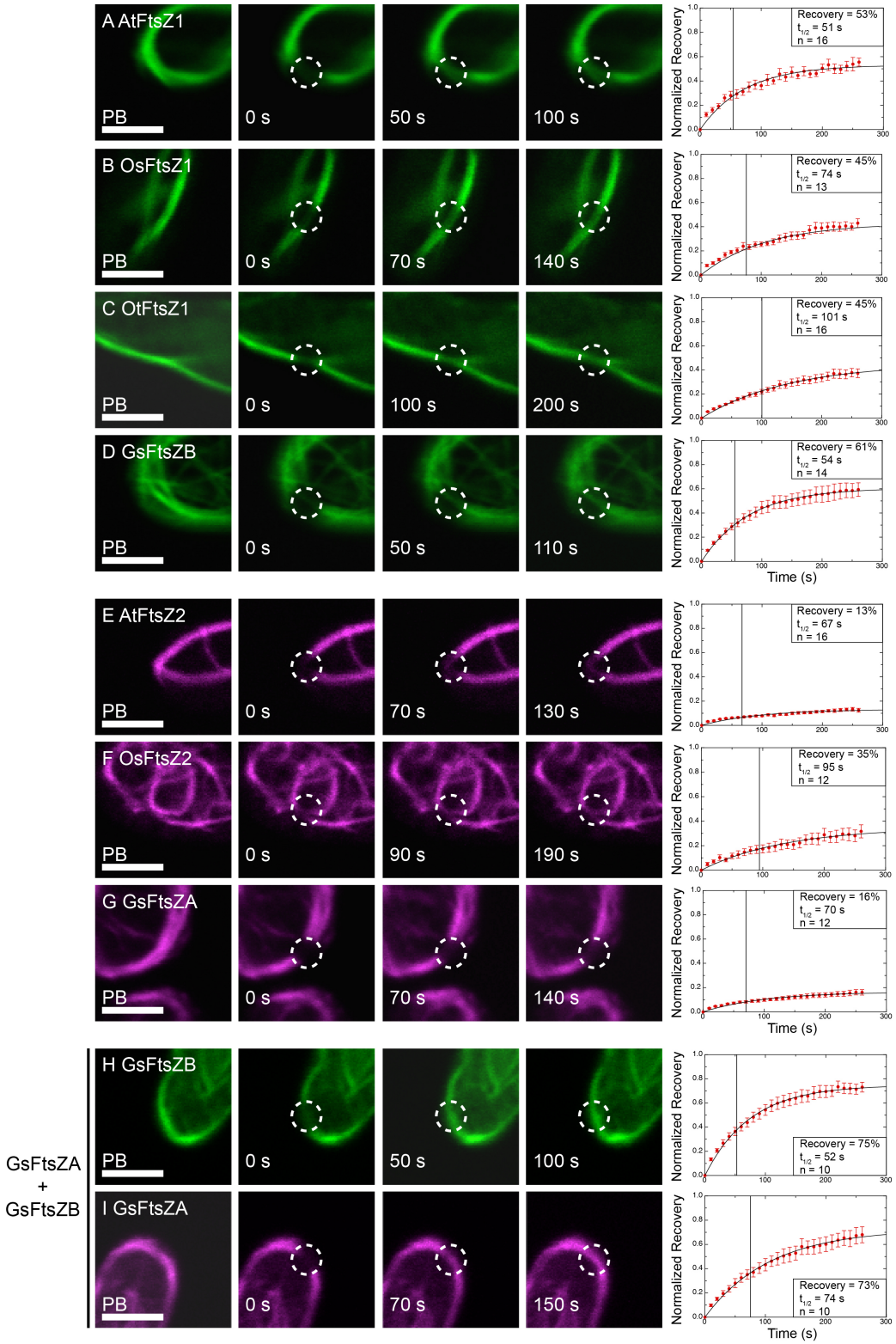

Figure 3.4: Greater polymer turnover dynamics in FtsZ1 are conserved across the green and red photosynthetic lineages. Cells expressing (A) AtFtsZ1-mVenus, (B)

Figure 3.4 (cont'd): OsFtsZ1-mVenus, (C) OtFtsZ1-mVenus, (D) GsFtsZB-mVenus, (E) AtFtsZ2-mCerulean, (F) OsFtsZ2-mCerulean, (G) GsFtsZA-mCerulean, and (H) GsFtsZB coexpressed with (I) GsFtsZA were analyzed by FRAP. From left to right, images represent fluorescence signal at the location of photobleaching (dashed circle) prior to bleaching (PB), at the time of bleaching (0 s), the time closest to the $t_{1/2}$, and the time closest to twice that of $t_{1/2}$. The average fluorescence recovery vs time plots are show at right. Data in each graph were normalized to the PB fluorescence signal (1 on the y-axis) and the fluorescence signal at the time of photobleaching (0 on the y-axis). Data shown in the boxes show the calculated $t_{1/2}$ (also indicated by the vertical black bar in the graph), maximum extent of recovery, and the number of independent FRAP experiments performed for each expression strain. The red brackets represent SEM at each time point. AtFtsZ1-mVenus, OsFtsZ1-mVenus, OtFtsZ1-mVenus, and GsFtsZB-mVenus fluorescence signals are falsely colored green. AtFtsZ2-mCerulean, OsFtsZ2-mCerulean, and GsFtsZA-mCerulean fluorescence signals are falsely colored magenta. Bars, 2 µm.

Fig. 3.4 F). GsFtsZA recovered with a $t_{1/2}$ of 70 s and a total extent of recovery of 16% (n = 12, Fig. 3.4 G).

We also performed FRAP experiments on coassembled GsFtsZs to assess if GsFtsZB was able enhance the turnover of GsFtsZA, as previously shown for AtFtsZ1 and AtFtsZ2 (TerBush and Osteryoung, 2012). GsFtsZB recovered with a $t_{1/2}$ of 52 s and to 75% of the pre-bleach intensity (n = 10, Fig. 3.4 H). Similarly, GsFtsZA recovered

with a $t_{1/2}$ of 74 s and to 73% of the pre-bleach intensity (n = 10, Fig. 3.4 I). In this coexpression strain, the rates of GsFtsZA and GsFtsZB turnover were similar to those in the single-expression strains. More importantly, the maximum extent of fluorescence recovery for GsFtsZA was greatly increased in the presence of GsFtsZB, similar to the effect of AtFtsZ1 on AtFtsZ2 (TerBush and Osteryoung, 2012). When coexpressed, OsFtsZ1 and OsFtsZ2 showed reduced expression in terms of the number of cells with visible coassembled filaments and fluorescence intensity, potentially due to codon usage in the rice FtsZ proteins not being optimal for expression in *S. pombe* (Fig. 3.3 B). Therefore, this coexpression strain was omitted from FRAP experiments due to these technical challenges and lack of confidence in the filament turnover data.

Overall, the FtsZ dynamics data indicate that both faster rates and greater extents of total recovery observed for Arabidopsis FtsZ1 than FtsZ2 filaments are conserved traits across both the green and red photosynthetic lineages (Fig. 3.5). Additionally, the ability of GsFtsZB to enhance the turnover of GsFtsZA in coassembled filaments shows that this is a trait also conserved across both the green and red photosynthetic lineages. All FRAP data are summarized in Table 3.1.

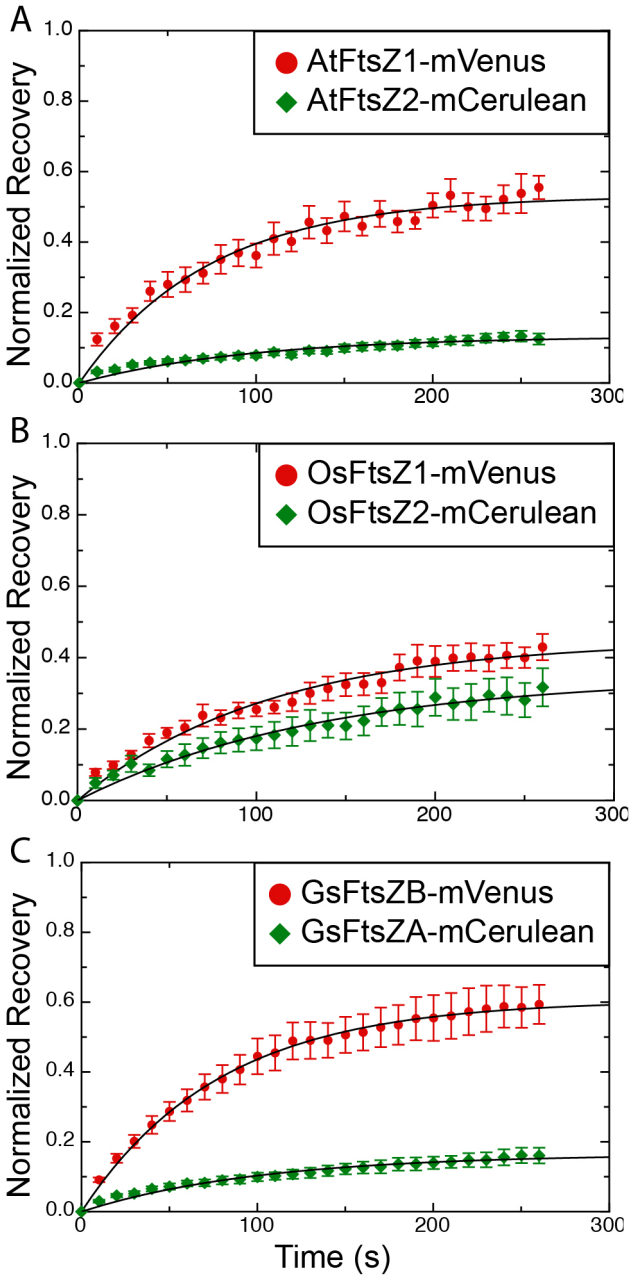

Figure 3.5: FtsZ1 and FtsZB homopolymers are more dynamic than FtsZ2 and FtsZA homopolymers. The average fluorescence recovery vs time plots comparing the normalized recovery of (A) AtFtsZ1-mVenus and AtFtsZ2-mCerulean, (B) OsFtsZ1-mVenus and OsFtsZ2-mCerulean, and (C) GsFtsZA-mCerulean and GsFtsZB-mVenus. Data in each graph were normalized to the PB fluorescence signal (1 on the y-axis) and

Figure 3.5 (cont'd): the fluorescence signal at the time of photobleaching (0 on the y-axis). AtFtsZ1-mVenus, OsFtsZ1-mVenus, and GsFtsZB-mVenus data are represented by red circles. AtFtsZ2-mCerulean, OsFtsZ2-mCerulean, and GsFtsZA-mCerulean data are represented by green diamonds. The brackets in the datasets represent the standard error of the mean (SEM) for the normalized recovery at every time-point.

Protein	$t_{1/2}$ (s)	% Recovery	n
AtFtsZ1-mVenus	51	53%	16
OsFtsZ1-mVenus	74	45%	13
$OsFtsZ1_{D249A}$-mVenus	101	21%	13
OtFtsZ1-mVenus	101	45%	16
$OtFtsZ1_{D224A}$-mVenus	61	20%	14
GsFtsZB-mVenus	54	61%	14
$GsFtsZB_{D300A}$-mVenus	87	35%	13
AtFtsZ2-mCerulean	67	13%	16
OsFtsZ2-mCerulean	95	35%	12
$OsFtsZ2_{D300A}$-mCerulean	372	30%	11
GsFtsZA-mCerulean	70	16%	12
$GsFtsZA_{D322A}$-mCerulean	51	10%	11
SeFtsZ-msfGFP	113	29%	14
$SeFtsZ_{D239A}$-msfGFP	46	8%	15
GsFtsZB-mVenus + GsFtsZA-mCerulean	52	75%	10
	74	73	10

Table 3.1: FRAP data for all single and coexpression strains. Time for the normalized and averaged half-time of recovery ($t_{1/2}$, s) and maximum percent recovery for each protein in each expression strain. n represents the number of independent FRAP experiments performed on each protein in each expression strain.

Effect of GTPase activity on FtsZ filament morphology and turnover

To further test the importance of GTPase activity for FtsZ filament morphology and turnover, we expressed mutant forms of each FtsZ from *O. sativa*, *O. tauri*, and *G. sulphuraria* in which the conserved T7 loop aspartate required for GTPase activity, but not GTP binding (Oliva et al., 2004; Scheffers et al., 2001) was changed to alanine. Mutation of this critical residue reduces GTPase activity of Arabidopsis and *E. coli* FtsZs to less than 10% and ~1% of their WT activities, respectively (Olson et al., 2010; Redick et al., 2005). Consistent with our previous findings for AtFtsZ1 and AtFtsZ2 (TerBush and Osteryoung, 2012), all putative GTPase-deficient FtsZs assembled into filamentous structures when expressed in *S. pombe* (Fig. 3.6). OsFtsZ1$_{D249A}$ assembled into a single long filament that curved around the interior contours of the cell or multiple straight filaments that were loosely associated (Fig. 3.6 A). Similarly, OtFtsZ1$_{D224A}$ assembled multiple straight filaments that did not bend around the contours of the cell interior (Fig.3.5 B). GsFtsZB$_{D300A}$ assembled straight or curved filaments that did not loop around the cell interior and were commonly loosely associated filaments (Fig. 3.6 C), similar to those of OsFtsZ1$_{D224A}$. OsFtsZ2$_{D300A}$ assembled filaments and rings with regions of variable thicknesses and spot-like structures (Fig. 3.6 D), while GsFtsZA$_{D322A}$ assembled large rings with regions of variable thickness, but were more frequently split and frayed into smaller filaments with less fluorescence intensity (Fig. 3.6 E).

We also performed FRAP experiments to further assess how GTPase activity affects the filament turnover characteristics of the FtsZs studied here. OsFtsZ1$_{D249A}$ recovered with a $t_{1/2}$ of 101 s and a total extent of recovery of 21% (Fig. 3.7 A, n = 13). OtFtsZ1$_{D224A}$ had a $t_{1/2}$ of 61 s and recovered to 20% of the pre-bleach fluorescence

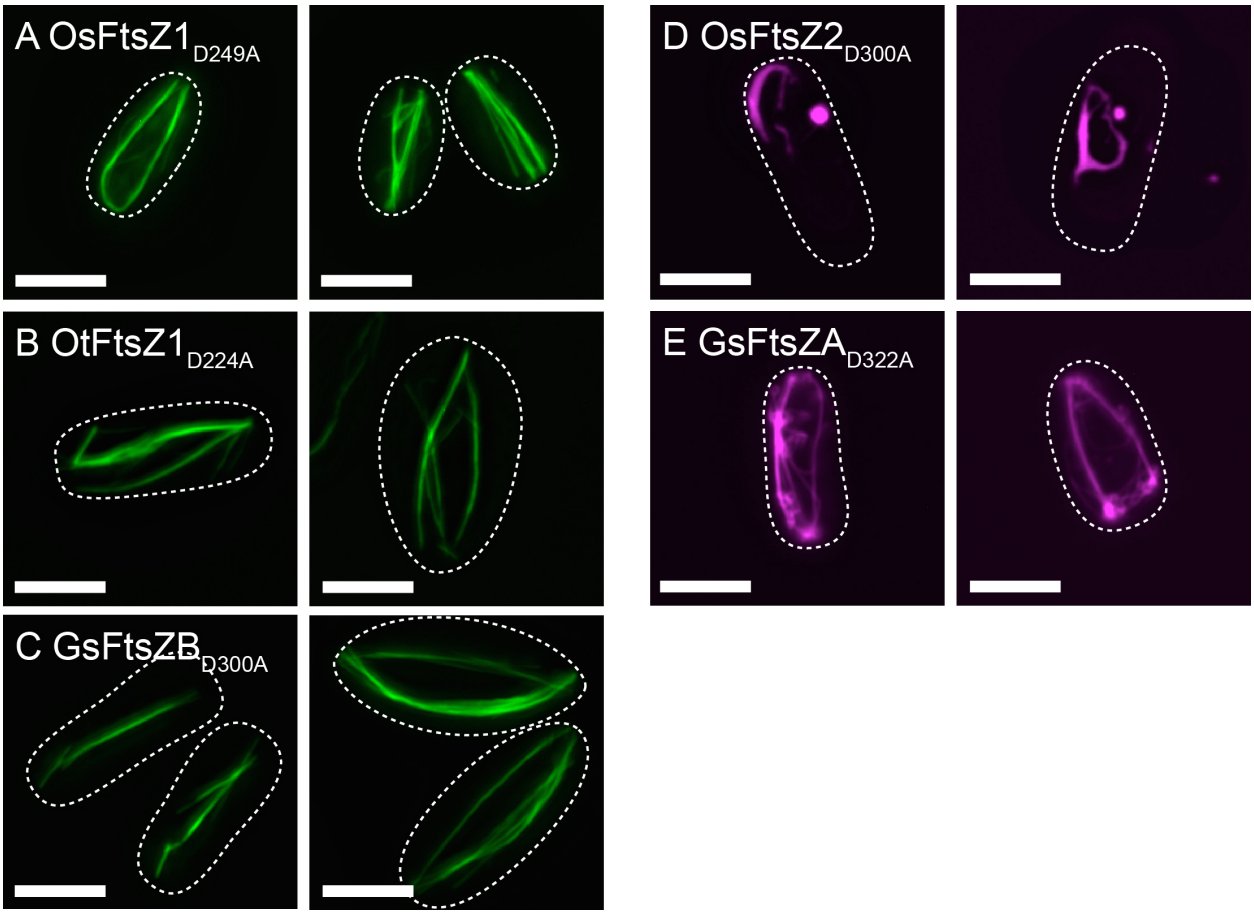

Figure 3.6: Putative GTPase-deficient mutants display altered filament morphologies. Epifluorescence micrographs of *S. pombe* cells expressing (A) OsFtsZ1(D249A)-mVenus, (B) $OtFtsZ1_{D224A}$-mVenus, (C) $GsFtsZB_{D300A}$-mVenus, (D) $OsFtsZ2_{D300A}$-mCerulean, and (E) $GsFtsZA_{D322A}$-mCerulean. $OsFtsZ1_{D249A}$-mVenus, $OtFtsZ1_{D224A}$-mVenus, and $GsFtsZB_{D300A}$-mVenus fluorescence signals are falsely colored green. $OsFtsZ2_{D300A}$-mCerulean and $GsFtsZA_{D322A}$-mCerulean fluorescence signals are falsely colored magenta. Dashed lines represent the cell outlines. Bars, 5 µm.

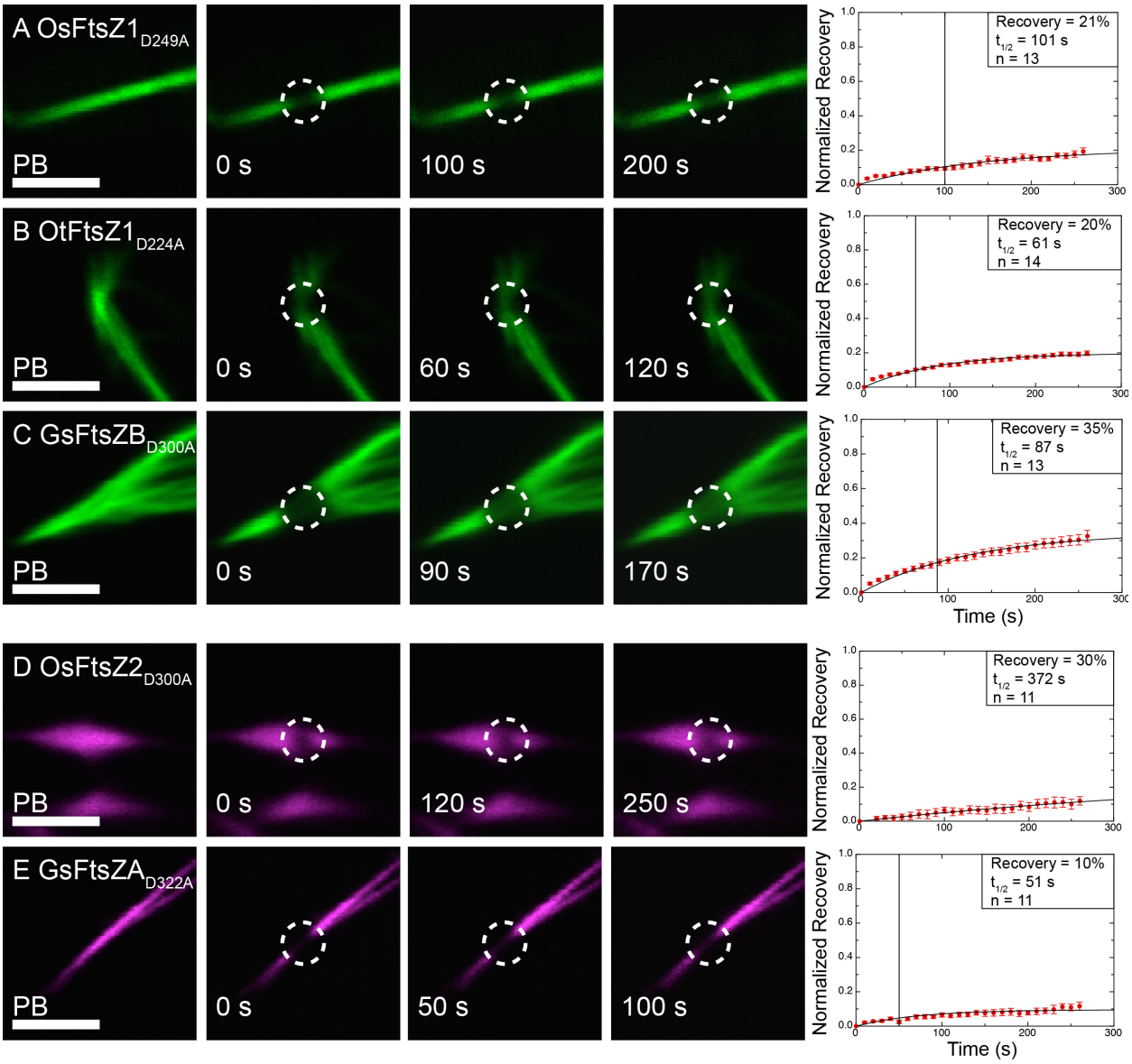

Figure 3.7: Putative FtsZ1 GTPase-deficient mutants show reduced, yet not abolished, polymer turnover, while putative FtsZ2 GTPase-deficient mutants lack polymer turnover. Cells expressing (A) OsFtsZ1$_{D249A}$-mVenus, (B) OtFtsZ1$_{D224A}$-mVenus, (C) GsFtsZB$_{D300A}$-mVenus, (D) OsFtsZ2$_{D300A}$-mCerulean, and (E) GsFtsZA$_{D322A}$-mCerulean were analyzed by FRAP. From left to right, images represent fluorescence signal at the location of photobleaching (dashed circle) prior to bleaching

Figure 3.7 (cont'd): (PB), at the time of bleaching (0 s), the time closest to the $t_{1/2}$, and the time closest to twice that of $t_{1/2}$. The average fluorescence recovery vs time plots are show at right. Data in each graph were normalized to the PB fluorescence signal (1 on the y-axis) and the fluorescence signal at the time of photobleaching (0 on the y-axis). Data shown in the boxes show the calculated $t_{1/2}$ (also indicated by the vertical black bar in the graph), maximum extent of recovery, and the number of independent FRAP experiments performed for each expression strain. The red brackets represent SEM at each time point. OsFtsZ1$_{D249A}$-mVenus, OtFtsZ1$_{D224A}$-mVenus, and GsFtsZB$_{D300A}$-mVenus fluorescence signals are falsely colored green. OsFtsZ2$_{D300A}$-mCerulean and GsFtsZA$_{D322A}$-mCerulean fluorescence signals are falsely colored magenta. Bars, 2 µm.

intensity (Fig. 3.7 B, n = 14). GsFtsZB$_{D300A}$ recovered with a $t_{1/2}$ of 87 s and to a maximum extent of 35% (Fig. 3.7 C, n = 13). OsFtsZ2$_{D300A}$ filaments had severely reduced turnover with a $t_{1/2}$ of 372 s and a maximum recovery of 30% (Fig. 3.7 D, n = 11). Likewise, GsFtsZA$_{D300A}$ recovered with a $t_{1/2}$ of 51 s and to 10% (Fig. 3.7 E, n = 11).

Taken together, these filament morphology and turnover experiments on putative GTPase-deficient FtsZs show that GTPase activity is important for normal FtsZ assembly and turnover across various photosynthetic eukaryote lineages. More importantly, these data show that, consistent with our previous results for Arabidopsis FtsZ1 and FtsZ2 (TerBush and Osteryoung, 2012), GTPase activity is critical for promoting filament turnover for FtsZ2s from diverse photosynthetic eukaryotes, but not solely responsible for turnover of FtsZ1/FtsZB filaments.

Analysis of cyanobacterial FtsZ filament morphology and turnover

To assess the inherent assembly and dynamic properties of cyanobacterial FtsZ, we expressed the single FtsZ from *Synechococcus elongatus* PCC 7942 (SeFtsZ) in *S. pombe* as a fluorescent fusion to monomeric superfolder GFP (msfGFP) (Costantini et al., 2012) and analyzed its filament morphology and turnover characteristics. SeFtsZ readily assembled into filaments in the *S. pombe* cytosol (Fig. 3.8 A). It commonly

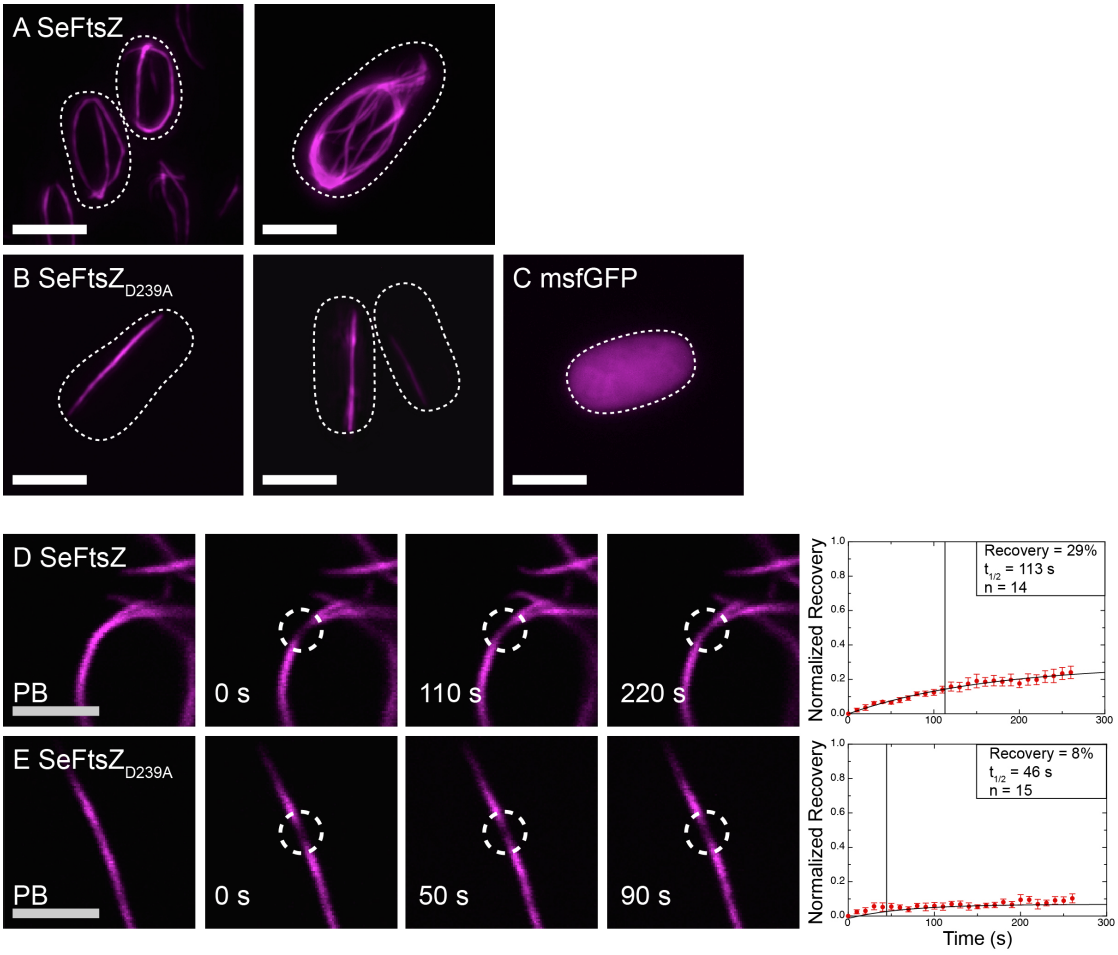

Figure 3.8: Cyanobacterial FtsZ filament morphology shows characteristics of FtsZ1 and FtsZ2 families, but polymer turnover is similar to that of FtsZ2 and FtsZA. (A-C) Epifluorescence micrographs of *S. pombe* cells expressing (A) SeFtsZ-

Figure 3.8 (cont'd): msfGFP, (B) SeFtsZ(D239A)-msfGFP, or (C) msfGFP. Dashed lines represent the cell outlines. (D-E) Cells expressing (D) SeFtsZ-msfGFP or (E) SeFtsZ(D239A)-msfGFP were analyzed by FRAP. From left to right, images represent fluorescence signal at the location of photobleaching (dashed circle) prior to bleaching (PB), at the time of bleaching (0 s), the time closest to the $t_{1/2}$, and the time closest to twice that of $t_{1/2}$. The average fluorescence recovery vs time plots are show at right. Data in each graph were normalized to the PB fluorescence signal (1 on the y-axis) and the fluorescence signal at the time of photobleaching (0 on the y-axis). Data shown in the boxes show the calculated $t_{1/2}$ (also indicated by the vertical black bar in the graph), maximum extent of recovery, and the number of independent FRAP experiments performed for each expression strain. The red brackets represent SEM at each time point. SeFtsZ-msfGFP, SeFtsZ(D239A)-msfGFP, and msfGFP fluorescence signals are falsely colored magenta. White bars, 5 μm. Grey bars, 2 μm.

formed long cables that looped around the cell (Fig. 3.8 A, left panel) and also large rings that split into loosely associated filaments (Fig. 3.8 A, right panel). We also expressed SeFtsZ as a putative GTPase-deficient mutant bearing the aspartate-to-alanine mutation in the conserved T7 loop ($SeFtsZ_{D239A}$) to assess how GTPase activity affects SeFtsZ assembly characteristics. $SeFtsZ_{D239A}$ assembled straight filaments that commonly were the length of the cell, but did not curve around the ends (Fig. 3.8 B). In control experiments, msfGFP adopted a completely diffuse localization pattern (Fig. 3.8 C). FRAP experiments showed that SeFtsZ fluorescence recovered back into the bleached region with a $t_{1/2}$ of 113 s and to 29% of the pre-bleach fluorescence intensity

(Fig. 3.8 D, n = 14). In contrast, SeFtsZ$_{D239A}$ had nearly abolished filament dynamics with a $t_{1/2}$ of 46 s but only recovering to 8% of the pre-bleach fluorescence intensity (Fig. 3.8 E, n = 15). These filament morphology and turnover data show that SeFtsZ possesses filament morphology properties of both FtsZ1/FtsZB and FtsZ2/FtsZA, but its filament turnover properties are highly similar to those of FtsZ2/FtsZA. The overall greater consistency of SeFtsZ filament morphology and turnover properties with those of eukaryotic FtsZ2/FtsZA supports the theory that the FtsZ2 and FtsZA families evolved from the probable single FtsZ in the ancestor of chloroplasts and that the FtsZ1 and FtsZB families evolved later by gene duplication events, in their respective photosynthetic lineages, and followed by functional divergence.

Previous data have shown that reversible photobleaching can greatly influence fluorescence recovery kinetics of proteins fused to GFP variants For example ion channel proteins previously shown to be immobile displayed 65.9% fluorescence recovery with a time constant of 0.36 s when fused to eCFP (Sinnecker et al., 2005). Therefore, in control experiments, we photobleached the entire contents of cells expressing a representative for each fluorescence protein used (mVenus, mCerulean, and msfGFP) and recorded fluorescence intensity over time to assess for the spontaneous recovery of bleached fluorescence proteins. In all cases, there was no substantial fluorescence recovery in the cells (Fig. 3.9). Combined with the low fluorescence recovery and long $t_{1/2}$ values of FtsZ proteins fused to mCerulean, these data indicate that reversible photobleaching does not influence the FtsZ dynamics data in this study.

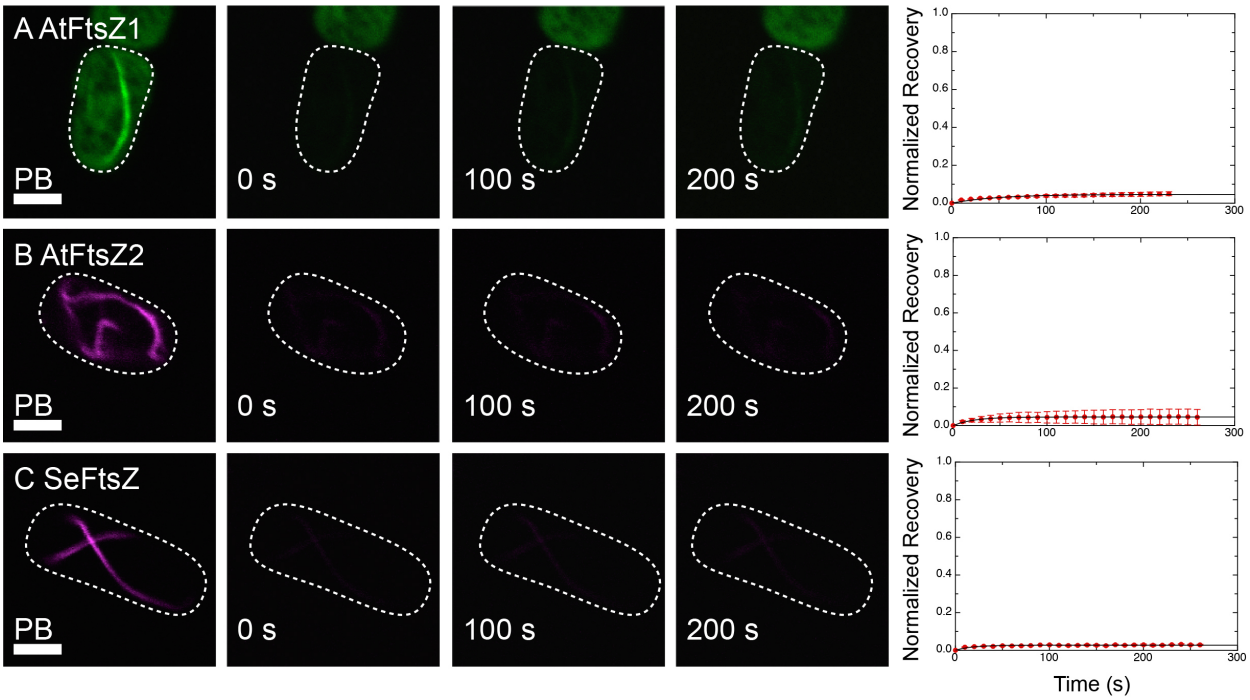

Figure 3.9: Photobleached FtsZ fusions do not spontaneously recover fluorescence. Cells expressing (A) AtFtsZ1-mVenus, (B) AtFtsZ2-mCerulean, and (C) SeFtsZ-msfGFP were analyzed by FRAP. At the photobleaching event, the entire content of the cells were bleached to assess if the fluorescence proteins could spontaneously recover their fluorescence intensity. From left to right, images represent fluorescence signal in the cell prior to bleaching (PB), at the time of bleaching (0 s), 100 s post-bleaching, and 200 s post-bleaching. The average fluorescence recovery vs time plots are show at right. Data in each graph were normalized to the PB fluorescence signal (1 on the y-axis) and the fluorescence signal at the time of photobleaching (0 on the y-axis). The recovery data were the average of 3 independent FRAP experiments for each expression strain (n = 3). The red brackets represent SEM at each time point.

Figure 3.9 (cont'd): AtFtsZ1-mVenus fluorescence signal is falsely colored green. AtFtsZ2-mCerulean and SeFtsZ-msfGFP fluorescence signals are falsely colored magenta. Bars, 2 μm.

Discussion

Studies analyzing the functional behavior of FtsZs from photosynthetic eukaryotes have begun to emerge (El-Kafafi et al., 2005; Johnson et al., 2015a; Johnson et al., 2015b; Olson et al., 2010; Smith et al., 2010; Smith et al., 2011; TerBush and Osteryoung, 2012). However, the vast majority of these data are for FtsZ1 and FtsZ2 from Arabidopsis, and there have been no studies to compare the behavior of FtsZ pairs from different photosynthetic organisms, especially between FtsZs from the green and red photosynthetic lineages. Performing such a comparative analysis *in vivo* would be highly challenging and time-consuming, as chloroplast division is highly sensitive to FtsZ expression level, FtsZ fluorescent fusions expressed from their native promoters produce low fluorescence signal amid high background chlorophyll autofluorescence in photosynthetic tissues, and transformation procedures for algal species are not well established. To date, *S. pombe* has proven to be a useful and robust expression system for gaining insight into the chloroplast division machinery, especially into the assembly and dynamics of FtsZs and the roles of the regulatory proteins that govern their assembly and positioning *in planta* (TerBush and Osteryoung, 2012; Zhang et al., 2013). We have found that FtsZ1 and FtsZ2 from Arabidopsis assemble filaments and coassemble into presumed heteropolymers that undergo dynamic turnover. These results are highly consistent with previous findings from *in vivo* and *in vitro* experiments on plant FtsZs (El-Kafafi et al., 2005; Johnson et al., 2015b; McAndrew et al., 2001; Olson et al., 2010; Smith et al., 2010; TerBush and Osteryoung, 2012; Vitha et al., 2001). A recent study analyzing the turnover of AtFtsZ1 and AtFtsZ2

in Z rings and filaments from live Arabidopsis epidermal cells showed that turnover rates were significantly longer than those we measure in *S. pombe*, likely the result of elaborate mechanisms for positioning and regulating Z-ring assembly and constriction (Johnson et al., 2015b; TerBush and Osteryoung, 2012). Nevertheless, in plants FtsZ1 still displayed greater dynamics than FtsZ2, which suggests that the results in *S. pombe* reflect the overall *in vivo* behavioral trends of FtsZ1 and FtsZ2. Therefore, the continued use of *S. pombe* to analyze the inherent filament assembly and turnover properties of FtsZs from various photosynthetic organisms, in order to assess functional conservation and variation, is highly advantageous, as fission yeast are easily transformed, grow and express proteins at a rapid rate, and possess none of the proteins that interact with and modulate FtsZ behavior *in planta*.

FtsZ filament morphology

When comparing the Arabidopsis FtsZ1-mVenus and FtsZ2-mCerulean filaments in this study with the Arabidopsis FtsZ1-eYFP and FtsZ2-eCFP filaments in our previous study (TerBush and Osteryoung, 2012), there is a distinct change in morphology, especially for FtsZ2. Previously, FtsZ1-eYFP assembled into large rings and single cables that looped around the cell compartment, while FtsZ2-eCFP assembled into small rings and intricate networks of filaments with regions of variable thickness. In this study, FtsZ1-mVenus assembled multiple cables that looped around the cell and occasionally into large rings, which likely formed by the annealing of cable ends (Fig. 3.1 A). Additionally, FtsZ2-mCerulean had a drastic shift in morphology, where it assembled into very regular rings, with a diameter the length of the cell interior

compartment, that had smaller filaments protruding off of the main structure (Fig. 3.1 E, left panel arrow). This shift in filament morphology was likely caused by changing from eYFP and eCFP, which are prone to dimerize at high concentrations in cellular environments, to mVenus and mCerulean bearing the A206K mutation, which eliminates the dimer interface and produces truly monomeric fluorescent proteins (Rizzo and Piston, 2005; Zacharias et al., 2002). This is consistent with the more loosely bundled appearance of FtsZ1-mVenus and may represent a more accurate filament morphology than observed in our previous study. However, the dynamic and colocalization properties of the AtFtsZ1-mVenus and AtFtsZ2-mCerulean are consistent with those of AtFtsZ1-eYFP and AtFtsZ2-eCFP, suggesting that the inherent behaviors of FtsZs fused to mVenus and mCerulean are consistent with those fused to eYFP and eCFP.

As we discussed in TerBush and Osteryoung (2012), we assume that the filaments observed in *S. pombe* represent bundles of individual polymers. With this in mind, we observe differences in bundling in FtsZ1 proteins from the various species analyzed. The representatives from *A. thaliana* and *O. sativa* (rice) form relatively tightly bundled cables, albeit OsFtsZ1 cables possess flared ends. However, *Ostreococcus tauri* (green alga) FtsZ1 shows more loosely associated bundles (Fig. 3.1 C), while *Galdieria sulphuraria* (red alga) FtsZB shows even less ability for individual polymers to laterally associate into bundles (Fig. 3.1 D). This reduced bundling activity is also evident in GsFtsZA, but to a lesser degree (Fig. 3.1 H). A previous study of *E. coli* and *B. subtilis* FtsZ showed that the C-terminal variable region (CTV), which includes the

amino acids downstream of the C-terminal peptide required for FtsZ interaction with membrane-associating proteins, promoted lateral assembly of individual polymers into bundles based on its degree of positive charge (Buske and Levin, 2012). Upon analyzing a multiple sequence alignment (Fig. 3.10), there seems to be a correlation in the appearance of FtsZ filament bundling in *S. pombe* and the number of positively charged amino acids in their CTVs (Fig. 1.3, Fig. 3.10 magenta box). Both OtFtsZ1 and GsFtsZA have a reduced CTV compared to those in AtFtsZ1/OsFtsZ1 and AtFtsZ2/OsFtsZ2, respectively, and display a moderate degree of loose bundling. GsFtsZB lacks the C-terminal region downstream of the conserved GTP-binding and hydrolysis domain all together (Fig. 3.10) and shows less filament bundling. Further studies on assembly and bundling activity *in vitro* will be necessary to test this point further, but our data do support a role for the CTV in promoting lateral interactions and bundling of polymers based on the degree of positive charge in this region.

We commonly observed that OsFtsZ2 assembled rings of two sizes, those that seemed more constrained by the interior dimensions of the yeast cell and those that were roughly 2 μm in diameter. However, rings of both diameters were evident in the coexpression strains for Arabidopsis and rice FtsZ. Similar small rings have been observed in transgenic plants (Johnson et al., 2015a; Zhang et al., 2013), suggesting that the small-diameter rings may represent an inherent curvature of plant FtsZ2 proteins and that plant FtsZ2s have two distinct states of polymer geometry, a straight and more curved conformation. Similar curvature patterns have been observed for *E. coli* FtsZ when polymerized with GDP (Erickson et al., 2010; Lu and Erickson, 1999;

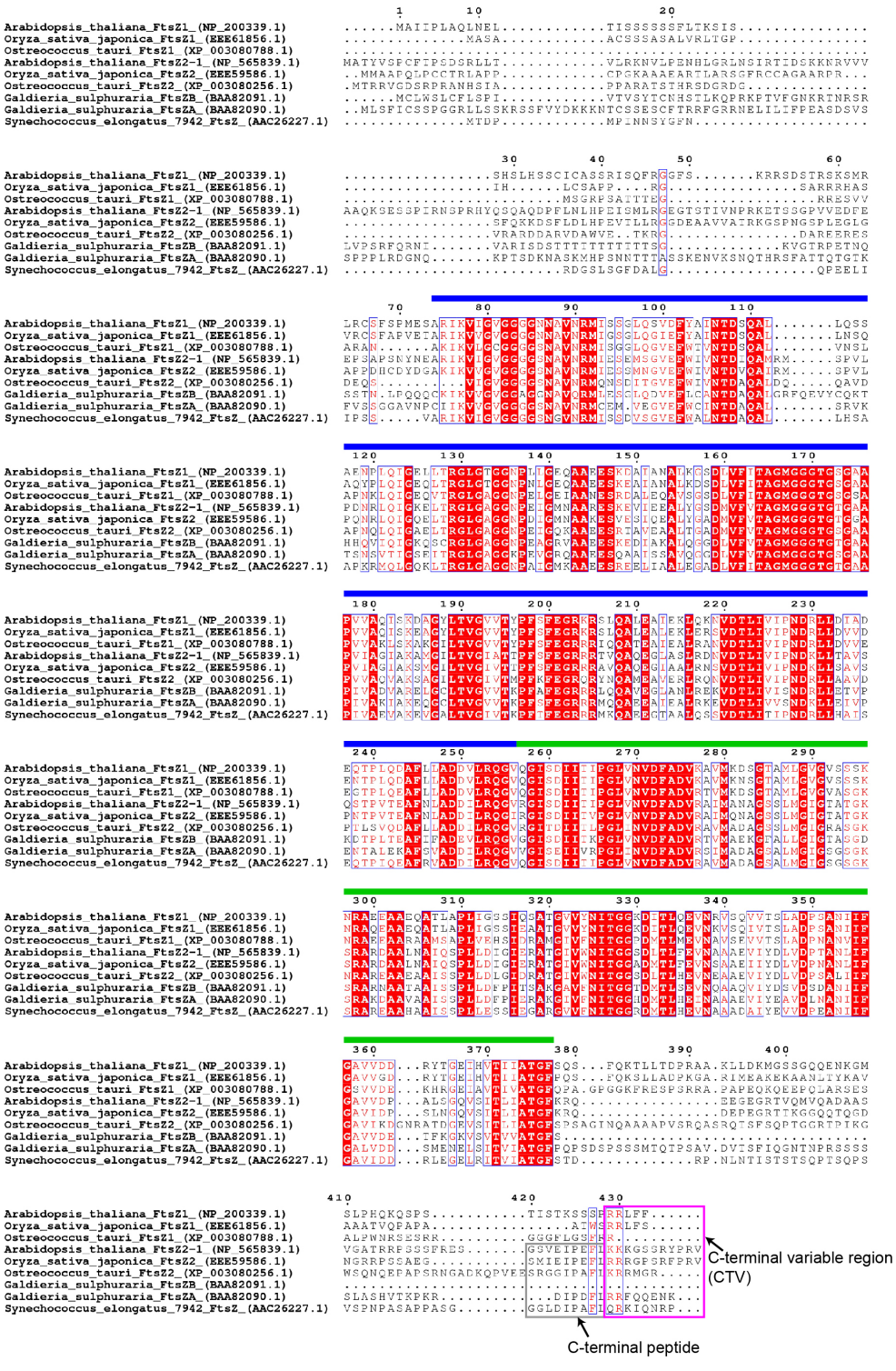

Figure 3.10: Multiple Sequence alignment of FtsZ proteins included in this survey.

Multiple protein alignment was performed for FtsZ homologs from *Arabidopsis thaliana*

Figure 3.10 (cont'd): (FtsZ1 - NP_200339.1 and FtsZ2 - NP_565839.1), *Oryza sativa japonica* (FtsZ1 - EEE61856.1 and FtsZ2 - EEE59586.1), *Ostreococcus tauri* (FtsZ1 - XP_003080788.1 and FtsZ2 - XP_003080256.1), *Galdieria sulphuraria* (FtsZB - BAA82091.1 and FtsZA - BAA82090.1), and *Synechococcus elongatus PCC 7942* (FtsZ - AAC26227.1) using MAFFT E-INS-i online server (Katoh and Standley, 2013) and graphic generated using ESPript 3.0 with a %Equivalent and global score of 0.7 sequence similarity depiction parameter (Robert and Gouet, 2014). Alignment identified a highly conserved GTP binding domain (blue bar), moderately conserved C-terminal domain (green bar), and conserved C-terminal peptide among FtsZ2/FtsZA and SeFtsZ (grey box). The later is consistent with previous reports highlighting the absence of the C-terminal peptides in FtsZ1's of land plants and green algae (TerBush et al., 2013). Illustrative of FtsZ divergence, *Galdieria sulphuraria* FtsZB lacks a large portion of the C-terminal region while FtsZA possesses the highly conserved C-terminal peptide. The C-terminal variable region (CTV) (Buske and Levin, 2012) is indicated by a magenta box.

Romberg et al., 2001), suggesting that GTP hydrolysis may be a step in the process of inducing polymer bending. This is supported by a recent study suggesting that *Mycobacterium tuberculosis* FtsZ undergoes a hinge-opening mechanism in response to GTP hydrolysis that induces protofilament bending (Li et al., 2013). However, another study on *E. coli* FtsZ showed that Z rings devoid of GTP hydrolysis assemble on tubular liposomes and start the constriction process, but that constriction is halted shortly thereafter, indicating that GTPase activity is not required for inducing constriction but for

sustaining it (Osawa and Erickson, 2011). Further structural analysis into inherent curvatures, mechanisms of protofilament bending, and force generation will be needed to clarify these issues for FtsZs from photosynthetic eukaryotes as well as bacteria.

As we observed previously, AtFtsZ1 and AtFtsZ2 coassembled into filaments that were similar to filaments formed by AtFtsZ2 alone. This was also observed for the coassembly of OsFtsZ1 and OsFtsZ2, suggesting that FtsZ2 structural dominance is a trait conserved across plant FtsZs. However, GsFtsZA and GsFtsZB coassembled into filament networks that had characteristics of both FtsZs but were more similar to those of GsFtsZB, including the ability to assemble large rings and loosely bundled filaments. However, due to lack of primary sequence conservation and poor transit peptide prediction tools, GsFtsZA and GsFtsZB were expressed with the N-terminal regions upstream of their conserved GTP-binding and hydrolysis domains removed. The assembly data for these proteins suggest that FtsZ2 structural dominance is a feature conserved among FtsZ pairs from both the green and red photosynthetic lineages. Additionally, they also suggest that the N-terminal region of FtsZs may influence FtsZ2's structural dominance over FtsZ1.

FtsZ filament turnover

All FtsZs in this study assembled filaments that underwent dynamic turnover. Invariably, the FtsZ1 representative from each pair displayed greater turnover dynamics, i.e., more rapid rates and greater total extents of recovery, indicating that this is a conserved trait for FtsZ pairs across both the green and red photosynthetic lineages (Fig. 3.5). GsFtsZB possessed the greatest filament turnover dynamics of any FtsZ

studied here. The high dynamic character coincided with the weakest apparent lateral interactions, suggesting the possibility that lateral packing of polymers may have a significant impact on the diffusion of assembly subunits into and out of bundles. However, the extent to which lateral interactions between polymers affect subunit diffusion may not be significant, as AtFtsZ1 displayed the highest degree of bundling of any FtsZ1/FtsZB studied here, yet filament turnover was near that of GsFtsZB. These data suggest that FtsZ filament turnover may be insensitive to the extent of lateral association and more influenced by another factor, such as FtsZ subunit interface stability. This hypothesis is also supported by GsFtsZA assembling filaments with the weakest apparent lateral interactions of any FtsZ2/FtsZA in this study, yet showed very low turnover properties. An alternative hypothesis is that the GsFtsZB studied here lacks its N-terminal region upstream of the conserved GTP-binding and hydrolysis domains and natively does not possess a C-terminal tail, which is found in all other FtsZs studied. This idea suggests the possibility that the N- and C-terminal regions may be important for promoting polymer stability and lateral interactions leading to bundling, as discussed above. In either case, additional studies will be required to verify the validity of these hypotheses by testing for subunit interface stability and the effect of the N- and C-terminal regions on FtsZ filament turnover and lateral association of individual polymers.

All putative GTPase-deficient FtsZs displayed reduced filament turnover characteristics compared to their WT counterparts (Fig. 3.11). While differences in the specific $t_{1/2}$ and total extent of recoveries were present in putative GTPase-deficient

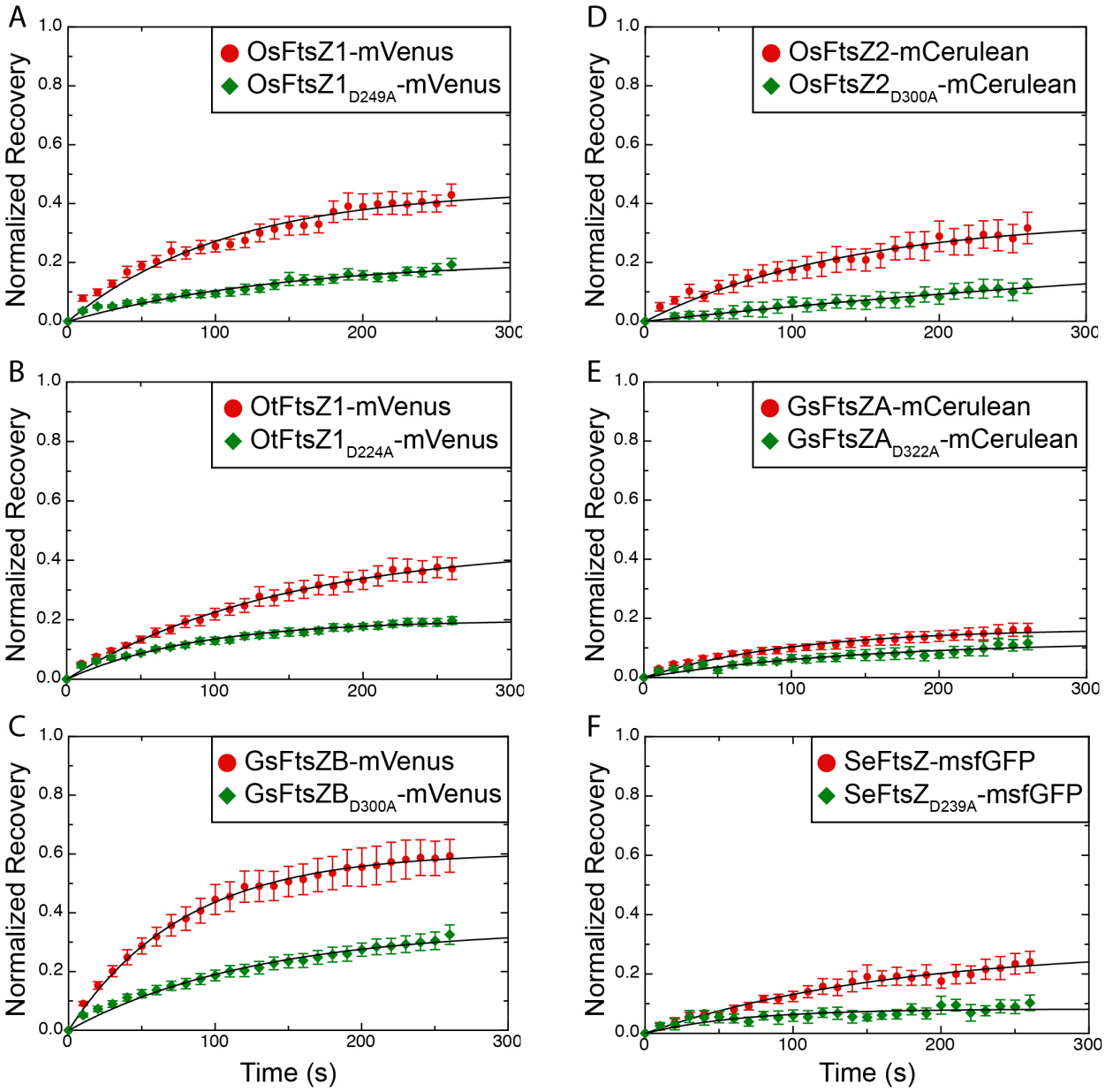

Figure 3.11: Putative GTPase-deficient FtsZ mutants have reduced polymer turnover dynamics than that of their WT FtsZ counterpart. The average fluorescence recovery vs time plots comparing the normalized recovery of (A) OsFtsZ1-mVenus and OsFtsZ1$_{D249A}$-mVenus, (B) OtFtsZ1-mVenus and OtFtsZ1$_{D224A}$-mVenus, and (C) GsFtsZB-mVenus and GsFtsZB$_{D300A}$-mVenus, (D) OsFtsZ2-mCerulean and

Figure 3.11 (cont'd): OsFtsZ2$_{D300A}$-mCerulean, (E) GsFtsZA-mCerulean and GsFtsZA$_{D322A}$-mCerulean, and (F) SeFtsZ-msfGFP and SeFtsZ$_{D239A}$-msfGFP. Data in each graph were normalized to the PB fluorescence signal (1 on the y-axis) and the fluorescence signal at the time of photobleaching (0 on the y-axis). OsFtsZ1-mVenus, OtFtsZ1-mVenus, GsFtsZB-mVenus, OsFtsZ2-mCerulean, GsFtsZA-mCerulean, and SeFtsZ-msfGFP data are represented by red circles. OsFtsZ1$_{D249A}$-mVenus, OtFtsZ1$_{D224A}$-mVenus, GsFtsZB$_{D300A}$-mVenus, OsFtsZ2$_{D300A}$-mCerulean, GsFtsZA$_{D322A}$-mCerulean, and SeFtsZ$_{D239A}$-msfGFP data are represented by green diamonds. The brackets represent SEM at each time point.

FtsZs from one species to the next, the overall findings were that FtsZ1/FtsZB filaments retained a significant degree of turnover, while FtsZ2/FtsZA filament turnover was nearly abolished across FtsZs from all species analyzed. These data are highly consistent with our previous results for AtFtsZ1-eYFP and AtFtsZ2-eCFP (TerBush and Osteryoung, 2012) and suggest that the hypothesis that the FtsZ1-FtsZ1 subunit interface is weak and prone to breakage, even in the absence of GTPase activity, may be extended to FtsZ1/FtsZB proteins across the green and red photosynthetic lineages. Similarly, these data suggest that the hypothesized FtsZ2-FtsZ2 strong subunit interface that is highly dependent on GTP hydrolysis for destabilization may also be extended.

In our previous study analyzing Arabidopsis FtsZ1 and FtsZ2, one of the critical findings was that AtFtsZ1 was able to enhance the turnover properties of AtFtsZ2 in presumed heteropolymers (TerBush and Osteryoung, 2012). Therefore, it was of great

evolutionary interest to assess if this is a conserved trait across the green and red photosynthetic lineages. In this study, we found that the extent of fluorescence recovery of the FtsZ2-like protein in the red alga *Galdieria sulphuraria*, GsFtsZA, was greatly enhanced in the presence of GsFtsZB relative to when GsFtsZA was expressed alone. However, the rate of filament turnover was unaffected. This is highly consistent with our previous findings for the effect of AtFtsZ1 on AtFtsZ2 turnover. These data indicate that the ability of FtsZ1 to augment the turnover of FtsZ2 in heteropolymers, and therefore potentially facilitate Z-ring constriction by enhancing remodeling, is a conserved trait across photosynthetic eukaryotes, even with the presumed independent gene duplication events that produced FtsZ1 and FtsZB in the green and red photosynthetic lineages, respectively, after their divergence (Miyagishima et al., 2004).

FtsZ evolution

The prevailing evolutionary theory states that chloroplasts arose when a free-living cyanobacterium was engulfed by a heterotrophic eukaryote and was subsequently enslaved, evolving into the organelles we see today (Gould et al., 2008). Further, it is believed that green-lineage FtsZ2 and red-lineage FtsZA are more ancient and are homologs of the single FtsZ in the common ancestor of chloroplasts. FtsZ1 and FtsZB arose later from independent gene duplication events in the green and red photosynthetic lineages, respectively (Miyagishima et al., 2004). These hypotheses are largely based on sequence homology and there has been no functional analysis for cyanobacterial FtsZ proteins to date. Therefore, this comparative analysis is a major

first step in elucidating the behaviors of cyanobacterial FtsZ and how they relate to FtsZs from photosynthetic eukaryotes.

SeFtsZ assembled well in *S. pombe*, possessing filament morphology that resembled the characteristics of both FtsZ1/FtsZB and FtsZ2/FtsZA families. The long looping cables formed by the WT protein and straight filaments formed by the putative GTPase-deficient mutant were highly consistent with filament morphologies for FtsZ1/FtsZB. SeFtsZ also assembled large rings with loosely associated bundles similar to those of FtsZ2/FtsZA. However, FRAP experiments show that SeFtsZ properties are completely consistent with those of the FtsZ2/FtsZA, as shown by a slow rate coupled with a low extent of turnover of the WT protein and the loss of filament turnover by the putative GTPase-deficient mutant. Overall, the higher functional similarity between SeFtsZ and FtsZ2/FtsZA is consistent with the theory that FtsZ2 and FtsZA are the direct homologs of the FtsZ present in the cyanobacterial endosymbiont and that FtsZ1/FtsZB arose later from gene duplication events.

Conclusions

Taken together, the comparative analyses presented in this study expand our understanding of how FtsZ function has been conserved across the photosynthetic lineages. Although minor differences in filament morphology and turnover exist from one species to the next, trends in the major behaviors of the FtsZ1/FtsZB and FtsZ2/FtsZA families persist, strongly suggesting that the distinct functions of FtsZ1/FtsZB promoting Z-ring constriction by enhancing remodeling and of FtsZ2/FtsZA as the structural determinants of the Z ring are well conserved and important for of Z-ring activity across

the green and red photosynthetic lineages. Additionally, this work provides the first functional characterization of a cyanobacterial FtsZ and supports the current theory that the direct homologs of the FtsZ from the endosymbiotic ancestor of chloroplasts are FtsZ2 and FtsZA, for the green and red photosynthetic lineages, respectively. These data also support that FtsZ1 and FtsZB arose later in their respective lineages and underwent convergent evolution to develop their unique function in Z-ring constriction.

Materials and Methods

Cloning of S. pombe Expression Constructs

FtsZ genes were cloned into the pREP41X and pREP42X expression vectors under the control of the *nmt1** promoter for analysis in *S. pombe* (Basi et al., 1993; Forsburg, 1993; Maundrell, 1993). Sequences encoding *Arabidopsis thaliana* FtsZ1 (NP_200339.1) and FtsZ2 (NP_565839.1) lacking the predicted transit peptide (the first 57 and 48 amino acids, respectively) were PCR-amplified from corresponding *S. pombe* expression plasmids (TerBush and Osteryoung, 2012) using primers AT262/AT298 and AT264/AT299, respectively. A monomeric variant of the yellow fluorescent protein Venus (mVenus) bearing the A206K mutation shown to eliminate the dimerization potential of GFP-derived fluorescent proteins (Nagai et al., 2002; Zacharias et al., 2002), generated in a bacterial expression vector provided by Desmond A. Moore and Harold P. Erickson (Duke University, Durham, NC), was PCR amplified with primers AT7/AT297. *mCerulean* (Addgene, Cambridge, MA) was PCR-amplified with primers AT7/AT297. *AtFtsZ1* and *mVenus* were cloned into *pREP41X* digested with BamH1 by the Gibson Assembly method (Gibson et al., 2009) to create *pREP41X-AtFtsZ1-mVenus*. *AtFtsZ2* and *mCerulean* were cloned into *pREP42X* digested with BamH1 by the Gibson Assembly method to create pREP42X-AtFtsZ2-mCerulean. We had the additional eukaryotic FtsZ CDS from *Oryza sativa*, *Ostreococcus tauri*, and *Galdieria sulphuraria* synthesized with codon optimization for expression in *Arabidopsis thaliana* from Integrated DNA Technologies (Coralville, IA) or Invitrogen (Carlsbad, CA). The sequence encoding OsFtsZ1 (EEE61856.1) lacking the predicted transit peptide (the

first 35 amino acids) was PCR-amplified with primers AT325/AT326 and cloned with *mVenus* into the same *pREP41X* digested with BamH1 with the Gibson assembly method to generate *pREP41X-OsFtsZ1-mVenus*. The sequence encoding OsFtsZ2 (EEE59586.1) lacking the predicted transit peptide (the first 20 amino acids) was PCR-amplified with primers AT327/AT328 and cloned with *mCerulean* into the same *pREP42X* digested with BamH1 with the Gibson assembly method to generate *pREP42X-OsFtsZ2-mCerulean*. The sequence encoding OtFtsZ1 (XP_003080788.1) lacking the predicted transit peptide (the first 18 amino acids) was PCR-amplified with primers AT329/AT330 and cloned with *mVenus* into the same *pREP41X* digested with BamH1 with the Gibson assembly method to generate *pREP41X-OtFtsZ1-mVenus*. The sequence encoding OtFtsZ2 (XP_003080256.1) lacking the predicted transit peptide (the first 35 amino acids) was PCR-amplified with primers AT331/AT332 and cloned with *mCerulean* into the same *pREP42X* digested with BamH1 with the Gibson assembly method to generate *pREP42X-OtFtsZ2-mCerulean*. Due to the lack of conservation in the N-terminal extension of red algal FtsZs and poor transit peptide prediction tools, we PCR-amplified *GsFtsZA* and *GsFtsZB* beginning at the start of the conserved GTP-binding domain. The sequence encoding GsFtsZA (BAA82090.1) lacking the first 120 amino acids was PCR-amplified with primers AT78/AT80 and joined to *mCerulean*, amplified with AT7/AT81, by primers AT78/AT81 by splicing by overlap extension and asymmetric PCR (Warrens et al., 1997). This fused gene fragment was cloned into *pREP42X* digested with Xho1 and BamH1 by conventional cloning techniques to create *pREP42X-GsFtsZA-mCerulean*. The sequence encoding GsFtsZB

(BAA82091.1) lacking the first 90 amino acids was PCR-amplified with primers AT76/AT77 and joined to *mVenus*, amplified with primers AT7/AT81, by primers AT76/AT81 by splicing by overlap extension and asymmetric PCR. This fused gene fragment was cloned into *pREP41X* digested with Xho1 and BamH1 by conventional cloning techniques to create *pREP41X-GsFtsZB-mVenus*. Generation of *pREP41-SeFtsZ-msfGFP* was performed by PCR-amplification of *FtsZ* (synpcc7942_2378) from *Synechococcus elongatus* PCC 7942 in two fragments. Fragment one, which consisted of nucleotides 1-240, was PCR-amplified with primers PSZ1F/PSZ1R. Piece two, which consisted of nucleotides 241-1182, was PCR-amplified with primers PSZ2F/PSZ2R. Amplification of *msfGFP*, which also bears the A206K mutation to eliminate dimerization (Costantini et al., 2012), was performed with primers PGFPF/PGFPR. All three PCR products were cloned into *pREP41* digested with Nde1 and BamH1 by the Gibson Assembly method. To generate the control constructs that expressed only mVenus or mCerulean, sequences encoding mVenus and mCerulean were PCR-amplified from *S. pombe* expression constructs with primers AT310 and AT297 and cloned into BamH1-digested *pREP41X* or *pREP42X*, respectively, by Gibson Assembly. To generate the control construct *pREP41-msfGFP*, *msfGFP* was PCR-amplified with primers PGF/PGR and cloned into *pREP41* digested with Nde1 and BamH1 by the Gibson Assembly method.

Putative GTPase-deficient mutants were created by introducing a single nucleotide substitution via overlapping primers and PCR amplification of the constructs described above. *pREP41X-OsFtsZ1*$_{D249A}$*-mVenus* was created by PCR amplification of

OsFtsZ1$_{D249A}$*-mVenus* in two pieces from *pREP41X-OsFtsZ1-mVenus* with primers AT325/AT340 and AT339/AT297 and cloned into *pREP41X* digested with BamH1 by Gibson Assembly. *pREP42X-OsFtsZ2*$_{D300A}$*-mCerulean* was created by PCR amplification of *OsFtsZ2*$_{D300A}$*-mCerulean* in two pieces from *pREP42X-OsFtsZ2-mCerulean* with primers AT327/AT342 and AT341/AT297 and cloned into *pREP42X* digested with BamH1 by Gibson Assembly. *pREP41X-OtFtsZ1*$_{D224A}$*-mVenus* was created by PCR amplification of *OtFtsZ1*$_{D224A}$*-mVenus* in two pieces from *pREP41X-OtFtsZ1-mVenus* with primers AT329/AT344 and AT343/AT297 and cloned into *pREP41X* digested with BamH1 by Gibson Assembly. *pREP42X-GsFtsZA*$_{D322A}$*-mCerulean* was created by PCR amplification of *GsFtsZA*$_{D322A}$*-mCerulean* in two pieces from *pREP42X-GsFtsZA-mCerulean* with primers AT296/AT294 and AT293/AT297 and cloned into *pREP42X* digested with BamH1 by Gibson Assembly. *pREP41X-GsFtsZB*$_{D300A}$*-mVenus* was created by PCR amplification of *GsFtsZB*$_{D300A}$*-mVenus* in two pieces from *pREP41X-GsFtsZ1-mVenus* with primers AT295/AT292 and AT291/AT297 and cloned into *pREP41X* digested with BamH1 by Gibson Assembly. *pREP41X-SeFtsZ*$_{D239A}$*-msfGFP* was created by PCR amplification of *SeFtsZ*$_{D239A}$*-msfGFP* in two pieces from *pREP41-SeFtsZ-msfGFP* with primers AT351/AT354 and AT353/AT352 and cloned into *pREP41X* digested with BamH1 by Gibson Assembly.

An expression construct was made to coexpress both GsFtsZA-mCerulean and GsFtsZB-mVenus from a single vector. The expression cassette from *pREP41X-GsFtsZB-mVenus*, including the *nmt1** promoter, *GsFtsZB-mVenus*, and *nmt1* terminator was PCR-amplified with primers AT109/AT110 and cloned into *pREP42X-*

GsFtsZA-mCerulean digested with AatII by Gibson Assembly. All primers used for cloning are listed in Table 3.2.

Table 3.2: List of primers used for cloning. Column 1: Primer designation. Column 2: Nucleotide sequence of each individual primer. Column 3: Indication of the presence or absence of a restriction site sequence engineered into the primer. See materials and methods section for additional details.

Primer	Sequence	Restriction Site
AT7	ATG GTG AGC AAG GGC GAG GAG CTG	N/A
AT76	TTT TTT CTC GAG ACC ATG CAG TGC AAG ATT AAG GTT GTG GGA GTT G	Xho1
AT77	GCC CTT GCT CAC CAT CTG CAT AGA GAA TCC GGT AGC CAC CAC AGT AAC	N/A
AT78	TTT TTT CTC GAG ACC ATG CCT TGC ATT ATC AAG GTT GTG GGA GTT G	Xho1
AT80	GCC CTT GCT CAC CAT CTG CAT CTT GTT CTC TTG CTG GAA CCT TCT AAG G	N/A
AT81	TTT TTT GGA TCC TTA CTT GTA CAG CTC GTC CAT GCC GAG	BamH1
AT109	GAT AAT AAT GGT TTC TTA GAC GTG TCG ATC GAC TCT AGA GGA TCA GAA AAT TAT C	N/A
AT110	GAA AAG TGC CAC CTG ACG TGC ATT ACT AAT AGA AAG GAT TAT TTC ACT TCT AAT TAC ACA AAT TCC G	N/A
AT262	GTT AAA TCA TAC CTC GAG GGA TCC ACC ATG AGG TCT AAG TCG ATG CGA TTG AGG	BamH1
AT264	GTT AAA TCA TAC CTC GAG GGA TCC ACC ATG GCC GCT CAG AAA TCT GAA TCT TCT	BamH1
AT291	GTG GAT TTC GCA GCT GTT AGA ACT GTG ATG	N/A
AT292	CT AAC AGC TGC GAA ATC CAC ATT CAC GAG	N/A
AT293	GTG GAT TTC GCT GCT GTG AGA TCT ATC ATG	N/A
AT294	CT CAC AGC AGC GAA ATC CAC ATT GAT GAG	N/A
AT297	GAC ATT CCT TTT ACC CGG GGA TCC TTA CTT GTA CAG CTC GTC CAT GCC GAG	BamH1

Table 3.2 (cont'd)

AT298	CTC GCC CTT GCT CAC CAT CTG CAT GAA GAA AAG TCT ACG GGG AGA AGA	N/A
AT299	CTC GCC CTT GCT CAC CAT CTG CAT GAC TCG GGG ATA ACG AGA GCT	N/A
AT325	GTT AAA TCA TAC CTC GAG GGA TCC ACC ATG GCA TCG GTT CGT TGC AGT TTT GCT CC	BamH1
AT326	CTC GCC CTT GCT CAC CAT CTG CAT ACT AAA CAA TCT CCT CGA CCA GGT AGC TG	N/A
AT327	GTT AAA TCA TAC CTC GAG GGA TCC ACC ATG GCA GCC GCA GAA GCT AGA ACA CTG	BamH1
AT328	CTC GCC CTT GCT CAC CAT CTG CAT AAC TCG TGG GAA CCT GGA GGG TC	N/A
AT329	GTT AAA TCA TAC CTC GAG GGA TCC ACC ATG GCT CGT GCC AAC GCT AAA ATA AAG GTA C	BamH1
AT330	CTC GCC CTT GCT CAC CAT CTG CAT TCT TCT GAA AGA CCC AAG AAA CCC CC	N/A
AT331	GTT AAA TCA TAC CTC GAG GGA TCC ACC ATG GCG AGA GAT GAT GCT CGA GTA GAT GC	BamH1
AT332	CTC GCC CTT GCT CAC CAT CTG CAT CCT GCC CAT ACG ACG TTT TAA GAA GGC	N/A
AT339	GTG GAC TTC GCT GCT GTT AAA GCT GTG ATG	N/A
AT340	TTT AAC AGC AGC GAA GTC CAC GTT AAC TAA ACC	N/A
AT341	C GTT GAC TTC GCT GCC GTT CGT GC	N/A
AT342	ACG AAC GGC AGC GAA GTC AAC GTT GAC	N/A
AT343	GTG GAC TTT GCA GCC GTG AGG ACT GTA	N/A
AT344	CCT CAC GGC TGC AAA GTC CAC GTT CAC	N/A
AT351	GTT AAA TCA TAC CTC GAG GGA TCC ACC ATG GCC ACC GAC CCT ATG CCG ATC AAC AAT TC	BamH1
AT352	GAC ATT CCT TTT ACC CGG GGA TCC CTA GGG TCG GTT TTG AAT TTT CCG TTG TAG G	BamH1
AT353	GAC TTT GCC GCC GTT CGC GCC	N/A
AT354	GCG AAC GGC GGC AAA GTC GAC G	N/A
PSZ1F	GACTTATAGTCGCTTTGTTAAATCAATGACGGATCCGATGCCAATTA	N/A
PSZ1R	ACTACCGCTGCCACTTCCCGCGGAATGCAGCAACGCCTGC	N/A
PSZ2F	GCACGGCATGGATGAACTCTACAAAGCCCCCAAGCGGATGCAGTTGGG	N/A

Table 3.2 (cont'd)

PSZ2R	AAGGGAGACATTCCTTTTACCCGGGCTAGGGTCGGTTTTGAATTTTCC	N/A
PGFPF	TTCCGCGGGAAGTGGCAGCGGTAGTATGAGTAAAGGTGAAGAACTG	N/A
PGFPR	TTTGTAGAGTTCATCCATGCCG	N/A
PGF	GACTTATAGTCGCTTTGTTAAATCAATGAGTAAAGGTGAAGAACTG	N/A
PGR	AAGGGAGACATTCCTTTTACCCGGGTCATTTGTAGAGTTCATCCATG	N/A

Transformation into S. pombe

FtsZ constructs were transformed into *S. pombe* using a lithium acetate procedure (http://www.sanfordburnham.org/labs/wolf/Protocols/Protocols/Fission%20Yeast/Nurse%20Lab%20Manual.htm). *S.pombe* (strain MBY192 [h^- leu1-32 ura4-D18]) cultures were grown in 50 mL of yeast extract plus supplements media (YES, http://www-bcf.usc.edu/~forsburg/media.html) for ~40 hours at 32°C. $5x10^8$ cells (50 mL at OD_{600} = 0.5) were harvested by centrifugation at 4,000*g* for 10 minutes at room temp. The resulting cell pellet was washed in 25 mL of TE (10 mM Tris-HCl, 1 mM EDTA, pH 7.5). The cells were pelleted again at 4,000*g* for 10 minutes at room temp. The cells were resuspended in 1 mL of TE and LiAc (100 mM lithium acetate, pH 7.5) and allowed to incubate at 30°C for 30 min. 200 µL of cells were aliquoted to a 2.0 mL microfuge tube that contained 20 µL of 10 µg/µL carrier sperm DNA (Agilent Technologies) and 1 µg of plasmid DNA (~2-3 µL in 2 mM Tris-HCl, pH 8.5) that had been incubating on ice. Cells were mixed by vortexing. For strains coexpressing 2 FtsZs from separate plasmids, 1 µg of each plasmid DNA was added to the transformation reaction to co-transform both plasmids into *S. pombe* at the same time. 1.2 mL of PEG solution (40% PEG, TE pH .5, and LiAc) was added to each tube and vortexed for 10 s. The tubes were incubated at 30°C for 30 min with shaking at 250

rpm. DMSO was added to 5% total volume (71 µL), the cells were vortexed again for 10 s, and then the tubes were incubated at 42°C for 15 min. The cells were pelleted at 7,000*g* for 30 s, and the supernatant was pipetted off. The cells were resuspended in 300 µL of TE and plated onto solid PMG with selection for each plasmid (-leucine for *pREP41* and *pREP41X*, -uracil for *pREP42X*, or -leucine/-uracil for strains with both *pREP41X* and *pREP42X*) and 15 µM thiamine to repress protein expression (Maundrell, 1990). The plates were allowed to grow at 32°C until colonies formed.

Growth and Expression of Transformed Cell Lines

Yeast strains containing the FtsZ fluorescent fusions described above were streaked for isolation on solid PMG with 15 µM thiamine, to repress expression. The plates also lacked leucine, uracil, or both to select for constructs pREP41/pREP41X, pREP42X, or both pREP41X and pREP42X, respectively. Plates were incubated at 32°C until colonies formed. Individual colonies were picked and used to inoculate 3 mL of liquid culture without thiamine to induce expression of the fusion proteins. These cultures were allowed to grow at 32°C with 250 rpm shaking for ~40 h to reach steady state conditions for polymer assembly and turnover.

Fluorescence Microscopy and FRAP Analysis

S. pombe cells grown in liquid PMG media under selection, as described above, were imaged by differential interference contrast (DIC) and epifluorescence microscopy, using a microscope (model DMRA2; Leica, Wetzlar, Germany) with an HCX PL FLUOTAR 100X (1.30 NA) oil-immersion objective (Leica) and a CCD camera (retiga Exi; QImaging, Burnaby, BC, Canada). 2 µL of liquid culture was pipetted onto a glass

poly-lysine coated slide and covered with a No. 1.5 coverslip. All imaging was performed at room temperature. Z stacks were taken with 0.5 μm increments. Images were acquired and subsequently de-blurred using nearest neighbor deconvolution at 70% haze removal using Image-Pro 7.0 software (Media Cybernetics). Additional image processing and analysis for epifluorescence micrographs was performed using Fiji software (ImageJ; http://fiji.sc/Fiji). Single-plane projections were generated from Z stacks using the maximum intensity algorithm and were falsely colored green for all FtsZ1 and FtsZB fluorescent signals and magenta for all FtsZ2, FtsZA, and cyanobacterial FtsZ fluorescent signals. Coexpression overlays were created with the merge channel tool, where colocalized fluorescence signals appear in white. Colocalization of fluorescence signals in coexpressing strains was quantified by creating a composite image of the 2 fluorescence signals from a deconvoluted Z stack, cropping the image to contain only the single cell being analyzed, unmerging the 2 channels, using the Coloc2 plugin within Fiji to calculate a Pearson's Correlation Coefficient (PCC) (Bolte and Cordelières, 2006), and averaging all PCC values for each coexpression strain, ± SEM.

Fluorescence Recovery After Photobleaching (FRAP) experiments were performed at room temperature on a laser-scanning confocal microscope (Fluoview 1,000 Spectral, Olympus) with a Plan FLN 60X (1.42 NA) oil-immersion objective with a 3.2X zoom. Just prior to performing each FRAP experiment, the high voltage setting for the photomultiplier tube was set so the greatest fluorescence signal in the image was just below saturation. FRAP data were collected with FV1000 ASW software (Olympus).

2 µL of liquid culture was pipetted onto a glass poly-lysine coated slide and covered with a No. 1.5 coverslip. All polymers were bleached for 20 ms at a % laser intensity so that one-half to two-thirds of the fluorescence signal was bleached, and continuous imaging was performed at the minimal laser intensity to minimize photobleaching but still provide adequate fluorescence signal. mVenus, mCerulean, and msfGFP fusion constructs were imaged and bleached with a 515, 458, and 488 nm laser, respectively. All time-course imaging for FRAP experiments were performed with 10 s intervals between time points. Three images were acquired before bleaching to calculate the average pre-bleach fluorescence intensity, and subsequent imaging occurred for an additional 260 s. Fluorescence intensity measurements were acquired for the region of photobleaching, a background sample, and an area of fluorescence signal that was away from the bleach region. Raw FRAP data was processed to produce photobleaching corrected and normalized recovery datasets (Rabut and Ellenberg, 2005). All datasets for each fluorescent fusion were averaged together to produce the average recovery dataset. Additionally, standard error of the mean (SEM) was calculated for normalized recovery at each time point. This average FRAP recovery dataset was used for curve-fitting using pro Fit software (QuantumSoft), where the data were fit to the single exponential equation $f(t) = A(1-e^{-kt})$. The time for one-half recovery of the fluorescence signal ($t_{1/2}$) was calculated as $t_{1/2} = \ln(1/2)/-k$.

Chapter 4

The N- and C-terminal Flanking Regions of Chloroplast FtsZ1 and FtsZ2 Influence Their Assembly Properties and Functional Relationship

This chapter is an adaptation and expansion of the methods manuscript presented in Appendix A.

Purification of full-length FtsZ1 and FtsZ2 was performed by Dr. Katie Porter, Department of Plant Biology at Michigan State University.

Abstract

Chloroplast division is driven by a macromolecular complex, which includes multiple ring structures that assemble at the mid-plastid. The centerpiece of the chloroplast division machinery is the stromal FtsZ ring, which is composed of two functionally distinct FtsZ isoforms, FtsZ1 and FtsZ2. My work in Chapter 2 utilizing *S. pombe* as a heterologous expression system showed that FtsZ1 and FtsZ2 possess distinct filament morphology and dynamic properties. However, the source of these distinct properties is poorly understood. FtsZs possess a core GTP-binding and hydrolysis domain that is highly conserved. However, they also contain N- and C-terminal flanking regions that show much less sequence conservation in FtsZs from various species and between FtsZ1 and FtsZ2 in a single organism. In this chapter, I compared the filament morphology and turnover characteristics of a series of Arabidopsis FtsZ1 and FtsZ2 truncation mutants in *S. pombe* to those of their full-length counterparts. I found that FtsZ1 and FtsZ2 proteins lacking the N- and/or C-terminal regions showed altered filament morphologies and those lacking both their N- and C-termini had reduced bundling activity *in vitro*. I also found that the N-terminal region of FtsZ2 is critical for its structural dominance over FtsZ1 in presumed heteropolymers. Finally, I show that the N- and C-terminal regions promote filament turnover, and that FtsZ1 and FtsZ2 lacking these regions show similar, yet still different, filament turnover characteristics. These data suggest that the N- and C-terminal regions directly promote polymer bundling and turnover. More importantly, these regions contribute to the distinct filament assembly and turnover characteristics of FtsZ1 and FtsZ2, but are not solely responsible for them.

Introduction

Chloroplasts are part of the main energy production pathway of plants and are present in high numbers in photosynthetic plant tissues. To maintain their populations as plant cells grow and divide, chloroplasts undergo division at their midpoint (Pyke, 1999). This process is facilitated by a macromolecular complex that involves the assembly of multiple ring structures both in the chloroplast interior (stroma) and outside the chloroplast within the cytosol (Osteryoung and Pyke, 2014). As chloroplasts arose from the endosymbiosis of an ancient cyanobacterium, many of the division components found in present-day chloroplasts are homologs of the bacterial cell division complex (Gould et al., 2008; Osteryoung and Pyke, 2014).

The central structure of chloroplast and bacterial cell division is the FtsZ ring (Z ring). In bacteria, the Z ring is the first structure of the division complex to assemble at the midcell and is composed of a single FtsZ protein (Bi and Lutkenhaus, 1991). Although FtsZ is a soluble protein, Z rings are tethered to the bacterial cell membrane via interaction with multiple membrane proteins (Addinall and Lutkenhaus, 1996; Liu et al., 1999). Once assembled, the Z ring acts as a scaffold for the recruitment of the downstream division components (Adams and Errington, 2009). FtsZ is a tubulin-like cytoskeletal GTPase that undergoes GTP-dependent assembly *in vitro*, where it polymerizes into single-stranded protofilaments, loose bundles, sheets, or helices depending on assembly conditions and the intrinsic biochemical properties of each particular FtsZ protein (Erickson et al., 2010). Additionally, it has been shown that electrostatic interactions, especially those involving the C-terminal variable region (CTV), influence the degree to which individual FtsZ protofilaments laterally interact (Buske and

Levin, 2012). Assembly stimulates GTPase activity, which destabilizes the subunit interface and promotes fragmentation and polymer turnover (Huecas et al., 2007). It has been demonstrated *in vitro* that when anchored to liposomes, assembled FtsZ rings and polymers exert a bending force on membranes based on a fixed direction of curvature (Osawa et al., 2008; Osawa et al., 2009). Furthermore, GTP hydrolysis is required for sustaining this contractile activity (Osawa and Erickson, 2011). Although the mechanism of force generation is not clear, it may be the result of a conformational switch involving a hinge-opening mechanism induced by GTP hydrolysis (Li et al., 2013).

In contrast to bacteria, chloroplasts possess two FtsZ families, FtsZ1 and FtsZ2 (Osteryoung et al., 1998). FtsZ1 and FtsZ2 are nuclear-encoded proteins that are translocated into the chloroplast via N-terminal transit peptides, which are cleaved upon import of the proteins into the stroma, where they coassemble into Z rings (McAndrew et al., 2001; Vitha et al., 2001). Z rings are tethered to the chloroplast membrane via the interaction between the integral membrane protein ARC6 and FtsZ2 through the C-terminal peptide conserved across FtsZ2 and bacterial FtsZ proteins (Ma and Margolin, 1999; Maple et al., 2005; TerBush et al., 2013; Vitha et al., 2003). Each FtsZ protein is critical for chloroplast division, as plants lacking either FtsZ1 or FtsZ2 show severe defects in chloroplast division, as indicated by larger and fewer chloroplasts per cell (Osteryoung et al., 1998). Genetic evidence has shown that FtsZ1 and FtsZ2 cannot substitute for one another *in vivo*, indicating that these proteins possess distinct functionality in chloroplast division (Schmitz et al., 2009). Other research has shown that FtsZ1 and FtsZ2 assemble into homopolymers, but always coassemble *in planta* and preferentially coassemble into heteropolymers *in vitro* (El-Kafafi et al., 2005; Lohse

et al., 2006; McAndrew et al., 2001; Olson et al., 2010; Smith et al., 2010; Vitha et al., 2001). Recent *in vivo* analysis has shown that both FtsZ1 and FtsZ2 undergo continual subunit exchange within Z rings, but that FtsZ1 is more dynamic (Johnson et al., 2015b). Additionally, FtsZ1 and FtsZ2 both possess GTPase activity, with FtsZ1 having higher activity than FtsZ2 (Olson et al., 2010; Smith et al., 2010).

In Chapter 2, I presented my research analyzing the intrinsic filament assembly and dynamic properties of FtsZ1 and FtsZ2 from Arabidopsis using *Schizosaccharomyces pombe* as a heterologous expression system (TerBush and Osteryoung, 2012). I found that FtsZ1 and FtsZ2 assembled filaments with distinct morphologies and that FtsZ1 filaments had greater turnover than FtsZ2 filaments. Additionally, I found that, when coassembled, FtsZ2 displayed structural dominance over FtsZ1 and that FtsZ1 enhanced FtsZ2 turnover. These findings led to the hypotheses that FtsZ2 plays a structural role in assembling the Z ring, while FtsZ1 may be important for enhancing Z-ring remodeling. However, the cause of these distinct behaviors was not clear. All FtsZs have a highly conserved GTP-binding and hydrolysis domain that is required for assembly (TerBush et al., 2013; Vaughan et al., 2004). However, this conserved domain is flanked by N- and C-terminal regions that vary in length and show poor conservation among FtsZ proteins (Fig. 4.1) (TerBush et al., 2013; Vaughan et al., 2004). Following my work in Chapter 2, I hypothesized that these N- and C-terminal flanking regions are at least partly responsible for the distinct behaviors of FtsZ1 and FtsZ2. Therefore, I generated a series of FtsZ truncations and analyzed their intrinsic filament assembly and dynamic properties in *S. pombe* to assess the roles these flanking regions may play in FtsZ behavior. I found that FtsZs lacking the

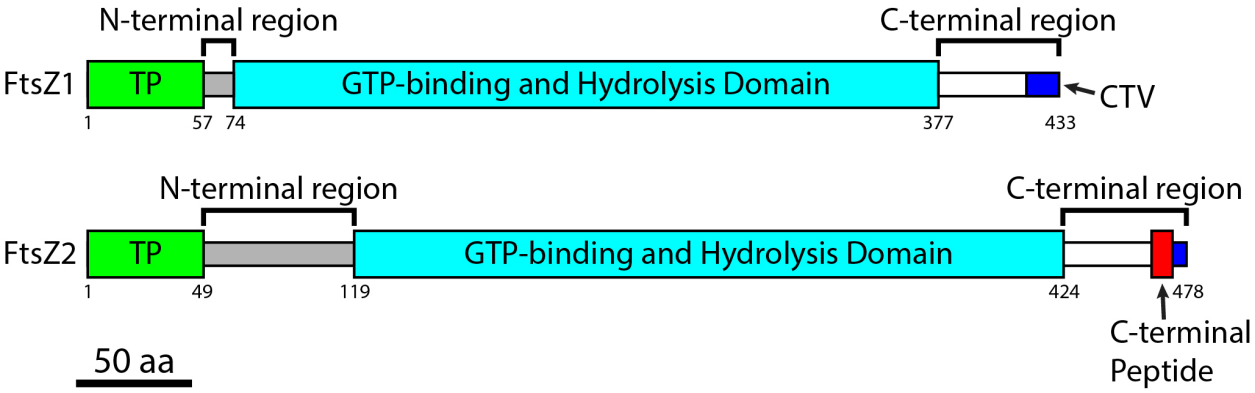

Figure 4.1: Domain architecture of *Arabidopsis* FtsZ1 and FtsZ2. Diagrams are drawn to scale. Colors represent the chloroplast transit peptide (green, TP), N-terminal extension (gray), GTP-binding and hydrolysis domain (cyan), C-terminal spacer (white), C-terminal peptide (red), and C-terminal variable region (blue). FtsZs expressed in this study do not include the TP. The N- and C-terminal regions are indicated by brackets. Black bar, 50 amino acids (aa).

N- and/or C-terminal regions show altered filament morphologies and reduced turnover. Interestingly, the filament turnover properties of FtsZ1 and FtsZ2 lacking their N- and C-termini were much more similar to each other than between those of their full-length counterparts. When coexpressed with FtsZ1, versions of FtsZ2 lacking the N-terminal region lost the structural dominance I described in Chapter 2 (TerBush and Osteryoung, 2012). Finally, purified and assembled FtsZ1 and FtsZ2 proteins lacking the N- and C-terminal regions showed a severe inhibition in lateral assembly into bundled structures. Taken together, these data indicate that the N- and C-terminal regions promote FtsZ bundling and filament turnover. They also indicate that these regions contribute to the

distinct assembly and dynamic properties of FtsZ1 and FtsZ2, while not being solely responsible for them.

Results

FtsZs lacking their N- and/or C-terminal regions show altered filament morphologies

To begin this comparative analysis, I expressed various forms of FtsZ1 and FtsZ2 C-terminally fused to monomeric fluorescence proteins in *S. pombe* and analyzed their filament morphology characteristics. As described in Chapter 3, full-length FtsZ1 lacking the predicted transit peptide ($FtsZ1_{FL}$) (Olson et al., 2010) assembled cables, presumably representing bundles of individual polymers (Erickson et al., 2010; Mukherjee and Lutkenhaus, 1999; Popp et al., 2009), that looped around the cell and annealed to form large rings conforming to the interior compartment of the yeast cell (Fig. 3.1 A, Fig. 4.2 A). These cables displayed minimal fraying of smaller filaments from the main cable structure. FtsZ1 lacking the N-terminal region ($FtsZ1_{\Delta NT}$, Fig. 4.1) also assembled cables (Fig. 4.2 B). However, there were more numerous cables, which also possessed a higher frequency of smaller filaments splitting off of the main structure. FtsZ1 lacking the C-terminal region ($FtsZ1_{\Delta CT}$) assembled straight or bent filaments and a large number of thinner filaments, with weaker fluorescence signal, fraying off of the main filament (Fig. 4.2 C). FtsZ1 lacking both the N- and C-terminal regions ($FtsZ1_{\Delta NCT}$) showed the most drastic change in filament morphology from $FtsZ1_{FL}$. $FtsZ1_{\Delta NCT}$ assembled multiple long filaments that looped around the cell, but these filaments were frequently frayed into several loosely associated filaments, suggesting a reduced level of lateral interactions and bundling between individual polymers (Fig. 4.2 D).

Full length FtsZ2 lacking the predicted transit peptide as described in Chapter 3 ($FtsZ2_{FL}$) (Olson et al., 2010) assembled large rings and an overall even fluorescence

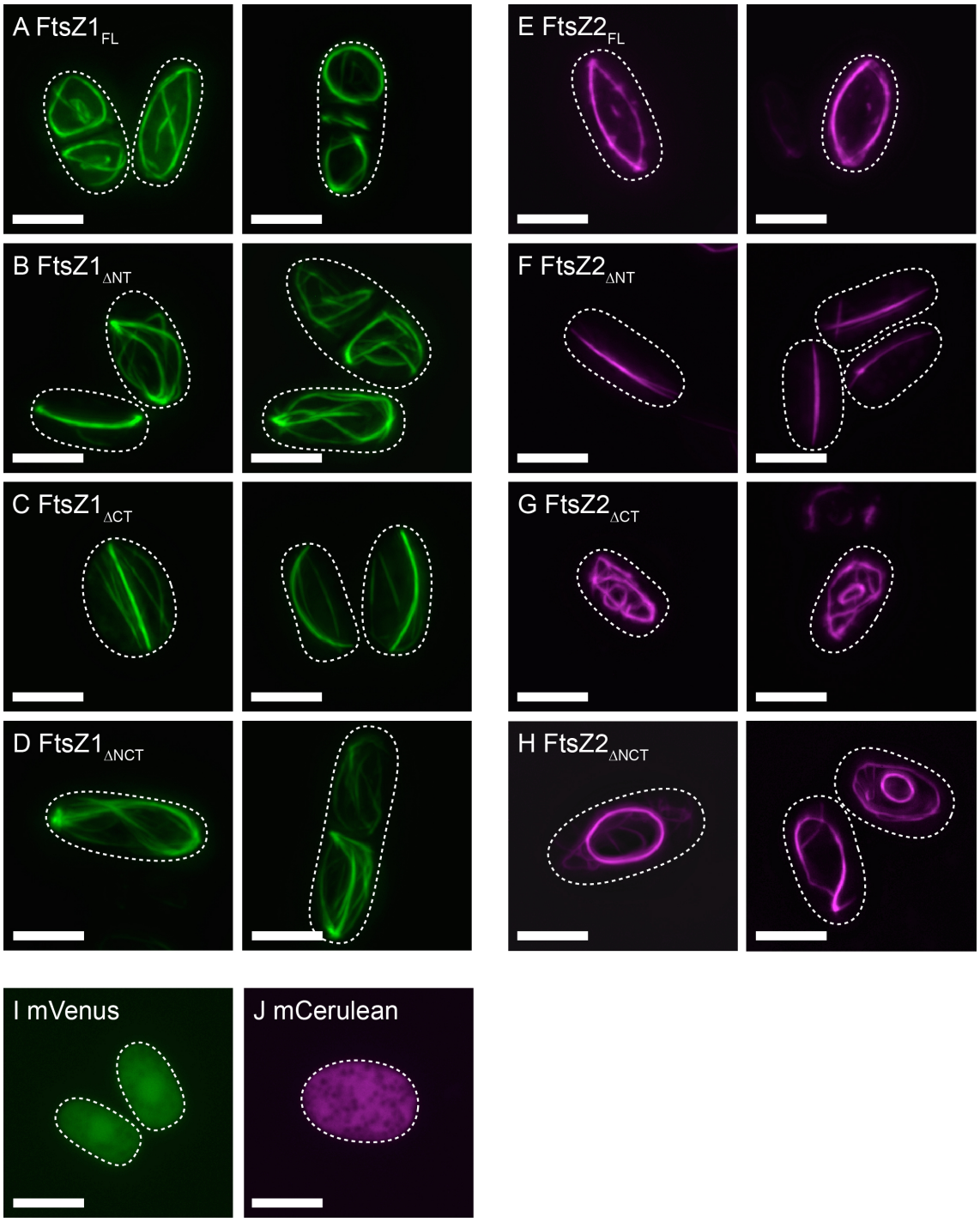

Figure 4.2: Filament morphologies for full-length and truncated forms of FtsZ1 and FtsZ2. Epifluorescence micrographs of *S. pombe* cells expressing (A) $FtsZ1_{FL}$-mVenus, (B) $FtsZ1_{\Delta NT}$-mVenus, (C) $FtsZ1_{\Delta CT}$-mVenus, (D) $FtsZ1_{\Delta NCT}$-mVenus, (E)

Figure 4.2 (cont'd): $FtsZ2_{FL}$-mCerulean, (F) $FtsZ2_{\Delta NT}$-mCerulean, (G) $FtsZ2_{\Delta CT}$-mCerulean, (H) $FtsZ2_{\Delta NCT}$-mCerulean, (I) mVenus, and (J) mCerulean. $FtsZ1_{FL}$-mVenus, $FtsZ1_{\Delta NT}$-mVenus, $FtsZ1_{\Delta CT}$-mVenus, $FtsZ1_{\Delta NCT}$-mVenus, and mVenus fluorescence signals are falsely colored green. $FtsZ2_{FL}$-mCerulean, $FtsZ2_{\Delta NT}$-mCerulean, $FtsZ2_{\Delta CT}$-mCerulean, $FtsZ2_{\Delta NCT}$-mCerulean, and mCerulean fluorescence signals are falsely colored magenta. The dashed lines represent the cell outlines. Bars, 5 μm.

distribution along the ring structure (Fig. 4.2 E). Similar to $FtsZ1_{FL}$, the dimensions of these rings appeared to conform to the interior dimensions of the yeast cell (Fig. 4.2 E). In contrast, FtsZ2 lacking the N-terminal region ($FtsZ2_{\Delta NT}$) assembled into straight filaments that had even fluorescence distribution and were up to the length of the cell (Fig. 4.2 F). A small number of the assembled filaments displayed forked and branching ends, suggesting that lateral interactions in this truncated form of FtsZ2 were partially inhibited. FtsZ2 lacking the C-terminal region ($FtsZ2_{\Delta CT}$) assembled more highly branched rings accompanied by several cross-linking filaments (Fig. 4.2 G). Additionally, $FtsZ2_{\Delta CT}$ assembled smaller rings of roughly 2 μm in diameter. FtsZ2 lacking both the N- and C-terminal regions ($FtsZ2_{\Delta NCT}$) assembled large rings, but these possessed cross-linking filaments, areas of loose bundling with smaller filaments splitting from the main structure, and small rings roughly 2 μm in diameter (Fig. 4.2 H). In control experiments, unfused mVenus and mCerulean displayed completely diffuse localization patterns (Fig. 4.2 I-J).

Coassembly of FtsZ1 and FtsZ2 is influenced by their N- and C-terminal flanking regions

To further analyze the effect of the N- and C-terminal regions on FtsZ filament morphology, I coexpressed $FtsZ1_{FL}$ with full-length and all truncated forms of FtsZ2 (Fig. 4.3). As shown in Chapter 3 (Fig. 3.3 A), $FtsZ1_{FL}$ and $FtsZ2_{FL}$ coassembled into ring structures that had cross-linking filaments and regions where the ring split into smaller filaments (Fig. 4.3 A). These proteins also assembled smaller rings similar to those assembled by $FtsZ2_{\Delta CT}$. I also assessed the degree of colocalization by calculating the Pearson's correlation coefficient (PCC), which gives a measure of the degree of overlap between the two fluorescence signals and how the intensities correlate (Bolte and Cordelières, 2006). $FtsZ1_{FL}$ and $FtsZ2_{FL}$ colocalized to a high degree with a PCC of 0.92 ± 0.01 (mean ± SEM, n = 23), as described in Chapter 3. In contrast, $FtsZ1_{FL}$ and $FtsZ2_{\Delta NT}$ coassembled into long, looping cables that resembled those formed by $FtsZ1_{FL}$ when expressed alone (Fig. 4.3 B). However, the $FtsZ1_{FL}$ fluorescence signal was slightly diffuse in this strain, resulting in a reduced PCC of 0.88 ± 0.01 (n = 12), a statistically significant decrease compared to when $FtsZ1_{FL}$ and $FtsZ2_{FL}$ were coassembled ($P < 0.01$). Similar to $FtsZ1_{FL}$ and $FtsZ2_{FL}$, $FtsZ1_{FL}$ and $FtsZ2_{\Delta CT}$ coassembled large rings with cross-linking filaments and small rings, with a high PCC of 0.92 ± 0.01 (n = 11, Fig. 4.3 C). $FtsZ1_{FL}$ and $FtsZ2_{\Delta NCT}$ coassembled into $FtsZ1_{FL}$-like cables. In this strain, $FtsZ1_{FL}$ showed a more apparent diffuse localization pattern than in the $FtsZ1_{FL}$ and $FtsZ2_{\Delta NT}$ coexpression strain (Fig. 4.3 B and D). Because of this,

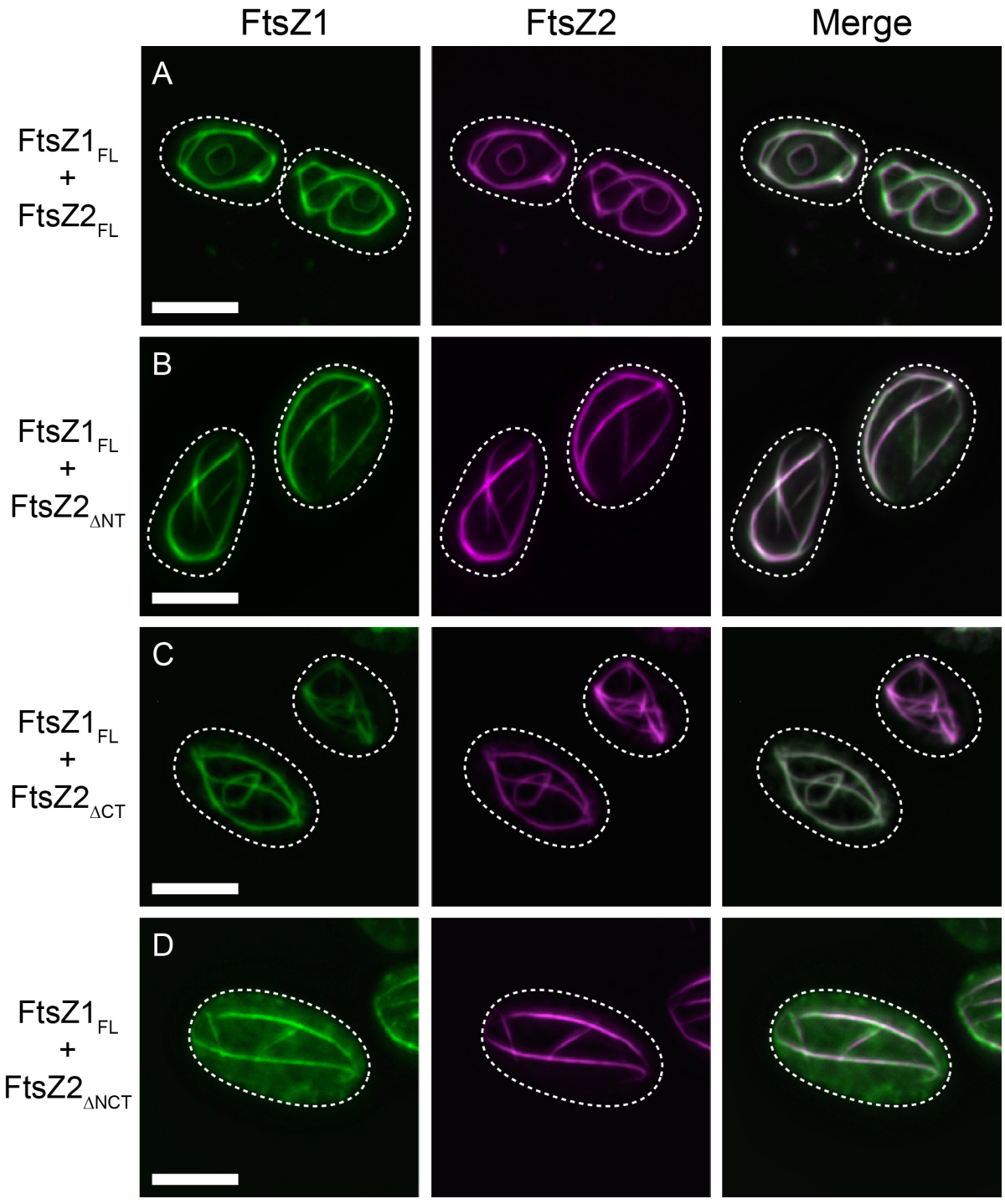

Figure 4.3: Coassembled filament morphologies for $FtsZ1_{FL}$ coexpressed with full-length and truncated forms of FtsZ2. Epifluorescence micrographs of *S. pombe* cells

Figure 4.3 (cont'd): coexpressing (A) $FtsZ1_{FL}$-mVenus and $FtsZ2_{FL}$-mCerulean, (B) $FtsZ1_{FL}$-mVenus and $FtsZ2_{\Delta NT}$-mCerulean, (C) $FtsZ1_{FL}$-mVenus and $FtsZ2_{\Delta CT}$-mCerulean, and (D) $FtsZ1_{FL}$-mVenus and $FtsZ2_{\Delta NCT}$-mCerulean. $FtsZ1_{FL}$-mVenus fluorescence signal is falsely colored green, while $FtsZ2_{FL}$-mCerulean, $FtsZ2_{\Delta NT}$-mCerulean, $FtsZ2_{\Delta CT}$-mCerulean, and $FtsZ2_{\Delta NCT}$-mCerulean fluorescence signals are falsely colored magenta. The white color in the merged images represent regions where the two fluorescence signals overlap and colocalize. Dashed lines represent cell outlines. Bars, 5 μm.

these proteins had a statistically significant reduction in their PCC (0.74 ± 0.02, n = 17, $P < 0.01$) compared to coassembled structures of $FtsZ1_{FL}$ and $FtsZ2_{FL}$.

I also coexpressed $FtsZ2_{FL}$ with the three truncated forms of FtsZ1 (Fig. 4.4). $FtsZ1_{\Delta NT}$ and $FtsZ2_{FL}$ coassembled into large rings with cross-linking filaments and small rings with a PCC of 0.91 ± 0.01 (n = 7, Fig. 4.4 A). $FtsZ1_{\Delta CT}$ and $FtsZ2_{FL}$ coassembled into similar structures with a high PCC of 0.90 ± 0.01 (n = 13, Fig. 4.4 B). $FtsZ1_{\Delta NCT}$ and $FtsZ2_{FL}$ also coassembled large and small rings, but the large rings were more frequently split with smaller filaments fraying off of the main structure. However, $FtsZ1_{\Delta NCT}$ and $FtsZ2_{FL}$ were also highly colocalized with a PCC of 0.89 ± 0.01 (n = 15, Fig. 4.4 C). Although there was slightly more filament splitting and fraying for coassembled filament structures of $FtsZ1_{\Delta NCT}$ and $FtsZ2_{FL}$, all combinations of $FtsZ2_{FL}$ with the truncated forms of FtsZ1 coassembled into structures resembling those coassembled by $FtsZ1_{FL}$ and $FtsZ2_{FL}$.

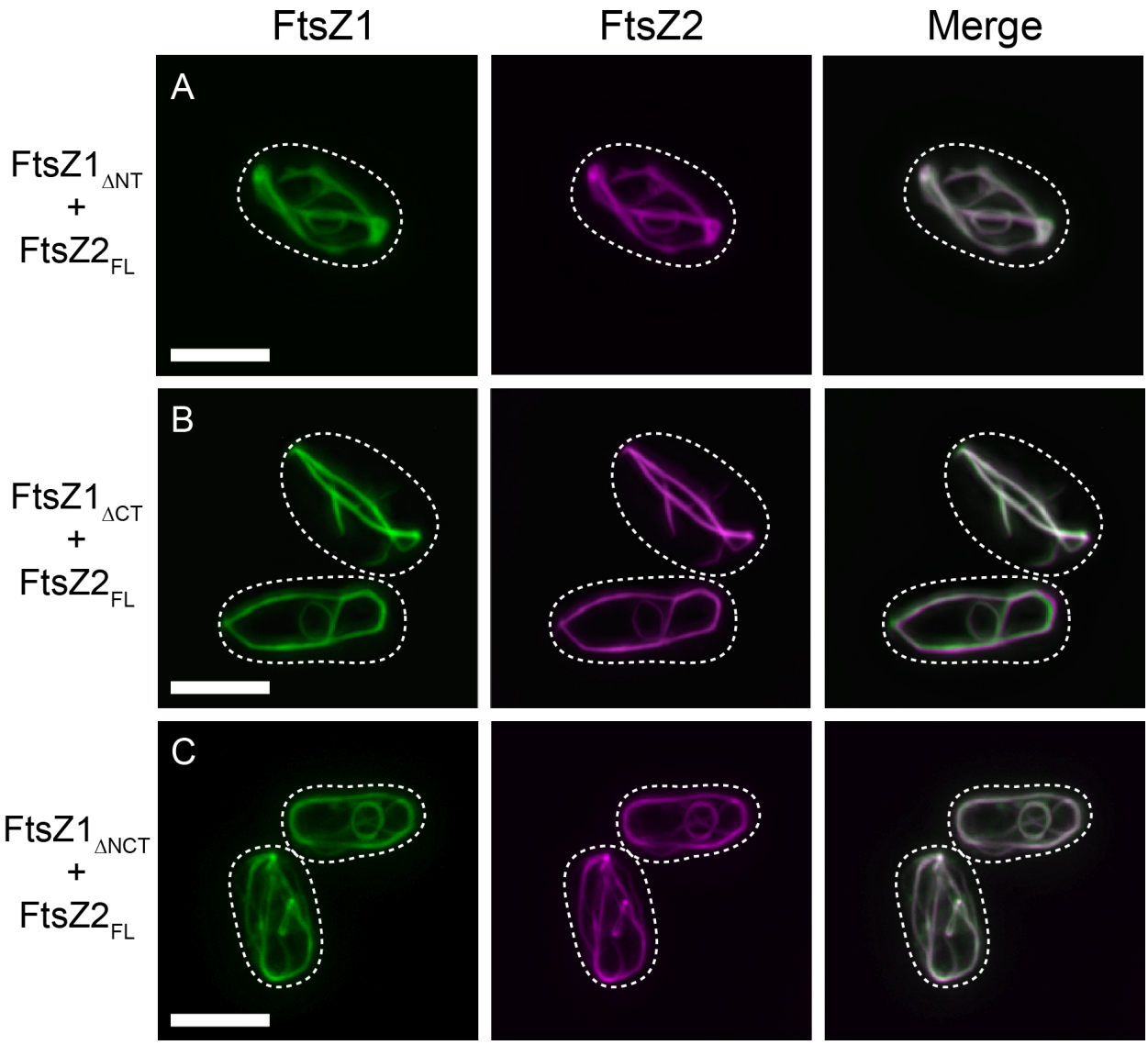

Figure 4.4: Coassembled filament morphologies for $FtsZ2_{FL}$ coexpressed with the truncated forms of FtsZ1. Epifluorescence micrographs of *S. pombe* cells coexpressing (A) $FtsZ1_{\Delta NT}$-mVenus and $FtsZ2_{FL}$-mCerulean, (B) $FtsZ1_{\Delta CT}$-mVenus and $FtsZ2_{FL}$-mCerulean, and (C) $FtsZ1_{\Delta NCT}$-mVenus and $FtsZ2_{FL}$-mCerulean. $FtsZ1_{\Delta NT}$-mVenus, $FtsZ1_{\Delta CT}$-mVenus, and $FtsZ1_{\Delta NCT}$-mVenus fluorescence signals are falsely colored green, while $FtsZ2_{FL}$-mCerulean fluorescence signal is falsely colored magenta.

Figure 4.4 (cont'd): The white color in the merged images represent regions where the two fluorescence signals overlap and colocalize. Dashed lines represent cell outlines. Bars, 5 μm.

Taken together, these filament morphology data show that the N- and C-terminal regions of FtsZ1 and FtsZ2 play critical roles in normal FtsZ assembly, including promoting lateral association of individual FtsZ polymers into bundles and inducing filament curvature. The coexpression data are consistent with our previous finding that FtsZ2 has a large influence on the morphology of coassembled filaments (TerBush and Osteryoung, 2012). However, these data expand our understanding of how FtsZ1 and FtsZ2 interact by showing that the N-terminal region of FtsZ2 contributes strongly to FtsZ2's structural dominance over FtsZ1, that the N- and C-terminal regions of FtsZ2 influence the extent of colocalization between FtsZ1 and FtsZ2, and that the N- and C-terminal regions of FtsZ1 may enhance bundling of coassembled structures.

FtsZs lacking their N- and C-terminal regions assemble but with inhibited lateral interactions

The results of the filament morphology experiments in *S. pombe* suggest that the N- and C-terminal regions influence FtsZ1 and FtsZ2 assembly properties. To further address this, purified full-length and N- and C-terminally truncated forms of FtsZ1 and FtsZ2 were purified and assembled in the presence of GTP, and the resulting structures were imaged by transmission electron microscopy (TEM, Fig. 4.5). $FtsZ1_{FL}$ readily assembled into polymers that laterally interacted to form bundled structures (Fig. 4.5 A).

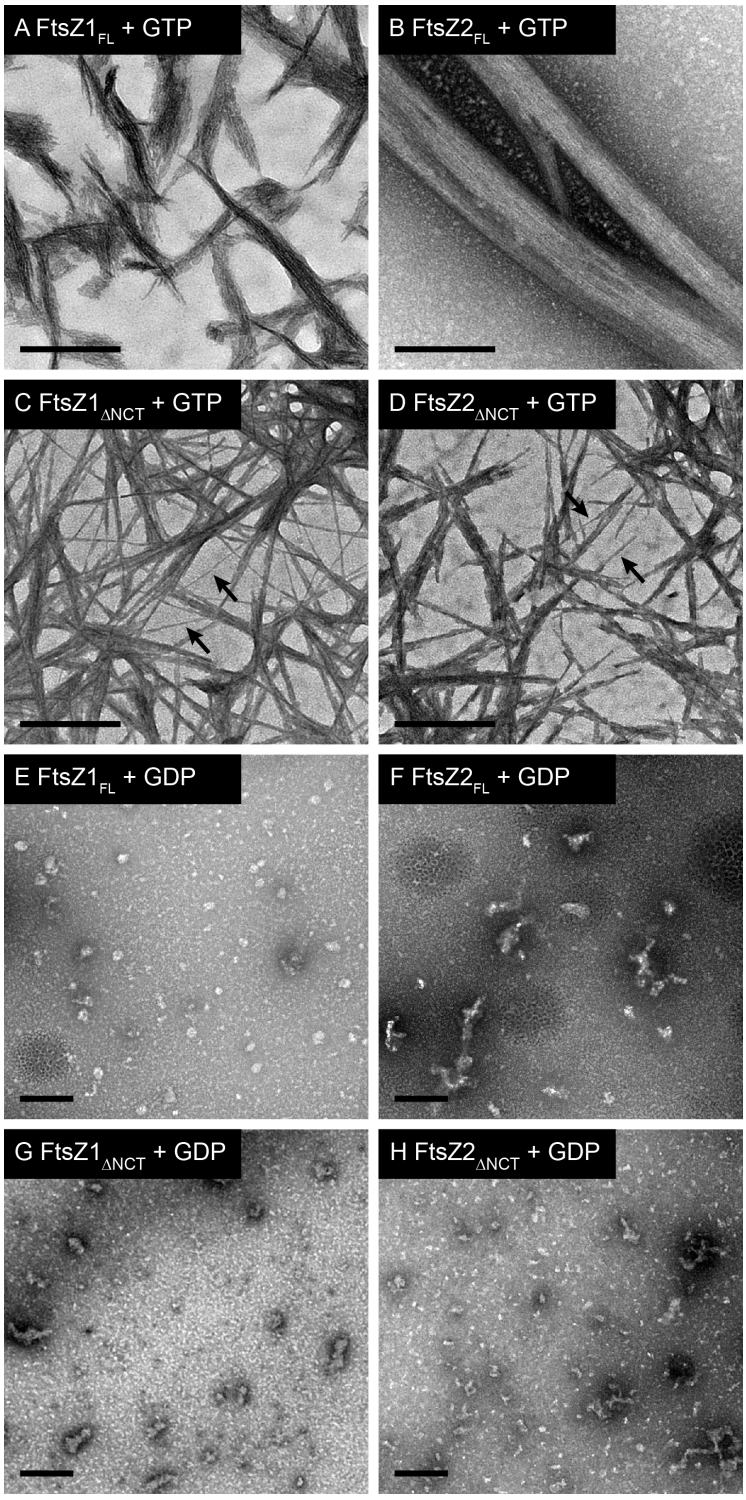

Figure 4.5: *In vitro* assembly of full-length and truncated forms of FtsZ1 and FtsZ2. Transmission electron micrographs of assembly reactions containing (A) $FtsZ1_{FL}$

Figure 4.5 (cont'd): with GTP, (B) $FtsZ2_{FL}$ with GTP, (C) $FtsZ1_{\Delta NCT}$ with GTP, (D) $FtsZ2_{\Delta NCT}$ with GTP, (E) $FtsZ1_{FL}$ with GDP, (F) $FtsZ2_{FL}$ with GDP, (G) $FtsZ1_{\Delta NCT}$ with GDP, and (H) $FtsZ2_{\Delta NCT}$ with GDP. All reactions contained 5 μM FtsZ and 500 μM nucleotide. Assembly was allowed to proceed for 5 minutes before the protein was loaded onto carbon-coated grids and stained with 2% uranyl acetate. (C-D) Arrows indicate polymers ~5-7 nm in width, which are likely single-stranded protofilaments. Bars, 200 nm.

Although the 3-dimensional geometry of these structures is not known, they appear to be small sheets of $FtsZ1_{FL}$ polymers that ranged from ~55-600 nm in length and ~30-90 nm in width. $FtsZ2_{FL}$ extensively assembled into large bundles that frequently split into smaller ones (Fig. 4.5 B). These bundles ranged from ~570-6,300 nm in length and ~40-180 nm in width. These bundled structures are in contrast to the single or double-stranded protofilaments previously assembled by full-length Arabidopsis FtsZ1 and FtsZ2 (Olson et al., 2010; Smith et al., 2010). However, those proteins were either purified out of inclusion bodies, which required denaturation and refolding, and only assembled in the presence of calcium as a stabilizing agent or had misplaced transit peptide cleavage sites. In contrast to full-length FtsZ1, $FtsZ1_{\Delta NCT}$ assembled thin protofilament bundles, indicating reduced lateral assembly (Fig. 4.5 C). These structures ranged from ~220-550 nm in length and ~6-40 nm in width. The thin filaments of ~6 nm in width likely represent single or double-stranded protofilaments, based on dimensions of bacterial FtsZ proteins (Romberg et al., 2001) (Fig. 4.5 C, arrows).

FtsZ2$_{\Delta NCT}$ also assembled into much smaller structures than its full-length counterpart (Fig. 4.5 D). FtsZ2$_{\Delta NCT}$ structures ranged from ~80-430 nm in length and ~5-35 nm in width. Protofilaments of ~5 nm in thickness were observed (Fig. 4.5 D, arrows), suggesting that FtsZ2$_{\Delta NCT}$ also assembled single or double-stranded protofilaments, but were not as prevalent as in FtsZ1$_{\Delta NCT}$ assembly reactions. In control reactions, FtsZs were assembled in the presence of GDP. Consistent with previous results (Olson et al., 2010), neither FtsZ1 nor FtsZ2 assembled polymerized structures when GDP was the only nucleotide present (Fig. 4.5 E-H). These TEM data show that full-length FtsZ1 and FtsZ2 assemble highly bundled structures and that their N- and C-termini greatly promote lateral association of polymers into bundled structures.

The N- and C-terminal regions influence FtsZ filament turnover

To continue my analysis, I performed fluorescence recovery after photobleaching (FRAP) experiments on the various truncated forms of FtsZ1 and FtsZ2 to assess their steady-state filament turnover characteristics. All constructs displayed recovery of fluorescence into the photobleached regions (Fig. 4.6). As shown in Chapter 3, the FtsZ1$_{FL}$ fluorescence signal recovered with a half-time ($t_{1/2}$) of 51 s and to 53% of the pre-bleach intensity (Fig. 3.4 A, n = 16). All three of the truncated FtsZ1 forms showed altered filament turnover characteristics. The FtsZ1$_{\Delta NT}$ fluorescence signal showed reduced recovery, with a $t_{1/2}$ of 95 s and to 53% of the pre-bleach intensity (Fig. 4.6 A, n = 13). The FtsZ1$_{\Delta CT}$ fluorescence signal displayed a $t_{1/2}$ of 90 s and a maximum recovery of 21% (Fig. 4.6 B, n = 14), while the FtsZ1$_{\Delta NCT}$ fluorescence signal recovered with a $t_{1/2}$ of 93 s and to a maximum extent of 37% (Fig. 4.6 C, n = 14).

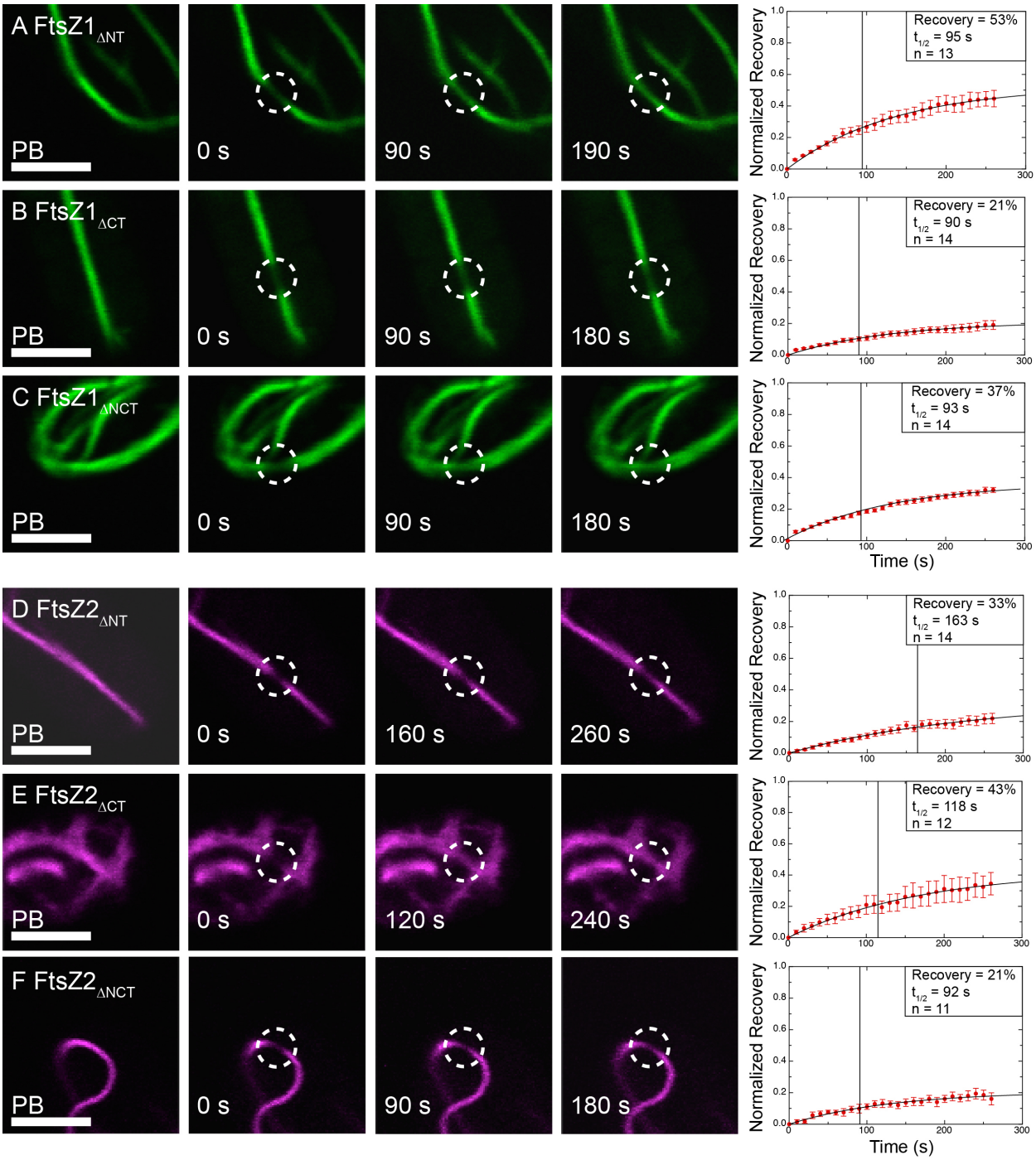

Figure 4.6: Steady-state polymer dynamics of the truncated forms of FtsZ1 and FtsZ2. Cells expressing (A) FtsZ1$_{\Delta NT}$-mVenus, (B) FtsZ1$_{\Delta CT}$-mVenus, (C) FtsZ1$_{\Delta NCT}$-mVenus, (D) FtsZ2$_{\Delta NT}$-mCerulean, (E) FtsZ2$_{\Delta CT}$-mCerulean, and (F) FtsZ2$_{\Delta NCT}$-

Figure 4.6 (cont'd): mCerulean were analyzed by FRAP. From left to right, the panels represent the fluorescence intensity in the bleached region (dashed circle) prior to bleaching (PB), at the time of bleaching (0 s), at the time closest to $t_{1/2}$, and at the time closest to twice $t_{1/2}$. The graphs to the right show the averaged and normalized fluorescence recovery vs time (sec) data. The data are normalized to the pre-bleach fluorescence intensity (1 on the y-axis) and the fluorescence intensity at the time of bleaching (0 on the y-axis). The data in the box are the calculated maximum percent fluorescence recovery, $t_{1/2}$ (also represented by the vertical bar), and the number of independent FRAP experiments performed (n). The red brackets represent the SEM for the normalized and averaged fluorescence recovery for each time point. FtsZ1$_{\Delta NT}$-mVenus, FtsZ1$_{\Delta CT}$-mVenus, and FtsZ1$_{\Delta NCT}$-mVenus fluorescence signals are falsely colored green. FtsZ2$_{\Delta NT}$-mCerulean, FtsZ2$_{\Delta CT}$-mCerulean, and FtsZ2$_{\Delta NCT}$-mCerulean fluorescence signals are falsely colored magenta. Bars, 2 μm.

As shown in Chapter 3, the FtsZ2$_{FL}$ fluorescence signal recovered with a $t_{1/2}$ of 67 s and to 13% of the pre-bleach intensity (Fig. 3.4 E, n = 16). Similar to the truncated FtsZ1 forms, all truncated forms of FtsZ2 showed altered filament turnover properties. The FtsZ2$_{\Delta NT}$ fluorescence signal recovered with the slowest $t_{1/2}$, 163 s, and to 33% of the pre-bleach intensity (Fig. 4.6 D, n = 14). The FtsZ2$_{\Delta CT}$ fluorescence signal recovered with a $t_{1/2}$ of 118 s and to 43% of the pre-bleach intensity (Fig. 4.6 E, n = 12), the greatest percent recovery among the FtsZ2 truncated forms. Finally, the FtsZ2$_{\Delta NCT}$ fluorescence signal recovered with a $t_{1/2}$ of 92 s and to 21% of the pre-bleach intensity (Fig. 4.6 F, n = 11). Taken together, the FRAP data show that all truncated forms FtsZ1

and FtsZ2 display reduced filament turnover dynamics compared to their full-length counterparts. Additionally, FtsZ1 and FtsZ2 proteins lacking their N- and C-terminal regions are more similar to each other in their turnover properties than are their full-length counterparts. These data indicate that the N- and C-terminal flanking regions promote FtsZ1 and FtsZ2 filament turnover and contribute to their distinct dynamic properties. However, these regions do not fully account for these differences.

Discussion

In recent years, studies have begun to elucidate the assembly and biochemical properties of plant FtsZ proteins (El-Kafafi et al., 2005; Johnson et al., 2015b; Lohse et al., 2006; Olson et al., 2010; Schmitz et al., 2009; Smith et al., 2010). My data in Chapter 2 (TerBush and Osteryoung, 2012) were consistent with those results and furthered our understanding of FtsZ function by showing that FtsZ1 and FtsZ2 have distinct filament assembly and dynamic properties: FtsZ1 directly enhances FtsZ2 turnover, and FtsZ2 displays morphological dominance over FtsZ1 in coassembled filaments. However, these results generated new questions regarding the source of the distinct behaviors of FtsZ1 and FtsZ2. I hypothesized that the poorly conserved N- and C-terminal regions (TerBush and Osteryoung, 2012; Vaughan et al., 2004) were to some extent responsible for the distinct assembly and dynamic properties of FtsZ1 and FtsZ2. To test my hypothesis, I compared the assembly and turnover properties of a series of truncated FtsZ proteins to those of their full-length counterparts. Performing such experiments *in planta* would be challenging on several fronts, including the recalcitrance of FtsZ proteins to fluorescence tagging *in vivo*, the potential of truncated FtsZ1 and FtsZ2 to not assemble *in planta*, weak fluorescence signal from constructs driven by FtsZ native promoters amid high chlorophyll autofluorescence, long generation times for Arabidopsis transgenic lines, and chloroplast movement induced by microscope illumination. Therefore, *S. pombe* represents a useful and efficient system in which to conduct this comparative analysis between full-length and truncated forms of FtsZ1 and FtsZ2.

Effect of the N- and C-termini on FtsZ filament morphology

As discussed in Chapter 2 (TerBush and Osteryoung, 2012), I assume that the assembled structures in *S. pombe* represent bundles of individual FtsZ polymers (Erickson et al., 2010; Mukherjee and Lutkenhaus, 1999; Popp et al., 2009). The FtsZ filament morphology data in this chapter are consistent with this hypothesis, as several of the truncated forms of FtsZ1 and FtsZ2 have large filaments splitting into smaller ones with less intense fluorescence signal (Fig. 4.2-3). All truncated forms of FtsZ1 and FtsZ2, with the exception of FtsZ2$_{\Delta NT}$, showed more filament splitting than did their full-length counterparts. These data suggest that the N- and C-termini of FtsZ1 and the C-terminus of FtsZ2 directly promote lateral association of polymers into bundles. This conclusion was confirmed in transmission electron micrographs showing that full-length FtsZ1 and FtsZ2 proteins assembled highly bundled structures *in vitro*, while those lacking their N- and C-terminal regions showed significantly reduced bundling (Fig. 4.5). A recent study on *E. coli* and *B. subtilis* FtsZs showed that the C-terminal variable region (CTV), which comprises the amino acids following the conserved C-terminal peptide required for FtsZ interaction with the membrane-tethering protein, was important for promoting lateral assembly of FtsZ polymers into bundles based on the degree of positive charge (Buske and Levin, 2012). As the CTVs of FtsZ1 and FtsZ2, and the N-terminal region of FtsZ1, have predicted pIs in the range of 10.8-12.0, they will all be positively charged at the pH of the chloroplast stroma (pH 7.5-7.9) (Hauser et al., 1995). Therefore, these regions could potentially promote bundling by charge shielding between the negatively charged GTP-binding and hydrolysis domains of FtsZ1 and FtsZ2 in polymers, which is consistent with the hypothesis that bacterial FtsZ

protofilaments are loosely held together by weak electrostatic interactions (Erickson et al., 2010). An alternative explanation is that these regions may make direct contacts in neighboring polymers within the bundle to stabilize lateral interactions, as shown for the bacteriophage encoded FtsZ-like protein PhuZ (Zehr et al., 2014). Additional experiments will be needed to further clarify the specific mechanisms by which the N- and C-terminal regions promote polymer bundling, which may be important for normal Z-ring assembly (Johnson et al., 2015a; Li et al., 2007; Milam et al., 2012).

$FtsZ1_{FL}$ and $FtsZ2_{FL}$ coassemble into $FtsZ2_{FL}$-like rings, but with more frequent filament splitting (Fig. 4.3). However, when $FtsZ1_{58\text{-}478}$ is coexpressed with forms of FtsZ2 lacking their N-terminal region ($FtsZ2_{\Delta NT}$ and $FtsZ2_{\Delta NCT}$), these proteins coassemble into cables that highly resemble $FtsZ1_{FL}$ when expressed alone, suggesting that the N-terminal region of FtsZ2 plays a critical role for maintaining FtsZ2 structural dominance in coassembled filaments. The predicted N-terminal region of FtsZ2, after cleavage of the chloroplast transit peptide, is 61 amino acids. While this region has low overall sequence conservation among FtsZ2 proteins across photosynthetic eukaryotes, there is a highly conserved motif among FtsZ2 proteins from vascular plants (residues 71-83 for Arabidopsis FtsZ2). Although there has been no data on the mechanistic function of the N-terminal region to date, this region may affect filament morphology by making specific contacts between FtsZ2 and other FtsZ1 or FtsZ2 subunits within the same or laterally associating polymers within a bundle. When $FtsZ1_{\Delta NCT}$ and $FtsZ2_{FL}$ were coexpressed, these proteins coassembled large and small rings similar to those assembled by $FtsZ1_{FL}$ and $FtsZ2_{FL}$. However, these structures showed an increased frequency of filament splitting, suggesting that FtsZ2 is not able to completely overcome

the reduced lateral association of $FtsZ1_{\Delta NCT}$ and that FtsZ1 does retain some influence on coassembled filament morphology.

In all coexpression strains in Chapters 2-3, FtsZ1 and FtsZ2 colocalize to a very high degree. However, when $FtsZ1_{FL}$ was coexpressed with $FtsZ2_{\Delta NT}$, there was a more diffuse localization of the $FtsZ1_{FL}$ fluorescence signal, resulting in a statistical reduction in the extent to which $FtsZ1_{FL}$ and $FtsZ2_{\Delta NT}$ colocalized in that coexpression strain as indicated by the reduced PCC (Fig. 4.3). $FtsZ1_{FL}$ and $FtsZ2_{\Delta NCT}$ colocalization was reduced further, as a lower PCC was measured and a diffuse $FtsZ1_{FL}$ fluorescence signal was readily visible in this strain. These results suggest that the N- and C-terminal flanking regions of FtsZ2 function together to promote normal heteropolymer formation of FtsZ1 and FtsZ2, with the N-terminus playing a more important role. The single and coexpressed filament morphology data in this chapter have suggested the N- and C-terminal flanking regions of FtsZ1 and FtsZ2 promote lateral assembly of FtsZ polymers as well as influencing coassembly characteristics. Additional experiments to analyze these properties will be necessary to further elucidate the details and mechanisms of homopolymer and heteropolymer assembly.

Effect of the N- and C-termini on FtsZ filament turnover

In *S. pombe*, all truncated forms of FtsZ1 and FtsZ2 showed reduced steady-state filament turnover characteristics when compared to their full-length counterparts (Fig 3.3 and Fig. 4.6). Truncated FtsZ1 proteins all showed increased $t_{1/2}$ measurements, while only truncations lacking the C-terminal region showed reduced fluorescence recovery. One explanation for these changes is that FtsZ1-FtsZ1 subunit interfaces are

stabilized for the various truncated forms of FtsZ1. In this situation, the rate at which polymers fragment and depolymerize into diffusible subunits would decrease, resulting in more of the FtsZ1 pool being locked into the immobile fraction. Thus, the result of more stable subunit interfaces would be an increase in $t_{1/2}$ values and less total fluorescence recovery, as previously seen for GTPase-deficient mutants of FtsZ1 and FtsZ2 (TerBush and Osteryoung, 2012). An alternative explanation is that lateral interactions between individual FtsZ polymers are stabilized. In this situation, the breakdown of FtsZ polymers into diffusible subunits would be unaffected, and the assembly-ready pool of FtsZ subunits, or mobile fraction, would be unaltered. However, more stable lateral interactions between polymers would likely inhibit diffusion of FtsZ subunits and thereby reduce their rate of diffusion. While the effect of stabilized subunit interfaces or increased lateral interactions cannot be completely separated from this analysis, the prior situation is more consistent for FtsZ1 proteins lacking their C-termini, as filament morphology in *S. pombe* (Fig. 4.2) and *in vitro* assembly (Fig. 4.5) show that FtsZ1 lacking the N- and/or C-terminal regions show a significant reduction in bundling. Taken together, these data suggest that in the wild-type FtsZ1 protein the N-terminus influences polymer turnover through destabilizing lateral interactions, whereas the C-terminus influences polymer turnover by destabilizing FtsZ1-FtsZ1 subunit interfaces, even in the absence of reduced lateral interactions.

Similar to FtsZ1, an explanation for the change in filament turnover for FtsZ2 lacking its N- and/or C-terminus is that the subunit interfaces are more stable than in filaments composed of full-length FtsZ2. However, filaments composed of truncated FtsZ2 show increased fluorescence recovery, indicating greater mobile fractions than

for full-length FtsZ2. This suggests that subunit interface stability is not the only driving force determining FtsZ2 filament turnover, but that lateral interactions also play an important role. The *S. pombe* filament morphology and TEM data suggest that FtsZ2 lacking its N- and C-terminal regions have severe reductions in lateral assembly (Fig. 4.2 and Fig 4.5). As a result of stabilized subunit interfaces, FtsZ2 filaments would break down more slowly, resulting in larger diffusible oligomers that would further depolymerize to replenish the assembly-ready pool. However, reduced lateral interactions would allow these diffusible oligomers to diffuse more readily in and out of bundles. Therefore, the mobile fraction may not necessarily be reduced but may be increased if diffusion occurs rapidly after rate-limiting polymer breakdown. It appears as though rate of breakdown, controlled by FtsZ2 subunit interface stability, and lateral interactions of diffusible oligomers both influence the turnover of FtsZ2 filaments. Additional experiments to analyze the lateral assembly of FtsZ polymers and FtsZ subunit interface stability will be necessary to further elucidate these mechanistic details.

In Chapters 2 and 3, I showed that full-length FtsZ1 and FtsZ2 assemble filaments with distinct turnover characteristics (Fig. 2.3 and Fig. 3.4). In contrast, $FtsZ1_{\Delta NCT}$ and $FtsZ2_{\Delta NCT}$ filaments possess near identical rates of turnover and exhibit more similar total fluorescence recoveries than do full-length FtsZ1 and FtsZ2 (Fig. 4.6). These data indicate that the N- and C-terminal regions directly contribute to the distinct filament turnover properties of FtsZ1 and FtsZ2. However, $FtsZ1_{\Delta NCT}$ has a greater mobile fraction than $FtsZ2_{\Delta NCT}$, suggesting that the GTP-binding and hydrolysis domain of FtsZ2 has greater potential for lateral interactions than that of FtsZ1 and contributes to the greater stability of FtsZ2 filaments. This hypothesis is consistent with the slightly

higher degree of bundling of FtsZ2$_{\Delta NCT}$ than FtsZ1$_{\Delta NCT}$ (Fig. 4.5). Taken together these filament turnover data suggest that the N- and C-terminal regions highly influence the overall filament turnover properties of FtsZ1 and FtsZ2 through a combination of influencing subunit interface stability and lateral association of individual polymers within bundles.

Materials and Methods

Cloning and transformation of S. pombe expression constructs

The *pREP41X-FtsZ1$_{FL}$-mVenus* and *pREP42X-FtsZ2$_{FL}$-mCerulean* constructs used in this study were the same as those generated in Chapter 3. All truncated *FtsZ1* and *FtsZ2* constructs were generated by PCR amplification from these two plasmids. To generate *pREP41X-FtsZ1$_{\Delta NT}$-mVenus*, *FtsZ1$_{\Delta NT}$* and *mVenus* were amplified by PCR with primers sets AT266/AT298 and AT7/AT297, respectively, and cloned into *pREP41X* digested with BamH1 by the Gibson Assembly method (Gibson et al., 2009). *FtsZ1$_{\Delta CT}$* was PCR-amplified with primers AT262/AT285. This gene fragment was cloned with *mVenus* into *pREP41X* digested with BamH1 by the Gibson Assembly method to generate *pREP41X-FtsZ1$_{\Delta CT}$-mVenus*. *FtsZ1$_{\Delta NCT}$* was PCR-amplified with primers AT266/AT285. This gene fragment was cloned with *mVenus* into *pREP41X* digested with BamH1 by the Gibson Assembly method to generate *pREP41X-FtsZ1$_{\Delta NCT}$-mVenus*. To generate *pREP42X-FtsZ2$_{\Delta NT}$-mCerulean*, *FtsZ2$_{\Delta NT}$* and *mCerulean* were PCR-amplified with primer sets AT268/AT299 and AT7/AT297, respectively. These gene fragments were cloned into *pREP42X* digested with BamH1 by the Gibson Assembly method. *FtsZ2$_{\Delta CT}$* was PCR amplified by primers AT264/AT287 and cloned with *mCerulean* into *pREP42X* digested with BamH1 by the Gibson Assembly method to generate *pREP42X-FtsZ2$_{\Delta CT}$-mCerulean*. *FtsZ2$_{\Delta NCT}$* was PCR amplified by primers AT268/AT287 and cloned with *mCerulean* into *pREP42X* digested with BamH1 by the Gibson Assembly method to generate *pREP42X-FtsZ2$_{\Delta NCT}$-mCerulean*. Control *pREP41X-mVenus* and *pREP42X-mCerulean* constructs were the same described in Chapter 3.

All constructs described above were transformed into *S. pombe* by the lithium acetate and heat shock method described in Chapter 3. All *S. pombe* strains coexpressing two constructs were generated by transforming both expression plasmids into *S. pombe* in the same reaction.

Cell growth conditions and expression from transformed S. pombe lines

S. pombe cells containing the expression constructs described above were grown on solid PMG media containing 15 μM thiamine to repress protein expression. Isolated colonies were picked and used to inoculate cultures in liquid PMG media to induce expression as described in Chapter 3.

Epifluorescence microscopy and FRAP analysis

FtsZ polymer morphology was observed by epifluorescence microscopy and turnover was analyzed by fluorescence recovery after photobleaching (FRAP) experiments as described in Chapter 3.

Cloning and transformation of bacterial expression constructs

Full length FtsZs lacking their predicted transit peptides, $FtsZ1_{FL}$ (AtFtsZ1-1, At5g55280) and $FtsZ2_{FL}$ (AtFtsZ2-1, At2g36250), were expressed from bacterial expression plasmids generated in Olson et al. (2010). To generate the construct expressing FtsZ1 that lacked its N- and C-terminal regions (amino acids 71-376, $FtsZ1_{\Delta NCT}$), $FtsZ1_{\Delta NCT}$ was amplified by PCR from another construct containing the FtsZ1 gene with primers AT72/AT40. Primer AT40 contained a 6X-His tag in the sequence to fuse the 6X-His tag at the C-terminus of $FtsZ1_{\Delta NCT}$. This gene product was

cloned into *pLW01* (provided to us by Dr. Lucy Waskell, University of Michigan) digested with Nco1 and Xho1 using standard restriction-based cloning techniques to generate *pLW01-FtsZ1*$_{\Delta NCT}$*-6XHis*. *pLW01-FtsZ2*$_{\Delta NCT}$*-6XHis* was generated by PCR amplification of *FtsZ2* lacking its N- and C-terminal regions (amino acids 118-423, FtsZ2$_{\Delta NCT}$) from another construct containing the full length *FtsZ2* gene lacking the predicted transit peptide with primers AT73/AT42. AT42 contained a 6X-His tag in its sequence to fuse it to the C-terminus of *FtsZ2*$_{\Delta NCT}$, upstream of the stop codon. This gene product was cloned into *pLW01* digested with Nco1 and Xho1 using standard restriction-based cloning techniques. All primers used for cloning are listed in Table 4.1.

Table 4.1: List of primers used for cloning. Column 1: Primer designation. Column 2: Nucleotide sequence of each individual primer. Column 3: Indication of the presence or absence of a restriction site sequence engineered into the primer. See materials and methods section for additional details.

Name	Sequence	Restriction Site
AT7	ATG GTG AGC AAG GGC GAG GAG CTG	N/A
AT40	TTT TTT CTC GAG CTA ATG ATG ATG ATG ATG ATG GCC TGT GGC GAT TAT CGT TAC ATG AAT	Xho1
AT42	TTT TTT CTC GAG TTA ATG ATG ATG ATG ATG ATG ACC CGT AGC TAT CAG GGT TAT GCT TAC	Xho1
AT72	TTT TTT CCA TGG AA TCT GCG AGA ATT AAG GTG ATT GGT GTC GGT	Nco1
AT73	TTT TTT CCA TGG AG GCG AGG ATT AAG GTT ATT GGT GTG	Nco1
AT262	GTT AAA TCA TAC CTC GAG GGA TCC ACC ATG AGG TCT AAG TCG ATG CGA TTG AGG	BamH1

Table 4.1 (cont'd)

AT264	GTT AAA TCA TAC CTC GAG GGA TCC ACC ATG GCC GCT CAG AAA TCT GAA TCT TCT	BamH1
AT266	GTT AAA TCA TAC CTC GAG GGA TCC ACC ATG GCG AGA ATT AAG GTG ATT GGT GTC GGT G	BamH1
AT268	GTT AAA TCA TAC CTC GAG GGA TCC ACC ATG GCG AGG ATT AAG GTT ATT GGT GTG GG	BamH1
AT285	CTC GCC CTT GCT CAC CAT CTG CAT GAA GCC TGT GGC GAT TAT CGT TAC ATG	N/A
AT287	CTC GCC CTT GCT CAC CAT CTG CAT GAA ACC CGT AGC TAT CAG GGT TAT GC	N/A
AT297	GAC ATT CCT TTT ACC CGG GGA TCC TTA CTT GTA CAG CTC GTC CAT GCC GAG	BamH1
AT298	CTC GCC CTT GCT CAC CAT CTG CAT GAA GAA AAG TCT ACG GGG AGA AGA	N/A
AT299	CTC GCC CTT GCT CAC CAT CTG CAT GAC TCG GGG ATA ACG AGA GCT	N/A

The bacterial expression constructs described above were transformed into Rosetta (DE3) cells (Novagen) containing a second plasmid overexpressing the *ftsQAZ* operon to improve expression of the Arabidopsis FtsZ proteins (Jeong and Lee, 2003). Rosetta cells were made chemically competent (Inoue et al., 1990). 200-400 ng of plasmid DNA was added to 100 µL of competent cells and allowed to incubate on ice for 30 minutes. The cells were placed in a water bath at 42°C and allowed to incubate for 90 sec. The cells were place on ice for 2 min before 900 µL of LB medium was added to each tube. The cells were then incubated at 37°C for 1 hr with shaking at 250 rpm. The cells were pelleted at 16,000*g* for 20 s and resuspended in 100 µL of LB medium. The cells were then plated on LB containing 100 µg/mL Carbenicillin, 100 µg/mL

Spectinomycin, and 25 µg/mL Chloramphenicol and allowed to grow at 37°C until colonies formed.

Protein expression and purification

Isolated colonies were used to inoculate 40 mL of LB with antibiotic selection (100 µg/mL Carbenicillin, 100 µg/mL Spectinomycin, and 25 µg/mL Chloramphenicol). These starter cultures were grown overnight at 37°C with shaking at 250 rpm. The next morning, the 40 mL starter culture was used to inoculate 800 mL of fresh LB with antibiotic selection (50 µg/mL Carbenicillin, 25 µg/mL Spectinomycin, 25 µg/mL Chloramphenicol). The expression cultures were incubated at 37°C with shaking at 250 rpm. When the OD_{600} reached 0.6-0.9, isopropyl β-D-thio-galactopyranoside was added to a final concentration of 600 µM. The expression cultures were then incubated at 14°C with shaking at 250 rpm for 36-40 hr. Cells were harvested by centrifugation at 8,000*g* for 20 minutes at 4°C. The supernatant was removed and the cell pellet from each 800 mL expression culture was resuspended in 20 mL of Extraction buffer (50 mM Tris-HCl, 300 mM NaCl, 10% glycerol, pH 8.0). The cell suspensions were frozen at -80°C until needed for purification.

The cells were thawed and lysozyme (LabScientific, Highlands, NJ) was added to a concentration of 1 mg/mL. The cells were incubated at 4°C with gentle rocking for 20 min. The cells were sonicated with a microtip sonicator for 4 intervals of 30 seconds with 5 min on ice between each interval. The sonicated solutions were centrifuged at 20,000*g* for 20 min at 4°C. The soluble fraction was collected and phenylmethanesulfonyl fluoride (PMSF, Sigma) was added to a final concentration of

1 mM. The cell supernatant was loaded onto 2 mL of Ni-NTA resin (Qiagen) already equilibrated into Extraction Buffer for 30 min with rocking at 4°C. The resin was washed with 2X with 15 mL of Extraction Buffer with 10 mM imidazole (Sigma) and 1% tween 20 (Fisher Scientific), 2X with 15 mL Extraction Buffer with 25 mM imidazole, and 1X with 15 mL of Extraction Buffer with 25 mM imidazole. The proteins were eluted from the Ni-NTA resin with 15 mL of Extraction Buffer with 300 mM imidazole and separated into 2 mL fractions. The first 5 2-mL elution fractions were pooled and dialyzed against HMK buffer (25 mM HEPES, 100 mM KCl, 5 mM $MgSO_4$, pH 7.0) 3X for 1 hr at 4°C with gentle stirring. The purified protein solution was centrifuged at 20,000*g* for 30 min at 4°C to remove insoluble proteins. Proteins were stored on ice for up to 2 weeks.

Assembly and TEM analysis

Each day the proteins were used for biochemical reactions, they were centrifuged at 52,000*g* for 20 min at 4°C to remove any aggregated or precipitated proteins before any assays were performed. Additionally, FtsZ concentration was measured with the bicinchoninic acid assay (BCA, ThermoFisher Scientific) immediately prior to assembly assays and TEM analysis.

FtsZ proteins were incubated at 5 μM total concentration in HMK buffer containing 0.5 mM GTP or GDP at room temperature. After 5 min, 5 μL of each reaction were pipetted onto a carbon-coated 400-mesh copper grid and stained with 2% aqueous uranyl acetate. Assembled structures were observed with a JEOL100 CXII (Japan Electron Optics Laboratories) transmission electron microscope at an

accelerating voltage of 100 kV. Transmission electron micrographs were acquired with an ORIUS Gatan camera and Gatan software (Gatan, Pleasanton, CA).

Chapter 5

Conclusions and Future Directions

Conclusions

Chloroplast FtsZs are cytoskeletal GTPases that drive the process of chloroplast division by the formation and subsequent constriction of the mid-plastid Z ring (Osteryoung and Pyke, 2014; TerBush et al., 2013). Although FtsZ1 and FtsZ2 always coassemble *in vivo*, they possess distinct functionality (McAndrew et al., 2001; Schmitz et al., 2009; Vitha et al., 2001). Much of the research on chloroplast FtsZs leading up to the work in this dissertation consisted of analysis of chloroplast morphology and FtsZ assembly patterns by light microscopy and immunolocalization, respectively, in various KO or overexpression mutants, Y2H assays to assess their interaction network, and *in vitro* biochemical analysis on purified FtsZs. My work sought to elucidate the distinct behaviors of FtsZ1 and FtsZ2 by analysis of their inherent filament assembly and turnover properties in the heterologous *S. pombe* expression system. Utilizing this system, I found that, in Chapter 2 (TerBush and Osteryoung, 2012), FtsZ1 and FtsZ2 proteins from Arabidopsis assemble filaments with distinct morphologies. FRAP experiments showed that FtsZ2 filaments are more stable than FtsZ1 filaments and that GTPase activity is critical for FtsZ2 subunit exchange but is likely not solely responsible for that of FtsZ1. When coexpressed, FtsZ1 and FtsZ2 coassembled into FtsZ2-like filaments and FtsZ1 enhanced the turnover of FtsZ2. These findings, combined with previous data, contributed to our understanding of how FtsZ1 and FtsZ2 proteins may work together to drive chloroplast division by suggesting that FtsZ2 serves as the main structural determinant of Z ring, while FtsZ1 enhances Z-ring remodeling, which has been shown to promote constriction of bacterial Z rings (Osawa and Erickson, 2011).

Following my work in Chapter 2, two main questions emerged that would constitute the rest of my graduate research. Firstly, the phylogenetically distinct FtsZ1 and FtsZ2 families are well-conserved among photosynthetic eukaryotes, and there has been very little research performed to characterize the function of FtsZ proteins from these diverse organisms (TerBush et al., 2013). Therefore, in Chapter 3, I performed a survey of filament assembly and turnover characteristics of FtsZ proteins from organisms among plants, green algae, red algae, and cyanobacteria. I found that the distinct filament morphological and turnover characteristics described for Arabidopsis FtsZ1 and FtsZ2 in Chapter 2 were conserved among FtsZs from the diverse organisms studied. These findings included distinct filament morphologies of the FtsZ1/FtsZB and FtsZ2/FtsZA proteins when expressed alone, FtsZ2/FtsZA morphological dominance over FtsZ1/FtsZB in coassembled filaments, the elevated turnover of FtsZ1/FtsZB filaments compared to those of FtsZ2/FtsZA, enhancement of GsFtsZA turnover when coassembled with GsFtsZB, and the dependency of FtsZ2/FtsZA, but not FtsZ1/FtsZB, proteins on GTPase activity for subunit exchange. I also performed the first characterization of a cyanobacterial FtsZ and found that its behavior is highly consistent with that of the FtsZ2/FtsZA family in plants and algae. These data suggest that the FtsZ1/FtsZB and FtsZ2/FtsZA families across photosynthetic eukaryotes maintain conserved roles in Z-ring assembly and constriction. Additionally, these data also support the evolutionary theory that green-lineage FtsZ2 and red-lineage FtsZA likely evolved from a single FtsZ in the common ancestor of chloroplasts.

Secondly, all FtsZ proteins maintain the conserved GTP-binding and hydrolysis domains responsible for assembly (Lowe and Amos, 1998; Oliva et al., 2004; Vaughan

et al., 2004). However, the N- and C-terminal regions flanking these domains show far less sequence conservation across FtsZ proteins from different organisms and between FtsZ1/FtsZB and FtsZ2/FtsZA proteins within a single organism (TerBush et al., 2013; Vaughan et al., 2004). Therefore, in Chapter 4, I examined the effect of the N- and C-terminal flanking regions on Arabidopsis FtsZ1 and FtsZ2 assembly, coassembly, and filament turnover. I found that FtsZ1 and FtsZ2 proteins lacking both their N- and C-termini displayed altered filament morphology and reduced lateral association into bundles when assembled *in vitro*. I also found that the N-terminal region of FtsZ2 is critical for its structural dominance over FtsZ1 in presumed heteropolymers. Finally, I showed that FtsZs lacking both their N- and C-terminal regions assemble filaments with reduced turnover properties that are much more similar to each other than filaments composed of their full-length counterparts are to each other. These data suggest that the N- and C-terminal regions promote polymer bundling and turnover, which are likely important for the association of individual FtsZ polymers to assemble into the higher-ordered Z ring and promote constriction activity (Li et al., 2007; Milam et al., 2012; Osawa and Erickson, 2011). More importantly, these regions also contribute to the distinct filament assembly and turnover properties of Arabidopsis FtsZ1 and FtsZ2, while not being solely responsible for them.

Future Directions

Taken together, the data presented within this dissertation have greatly enhanced our understanding of how FtsZ1 and FtsZ2 may work together to drive chloroplast division in diverse photosynthetic eukaryotes and begun to identify the structural features that promote their unique behaviors. While illuminating, these studies

generated many hypotheses and questions in regards to assembly, mechanisms of constriction, organization of chloroplast Z rings, and the relative stability of FtsZ interfaces within polymers. In this final chapter of my dissertation, I would like to outline future directions of FtsZ research that would answer many of the questions raised throughout my graduate research. The rest of my discussion on this topic will focus on two directions that chloroplast FtsZ research should go to cover FtsZ functionality more thoroughly. These aims include (1) mechanisms of Z-ring assembly and constriction and (2) regulation of FtsZ assembly and dynamics.

Mechanisms of Z-ring assembly and constriction

The first major hypothesis that came out of my research in Chapter 2 (TerBush and Osteryoung, 2012) and stated that the subunit interface between two Arabidopsis FtsZ1 proteins is weaker than the interface between two FtsZ2 proteins and is therefore more prone to breaking. FtsZ1 has been shown to possess greater GTPase activity than FtsZ2 (Olson et al., 2010; Smith et al., 2010), and GTPase activity is correlated with turnover dynamics of bacterial Z rings *in vivo* and polymers *in vitro* (Chen et al., 2007; Chen and Erickson, 2009; Huecas et al., 2007; Mukherjee and Lutkenhaus, 1998; Srinivasan et al., 2008). However, it is unlikely that GTPase activity plays the only role in determining subunit interface stability, as filaments composed of GTPase-deficient $FtsZ1_{D275A}$ retained a substantial amount of turnover while those composed of $FtsZ2_{D322A}$ were completely static (TerBush and Osteryoung, 2012). Therefore, comparison of FtsZ1-FtsZ1, FtsZ2-FtsZ2 and FtsZ1-FtsZ2 subunit interface stability is the logical follow-up experiment to test this hypothesis directly.

AlphaScreen™ (PerkinElmer®) is a new technology that can be used to assess the association between two proteins based on the proximity of “donor” and “acceptor” beads conjugated to proteins of interest. To gain insight into an isolated subunit interface, the effect of polymerization must be eliminated. Therefore, it would be advantageous in this context to perform this assay by purifying epitope-tagged N-terminal GTP-binding and C-terminal domains of chloroplast FtsZs ($FtsZ_N$ and $FtsZ_C$), which would only be able to form a single interface and not polymerize further. The more stable the FtsZ subunit interface is in the presence of GTP or a non-hydrolysable analog, the longer the beads will be held in proximity to each other before the interface breaks down and the larger the output signal from this assay. Therefore, a lower output reading for $FtsZ1_N$/$FtsZ1_C$ pairs than $FtsZ2_N$/$FtsZ2_C$, $FtsZ1_N$/$FtsZ2_C$, or $FtsZ2_N$/$FtsZ1_C$ pairs would indicate that the FtsZ1-FtsZ1 subunit interface is inherently weaker than interfaces between the other possible $FtsZ_N$/$FtsZ_C$ combinations. Additionally, AlphaScreen™ technology will be useful in determining the K_ds between the various subunit combinations of chloroplast FtsZs.

Alternatively, isothermal titration calorimetry (ITC) can be used to measure the heat of FtsZ self-association under various conditions, such as between the various possible $FtsZ_N$/$FtsZ_C$ combinations. Previously, ITC was performed to investigate whether *E. coli* FtsZ undergoes isodesmic or cooperative assembly (Caplan and Erickson, 2003). Differences in heat generated by association between $FtsZ_N$/$FtsZ_C$ proteins will give information on interface stability as well as potential assembly mechanisms. Another method by which to test for protein interface stability is by utilizing a Biacore system (GE Healthcare Life Sciences) and surface plasmon resonance. The

advantage of this system is that Biacore require no tagging of $FtsZ_N$ $FtsZ_C$ proteins and provides information on affinity and kinetics of association.

In Chapter 4, I found that filaments composed of various forms of FtsZ1 and FtsZ2 lacking their N- and/or C-termini showed reduced turnover compared to those composed of full-length FtsZ1 and FtsZ2. These data led to the hypothesis that the N- and C-terminal flanking regions of FtsZ1 and FtsZ2 promote filament turnover by destabilizing subunit interfaces between FtsZ proteins. Utilizing the AlphaScreen™ assay described above to assess the relative stability of interfaces between $FtsZ_N$ and $FtsZ_C$ with and without their N- and C-terminal flanking regions would serve as an excellent assay for testing this hypothesis. Additionally in Chapter 4, I showed that the N- and C-terminal regions promote the distinct assembly and turnover characteristics of FtsZ1 and FtsZ2. Generating domain-swapping constructs, where the N- and C-terminal regions of FtsZ1 on fused onto the GTP-binding and hydrolysis domains of FtsZ2, and vice versa, and analyzing their filament morphology and turnover characteristics would be an excellent follow-up experiment to support this conclusion.

Another critical area of future FtsZ research is further elucidating how FtsZ1 and FtsZ2 interact. For instance, I showed in Chapters 2 and 3 that FtsZ1 from Arabidopsis and FtsZB from *Galdieria sulphuraria* augment the turnover of AtFtsZ2 and GsFtsZA, respectively, in presumed heteropolymers (Fig. 2.6, Fig. 3.4 D & G-I). These data suggest that FtsZ1 proteins may be considered disassembly factors for FtsZ2s. Further experiments should focus on how FtsZ1 and FtsZ2 interact and the ability of FtsZ1 to reduce the extent of assembly of FtsZ2 *in vitro*. For example, FRAP data on coassembled heterologous FtsZ pairs in *S. pombe* showing that AtFtsZ1 augments

GsFtsZA and GsFtsZB augments AtFtsZ2 turnover would suggest that the interaction between FtsZ1/FtsZB and FtsZ2/FtsZA resulting in increased FtsZ2/FtsZA turnover is not dependent on any specific interaction between the two proteins. Similar experiments combining FtsZ1 and FtsZ2 proteins from different species to assess FtsZ2 dominance over heteropolymer morphology would also suggest such a mechanism. Additionally, the extent of assembly may be measured by light scattering, as our lab performed previously (Olson et al., 2010). If FtsZ1 reduces the extent of FtsZ2 assembly, then spiking FtsZ1 into preassembled FtsZ2 would result in a reduced signal output in light scattering assays following similar kinetics to what I observed for heteropolymer turnover in *S. pombe*. However, the data from this assay are influenced by the occurrence of bundling. Therefore, a reduction in signal could be the result of either reduced bundling or longitudinal assembly. Another option to isolate the longitudinal interaction between FtsZ proteins is by monitoring changes in fluorescence of a tryptophan residue buried in the nucleotide-binding site of FtsZ to measure assembly kinetics, which has previously been used to study the assembly kinetics of *E. coli* FtsZ (Chen et al., 2005). In addition to monitoring the extent of FtsZ2 assembly, aliquots for transmission electron microscopy (TEM) analysis will be taken at specific time points and FtsZ1 concentrations, determined from the light scattering assays, to visually inspect any changes in assembled structures. For example, a dose-dependent reduction in bundle width and/or length or increase in bundle splitting with increasing FtsZ1 concentration would support the hypothesis that FtsZ1 stimulates FtsZ2 disassembly.

One of the main questions in chloroplast FtsZ research is the composition of FtsZ heteropolymers. Unlike tubulins, which assemble strictly at a one-to-one ratio, some data suggest that chloroplast FtsZ1 and FtsZ2 display variability in the ratios at which they coassemble (Olson et al., 2010). However, these experiments need to be followed up to revisit the preferred composition of heteropolymers. The AlphaScreen^{TM} assay should provide an excellent platform for this analysis. The $FtsZ_N$ and $FtsZ_C$ half-proteins I discussed above will serve as the 100% heterodimer control, while assembling full-length FtsZ1 or FtsZ2 homopolymers, with an equal proportion of each FtsZ conjugated to the donor and acceptor beads, will serve as the random composition control. By mixing full-length FtsZ1 conjugated to the donor and FtsZ2 conjugated to the acceptor, or vice versa, analyzing where the output signal intensity falls on the spectrum between the 100% dimer and random distribution controls will provide the first direct evidence of heteropolymer organization. However, full-length FtsZ1 and FtsZ2 heteropolymers have been shown to assemble large bundles (Olson et al., 2010), which may skew the results from this analysis. Therefore, using proteins that have severely inhibited bundling activity, such as the $FtsZ1_{\Delta NCT}$ and $FtsZ2_{\Delta NCT}$ forms I analyzed by TEM in Chapter 4 (Fig. 4.5 C-D), will minimize the effect of bundling on this assay.

While the characteristics of FtsZ filament assembly and turnover are of great interest, the ultimate questions regard Z-ring functionality. For example, the observation that FtsZ1 augments FtsZ2 turnover in presumed heteropolymers in *S. pombe* led to the hypothesis that altering Z-ring composition may be a mechanism by which Z-ring constriction is modulated (TerBush and Osteryoung, 2012). While FtsZ1 and FtsZ2 always colocalize *in planta* when both are present and their molar ratios do not change

over development in whole rosettes, which is contradictory the idea that the two FtsZs may be present in Z rings at variable ratios (McAndrew et al., 2001; Vitha et al., 2001; McAndrew et al., 2008), this model poses an appealing mechanism for controlling Z-ring activity. Therefore, investigations into the effect of altering the ratio between FtsZ1 and FtsZ2 on Z-ring assembly and constriction will help to elucidate the workings of Z rings.

Recent *in vitro* work on *E. coli* FtsZ fused to a membrane-associating peptide showed that it assembles Z rings on tubular liposomes and generates contractile force without the presence of any additional proteins (Osawa et al., 2008; Osawa and Erickson, 2011). This system presents an excellent method to generate the first direct evidence to support or negate the hypothesis that altering the ratio of FtsZ1 to FtsZ2 modulates Z-ring assembly and force generation. For example, I expect FtsZ2 alone to form stable Z rings with low turnover and therefore slow rates contractile activity. As the ratio of FtsZ1 increases, I expect Z-ring remodeling to increase and therefore increase the rate of constriction, but not necessarily generation of more constriction force resulting in deeper levels of deforming the liposome membrane, as this may be an inherent property of the structure-determining FtsZ2. One beneficial technical aspect of this experiment is that the low rate of GTP hydrolysis of FtsZ1 and FtsZ2 will provide ample time to find and image Z-rings before the GTP is used up and Z rings disassemble.

FtsZ2 has been shown to assemble Z rings in small chloroplasts in *ftsZ1* null plants (Yoder et al., 2007). However, this rarely occurs, as the majority of chloroplasts in this mutant background are severely enlarged, indicating that FtsZ2 is not sufficient for driving normal chloroplast division on its own. Additionally, the ratio of FtsZ1 to FtsZ2

has previously been shown to remain at a constant 1:2 ratio in whole rosettes of Arabidopsis throughout development (McAndrew et al., 2008). However, it remains unknown whether or not the ratio between FtsZ1 and FtsZ2 changes in individual chloroplasts or Z rings during development or throughout a single contractile cycle. Therefore, investigation into *in planta* FtsZ levels is of great importance for addressing the hypothesis that altering the ratio between FtsZ1 and FtsZ2 in Z rings is a mechanism to modulate Z-ring constriction.

Through the course of my graduate studies, I have complemented the Arabidopsis *ftsZ1* KO mutant with an FtsZ1-mCerulean construct, where single mid-plastid Z rings can be seen by epifluorescence microscopy (Fig. 2.1 A-C). Furthermore, I have generated an FtsZ2-mCerulean construct that nearly complements the *ftsZ2-1* KO mutant and possesses single mid-plastid Z rings in chloroplasts of normal size (data not shown). I created these stable transgenic lines in order to perform quantitative imaging to compare the relative levels of FtsZ1 and FtsZ2 in chloroplasts and Z rings at different developmental stages and at different points during the constriction process, as well as assess FtsZ1 and FtsZ2 turnover properties *in planta*. While these Z rings can be readily visualized and imaged by epifluorescence microscopy (Fig. 2.1 C), imaging by confocal laser scanning microscopy is highly challenging due to poor signal-to-noise ratios resulting from FtsZ fusions expressed at low levels from their native promoter amid chlorophyll autofluorescence, especially for time-course imaging needed to analyze the turnover properties of these fluorescently tagged FtsZs. These issues can be mitigated by increasing the signal-to-noise ratio by either selecting a brighter and more stable fluorescence tag, such as msfGFP, or by improving the optics on the

confocal microscope used for quantitative imaging. The Center for Advanced Microscopy at Michigan State University has recently acquired a Nikon A1Rsi super resolution confocal laser scanning microscope (CLSM), which has a more sensitive PMT and should improve the signal-to-noise ratio in these transgenic lines. However, imaging fusions to mCerulean requires excitation with a 458 nm laser, which activates the blue-light-induced chloroplast avoidance response and makes time-course imaging much more difficult in live cells. Therefore, changing to the msfGFP fluorescent tag would mitigate that challenge as well.

Regulation of FtsZ assembly and dynamics

ARC3 is a critical component for regulating Z-ring assembly and positioning (Shimada et al., 2004). Although ARC3 had already been shown to interact with FtsZ1 by Y2H and bimolecular fluorescence complementation (BiFC) experiments (Maple et al., 2007; Zhang et al., 2013), my work in Chapter 2 was the first to show that ARC3 lacking its membrane occupation and recognition nexus (MORN) domain directly antagonizes the assembly of FtsZ1 (TerBush and Osteryoung, 2012). Soon after, follow-up Y2H and *S. pombe* coexpression experiments showed that ARC3 interacts with and antagonizes the assembly of FtsZ2 as well (Zhang et al., 2013). While these experiments were a major step forward in elucidating the function of ARC3, the mechanism by which it interacts with FtsZ1 and FtsZ2 was still not well understood. ARC3 is a chimeric protein with an N-terminal FtsZ-like region and the C-terminal MORN domain (Shimada et al., 2004). The presence of the FtsZ-like domain suggests that ARC3's mechanism of action is integration into FtsZ polymers through interaction with the GTP-binding and hydrolysis domains to disrupt normal assembly. ARC3 has

also been shown to antagonize the assembly of *E. coli* FtsZ (Zhang et al., 2013), supporting this hypothesis. However, ARC3 lacks many of the conserved GTP-binding and hydrolysis motifs conserved across bacterial and eukaryotic FtsZs, and is therefore unlikely to bind and hydrolyze GTP (Shimada et al., 2004). Additionally, ARC3 also has a ~10 amino acid insertion in the "T7" loop that may interfere with interaction with the top interface of FtsZs, suggesting that ARC3 may act as a capping protein and thereby inhibit assembly. However, a recent study showed that FtsZ1 and FtsZ2 turnover in chloroplast Z rings is stabilized in the absence of ARC3, suggesting that ARC3 functions by destabilizing FtsZ polymers and not inhibiting their assembly (Johnson et al., 2015). Further research into whether or not ARC3 functions by preventing FtsZ assembly or destabilizing FtsZ polymers *in vitro* will shed light onto the mechanism by which ARC3 acts on FtsZ. For example, addition of ARC3 into reactions containing preassembled FtsZ polymers being monitored by light scattering or tryptophan fluorescence will result in a reduction in assembly signal in a dose-dependent manner if ARC3 induces breakdown of FtsZ structures. Additionally, initiating FtsZ assembly in the presence and absence of ARC3 will yield insight into whether ARC3 functions by inhibiting FtsZ polymerization.

Further investigation into the interaction network that recruits and activates ARC3 should also be performed. As indicated above, previous work has established that ARC3 lacking the MORN domain ($ARC3_{41-598}$) interacts with and antagonizes the assembly of both FtsZ1 and FtsZ2 (TerBush and Osteryoung, 2012; Zhang et al., 2013). However, Y2H assays have shown that full length ARC3 does not interact with FtsZ1 or FtsZ2 but interacts with Paralog of ARC6 (PARC6) (Glynn et al., 2009; Zhang et al.,

2013; Zhang, Chen et al., 2015). From these data, we hypothesized that PARC6 interacts with and sequesters the MORN domain of ARC3, thereby activating ARC3 for its regulatory activity on FtsZ. Reconstituting this interaction network in *S. pombe* represents an excellent method to test this hypothesis. Utilizing coexpression plasmids I described in Appendix A (Fig. A.5 A), we will express FtsZ1 and/or FtsZ2 with full length ARC3 or $ARC3_{41\text{-}598}$ in the presence and absence of the stromal domain of PARC6. Inhibited FtsZ assembly in the presence of ARC3 with PARC6 but no inhibition in the presence of ARC3 without PARC6 would be strong evidence supporting the role of PARC6 in sequestering ARC3's MORN domain to activate ARC3 to antagonize the assembly of FtsZ. The negative control experiment will be full-length ARC3 coexpressed with FtsZ1 and/or FtsZ2, while FtsZ1 and/or FtsZ2 coexpressed with $ARC3_{41\text{-}598}$ will serve as the positive control.

In contrast to the negative regulatory effect of ARC3, ARC6 has been shown by genetic experiments to be a positive regulator of FtsZ assembly and a critical component of the chloroplast division complex through its interaction with FtsZ2 (Maple et al., 2005; Pyke et al., 1994; Vitha et al., 2003). After visualization of FtsZ assembly in *arc6* null and overexpression lines, ARC6 was hypothesized to stabilize FtsZ polymers, potentially through tethering the Z ring to the chloroplast inner envelope membrane (Vitha et al., 2003). In Appendix A, I showed that FtsZ2 filaments in the presence of the stromal domain of ARC6 ($ARC6_{68\text{-}614}$) are more stable than those in the absence of $ARC6_{68\text{-}614}$. These data show that ARC6 stabilizes FtsZ2 filaments directly without the need for membrane association (Fig. A.4 & Fig. A.5) and suggest that FtsZ2 filament stabilization is due to increased lateral packing of polymers within the bundle. Additional

experiments to test the mechanism by which ARC6 stabilizes FtsZ2 filaments should be performed. One possibility is that ARC6 stabilizes the subunit interface of FtsZ2. In this case, any stabilization of this interface would result in a reduction in FtsZ2 GTPase activity. Therefore, assessing FtsZ2 GTPase activity in the presence and absence of $ARC6_{68\text{-}614}$ will yield insight into this hypothesis. Similarly, performing the AlphaScreen™ experiment with $FtsZ2_N$ and $FtsZ2_C$ half-proteins in the presence and absence of $ARC6_{68\text{-}614}$ may also yield data on any ARC6-induced subunit interface stabilization. In contrast, the effect of $ARC6_{68\text{-}614}$ on FtsZ2 assembled structures should be assessed. Inducing assembly of FtsZ2 in the presence and absence of $ARC6_{68\text{-}614}$ and observing assembled structures by TEM will show any major rearrangements of FtsZ2 bundles.

Summary

My work throughout this dissertation has substantially enhanced our understanding of how FtsZ1 and FtsZ2 drive chloroplast division. The findings in Chapter 2 (TerBush and Osteryoung, 2012) led to the first proposed roles of the FtsZ1 and FtsZ2 families in chloroplast division. My work in Chapter 3 served to further elucidate the evolution and conservation of the phylogenetically distinct FtsZ1/FtsZB and FtsZ2/FtsZA families. I also presented the first characterization of a cyanobacterial FtsZ, which provided functional data to support the evolution of the FtsZ2 and FtsZA families from the cyanobacterial endosymbiont FtsZ and subsequent evolution of the FtsZ1 and FtsZB families through gene duplication events. My work in Chapter 4 provided insight into the regions of FtsZs that govern their assembly and turnover properties and showed that the N- and C-terminal regions contribute to the distinct behaviors of FtsZ1 and FtsZ2, while not being solely responsible for them. My work in

this dissertation has also contributed to our understanding of the mechanisms by which Z-ring assembly and dynamics are regulated. In Chapter 2 (TerBush and Osteryoung, 2012), I showed for the first time that ARC3 directly antagonizes FtsZ1 assembly. In Appendix A, I showed that ARC6 stabilizes FtsZ2 filaments in the absence of its proposed *in planta* membrane-tethering function. These studies have also established the *S. pombe* heterologous expression system as a useful and robust tool for assessing the inherent filament assembly and dynamic properties of chloroplast FtsZ1 and FtsZ2 and the mechanisms by which they are regulated. This system will likely be broadly useful for the analysis of other cytoskeletal elements from prokaryotes and other organelles as well. Finally, the data presented within these studies have laid much groundwork for future research into the activity of chloroplast FtsZs, including generating several testable hypotheses on FtsZ polymer stability, Z-ring organization, mechanisms of generating constriction force, and mechanisms by which FtsZ assembly is regulated.

Appendix

Functional Analysis of the Chloroplast Division Complex Using

Schizosaccharomyces pombe as a Heterologous Expression System

This research has been submitted to *Microsc Microanal* for publication in a special Plant Biology issue due to be published in spring of 2016.

Minor edits have been made to this manuscript to conform to dissertation formatting requirements and Figure callouts.

The *pREP41X-ARC6*$_{68\text{-}614}$*-mVenus* expression construct was generated and imaged by Chris Porzondek, Biochemistry and Molecular Biology and Neuroscience Undergraduate Programs at Michigan State University.

Abstract

Chloroplast division is driven by a macromolecular complex that assembles at the mid-plastid. The central structure in this complex is the cytoskeletal FtsZ ring (Z ring), which is composed of the functionally distinct proteins FtsZ1 and FtsZ2. Recent studies in the heterologous *Schizosaccharomyces pombe* system showed that Arabidopsis FtsZ1 and FtsZ2 polymers have distinct assembly and turnover characteristics. To further analyze these FtsZs, we employed this system to compare the assembly and dynamic properties of FtsZ1 and FtsZ2 lacking their divergent N- and C-termini with those of their full-length counterparts. Our data provide evidence that the N- and C-termini promote polymer bundling and turnover in both FtsZs, but that they also contribute to the distinct behaviors of FtsZ1 and FtsZ2 filaments. We also assessed the effect of the FtsZ2 binding protein ARC6 on FtsZ2 polymer dynamics, and found that ARC6 interacts with and stabilizes FtsZ2 filaments in *S. pombe* independent of its presumed Z-ring tethering function *in planta*. Finally, we generated FtsZ1-FtsZ2 coexpression constructs to facilitate reconstitution of more complex interaction networks. Our experiments yield new insight into factors influencing FtsZ assembly and dynamics and highlight the utility of *S. pombe* for analysis of chloroplast FtsZs and their assembly regulators.

Introduction

Chloroplasts arose from the endosymbiosis of an ancient cyanobacterium and are present in high numbers in several green tissues of plants (Gould et al., 2008). To maintain these high population numbers as plant cells grow and divide, chloroplasts undergo growth and binary fission, where a constriction forms at the chloroplast midpoint and narrows until the two daughter chloroplasts are formed (Osteryoung and Pyke, 2014). Chloroplast division is driven by a large macromolecular complex that includes the formation of ring structures on both the stromal and cytosolic sides of the chloroplast membranes (Osteryoung and Pyke, 2014). Consistent with chloroplasts' origin from an engulfed cyanobacterium by a heterotrophic eukaryote, many of the division proteins in the chloroplast interior (stroma) are homologs of bacterial cell division components. However, over evolutionary time, chloroplasts have acquired additional division proteins of eukaryotic origin.

The centerpiece of the chloroplast division machinery is the cytoskeletal protein FtsZ, which assembles into the mid-plastid FtsZ ring (Z ring). The Z ring establishes the chloroplast division site and likely provides at least some of the constriction force in the early stages of chloroplast division, as shown for bacterial Z rings (Osawa et al., 2008). The chloroplast Z ring is composed of two functionally distinct FtsZ isoforms, FtsZ1 and FtsZ2 (Miyagishima et al., 2001; Osteryoung et al., 1998; Osteryoung and Vierling, 1995; Schmitz et al., 2009; Vitha et al., 2001). FtsZ1 and FtsZ2 are tubulin-like GTPases that are capable of self-assembly as homopolymers *in vitro* but are always colocalized *in vivo* and preferentially coassemble into heteropolymers *in vitro* (El-Kafafi

et al., 2005; Lohse et al., 2006; McAndrew et al., 2001; Olson et al., 2010; Smith et al., 2010; Vitha et al., 2001). Several stromal regulatory proteins of both bacterial and eukaryotic origin function together to antagonize FtsZ assembly at the chloroplast poles, thereby only allowing Z-ring formation at the chloroplast midpoint (Colletti et al., 2000; Glynn et al., 2009; Itoh et al., 2001; Maple et al., 2002; Nakanishi et al., 2009; Shimada et al., 2004; Zhang et al., 2013). Although FtsZ1 and FtsZ2 are soluble proteins in the chloroplast stroma, Z rings are tethered to the chloroplast membrane via interaction of FtsZ2 with the integral membrane protein ARC6 (Glynn et al., 2008; Maple et al., 2005; Schmitz et al., 2009; Vitha et al., 2003). ARC6 plays a major role in coordinating the stromal Z ring and cytosolic dynamin-like DRP5B ring across the envelope membranes (Gao et al., 2003; Glynn et al., 2008).

Much work has gone into understanding the interactions between the chloroplast division components as well as their mechanistic functions. Most of our understanding has come from various genetic experiments observing chloroplast morphology by light microscopy and FtsZ assembly patterns by immunofluorescence microscopy in various mutant backgrounds, and from yeast two-hybrid and other interaction assays to elucidate the interaction networks (Glynn et al., 2008; Glynn et al., 2009; Maple et al., 2005; Maple et al., 2007; Marrison et al., 1999; McAndrew et al., 2001; Miyagishima et al., 2001; Mori et al., 2001; Osteryoung et al., 1998; Schmitz et al., 2009; Vitha et al., 2003; Vitha et al., 2001; Yoshida et al., 2010; Zhang et al., 2013). One of the necessary next steps is analysis of the division proteins in live cells to assess the mechanistic function of each and understand how these proteins work together to drive division.

Conducting such experiments *in planta* requires fluorescence microscopy of tagged chloroplast division components, which can be challenging for several reasons, including the intolerance of some division components to fluorescent protein tagging, sensitivity of chloroplast division to altered levels of division proteins, transgene instability, long generation times, weak fluorescence signals from constructs driven by native promoters amid high background noise due to chlorophyll autofluorescence, and chloroplast movement in response to illumination on a microscope. An expression system in a cellular environment in which analysis of the inherent behaviors of FtsZ1 and FtsZ2 could be easily observed, as well as how FtsZ1 and FtsZ2 properties are modulated by various regulatory proteins, can enhance our understanding of chloroplast division mechanisms.

Srinivasan et al. (2008) expressed various bacterial FtsZs as fluorescent fusions in the fission yeast *Schizosaccharomyces pombe* and studied their polymer assembly and dynamic properties. They found that FtsZ from *Escherichia coli* and *Mycobacterium tuberculosis* assembled filaments in the yeast cytosol that displayed turnover characteristics consistent with previous *in vivo* and *in vitro* findings (Anderson et al., 2004; Chen et al., 2007; Chen and Erickson, 2005), suggesting that FtsZ behavior in *S. pombe* accurately reflects its *in vivo* behavior. This study paved the way for TerBush and Osteryoung (2012) to study *Arabidopsis thaliana* FtsZ1 and FtsZ2 in fission yeast, where they found that FtsZ1 and FtsZ2 have distinct filament morphology and turnover characteristics. Their data, viewed in the context of prior genetic studies (Osteryoung et al., 1998; Schmitz et al., 2009; Yoder et al., 2007), suggested that FtsZ2 is the structural

determinant for chloroplast Z rings while FtsZ1 promotes Z-ring constriction by enhancing turnover. Additional experiments in fission yeast were instrumental in establishing that the FtsZ-positioning factor ARC3 acts to directly antagonize FtsZ assembly (TerBush and Osteryoung, 2012; Zhang et al., 2013). These initial studies have shown fission yeast to be a robust tool for analysis of FtsZ organization and dynamics, and provided evidence on how chloroplast division regulatory proteins modulate FtsZ behavior. *S. pombe* cells can be grown quickly and are easily transformed, and, as *S. pombe* and chloroplasts share no division components, individual chloroplast division proteins can be studied in isolation or in combination with specific regulatory proteins in a cellular environment. Thus *S. pombe* can be a valuable complement to other experimental tools for elucidating the functions and interactions of the chloroplast division components.

Here, we utilize *S. pombe* to analyze the role of specific regions of FtsZ1 and FtsZ2 on their filament morphology and turnover characteristics as well as assessing the effect ARC6 has on FtsZ2 filament stability. These studies illustrate that the N- and C-terminal regions of FtsZ1 and FtsZ2 promote lateral interactions and polymer turnover, while ARC6 directly stabilizes FtsZ2 polymers in the absence of its membrane tethering function. We also discuss technical limitations and advantages of performing experiments in fission yeast.

Results

Effect of N- and C-terminal truncations on FtsZ filament morphology

FtsZs possess a highly conserved GTP-binding and hydrolysis domain and N- and C-terminal regions with far less sequence conservation (TerBush et al., 2013; Vaughan et al., 2004). We hypothesized that the poorly conserved N- and C-terminal flanking regions play a role in determining the distinct behavior of FtsZ1 and FtsZ2. Therefore, we compared the polymer assembly characteristics of chloroplast FtsZs lacking the N- and C-terminal regions with those of full length FtsZs expressed in *S. pombe*. Full-length FtsZ1 lacking its predicted transit peptide (amino acids 58-433) (Olson et al., 2010) and the truncated form of FtsZ1 (amino acids 74-377) were fused at their C-termini to mVenus, a monomeric version of the yellow fluorescence protein, to create $FtsZ1_{58-433}$-mVenus and $FtsZ1_{74-377}$-mVenus. The equivalent FtsZ2 proteins were fused at their C-termini to mCerulean, creating $FtsZ2_{49-478}$-mCerulean and $FtsZ2_{119-424}$-mCerulean. Consistent with previous experiments in *S. pombe* (TerBush and Osteryoung, 2012), $FtsZ1_{58-433}$-mVenus assembled multiple cables, presumably representing bundles of individual polymers (Erickson et al., 2010; Mukherjee and Lutkenhaus, 1999; Popp et al., 2009), that looped around the cell and annealed to form large rings conforming to the interior compartment of the yeast cell (Fig. A.1 A). These cables displayed minimal fraying of smaller filaments from the main cable structure. $FtsZ1_{74-377}$-mVenus also assembled multiple long filaments that looped around the cell, but these filaments were frequently frayed into several loosely associated filaments,

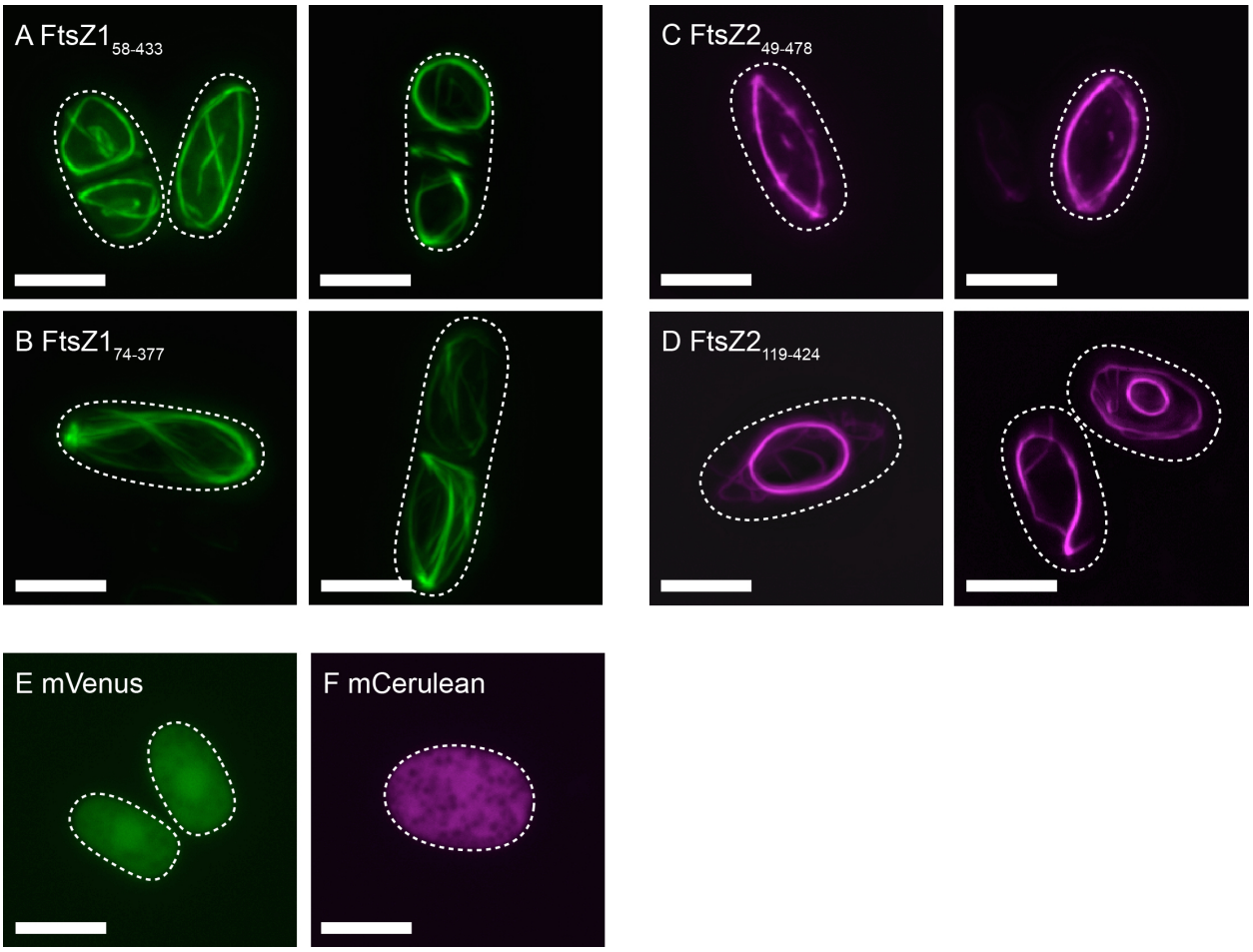

Figure A.1: Polymer morphologies of full-length FtsZ1 and FtsZ2 and constructs lacking their N- and C-terminal regions in *S. pombe*. Epifluorescence micrographs of (A) FtsZ1$_{58-433}$-mVenus, (B) FtsZ1$_{74-377}$-mVenus, (C) FtsZ2$_{49-478}$-mCerulean, (D) FtsZ2$_{119-424}$-mCerulean, (E) mVenus, and (F) mCerulean fluorescence signals in expressing yeast cells. FtsZ1$_{58-433}$-mVenus, FtsZ1$_{74-377}$-mVenus, and mVenus fluorescence signals are falsely colored green. FtsZ2$_{49-478}$-mCerulean, FtsZ2$_{119-424}$-mCerulean, and mCerulean fluorescence signals are falsely colored magenta. Dotted line represents the cell outline. Bars, 5 µm.

suggesting a reduced level of lateral interactions and bundling between individual polymers (Fig. A.1 B).

FtsZ2$_{49-478}$-mCerulean assembled large rings and an overall even fluorescence distribution along the ring structure (Fig. A.1 C). Similar to FtsZ1$_{58-433}$-mVenus, the dimensions of these rings appeared to be controlled by the interior dimensions of the yeast cell. FtsZ2$_{119-424}$-mCerulean also assembled large rings, but these possessed cross-linking filaments, areas of loose bundling with smaller filaments splitting from the main structure, and small rings roughly 2 μm in diameter (Fig. A.1 D). In control experiments, unfused mVenus and mCerulean displayed completely diffuse localization patterns (Fig. A.1 E-F).

Effect of N- and C-terminal truncations on steady-state turnover of FtsZ polymers

Another important aspect of FtsZ behavior is dynamic, steady-state turnover of polymers (Anderson et al., 2004; Chen and Erickson, 2005; Osawa and Erickson, 2011; Srinivasan et al., 2008; Stricker et al., 2002). Therefore, we performed fluorescence recovery after photobleaching (FRAP) experiments on the full-length and truncated forms of FtsZ examined above to determine the effect the N- and C-terminal regions have on FtsZ polymer turnover. The fluorescence signal in FtsZ1$_{58-433}$-mVenus filaments exhibited an average recovery half-time ($t_{1/2}$) of 51 s and a maximum percent recovery of 53% of the pre-bleach intensity (n = 16 cells, Fig. A.2 A). The truncated FtsZ1$_{74-377}$-mVenus was less dynamic, with a $t_{1/2}$ of 93 s and a maximum recovery of 37% (n = 14, Fig. A.2 B). For FtsZ2$_{49-478}$-mCerulean, the fluorescence signal recovered with a $t_{1/2}$ of 67 s and to 13% of the pre-bleach intensity (n = 16, Fig. A.2 C). FtsZ2$_{119-424}$-mCerulean

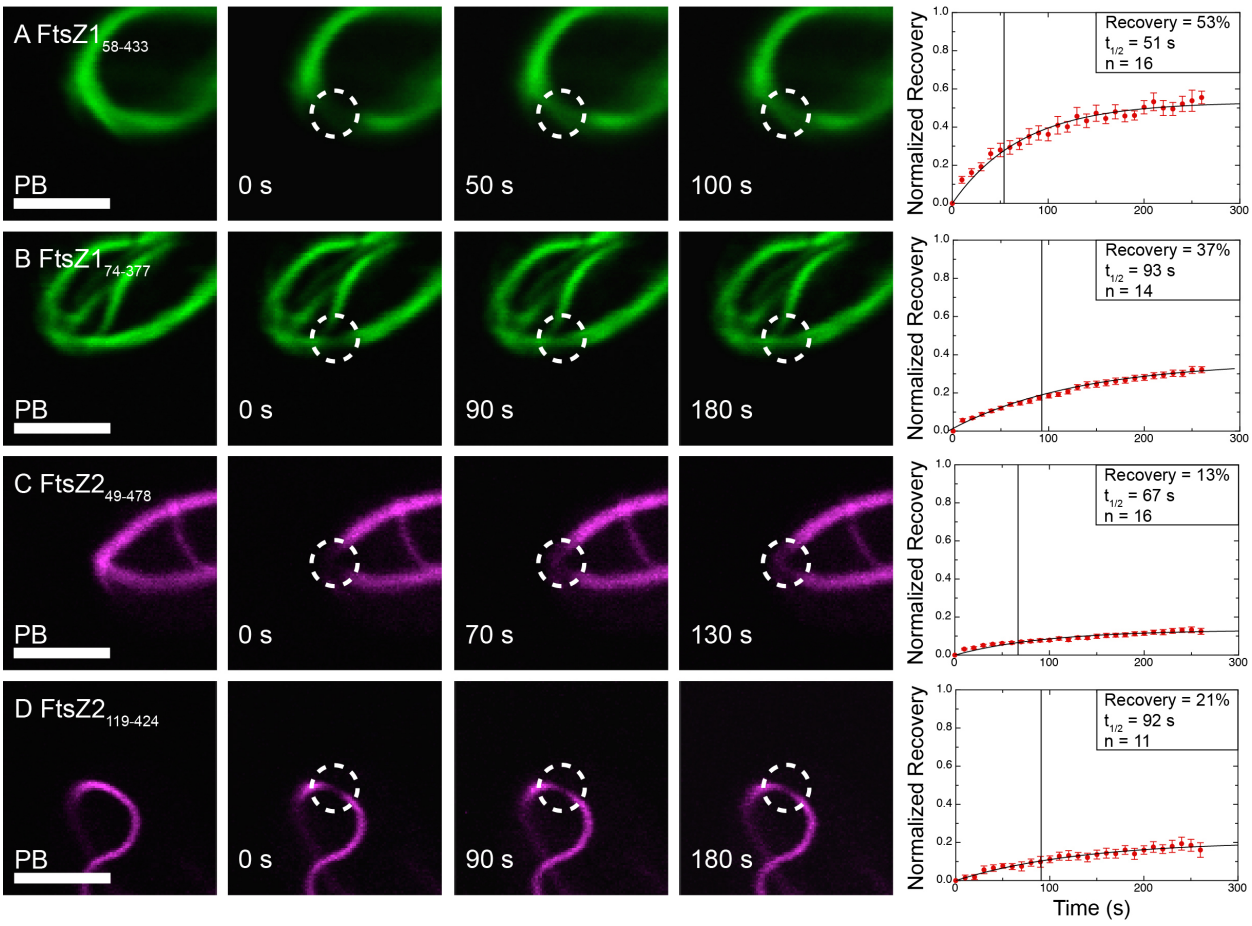

Figure A.2: Analysis of polymer dynamics for FtsZ1 and FtsZ2 proteins lacking their N- and C-terminal regions. Cells expressing (A) $FtsZ1_{74\text{-}377}$-mVenus and (B) $FtsZ2_{119\text{-}424}$-mCeruelan were analyzed by FRAP. From left to right, the panels represent the fluorescence intensity in the bleached region (dashed circle) prior to bleaching (PB), at the time of bleaching (0 s), at the time closest to $t_{1/2}$, and at the time closest to twice that of $t_{1/2}$. The graphs to the right show the normalized average fluorescence recovery vs time (s). The data are normalized to the pre-bleach fluorescence intensity (1 on the y-axis) and the fluorescence intensity at the time of bleaching (0 on the y-axis). The data in the box are the calculated maximum fluorescence recovery and $t_{1/2}$ (also represented by the vertical bar) as well as the number of independent FRAP

Figure A.2 (cont'd): experiments performed (N). The red brackets represent SEM at each time point. The FtsZ1$_{74-377}$-mVenus and FtsZ2$_{119-424}$-mCeruelan fluorescence signals are falsely colored green and magenta, respectively. Bars, 2 μm.

recovered with a $t_{1/2}$ of 92 s and to a maximum of 21% (n = 11, Fig. A.2 D). The slower recovery rates for the truncated proteins relative to those of their full-length counterparts, as well as the decreased extent of recovery of FtsZ1$_{74-377}$-mVenus compared to that of FtsZ1$_{58-433}$-mVenus, indicate that FtsZ1$_{74-377}$-mVenus and FtsZ2$_{119-424}$-mCerulean homopolymers are more stable than those composed of the full-length proteins. These data suggest that the N- and/or C-terminal regions of FtsZ1 and FtsZ2 directly promote polymer turnover. All FRAP data are summarized in Table A.1.

Protein	$t_{1/2}$ (s)	% Recovery	n
FtsZ1$_{58-433}$-mVenus	51	53%	16
FtsZ1$_{74-377}$-mVenus	93	37%	14
FtsZ2$_{49-478}$-mCerulean	67	13%	16
FtsZ2$_{119-424}$-mCerulean	92	21%	11
ARC6$_{68-614}$-mVenus + FtsZ2$_{49-478}$-eCFP	64	44%	14
	130	28%	11

Table A.1: Summary of FRAP data from all single and coexpression strains. Time for the normalized and averaged half-time of recovery ($t_{1/2}$, s) and maximum percent recovery for each protein in each expression strain. n represents the number of independent FRAP experiments performed on each protein in each expression strain.

Effect of ARC6 on FtsZ2 filament dynamics

The chloroplast division complex includes over a dozen different protein components that form an intricate interaction network (Osteryoung and Pyke, 2014). Several of the stromal proteins directly interact with and regulate the assembly of FtsZ1 and FtsZ2. One such critical interaction is between FtsZ2 and ARC6, an inner envelope transmembrane protein that interacts specifically with FtsZ2 and is thought to tether the Z ring to the membrane (Glynn et al., 2008; Maple et al., 2005; Vitha et al., 2003). Previous genetic experiments in Arabidopsis suggest that ARC6 promotes assembly of and stabilizes FtsZ polymers at the division site (Vitha et al., 2003). However, these conclusions came from immunolocalization of FtsZ2 in fixed leaves in *arc6* null and ARC6 overexpression lines. To further investigate the effect of ARC6 on FtsZ2 polymer stability, we coexpressed the stromal region of ARC6 (Vitha et al., 2003) fused at its C terminus to mVenus ($ARC6_{68\text{-}614}$-mVenus) with full length FtsZ2 C-terminally fused to eCFP ($FtsZ2_{49\text{-}478}$-eCFP) (TerBush and Osteryoung, 2012) and analyzed $FtsZ2_{49\text{-}478}$-eCFP polymer morphology and steady-state turnover characteristics. When expressed independently, $ARC6_{68\text{-}614}$-mVenus adopted a completely diffuse localization pattern (Fig. A.3 A), while $FtsZ2_{49\text{-}478}$-eCFP assembled an intricate network of interconnected filaments (Fig. A.3 B), as described previously (TerBush and Osteryoung, 2012). When $ARC6_{68\text{-}614}$-mVenus and $FtsZ2_{49\text{-}478}$-eCFP were coexpressed, they colocalized into a network of interconnected filaments with a Pearson's Correlation Coefficient (PCC) of 0.92 ± 0.01 (mean ± SEM, n = 18, Fig. A.3 C), consistent with previous yeast two-hybrid and biomolecular fluorescence complementation assays (Glynn et al., 2009; Maple et

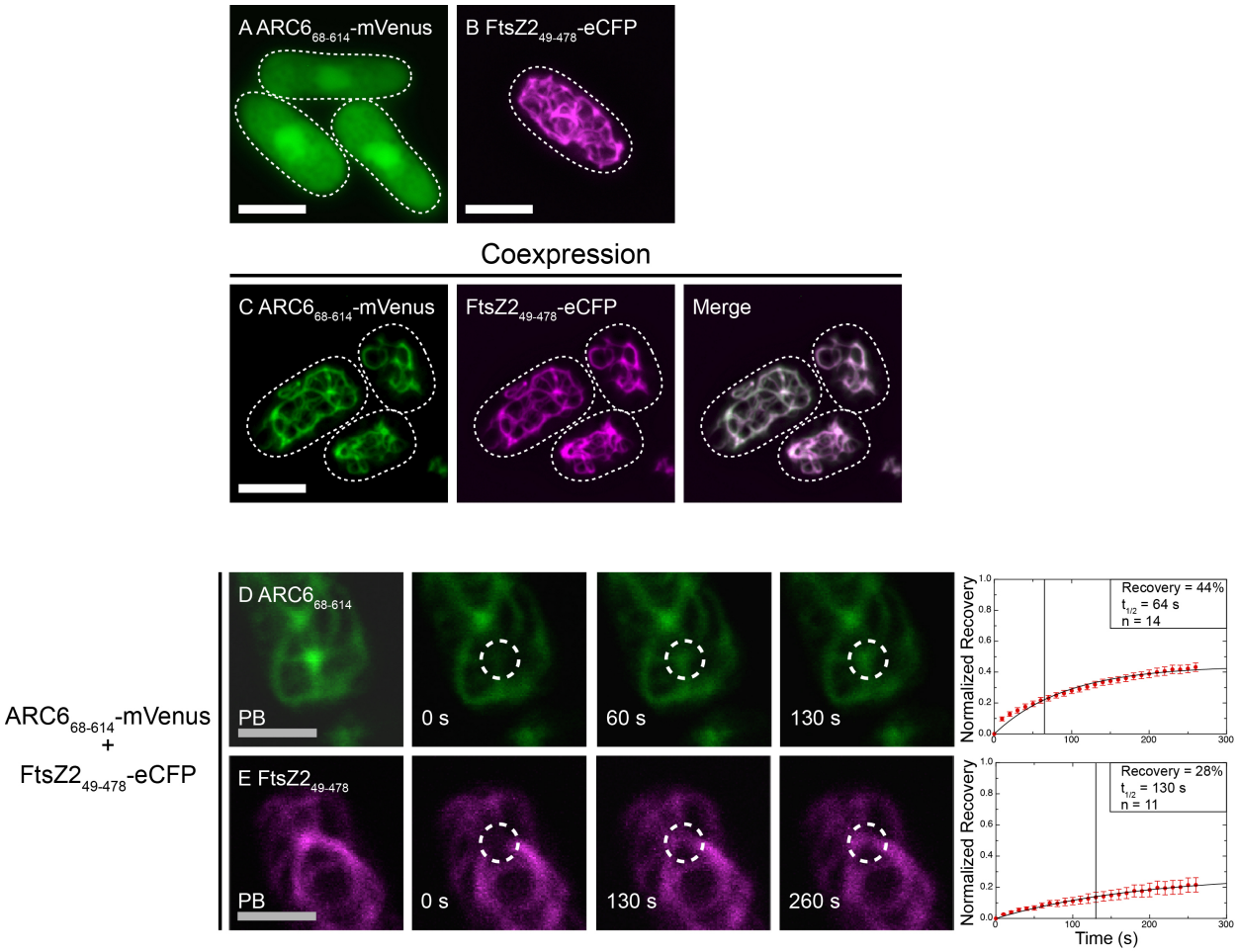

Figure A.3: FtsZ2 polymer morphology and dynamics in the presence of the stromal region of ARC6. (A-B) Epifluorescence micrographs of cells expressing (A) ARC6$_{68-614}$-mVenus, (B) FtsZ2$_{49-478}$-mCerulean, and (C) ARC6$_{68-614}$-mVenus and FtsZ2$_{49-478}$-mCerulean. (D-E) Cells expressing (D) ARC6$_{68-614}$-mVenus and (E) FtsZ2$_{119-424}$-eCFP were analyzed by FRAP. From left to right, the panels represent the fluorescence intensity in the bleached region (dashed circle) prior to bleaching (PB), at the time of bleaching (0 s), at the time closest to $t_{1/2}$, and at the time closest to twice that of $t_{1/2}$. The graphs to the right show the average fluorescence recovery vs time (s). The data are normalized to the pre-bleach fluorescence intensity (1 on the y-axis) and the

Figure A.3 (cont'd): fluorescence intensity at the time of bleaching (0 on the y-axis). The data in the box are the calculated maximum fluorescence recovery and $t_{1/2}$ (also represented by the vertical bar) as well as the number of independent FRAP experiments performed (N). The red brackets represent SEM at each time point. $ARC6_{68-614}$-mVenus fluorescence signal is falsely colored green, while $FtsZ2_{119-424}$-eCFP fluorescence signal is falsely colored magenta. (A-C) Dashed lines represent cell outlines. White Bars, 5 μm. Grey Bars, 2 μm.

al., 2005). These networks highly resembled those assembled by $FtsZ2_{49-478}$-eCFP when expressed alone (Fig. A.3 B).

We used FRAP to investigate the steady-state polymer dynamics of $ARC6_{68-614}$-mVenus and $FtsZ2_{49-478}$-eCFP in this coexpression strain. $ARC6_{68-614}$-mVenus displayed fluorescence recovery back into the bleached region with an average $t_{1/2}$ of 64 s and total recovery of 44% (n = 14, Fig. A.3 D). $FtsZ2_{49-478}$-eCFP fluorescence recovered with an average $t_{1/2}$ of 130 s and total recovery of 28% (n = 11, Fig. A.3 E). The $t_{1/2}$ for $FtsZ2_{49-478}$-eCFP in the presence of $ARC6_{68-614}$-mVenus was significantly greater than that reported previously for $FtsZ2_{49-478}$-eCFP expressed alone ($P < 0.05$, average $t_{1/2}$ of 87 s and total recovery of 31%) (TerBush and Osteryoung, 2012). The total fluorescence recovery was slightly decreased compared to that when $FtsZ2_{49-478}$-eCFP was expressed alone (Fig. A.4). However, the difference in total recovery was not

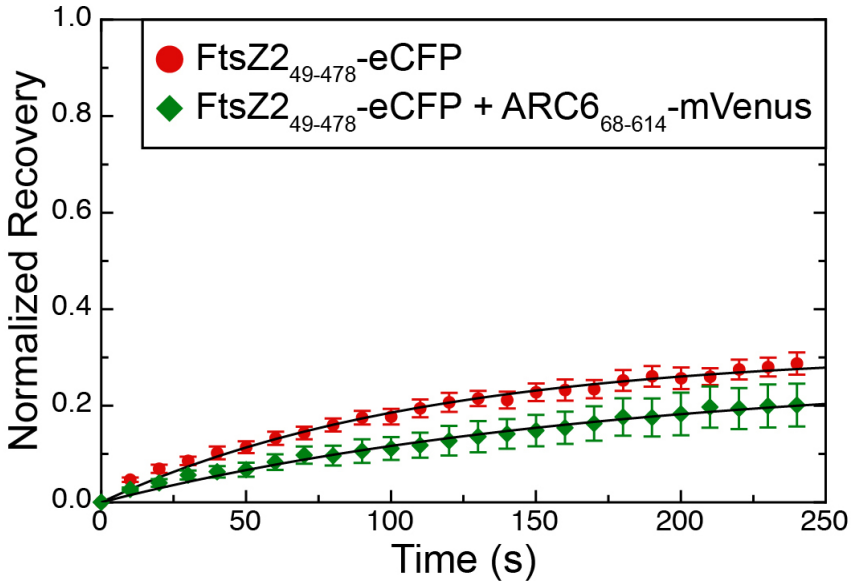

Figure A.4: Graph comparing fluorescence recovery of FtsZ2 alone and when coexpressed with ARC6. The normalized average fluorescence recovery vs time graph for FtsZ2$_{49-478}$-eCFP alone (red circle) and in the presence of ARC6$_{68-614}$-mVenus (green diamond). Data in each graph were normalized to the pre-bleach fluorescence intensity (1 on the y-axis) and the fluorescence intensity at the time of photobleaching (0 on the y-axis). The brackets indicate SEM at each time point.

statistically significant ($P > 0.05$). These data indicate that ARC6$_{68-614}$-mVenus significantly decreases the rate of FtsZ2 polymer turnover without altering the mobile and immobile fractions in *S. pombe*, consistent with the stabilizing effect of ARC6 overexpression on FtsZ filament formation *in vivo* (Vitha et al., 2003).

Generation of coexpression plasmids for analysis of multiple proteins

One drawback to expression in *S. pombe* is the presence of only two selectable markers in the MBY192 strain based on complementation of leucine and uracil

auxotrophy (Srinivasan et al., 2008). As the chloroplast division machinery is composed of multiple proteins in addition to FtsZ1 and FtsZ2, the ability to reconstitute more elaborate interaction networks in *S. pombe* would be highly advantageous for increasing our understanding of chloroplast division. Therefore, we generated a construct to coexpress both FtsZ1$_{58-433}$-eYFP and FtsZ2$_{49-478}$-eCFP from the same plasmid backbone (Fig. A.5 A). As seen previously (TerBush and Osteryoung, 2012), FtsZ1$_{58-433}$-eYFP and FtsZ2$_{49-478}$-eCFP expressed from separate plasmids coassembled into an FtsZ2-like network of interconnected filaments with a PCC of 0.91 ± 0.01 (n = 14) (Fig. A.5 B). When expressed from the coexpression plasmid, FtsZ1$_{58-433}$-eYFP and FtsZ2$_{49-478}$-eCFP also coassembled into an FtsZ2-like network of filaments (Fig. A.5 C), which was morphologically indistinguishable from the filament network observed when the proteins were coexpressed from separate plasmids (Fig. A.5 B). In the strain with the coexpression plasmid, the FtsZ1$_{58-433}$-eYFP and FtsZ2$_{49-478}$-eCFP fluorescence signals colocalized with a PCC of 0.93 ± 0.01 (n = 16), which was not statistically different from when FtsZ1$_{58-433}$-eYFP and FtsZ2$_{49-478}$-eCFP were expressed from separate plasmids ($P > 0.05$). Thus, these coexpression plasmids will allow for the analysis of 3 or 4-part interaction networks and greatly increase our understanding of the regulation of chloroplast division.

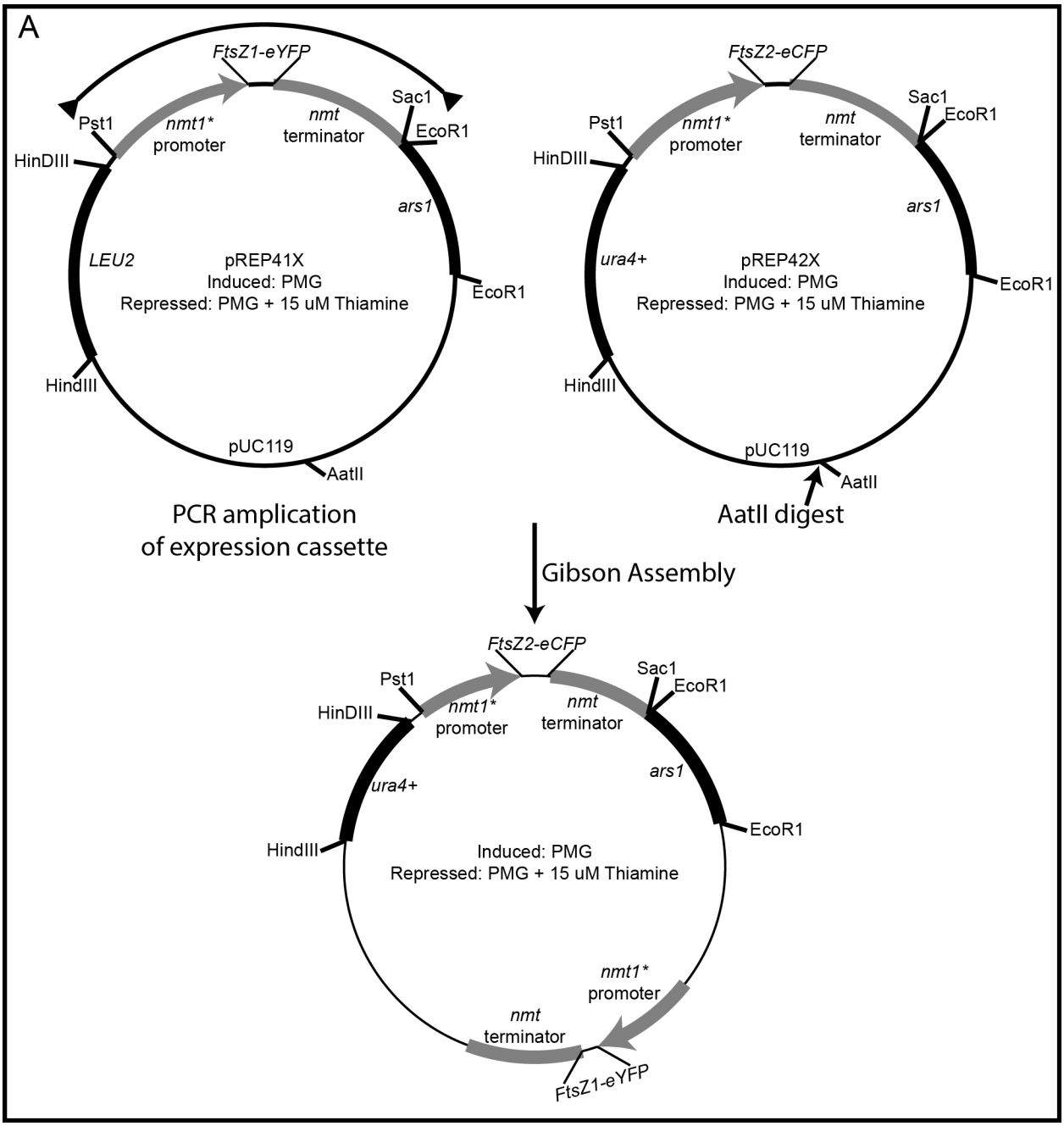

Figure A.5: Construction of an FtsZ coexpression plasmid and comparison to coexpression from separate plasmids. (A) A diagram displaying how the single plasmid to express both FtsZ1$_{74-377}$-eYFP and FtsZ2$_{49-478}$-eCFP was generated.

Figure A.5 (cont'd):

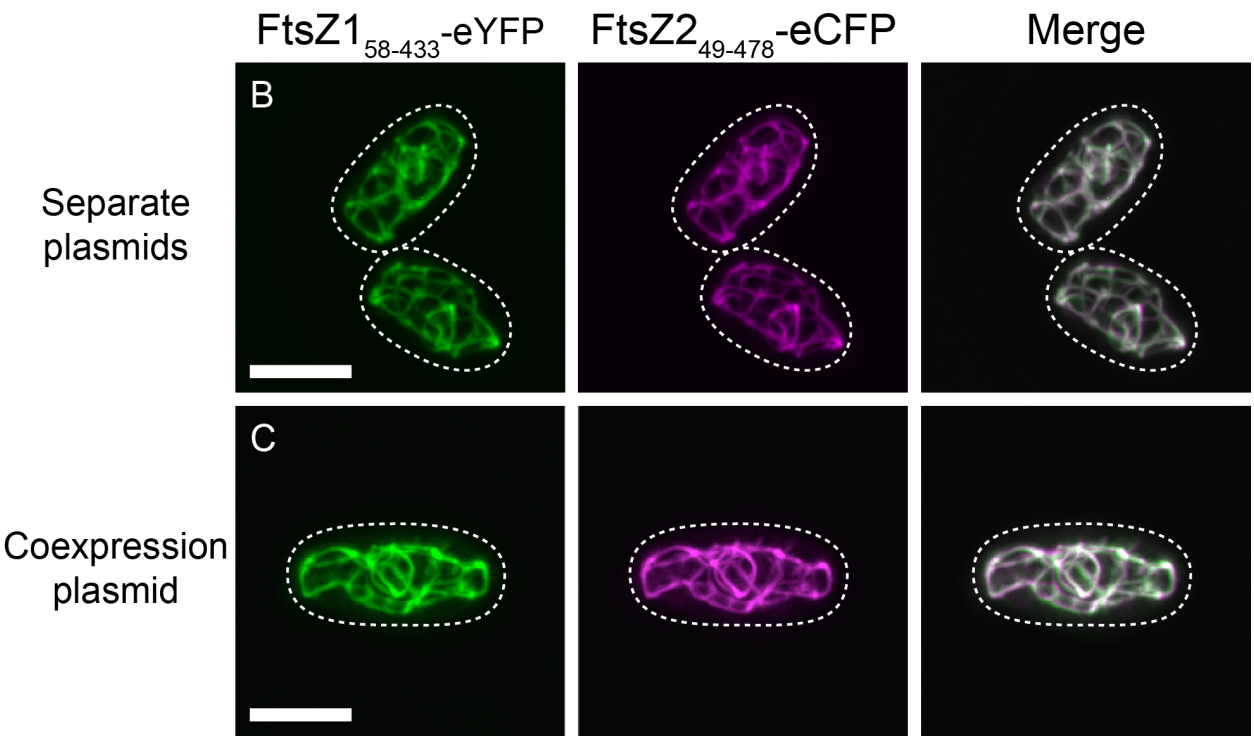

(B-C) Epifluorescence micrographs of cells expressing FtsZ1$_{74-377}$-eYFP and FtsZ2$_{49-478}$-eCFP from (B) separate plasmids or (C) from the coexpression plasmid. The FtsZ1$_{74-377}$-eYFP and FtsZ2$_{49-478}$-eCFP fluorescence signals are falsely colored green and magenta, respectively. Regions of white color in the merged panels represent overlap between the FtsZ1$_{74-377}$-eYFP and FtsZ2$_{49-478}$-eCFP fluorescence signals. Dashed lines represent cell outlines. Bars, 5 μm.

Discussion

Technical aspects of the S. pombe system

Analysis of the inherent behaviors of various chloroplast division components in *S. pombe* has advanced our understanding of how chloroplast division occurs. However, there are technical aspects to expression in fission yeast of which one must be aware. For example, the *pREP* series of plasmids does not integrate into the yeast genome (Maundrell, 1993). Therefore, expression from cell to cell is variable. Upon expression of fluorescent proteins from *pREP41X* and *pREP42X*, a range of protein levels will be observed, as indicated by no or little fluorescence signal to quite intense fluorescence signal. This trait is both advantageous and disadvantageous at the same time. In our experiments, the variation in expression has allowed for the effect of protein level on polymer morphology and turnover to be assessed in a single culture, as performed in TerBush and Osteryoung (2012), where fluorescence intensity was used as a measure of relative protein content. However, this trait also makes it more challenging to assess culture-wide traits, such as average protein content per cell. More elaborate quantification techniques are required to perform this type of analysis, which may include the use of a construct that integrates into the genome and results in more even protein expression. Such an approach was used to quantify the number of molecules per cell for 28 different cytoskeletal and signaling proteins in *S. pombe* cells using a combination of quantitative western blotting and fluorescence microscopy (Wu and Pollard, 2005). While there are *pREP* plasmids that yield varying degrees of expression due to stepwise deletions of the TATA box in the *nmt1* promoter (Basi et al.,

1993; Forsburg, 1993), the use of these vectors to analyze the effect of protein level on FtsZ polymer morphology and dynamics requires comparison of separate cultures.

Another consideration is the effect of FtsZ polymer morphology on quantification of colocalization using Pearson's correlation coefficients (PCC), which measure the extent of fluorescence signal overlap and how the two fluorescence intensities correlate (Bolte and Cordelières, 2006). We have used colocalization analysis in *S. pombe* to assess the interaction of FtsZ1 and FtsZ2 with various proteins that regulate their assembly (TerBush and Osteryoung, 2012; Zhang et al., 2013)(Fig. A.3). However, one must be careful when interpreting colocalization data, as FtsZ filament morphology may influence quantified data output. For example, $FtsZ1_{58-433}$-eYFP assembles single cables and large rings, while $FtsZ2_{49-478}$-eCFP assembles extensive networks of filaments (TerBush and Osteryoung, 2012). If these proteins were coexpressed with a diffusely localized fluorescent protein that does not interact with FtsZ1 or FtsZ2, then $FtsZ2_{49-478}$-eCFP would naturally have more fluorescence signal overlap with the coexpressed protein due to the $FtsZ2_{49-478}$-eCFP networks filling more of the cell volume than the $FtsZ1_{58-433}$-eYFP cables. Even though the proteins do not interact, this would artificially result in a greater PCC value between the fluorescent protein and $FtsZ2_{49-478}$-eCFP than $FtsZ1_{58-433}$-eYFP. Thus, the filament morphology of FtsZs must be taken into account when performing colocalization analysis with proteins that show weak interaction and diffuse localization patterns. Including appropriate controls, such as coexpressing each form of FtsZ with a diffuse fluorescence protein, provides excellent controls for such experiments.

Effect of the N- and C-termini on FtsZ polymer morphology and turnover

The coassembly of FtsZ1 and FtsZ2 into the mid-plastid Z ring is a critical aspect of chloroplast FtsZ function *in vivo*. Previous *in vivo* and *in vitro* data show that FtsZ1 and FtsZ2 assemble homopolymers and coassemble heteropolymers that display active polymer turnover (El-Kafafi et al., 2005; Johnson et al., 2015; McAndrew et al., 2001; Olson et al., 2010; Smith et al., 2010; Vitha et al., 2001). For *S. pombe* to be a valid system for the analysis of FtsZ behavior, chloroplast FtsZ fluorescent fusions must also possess these properties in the yeast cytosol. Our initial work with *S. pombe* demonstrated that $FtsZ1_{58\text{-}433}$-eYFP and $FtsZ2_{49\text{-}478}$-eCFP assemble as homopolymers and coassemble into heteropolymers that undergo active subunit exchange, and furthered our understanding on the distinct behaviors of FtsZ1 and FtsZ2 (TerBush and Osteryoung, 2012). However, these new discoveries led to new questions, including how the divergent N- and C-termini in these proteins affect their assembly and dynamic properties and whether or not FtsZ1-FtsZ1 or FtsZ1-FtsZ2 interfaces are inherently less stable than those of FtsZ2-FtsZ2. Our finding that $FtsZ1_{74\text{-}377}$-mVenus and $FtsZ2_{119\text{-}424}$-mCerulean assemble more loosely bundled filaments than full-length proteins in yeast (Fig. A.1) suggests that the N- and/or C-terminal regions enhance polymer bundling. $FtsZ2_{119\text{-}424}$-mCerulean filaments showed a higher degree of bundling than $FtsZ1_{74\text{-}377}$-mVenus filaments, suggesting that the conserved GTP-binding and hydrolysis domain of FtsZ2 by itself has a greater capacity for lateral interactions than that of FtsZ1, which may contribute to the greater stability of FtsZ2 polymers (TerBush and Osteryoung, 2012) (Fig. A.2). A recent study of *E. coli* and *B. subtilis* FtsZs showed that the C-

terminal variable region (CTV), which comprises the amino acids following the conserved C-terminal peptide required for FtsZ interaction with the membrane-tethering protein, was important for promoting lateral assembly of FtsZ polymers into bundles based on the degree of positive charge (Buske and Levin, 2012). The loose bundling of $FtsZ1_{74\text{-}377}$-mVenus and $FtsZ2_{119\text{-}424}$-mCerulean are consistent with these data, as both FtsZ1 and FtsZ2 possess CTVs with a positive charge. Therefore, their CTVs could potentially promote bundling by charge shielding between the negatively charged GTP-binding and hydrolysis domains of FtsZ1 and FtsZ2 in filaments. An alternative explanation is that the FtsZ N- and C-terminal regions make direct contacts to other polymers in the bundle to stabilize lateral interactions, as shown for the bacteriophage-encoded FtsZ-like protein PhuZ (Zehr et al., 2014).

Several studies on bacterial FtsZs have shown that FtsZ subunit exchange is widely conserved and is important for sustaining Z-ring constriction, although the dynamics vary from species to species and under different assembly conditions, (Chen et al., 2007; Chen and Erickson, 2009; Osawa and Erickson, 2011; Srinivasan et al., 2008). Consistent with our previous findings in *S. pombe* (TerBush and Osteryoung 2012), a recent study in live chloroplasts showed that FtsZ1 and FtsZ2 bearing fluorescent tags undergo active turnover in Z rings and polymers in transgenic Arabidopsis plants, and that FtsZ1 has greater turnover than FtsZ2 (Johnson et al., 2015). However, performing comparative *in planta* analyses of truncated FtsZs would be challenging on several fronts (as discussed in the Introduction). Therefore, performing polymer turnover experiments in *S. pombe* facilitates comparative studies to assess intrinsic behaviors of

FtsZ proteins. In our previous study (TerBush and Osteryoung, 2012), we found that FtsZ1 homopolymers had a faster turnover rate and much greater total fluorescence recovery than FtsZ2 homopolymers. In the current study, FtsZ1$_{74-377}$-mVenus and FtsZ2$_{119-424}$-mCerulean exhibited nearly identical polymer turnover rates and their recovery percentages, though still different, were more similar than those of their full-length counterparts (Fig. A.2). Taken together, these data suggest that the N- and C-terminal regions enhance bundling while also promoting polymer turnover. Importantly, the more consistent, yet still different, behavior of FtsZ1$_{74-377}$-mVenus and FtsZ2$_{119-424}$-mCerulean homopolymers than of full-length FtsZ1$_{58-433}$-mVenus and FtsZ2$_{49-478}$-mCerulean homopolymers also suggest that the N- and/or C-terminal regions contribute to the distinct polymer assembly and turnover characteristics of FtsZ1 and FtsZ2, but are not solely responsible for them.

Effect of ARC6 on FtsZ2 polymer stability

When coexpressed, ARC6$_{68-614}$-mVenus and FtsZ2$_{49-478}$-eCFP colocalized to a high degree, indicating that these proteins directly interact in the yeast cytosol. This finding is consistent with previous Y2H experiments (Glynn et al., 2008; Maple et al., 2005). Previous attempts to complement an Arabidopsis *ftsZ2* null mutant with a C-terminal FtsZ2 fusion protein failed (Johnson et al., 2015; TerBush and Osteryoung, 2012), we presumed because the C-terminal tag interfered with the interaction between the FtsZ2 C-terminal peptide and ARC6 (TerBush and Osteryoung, 2012). However, the fact that ARC6$_{68-614}$-mVenus directly interacts with FtsZ2$_{49-478}$-eCFP in *S. pombe* suggests that the lack of complementation *in vivo* may not be due to lack of interaction

with ARC6. One alternative explanation could be that the C-terminal fusion to FtsZ2 interferes with ionic interactions between individual FtsZ polymers in the Z ring. Additional experiments will be needed to clarify this issue.

Our FRAP experiments on cells coexpressing $ARC6_{68-614}$-mVenus and $FtsZ2_{49-478}$-eCFP showed that $ARC6_{68-614}$-mVenus had a faster rate and greater extent of fluorescence recovery than $FtsZ2_{49-478}$-eCFP. The fact that $ARC6_{68-614}$-mVenus does not polymerize into large filamentous structures but adopts a diffuse localization pattern when expressed alone, even though BiFC data suggest that ARC6 may self-interact and form homodimers (Maple et al., 2005), indicates that the only factor binding $ARC6_{68-614}$-mVenus to the network of interconnected filaments in the coexpression strain is $FtsZ2_{49-478}$-eCFP. Therefore, we presume that any $ARC6_{68-614}$-mVenus not bound to $FtsZ2_{49-478}$-eCFP is freely diffusible, resulting in a greater ability to diffuse in and out of the filament. These data also suggest that not all of $ARC6_{68-614}$-mVenus is bound to $FtsZ2_{49-478}$-eCFP and that the interaction between the two proteins may be somewhat transient. Further analysis into the kinetics of the ARC6-FtsZ2 interaction will be needed to elucidate these details.

More importantly, we found that $FtsZ2_{49-478}$-eCFP fluorescence recovery in the presence of $ARC6_{68-614}$-mVenus was significantly slower than when $FtsZ2_{49-478}$-eCFP was expressed alone. However, there was no difference in the total extent of fluorescence recovery in the presence or absence of $ARC6_{68-614}$-mVenus (Fig. A.4). These data indicate that ARC6 directly stabilizes FtsZ2 polymers, as suggested by previous genetic work *in planta* (Vitha et al., 2003). However, in *S. pombe,* stabilization

by ARC6 occurred independently of its *in vivo* membrane-tethering function. One potential explanation for this effect is that ARC6 stabilizes the FtsZ2-FtsZ2 subunit interface, reducing the rate of polymer fragmentation. In this situation, the rate at which polymers break down into diffusible subunits would decrease and more of the FtsZ2 pool would be locked into the immobile faction. As a result, one would see a decrease in both the rate of polymer turnover and total fluorescence recovery, as seen previously for the GTPase-deficient mutant $FtsZ2_{D322A}$-eCFP that assembles static filaments (TerBush and Osteryoung, 2012). However, total fluorescence recovery of $FtsZ2_{49-478}$-eCFP is unaffected by the presence of $ARC6_{68-614}$-mVenus. Therefore, a more likely possibility is that ARC6 stabilizes bundles by increasing the packing of or promoting more favorable lateral interactions between individual FtsZ2 polymers. In this situation, the frequency of FtsZ2 polymer breakage would be unaffected, but the increased interactions between FtsZ2 polymers may reduce diffusion of FtsZ2 subunits in and out of filaments. This situation is consistent with our data. However, more experiments are needed to understand how ARC6 specifically stabilizes FtsZ2 assembly and bundling.

Conclusions

The use of *S. pombe* has allowed us to elucidate inherent polymer assembly and dynamic properties of chloroplast FtsZ1 and FtsZ2, as well as identify potential contributors to their distinct behaviors. We have also begun to understand the functional interplay between FtsZ1 and FtsZ2 and how several regulatory proteins modulate their assembly. While protein behavior in this system must be interpreted with the *in vivo* biological context in mind, as with any non-native system, the resulting data have been

valuable for enhancing our understanding of the chloroplast division machinery, particularly the assembly and dynamics of the FtsZs and roles of their assembly regulators. Thus, *S. pombe* represents an advantageous and robust tool for studying the workings of the chloroplast division complex. Previous studies of bacterial FtsZ and MreB in *S. pombe* (Srinivasan et al., 2007; Srinivasan et al., 2008) indicates this system may also be broadly useful for analysis of an array of cytoskeletal elements from prokaryotes as well as organelles.

Materials and Methods

Cloning and transformation into S. pombe

FtsZ genes were cloned into the *pREP41X* and *pREP42X* expression vectors under the control of the *nmt1** promoter for analysis in *S. pombe* (Basi et al., 1993; Forsburg, 1993; Maundrell, 1993). All primers used for cloning are listed in Supplemental Table 1. Sequences encoding *Arabidopsis thaliana* FtsZ1 (AtFtsZ1-1, At5g55280, NP_200339.1) and FtsZ2 (AtFtsZ2-1, At2g36250, NP_565839.1) lacking their predicted transit peptides (the first 57 and 48 amino acids, respectively (Olson et al., 2010)) were PCR-amplified from the corresponding *S. pombe* expression plasmids (TerBush and Osteryoung, 2012) using primers AT262/AT298 and AT264/AT299, respectively. A monomeric variant of the yellow fluorescent protein Venus (mVenus) bearing the A206K mutation shown to eliminate the dimerization potential of GFP-derived fluorescent proteins (Nagai et al., 2002; Zacharias et al., 2002), generated in a bacterial expression vector provided by Desmond A. Moore and Harold P. Erickson (Duke University, Durham, NC), was PCR-amplified with primers AT7/AT297. The sequence encoding mCerulean (Addgene, Cambridge, MA) was PCR-amplified with primers AT7/AT297. *FtsZ1*$_{58\text{-}433}$ and *mVenus* were cloned into *pREP41X* digested with BamH1 using the Gibson Assembly method (Gibson et al., 2009) to create *pREP41X-FtsZ1*$_{58\text{-}433}$*-mVenus*. *FtsZ2*$_{49\text{-}478}$ and *mCerulean* were cloned into *pREP42X* digested with BamH1 by Gibson Assembly to create *pREP42X-FtsZ2*$_{49\text{-}478}$*-mCerulean*. To generate *pREP41X-FtsZ1*$_{74\text{-}377}$*-mVenus*, *FtsZ1*$_{74\text{-}377}$ was PCR-amplified from a previous *S. pombe* expression vector with primers AT266 and AT285. *mVenus* was PCR-

amplified from an *S. pombe* expression vector with primers AT7 and AT297. These gene fragments were cloned into *pREP41X* digested with BamH1 by Gibson Assembly. To generate *pREP42X-FtsZ2*$_{119\text{-}424}$*-mCerulean*, *FtsZ2*$_{119\text{-}424}$ was PCR-amplified from another *S. pombe* expression construct with primers AT268 and AT288. *mCerulean* (Addegene, Cambridge, MA) (Rizzo and Piston, 2005) was PCR-amplified from an *S. pombe* expression vector with primers AT7 and AT297. These gene fragments were cloned into *pREP42X* digested with BamH1 by Gibson Assembly. To generate the control constructs that expressed only mVenus or mCerulean, sequences encoding mVenus and mCerulean were PCR-amplified from *S. pombe* expression constructs with primers AT310 and AT297 and cloned into BamH1-digested *pREP41X* or *pREP42X*, respectively, by Gibson Assembly. The sequence encoding the stromal region of *Arabidopsis thaliana* ARC6 (At5g42480) was amplified from a bacterial expression plasmid by PCR with primers AT168 and AT139. *mVenus* was PCR-amplified with primers AT95 and AT147. These gene fragments were cloned into *pREP41X* digested with Xho1 and BamH1 by Gibson Assembly to create *pREP41X-ARC6*$_{68\text{-}614}$*-mVenus*. *pREP41X-FtsZ1*$_{58\text{-}433}$*-eYFP* and *pREP42X-FtsZ2*$_{49\text{-}478}$*-eCFP* were the same constructs as described in TerBush and Osteryoung (2012). A construct for coexpressing FtsZ1$_{58\text{-}433}$-eYFP and FtsZ2$_{49\text{-}478}$-eCFP from two expression cassettes in a single plasmid backbone was generated by PCR amplification of the entire expression cassette from *pREP41X-FtsZ1*$_{58\text{-}433}$*-eYFP*, including the *nmt1** promoter, *FtsZ1*$_{58\text{-}433}$*-eYFP* gene, and the *nmt* terminator, with primers AT109 and AT110 and cloned into *pREP42X-FtsZ2*$_{49\text{-}}$

$_{478}$-*eCFP* digested with AatII using Gibson Assembly. All primers used for cloning are summarized in Table A.2.

All constructs were transformed into *S. pombe* (strain MBY192 [*h*$^-$ *leu1-32 ura4-D18*] (Srinivasan et al., 2008)) by a modified lithium acetate protocol (http://www.sanfordburnham.org/labs/wolf/Protocols/Protocols/Fission%20Yeast/Nurse%20Lab%20Manual.htm). *S. pombe* cells were grown in 50 mL of yeast extract with supplements media (YES, http://www-bcf.usc.edu/~forsburg/media.html) for ~40 h at 32°C. 5x10^8 cells (50 mL at OD_{600} = 0.5) were collected by centrifugation at 4,000*g* at room temp for 10 min. The supernatant was removed and the cell pellet was resuspended and washed in 25 mL of TE (10 mM Tris-HCl, 1 mM EDTA, pH 7.5). The cells were pelleted again at 4,000*g* at room temp for 10 min. The supernatant was removed and the cell pellet was resuspended in 1 mL of TE + LiAc (100 mM lithium acetate, pH 7.5). The cells were incubated in a water bath at 30°C for 30 min. 200 µL of cells were added to a 2.0 mL microfuge tube already containing 20 µL of 10 µg/µL carrier sperm DNA (Agilent Technologies) and 1 µg of plasmid DNA (~2-3 µL in 2 mM Tris-HCl, pH 8.5) that was previously incubating on ice. Cells were mixed by vortexing. For *S. pombe* strains being transformed by 2 plasmids at the same time, 1 µg of each plasmid was added to the transformation reaction. 1.2 mL of PEG solution (40% PEG, TE pH 7.5, and LiAc) was added to each transformation reaction and the solution was mixed by vortexing for 10 sec. The cells were then incubated at 30°C with shaking at 250 rpm for 30 min. DMSO was added to 5% of the total volume (71 µL). The transformation reactions were placed in a 42°C water bath for

Name	Sequence (5' to 3')	Restriction Site
AT7	ATG GTG AGC AAG GGC GAG GAG CTG	N/A
AT95	GGT TCT GGT TCT GGT TCT ATG GTG AGC AAG GGC GAG GAG CTG	N/A
AT109	GAT AAT AAT GGT TTC TTA GAC GTG TCG ATC GAC TCT AGA GGA TCA GAA AAT TAT C	N/A
AT110	GAA AAG TGC CAC CTG ACG TGC ATT ACT AAT AGA AAG GAT TAT TTC ACT TCT AAT TAC ACA AAT TCC G	N/A
AT139	AGA ACC AGA ACC AGA ACC CTC CTT TAA CAT ATC AGC AAC GGA CAT TTC AAC	N/A
AT147	GAC ATT CCT TTT ACC CGG G TTA CTT GTA CAG CTC GTC CAT GCC GAG	N/A
AT168	GTC GCT TTG TTA AAT CAT ACC ACC ATG GCC GCC ACT CTC GTC TCT CCG CC	Xho1
AT266	GTT AAA TCA TAC CTC GAG GGA TCC ACC ATG GCG AGA ATT AAG GTG ATT GGT GTC GGT G	BamH1
AT268	GTT AAA TCA TAC CTC GAG GGA TCC ACC ATG GCG AGG ATT AAG GTT ATT GGT GTG GG	BamH1
AT285	CTC GCC CTT GCT CAC CAT CTG CAT GAA GCC TGT GGC GAT TAT CGT TAC ATG	N/A
AT288	CTC GCC CTT GCT CAC CAT CTG CAT TTC TCT AAA GGA AGA AGA GGG TCT TCT TGT AG	N/A
AT297	GAC ATT CCT TTT ACC CGG GGA TCC TTA CTT GTA CAG CTC GTC CAT GCC GAG	BamH1
AT310	GTT AAA TCA TAC CTC GAG GGA TCC ACC ATG GTG AGC AAG GGC GAG GAG CTG	BamH1

Table A.2: List of primers used for cloning. Column 1: Primer designation. Column 2: Nucleotide sequence of each individual primer. Column 3: Indication of the presence or absence of a restriction site sequence engineered into the primer. See materials and methods section for additional details.

15 min to heat-shock the cells. The cells were pelleted at 7,000*g* for 30 s, and the supernatant was discarded. The cell pellets were resuspended in 300 µL of TE and plated on solid PMG media with selection (http://www-bcf.usc.edu/~forsburg/media.html, -leucine for *pREP41X*, -uracil for *pREP42X* and the coexpression construct, or -leucine/-uracil for *pREP41X* and *pREP42X*). Plates contained 15 µM thiamine to repress protein expression from the *nmt1** promoter (Maundrell, 1990).

Cell growth conditions and expression from transformed S. pombe lines

S. pombe expression strains containing the constructs described above were streaked for isolation on solid PMG with selection and containing 15 µM thiamine to repress protein expression. Plates were incubated at 32°C until colonies formed, which was usually after 3-5 days. Individual cells were picked and used to inoculate liquid PMG with selection but lacking thiamine. Liquid cultures were incubated at 32°C with shaking at 250 rpm for ~40 h to reach full expression and presumed steady-state conditions for FtsZ polymer assembly and turnover before fluorescence microscopy experiments were performed.

Epifluorescence microscopy

Cells grown in liquid PMG were imaged by differential interference contrast (DIC) and epifluorescence microscopy with a Leica microscope (model DMRA2; Leica, Wetzlar, Germany) equipped with an HCX PL FLUOTAR 100X (1.30 NA) oil-immersion objective (Leica) and a CCD camera (retiga Exi, QImaging, Burnaby, BC, Canada). 2 µL of cells were pipetted onto a glass slide coated with poly-lysine and covered with a No. 1.5 coverslip. Epifluorescence imaging was performed at room temperature. Z-stacks

were collected with 0.5 µm increments and deblurred by performing Nearest Neighbor deconvolution at 70% haze removal with Image-Pro 7.0 software (Media Cybernetics). Additional image processing for epifluorescence micrographs was performed using Fiji (ImageJ; http://fiji.sc/Fiji). Single-plane projections were generated from Z-stacks using the maximum intensity algorithm and were falsely colored green for FtsZ1-mVenus, ARC6-mVenus, and mVenus fluorescence signals. Images depicting FtsZ2-mCerulean or mCerulean fluorescence signals were falsely colored magenta. Colocalization overlays were created with the merge tool in Fiji and the white color represents regions where the two fluorescence signals overlap. The degree of colocalization in coexpression strains was calculated by creating a composite deconvoluted Z-stack of both fluorescence signals, cropping the image to contain only the individual cell being analyzed, unmerging the Z-stacks, and using the Coloc2 tool in Fiji to calculate a Pearson's correlation coefficient (PCC) for a number of cells (Bolte and Cordelières, 2006). The individual PCC values for each coexpression strain were averaged and a standard error of the mean (SEM) was calculated for each coexpression strain.

Fluorescence Recovery After Photobleaching

Fluorescence Recovery After Photobleaching (FRAP) experiments were performed at room temperature on an Olympus FV1000 spectral laser-scanning confocal microscope equipped with a Plan FLN 60X (1.42 NA) oil-immersion objective and a 3.2X zoom. Immediately before each image acquisition, the high voltage for the photomultiplier tube was set so the greatest fluorescence signal in the cell was just below saturation. FRAP data were collected with FV1000 ASW software (Olympus). 2

µL of liquid *S. pombe* culture expressing a fluorescent fusion protein was pipetted onto a glass slide coated with poly-lysine and covered with a No. 1.5 coverslip. All fluorescence signals were photobleached for 20 ms at a laser intensity so that one-half to two-thirds of the fluorescence signal was bleached. Time-lapse imaging was performed with the minimal laser intensity that allowed for adequate fluorescence signal intensity but minimized photobleaching. mVenus and mCerulean fluorescence signals were imaged and bleached with the 515 nm and 458 nm lasers, respectively. Three images were acquired before the photobleaching event with an interval of 10 s to calculate the average pre-bleach fluorescence intensity. Imaging following the photobleaching event occurred for 260 s with an interval of 10 s between image acquisitions. Fluorescence intensity measurements were taken at the location of photobleaching, at a region of background signal to account for random noise, and at a region of fluorescence signal away from the photobleached location to account for photobleaching due to the continual imaging. Each raw FRAP dataset was processed to generate a photobleach-corrected and normalized fluorescence recovery dataset, with 1 being the average pre-FRAP fluorescence intensity and 0 being the fluorescence intensity at the time of photobleaching (Rabut and Ellenberg, 2005). Each processed FRAP dataset for each fluorescence protein in each expression strain was averaged together to generate an average fluorescence recovery dataset. SEM was calculated for the normalized average fluorescence recovery at each time point. The normalized average FRAP recovery dataset was used for curve-fitting in pro Fit software (QuantumSoft). The data were fit to the single exponential $f(t) = A(1-e^{-kt})$ equation. The

time it took for fluorescence signals to recover to one-half of the maximum recovery ($t_{1/2}$) was calculated as $t_{1/2} = \ln(1/2)/-k$. For statistical comparison of $FtsZ2_{49\text{-}478}$-eCFP turnover properties in the presence and absence of $ARC6_{68\text{-}614}$-mVenus, the individual raw FRAP datasets of $FtsZ2_{49\text{-}478}$-eCFP in the presence of $ARC6_{68\text{-}614}$-mVenus were normalized and used for curve-fitting to create $t_{1/2}$ and % recovery data for each FRAP run. This dataset was compared to our previous FRAP $t_{1/2}$ and % recovery data, prepared in the same manner, for when $FtsZ2_{49\text{-}478}$-eCFP was expressed alone (TerBush and Osteryoung, 2012) by Student's t-test.

BIBLIOGRAPHY

BIBLIOGRAPHY

Adams, D.W., and J. Errington. 2009. Bacterial cell division: assembly, maintenance and disassembly of the Z ring. *Nat Rev Microbiol*. 7:642-653.

Addinall, S.G., and J. Lutkenhaus. 1996. FtsA is localized to the septum in an FtsZ-dependent manner. *J Bacteriol*. 178:7167-7172.

Anderson, D.E., F.J. Gueiros-Filho, and H.P. Erickson. 2004. Assembly dynamics of FtsZ rings in Bacillus subtilis and Escherichia coli and effects of FtsZ-regulating proteins. *J Bacteriol*. 186:5775-5781.

Aylett, C.H.S., J. Löwe, and L.A. Amos. 2011. New insights into the mechanisms of cytomotive actin and tubulin filaments. *International review of cell and molecular biology*. 292:1-71.

Balmer, Y., A. Koller, G. del Val, W. Manieri, P. Schurmann, and B.B. Buchanan. 2003. Proteomics gives insight into the regulatory function of chloroplast thioredoxins. *P Natl Acad Sci USA*. 100:370-375.

Basi, G., E. Schmid, and K. Maundrell. 1993. TATA box mutations in the Schizosaccharomyces pombe nmt1 promoter affect transcription efficiency but not the transcription start point or thiamine repressibility. *Gene*. 123:131-136.

Beech, P.L., T. Nheu, T. Schultz, S. Herbert, T. Lithgow, P.R. Gilson, and G.I. McFadden. 2000. Mitochondrial FtsZ in a chromophyte alga. *Science*. 287:1276-1279.

Bi, E., and J. Lutkenhaus. 1991. Ftsz Ring Structure Associated with Division in Escherichia-Coli. *Nature*. 354:161-164.

Bolte, S., and F.P. Cordelières. 2006. A guided tour into subcellular colocalization analysis in light microscopy. *J Microsc*. 224:213-232.

Buske, P.J., and P.A. Levin. 2012. Extreme C terminus of the bacterial cytoskeletal protein FtsZ plays a fundamental role in assembly independent of modulatory proteins. *J Biol Chem*.

Buske, P.J., and P.A. Levin. 2013. A flexible C-terminal linker is required for proper FtsZ assembly in vitro and cytokinetic ring formation in vivo. *Mol Microbiol*. 89:249-263.

Caplan, M.R., and H.P. Erickson. 2003. Apparent cooperative assembly of the bacterial cell division protein FtsZ demonstrated by isothermal titration calorimetry. *J Biol Chem*. 278:13784–13788.

Chen, Y., D.E. Anderson, M. Rajagopalan, and H.P. Erickson. 2007. Assembly dynamics of Mycobacterium tuberculosis FtsZ. *J Biol Chem*. 282:27736-27743.

Chen, Y., K. Bjornson, S.D. Redick, and H.P. Erickson. 2005. A rapid fluorescence assay for FtsZ assembly indicates cooperative assembly with a dimer nucleus. *Biophys J*. 88:505-514.

Chen, Y., and H.P. Erickson. 2005. Rapid in vitro assembly dynamics and subunit turnover of FtsZ demonstrated by fluorescence resonance energy transfer. *J Biol Chem*. 280:22549-22554.

Chen, Y., and H.P. Erickson. 2009. FtsZ filament dynamics at steady state: subunit exchange with and without nucleotide hydrolysis. *Biochemistry*. 48:6664-6673.

Clough, S.J., and A.F. Bent. 1998. Floral dip: a simplified method for Agrobacterium-mediated transformation of Arabidopsis thaliana. *Plant J*. 16:735-743.

Colletti, K.S., E.A. Tattersall, K.A. Pyke, J.E. Froelich, K.D. Stokes, and K.W. Osteryoung. 2000. A homologue of the bacterial cell division site-determining factor MinD mediates placement of the chloroplast division apparatus. *Curr Biol*. 10:507-516.

Costantini, L.M., M. Fossati, M. Francolini, and E.L. Snapp. 2012. Assessing the tendency of fluorescent proteins to oligomerize under physiologic conditions. *Traffic*. 13:643-649.

Dajkovic, A., G. Lan, S.X. Sun, D. Wirtz, and J. Lutkenhaus. 2008. MinC spatially controls bacterial cytokinesis by antagonizing the scaffolding function of FtsZ. *Curr Biol*. 18:235-244.

de Boer, P.A. 2010. Advances in understanding E. coli cell fission. *Curr Opin Microbiol*. 13:730-737.

de Pater, S., M. Caspers, M. Kottenhagen, H. Meima, R. ter Stege, and N. de Vetten. 2006. Manipulation of starch granule size distribution in potato tubers by modulation of plastid division. *Plant biotechnology journal*. 4:123-134.

El-Kafafi, E.-S., S. Mukherjee, M. El-Shami, J.-L. Putaux, M.A. Block, I. Pignot-Paintrand, S. Lerbs-Mache, and D. Falconet. 2005. The plastid division proteins, FtsZ1 and FtsZ2, differ in their biochemical properties and sub-plastidial localization. *Biochem J*. 387:669-676.

El-Kafafi, E.S., M. Karamoko, I. Pignot-Paintrand, D. Grunwald, P. Mandaron, S. Lerbs-Mache, and D. Falconet. 2008. Developmentally regulated association of plastid

division protein FtsZ1 with thylakoid membranes in Arabidopsis thaliana. *Biochem J*. 409:87-94.

Erickson, H.P., D.E. Anderson, and M. Osawa. 2010. FtsZ in bacterial cytokinesis: cytoskeleton and force generator all in one. *Microbiol Mol Biol R*. 74:504-528.

Falconet, D. 2012. Origin, Evolution and Division of Plastids. *In* Photosynthesis: Plastid Biology, Energy Conversion and Carbon Assimilation. Vol. 34. Dordrecht; New York: Springer. 35-61.

Forsburg, S.L. 1993. Comparison of Schizosaccharomyces pombe expression systems. *Nucleic Acids Res*. 21:2955-2956.

Fu, G., T. Huang, J. Buss, C. Coltharp, Z. Hensel, and J. Xiao. 2010. In vivo structure of the E. coli FtsZ-ring revealed by photoactivated localization microscopy (PALM). *PLoS Biol*. 5:e12680.

Fujiwara, M., and S. Yoshida. 2001. Chloroplast targeting of chloroplast division FtsZ2 proteins in Arabidopsis. *Biochemical and biophysical research communications*. 287:462-467.

Gao, H., D. Kadirjan-Kalbach, J.E. Froehlich, and K.W. Osteryoung. 2003. ARC5, a cytosolic dynamin-like protein from plants, is part of the chloroplast division machinery. *Proc Natl Acad Sci USA*. 100:4328-4333.

Gardner, K.A.J.A., D.A. Moore, and H.P. Erickson. 2013. The C-terminal linker of Escherichia coli FtsZ functions as an intrinsically disordered peptide. *Mol Microbiol*. 89:264-275.

Gargano, D., J. Maple-Grodem, and S.G. Moller. 2012. In vivo phosphorylation of FtsZ2 in Arabidopsis thaliana. *Biochem J*. 446:517-521.

Gibson, D.G., L. Young, R.-Y. Chuang, J.C. Venter, C.A. Hutchison, and H.O. Smith. 2009. Enzymatic assembly of DNA molecules up to several hundred kilobases. *Nat Methods*. 6:343-345.

Gilson, P.R., X.C. Yu, D. Hereld, C. Barth, A. Savage, B.R. Kiefel, S. Lay, P.R. Fisher, W. Margolin, and P.L. Beech. 2003. Two Dictyostelium orthologs of the prokaryotic cell division protein FtsZ localize to mitochondria and are required for the maintenance of normal mitochondrial morphology. *Eukaryotic cell*. 2:1315-1326.

Glynn, J.M., J.E. Froehlich, and K.W. Osteryoung. 2008. Arabidopsis ARC6 coordinates the division machineries of the inner and outer chloroplast membranes through interaction with PDV2 in the intermembrane space. *Plant Cell*. 20:2460-2470.

Glynn, J.M., S.Y. Miyagishima, D.W. Yoder, K.W. Osteryoung, and S. Vitha. 2007. Chloroplast division. *Traffic*. 8:451-461.

Glynn, J.M., Y. Yang, S. Vitha, A.J. Schmitz, M. Hemmes, S.-Y. Miyagishima, and K.W. Osteryoung. 2009. PARC6, a novel chloroplast division factor, influences FtsZ assembly and is required for recruitment of PDV1 during chloroplast division in Arabidopsis. *Plant J*. 59:700-711.

Gould, S.B., R.F. Waller, and G.I. McFadden. 2008. Plastid evolution. *Annu Rev Plant Biol*. 59:491-517.

Hauser, M., H. Eichelmann, U. Heber, and A. Laisk. 1995. Chloroplast Ph Values and Buffer Capacities in Darkened Leaves as Revealed by Co2 Solubilization in-Vivo. *Planta*. 196:199-204.

Hopkins, J.F., D.F. Spencer, S. Laboissiere, J.A. Neilson, R.J. Eveleigh, D.G. Durnford, M.W. Gray, and J.M. Archibald. 2012. Proteomics reveals plastid- and periplastid-targeted proteins in the chlorarachniophyte alga Bigelowiella natans. *Genome biology and evolution*. 4:1391-1406.

Hu, Z., A. Mukherjee, S. Pichoff, and J. Lutkenhaus. 1999. The MinC component of the division site selection system in Escherichia coli interacts with FtsZ to prevent polymerization. *Proc Natl Acad Sci USA*. 96:14819-14824.

Huecas, S., C. Schaffner-Barbero, W. García, H. Yébenes, J.M. Palacios, J.F. Díaz, M. Menéndez, and J.M. Andreu. 2007. The interactions of cell division protein FtsZ with guanine nucleotides. *J Biol Chem*. 282:37515-37528.

Inoue, H., H. Nojima, and H. Okayama. 1990. High-Efficiency Transformation of Escherichia-Coli with Plasmids. *Gene*. 96:23-28.

Itoh, R., M. Fujiwara, N. Nagata, and S. Yoshida. 2001. A chloroplast protein homologous to the eubacterial topological specificity factor minE plays a role in chloroplast division. *Plant Physiol*. 127:1644-1655.

Jennings, P.C., G.C. Cox, L.G. Monahan, and E.J. Harry. 2010. Super-resolution imaging of the bacterial cytokinetic protein FtsZ. *Micron*.

Jeong, K.J., and S.Y. Lee. 2003. Enhanced production of recombinant proteins in Escherichia coli by filamentation suppression. *Appl Environ Microb*. 69:1295-1298.

Johnson, C.B., Z. Long, Z. Luo, R.S. Shaik, M.W. Sung, S. Vitha, and A. Holzenburg. 2015a. In situ structure of FtsZ mini-rings in Arabidopsis chloroplasts. *Adv Struc Chem Img*:1-12.

Johnson, C.B., R. Shaik, R. Abdallah, S. Vitha, and A. Holzenburg. 2015b. FtsZ1/FtsZ2 Turnover in Chloroplasts and the Role of ARC3. *Micros Microanal*:1-11.

Johnson, C.B., L.K. Tang, A.G. Smith, A. Ravichandran, Z. Luo, S. Vitha, and A. Holzenburg. 2013. Single Particle Tracking Analysis of the Chloroplast Division Protein FtsZ Anchoring to the Inner Envelope Membrane. *Micros Microanal*. 19:1-6.

Kadirjan-Kalbach, D.K., D.W. Yoder, M.E. Ruckle, R.M. Larkin, and K.W. Osteryoung. 2012. FtsHi1/ARC1 is an Essential Gene in Arabidopsis that Links Chloroplast Biogenesis and Division. *Plant J*.

Karamoko, M., E.S. El-Kafafi, P. Mandaron, S. Lerbs-Mache, and D. Falconet. 2011. Multiple FtsZ2 isoforms involved in chloroplast division and biogenesis are developmentally associated with thylakoid membranes in Arabidopsis. *FEBS Lett*. 585:1203-1208.

Katoh, K., and D.M. Standley. 2013. MAFFT multiple sequence alignment software version 7: improvements in performance and usability. *Mol Biol Evol*. 30:772-780.

Kelley, L.A., and M.J. Sternberg. 2009. Protein structure prediction on the Web: a case study using the Phyre server. *Nature protocols*. 4:363-371.

Kiefel, B.R., P.R. Gilson, and P.L. Beech. 2004. Diverse eukaryotes have retained mitochondrial homologues of the bacterial division protein FtsZ. *Protist*. 155:105-115.

Kiessling, J., A. Martin, L. Gremillon, S.A. Rensing, P. Nick, E. Sarnighausen, E.L. Decker, and R. Reski. 2004. Dual targeting of plastid division protein FtsZ to chloroplasts and the cytoplasm. *EMBO Rep*. 5:889-894.

Leech, R.M., and N.R. Baker. 1983. The development of photosynthetic capacity in leaves. *In* The Growth and Functioning of Leaves. J.E. Dale and F.L. Milthorpe, editors. Cambridge University Press, Cambridge.

Li, Y., J. Hsin, L. Zhao, Y. Cheng, W. Shang, and K.C. Huang. 2013. FtsZ Protofilaments Use a Hinge-Opening Mechanism for Constrictive Force Generation. *Science*.

Li, Z., M.J. Trimble, Y.V. Brun, and G.J. Jensen. 2007. The structure of FtsZ filaments in vivo suggests a force-generating role in cell division. *EMBO J*. 26:4694-4708.

Liu, Z., A. Mukherjee, and J. Lutkenhaus. 1999. Recruitment of ZipA to the division site by interaction with FtsZ. *Mol Microbiol*. 31:1853-1861.

Lohse, S., B. Hause, G. Hause, and T. Fester. 2006. FtsZ characterization and immunolocalization in the two phases of plastid reorganization in arbuscular mycorrhizal roots of Medicago truncatula. *Plant Cell Physiol*. 47:1124-1134.

Lowe, J., and L.A. Amos. 1998. Crystal structure of the bacterial cell-division protein FtsZ. *Nature*. 391:203-206.

Lu, C., and H.P. Erickson. 1999. The straight and curved conformation of FtsZ protofilaments-evidence for rapid exchange of GTP into the curved protofilament. *Cell Struct Funct*. 24:285-290.

Lu, C., J. Stricker, and H.P. Erickson. 1998. FtsZ from Escherichia coli, Azotobacter vinelandii, and Thermotoga maritima--quantitation, GTP hydrolysis, and assembly. *Cell Motil Cytoskeleton*. 40:71-86.

Lutkenhaus, J. 2007. Assembly dynamics of the bacterial MinCDE system and spatial regulation of the Z ring. *Annu Rev Biochem*. 76:539-562.

Ma, X., D.W. Ehrhardt, and W. Margolin. 1996. Colocalization of cell division proteins FtsZ and FtsA to cytoskeletal structures in living Escherichia coli cells by using green fluorescent protein. *Proc Natl Acad Sci USA*. 93:12998-13003.

Ma, X.L., and W. Margolin. 1999. Genetic and functional analyses of the conserved C-terminal core domain of Escherichia coli FtsZ. *J Bacteriol*. 181:7531-7544.

Maple, J., C. Aldridge, and S.G. Møller. 2005. Plastid division is mediated by combinatorial assembly of plastid division proteins. *Plant J*. 43:811-823.

Maple, J., N.H. Chua, and S.G. Moller. 2002. The topological specificity factor AtMinE1 is essential for correct plastid division site placement in Arabidopsis. *Plant J*. 31:269-277.

Maple, J., and S.G. Moller. 2010. The complexity and evolution of the plastid-division machinery. *Biochem Soc Trans*. 38:783-788.

Maple, J., L. Vojta, J. Soll, and S.G. Moller. 2007. ARC3 is a stromal Z-ring accessory protein essential for plastid division. *EMBO Rep*. 8:293-299.

Margolin, W. 2005. FtsZ and the division of prokaryotic cells and organelles. *Nat Rev Mol Cell Biol*. 6:862-871.

Marrison, J.L., S.M. Rutherford, E.J. Robertson, C. Lister, C. Dean, and R.M. Leech. 1999. The distinctive roles of five different ARC genes in the chloroplast division process in Arabidopsis. *Plant J*. 18:651-662.

Martin, A., D. Lang, J. Heckmann, A.D. Zimmer, M. Vervliet-Scheebaum, and R. Reski. 2009. A uniquely high number of ftsZ genes in the moss Physcomitrella patens. *Plant Biol*. 11:744-750.

Mateos-Gil, P., A. Paez, I. Hörger, G. Rivas, M. Vicente, P. Tarazona, and M. Vélez. 2012. Depolymerization dynamics of individual filaments of bacterial cytoskeletal protein FtsZ. *Proc Natl Acad Sci USA*.

Maundrell, K. 1990. nmt1 of fission yeast. A highly transcribed gene completely repressed by thiamine. *J Biol Chem*. 265:10857-10864.

Maundrell, K. 1993. Thiamine-repressible expression vectors pREP and pRIP for fission yeast. *Gene*. 123:127-130.

Mazouni, K., F. Domain, C. Cassier-Chauvat, and F. Chauvat. 2004. Molecular analysis of the key cytokinetic components of cyanobacteria: FtsZ, ZipN and MinCDE. *Mol Microbiol*. 52:1145-1158.

McAndrew, R.S., J.E. Froehlich, S. Vitha, K.D. Stokes, and K.W. Osteryoung. 2001. Colocalization of plastid division proteins in the chloroplast stromal compartment establishes a new functional relationship between FtsZ1 and FtsZ2 in higher plants. *Plant Physiol*. 127:1656-1666.

McAndrew, R.S., B.J.S.C. Olson, D.K. Kadirjan-Kalbach, C.L. Chi-Ham, S. Vitha, J.E. Froehlich, and K.W. Osteryoung. 2008. In vivo quantitative relationship between plastid division proteins FtsZ1 and FtsZ2 and identification of ARC6 and ARC3 in a native FtsZ complex. *Biochem J*. 412:367-378.

Milam, S.L., M. Osawa, and H.P. Erickson. 2012. Negative-Stain Electron Microscopy of Inside-Out FtsZ Rings Reconstituted on Artificial Membrane Tubules Show Ribbons of Protofilaments. *Biophys J*. 103:59-68.

Mingorance, J., G. Rivas, M. Vélez, P. Gómez-Puertas, and M. Vicente. 2010. Strong FtsZ is with the force: mechanisms to constrict bacteria. *Trends Microbiol*. 18:348-356.

Mingorance, J., M. Tadros, M. Vicente, J.M. González, G. Rivas, and M. Vélez. 2005. Visualization of single Escherichia coli FtsZ filament dynamics with atomic force microscopy. *J Biol Chem*. 280:20909-20914.

Miyagishima, S.-Y. 2005. Origin and evolution of the chloroplast division machinery. *J Plant Res*. 118:295-306.

Miyagishima, S.-Y., and Y. Kabeya. 2010. Chloroplast division: squeezing the photosynthetic captive. *Curr Opin Microbiol*. 13:738-746.

Miyagishima, S.-Y., H. Nozaki, K. Nishida, K. Nishida, M. Matsuzaki, and T. Kuroiwa. 2004. Two types of FtsZ proteins in mitochondria and red-lineage chloroplasts: the duplication of FtsZ is implicated in endosymbiosis. *J Mol Evol*. 58:291-303.

Miyagishima, S.-Y., K. Suzuki, K. Okazaki, and Y. Kabeya. 2012. Expression of the nucleus-encoded chloroplast division genes and proteins regulated by the algal cell cycle. *Mol Biol Evol*. 29:2957-2970.

Miyagishima, S.-Y., M. Takahara, T. Mori, H. Kuroiwa, T. Higashiyama, and T. Kuroiwa. 2001. Plastid division is driven by a complex mechanism that involves differential transition of the bacterial and eukaryotic division rings. *Plant Cell*. 13:2257-2268.

Miyagishima, S.Y. 2011. Mechanism of plastid division: from a bacterium to an organelle. *Plant Physiol*. 155:1533-1544.

Miyagishima, S.Y., H. Nakanishi, and Y. Kabeya. 2011. Structure, regulation, and evolution of the plastid division machinery. *International review of cell and molecular biology*. 291:115-153.

Mori, T., H. Kuroiwa, M. Takahara, S.Y. Miyagishima, and T. Kuroiwa. 2001. Visualization of an FtsZ ring in chloroplasts of Lilium longiflorum leaves. *Plant Cell Physiol*. 42:555-559.

Mukherjee, A., and J. Lutkenhaus. 1998. Dynamic assembly of FtsZ regulated by GTP hydrolysis. *EMBO J*. 17:462-469.

Mukherjee, A., and J. Lutkenhaus. 1999. Analysis of FtsZ assembly by light scattering and determination of the role of divalent metal cations. *J Bacteriol*. 181:823-832.

Nagai, T., K. Ibata, E.S. Park, M. Kubota, K. Mikoshiba, and A. Miyawaki. 2002. A variant of yellow fluorescent protein with fast and efficient maturation for cell-biological applications. *Nat Biotechnol*. 20:87-90.

Nakanishi, H., K. Suzuki, Y. Kabeya, and S.Y. Miyagishima. 2009. Plant-specific protein MCD1 determines the site of chloroplast division in concert with bacteria-derived MinD. *Curr Biol*. 19:151-156.

Nishida, K., M. Takahara, S.Y. Miyagishima, H. Kuroiwa, M. Matsuzaki, and T. Kuroiwa. 2003. Dynamic recruitment of dynamin for final mitochondrial severance in a primitive red alga. *P Natl Acad Sci USA*. 100:2146-2151.

Nishikawa, T., H. Kajitani, M. Sato, Y. Mogi, Y. Moriyanna, and S. Kawano. 2010. Isolation of chloroplast FtsZ and AtpC, and analysis of protein targeting into the complex chloroplast of the haptophyte Pavlova pinguis. *Cytologia*. 75:203-210.

Nishikawa, T., Y. Moriyama, M. Sato, T. Sano, S. Hasezawa, S. Ota, and S. Kawano. 2012. Isolation of mitochondrial and plastid ftsZ genes and analysis of the organelle targeting sequence in the diatom Chaetoceros neogracile (Diatoms, Bacillariophyceae). *Phycol Res*. 60:123-136.

Oliva, M.A., S.C. Cordell, and J. Löwe. 2004. Structural insights into FtsZ protofilament formation. *Nat Struct Biol*. 11:1243-1250.

Oliva, M.A., D. Trambaiolo, and J. Löwe. 2007. Structural insights into the conformational variability of FtsZ. *J Mol Biol*. 373:1229-1242.

Olson, B.J.S.C., Q. Wang, and K.W. Osteryoung. 2010. GTP-dependent heteropolymer formation and bundling of chloroplast FtsZ1 and FtsZ2. *J Biol Chem*. 285:20634-20643.

Osawa, M., D.E. Anderson, and H.P. Erickson. 2008. Reconstitution of contractile FtsZ rings in liposomes. *Science*. 320:792-794.

Osawa, M., D.E. Anderson, and H.P. Erickson. 2009. Curved FtsZ protofilaments generate bending forces on liposome membranes. *EMBO J*. 28:3476-3484.

Osawa, M., and H.P. Erickson. 2011. Inside-out Z rings--constriction with and without GTP hydrolysis. *Mol Microbiol*. 81:571-579.

Osteryoung, K.W., and R.S. McAndrew. 2001. The Plastid Division Machine. *Annual review of plant physiology and plant molecular biology*. 52:315-333.

Osteryoung, K.W., and J. Nunnari. 2003. The division of endosymbiotic organelles. *Science*. 302:1698-1704.

Osteryoung, K.W., and K.A. Pyke. 2014. Division and Dynamic Morphology of Plastids. *Ann Rev Plant Biol*. 65:443-472.

Osteryoung, K.W., K.D. Stokes, S.M. Rutherford, A.L. Percival, and W.Y. Lee. 1998. Chloroplast division in higher plants requires members of two functionally divergent gene families with homology to bacterial ftsZ. *Plant Cell*. 10:1991-2004.

Osteryoung, K.W., and E. Vierling. 1995. Conserved cell and organelle division. *Nature*. 376:473-474.

Popp, D., M. Iwasa, A. Narita, H.P. Erickson, and Y. Maeda. 2009. FtsZ condensates: an in vitro electron microscopy study. *Biopolymers*. 91:340-350.

Pyke, K. 1999. Plastid division and development *Plant Cell*. 11:549-556.

Pyke, K.A. 2010. Plastid division. *AoB Plants*. 2010:plq016.

Pyke, K.A., and R.M. Leech. 1991. Rapid Image Analysis Screening Procedure for Identifying Chloroplast Number Mutants in Mesophyll Cells of Arabidopsis thaliana (L.) Heynh. *Plant Physiol*. 96:1193-1195.

Pyke, K.A., and R.M. Leech. 1992. Chloroplast Division and Expansion Is Radically Altered by Nuclear Mutations in Arabidopsis thaliana. *Plant Physiol*. 99:1005-1008.

Pyke, K.A., S.M. Rutherford, E.J. Robertson, and R.M. Leech. 1994. arc6, A Fertile Arabidopsis Mutant with Only Two Mesophyll Cell Chloroplasts. *Plant Physiol*. 106:1169-1177.

Rabut, G., and J. Ellenberg. 2005. Photobleaching techniques to study mobility and molecular dynamics of proteins in live cells: FRAP, iFRAP, and FLIP. *In* Live Cell Imaging: A Laboratory Manual. R.D.a.S.D.L. Goldman, editor. Cold Spring Harbor Laboratory Press, Cold Spring Harbor, NY. 101-126.

Raymond, A., S. Lovell, D. Lorimer, J. Walchli, M. Mixon, E. Wallace, K. Thompkins, K. Archer, A. Burgin, and L. Stewart. 2009. Combined protein construct and synthetic gene engineering for heterologous protein expression and crystallization using Gene Composer. *Bmc Biotechnol*. 9.

Redick, S.D., J. Stricker, G. Briscoe, and H.P. Erickson. 2005. Mutants of FtsZ targeting the protofilament interface: effects on cell division and GTPase activity. *J Bacteriol*. 187:2727-2736.

Rizzo, M., and D. Piston. 2005. Optimization of Cyan Fluorescent Protein Fluorescence for Förster Resonance Energy Transfer. *Micros Microanal*. 11:1-2.

Robert, X., and P. Gouet. 2014. Deciphering key features in protein structures with the new ENDscript server. *Nucleic Acids Res*. 42:W320-324.

Romberg, L., M. Simon, and H.P. Erickson. 2001. Polymerization of Ftsz, a bacterial homolog of tubulin. is assembly cooperative? *J Biol Chem*. 276:11743-11753.

Sato, M., T. Nishikawa, H. Kajitani, and S. Kawano. 2007. Conserved relationship between FtsZ and peptidoglycan in the cyanelles of Cyanophora paradoxa similar to that in bacterial cell division. *Planta*. 227:177-187.

Scheffers, D.J., J.G. de Wit, T. den Blaauwen, and A.J. Driessen. 2001. Substitution of a conserved aspartate allows cation-induced polymerization of FtsZ. *FEBS Lett*. 494:34-37.

Schmitz, A.J., J.M. Glynn, B.J.S.C. Olson, K.D. Stokes, and K.W. Osteryoung. 2009. Arabidopsis FtsZ2-1 and FtsZ2-2 are functionally redundant, but FtsZ-based

plastid division is not essential for chloroplast partitioning or plant growth and development. *Mol Plant*. 2:1211-1222.

Shimada, H., M. Koizumi, K. Kuroki, M. Mochizuki, H. Fujimoto, H. Ohta, T. Masuda, and K. Takamiya. 2004. ARC3, a chloroplast division factor, is a chimera of prokaryotic FtsZ and part of eukaryotic phosphatidylinositol-4-phosphate 5-kinase. *Plant Cell Physiol*. 45:960-967.

Sinnecker, D., Voigt, P., Hellwig, N., & Schaefer, M. (2005). Reversible photobleaching of enhanced green fluorescent proteins. *Biochemistry*, *44*(18), 7085–7094.

Smith, A.G., C.B. Johnson, S. Vitha, and A. Holzenburg. 2010. Plant FtsZ1 and FtsZ2 expressed in a eukaryotic host: GTPase activity and self-assembly. *FEBS Lett*. 584:166-172.

Smith, A.G., C.B. Johnson, S. Vitha, and A. Holzenburg. 2011. Oligomerization of plant FtsZ1 and FtsZ2 plastid division proteins. *Arch Biochem Biophys*:1-8.

Srinivasan, R., M. Mishra, M. Murata-Hori, and M.K. Balasubramanian. 2007. Filament formation of the Escherichia coli actin-related protein, MreB, in fission yeast. *Curr Biol*. 17:266-272.

Srinivasan, R., M. Mishra, L. Wu, Z. Yin, and M.K. Balasubramanian. 2008. The bacterial cell division protein FtsZ assembles into cytoplasmic rings in fission yeast. *Genes Dev*. 22:1741-1746.

Stokes, K.D., R.S. McAndrew, R. Figueroa, S. Vitha, and K.W. Osteryoung. 2000. Chloroplast division and morphology are differentially affected by overexpression of FtsZ1 and FtsZ2 genes in Arabidopsis. *Plant Physiol*. 124:1668-1677.

Strauss, M.P., A.T.F. Liew, L. Turnbull, C.B. Whitchurch, L.G. Monahan, and E.J. Harry. 2012. 3D-SIM Super Resolution Microscopy Reveals a Bead-Like Arrangement for FtsZ and the Division Machinery: Implications for Triggering Cytokinesis. *PLoS Biol*. 10:e1001389.

Strepp, R., S. Scholz, S. Kruse, V. Speth, and R. Reski. 1998. Plant nuclear gene knockout reveals a role in plastid division for the homolog of the bacterial cell division protein FtsZ, an ancestral tubulin. *Proc Natl Acad Sci USA*. 95:4368-4373.

Stricker, J., and H.P. Erickson. 2003. In vivo characterization of Escherichia coli ftsZ mutants: effects on Z-ring structure and function. *J Bacteriol*. 185:4796-4805.

Stricker, J., P. Maddox, E.D. Salmon, and H.P. Erickson. 2002. Rapid assembly dynamics of the Escherichia coli FtsZ-ring demonstrated by fluorescence recovery after photobleaching. *P Natl Acad Sci USA*. 99:3171-3175.

Suppanz, I., E. Sarnighausen, and R. Reski. 2007. An integrated physiological and genetic approach to the dynamics of FtsZ targeting and organisation in a moss, Physcomitrella patens. *Protoplasma*. 232:1-9.

Takano, H., and K. Takechi. 2010. Plastid peptidoglycan. *Biochimica et biophysica acta*. 1800:144-151.

TerBush, A.D., and K.W. Osteryoung. 2012. Distinct functions of chloroplast FtsZ1 and FtsZ2 in Z-ring structure and remodeling. *J Cell Biol*. 199:623-637.

TerBush, A.D., Y. Yoshida, and K.W. Osteryoung. 2013. FtsZ in chloroplast division: structure, function and evolution. *Curr Opin Cell Biol*. 25:461-470.

Vaughan, S., B. Wickstead, K. Gull, and S.G. Addinall. 2004. Molecular evolution of FtsZ protein sequences encoded within the genomes of archaea, bacteria, and eukaryota. *J Mol Evol*. 58:19-29.

Vieler, A., G. Wu, C.H. Tsai, B. Bullard, A.J. Cornish, C. Harvey, I.B. Reca, C. Thornburg, R. Achawanantakun, C.J. Buehl, M.S. Campbell, D. Cavalier, K.L. Childs, T.J. Clark, R. Deshpande, E. Erickson, A. Armenia Ferguson, W. Handee, Q. Kong, X. Li, B. Liu, S. Lundback, C. Peng, R.L. Roston, Sanjaya, J.P. Simpson, A. TerBush, J. Warakanont, S. Zauner, E.M. Farre, E.L. Hegg, N. Jiang, M.H. Kuo, Y. Lu, K.K. Niyogi, J. Ohlrogge, K.W. Osteryoung, Y. Shachar-Hill, B.B. Sears, Y. Sun, H. Takahashi, M. Yandell, S.H. Shiu, and C. Benning. 2012. Genome, Functional Gene Annotation, and Nuclear Transformation of the Heterokont Oleaginous Alga Nannochloropsis oceanica CCMP1779. *PLoS genetics*. 8:e1003064.

Vitha, S., J.E. Froehlich, O. Koksharova, K.A. Pyke, H. van Erp, and K.W. Osteryoung. 2003. ARC6 is a J-domain plastid division protein and an evolutionary descendant of the cyanobacterial cell division protein Ftn2. *Plant Cell*. 15:1918-1933.

Vitha, S., R.S. McAndrew, and K.W. Osteryoung. 2001. FtsZ ring formation at the chloroplast division site in plants. *J Cell Biol*. 153:111-119.

Wang, X.D., J.A. Huang, A. Mukherjee, C. Cao, and J. Lutkenhaus. 1997. Analysis of the interaction of FtsZ with itself, GTP, and FtsA. *J Bacteriol*. 179:5551-5559.

Warrens, A.N., M.D. Jones, and R.I. Lechler. 1997. Splicing by overlap extension by PCR using asymmetric amplification: an improved technique for the generation of hybrid proteins of immunological interest. *Gene*. 186:29-35.

Wass, M.N., L.A. Kelley, and M.J.E. Sternberg. 2010. 3DLigandSite: predicting ligand-binding sites using similar structures. *Nucleic Acids Res*. 38:W469-W473.

Webster, W.A., and G.I. McFadden. 2009. Organelle division: dynamin-related proteins in apicomplexans. *Curr Biol*. 19:R334-336.

Wu, J.-Q., and T.D. Pollard. 2005. Counting cytokinesis proteins globally and locally in fission yeast. *Science*. 310:310-314.

Yang, Y., J.M. Glynn, B.J.S.C. Olson, A.J. Schmitz, and K.W. Osteryoung. 2008. Plastid division: across time and space. *Curr Opin Plant Biol*. 11:577-584.

Yang, Y., T.L. Sage, Y. Liu, T.R. Ahmad, W.F. Marshall, S.H. Shiu, J.E. Froehlich, K.M. Imre, and K.W. Osteryoung. 2011. CLUMPED CHLOROPLASTS 1 is required for plastid separation in Arabidopsis. *Proc Natl Acad Sci USA*. 108:18530-18535.

Yoder, D.W., D. Kadirjan-Kalbach, B.J.S.C. Olson, S.Y. Miyagishima, S.L. DeBlasio, R.P. Hangarter, and K.W. Osteryoung. 2007. Effects of mutations in arabidopsis FtsZ1 on plastid division, FtsZ ring formation and positioning, and FtsZ filament morphology in vivo. *Plant Cell Physiol*. 48:775-791.

Yoshida, Y., H. Kuroiwa, S. Hirooka, T. Fujiwara, M. Ohnuma, M. Yoshida, O. Misumi, S. Kawano, and T. Kuroiwa. 2009. The Bacterial ZapA-like Protein ZED Is Required for Mitochondrial Division. *Curr Biol*. 19:1491-1497.

Yoshida, Y., H. Kuroiwa, O. Misumi, M. Yoshida, M. Ohnuma, T. Fujiwara, F. Yagisawa, S. Hirooka, Y. Imoto, K. Matsushita, S. Kawano, and T. Kuroiwa. 2010. Chloroplasts divide by contraction of a bundle of nanofilaments consisting of polyglucan. *Science*. 329:949-953.

Yun, M.S., and Y. Kawagoe. 2009. Amyloplast Division Progresses Simultaneously at Multiple Sites in the Endosperm of Rice. *Plant Cell Physiol*. 50:1617-1626.

Yun, M.S., and Y. Kawagoe. 2010. Septum Formation in Amyloplasts Produces Compound Granules in the Rice Endosperm and is Regulated by Plastid Division Proteins. *Plant Cell Physiol*. 51:1469-1479.

Zacharias, D.A., J.D. Violin, A.C. Newton, and R.Y. Tsien. 2002. Partitioning of lipid-modified monomeric GFPs into membrane microdomains of live cells. *Science*. 296:913-916.

Zehr, E.A., J.A. Kraemer, M.L. Erb, J.K.C. Coker, E.A. Montabana, J. Pogliano, and D.A. Agard. 2014. The structure and assembly mechanism of a novel three-stranded tubulin filament that centers phage DNA. *Structure*. 22:539-548.

Zhang, M., A.J. Schmitz, D.K. Kadirjan-Kalbach, A.D. TerBush, and K.W. Osteryoung. 2013. Chloroplast division protein ARC3 regulates chloroplast FtsZ-ring

assembly and positioning in arabidopsis through interaction with FtsZ2. *Plant Cell*. 25:1787-1802.

Zhang, M., Chen, C., J. Froehlich, A.D. TerBush and K.W. Osteryoung. 2015. Roles of Arabidopsis PARC6 in coordination of the chloroplast division complex and negative regulation of FtsZ assembly. *Plant Physiol*. doi:10.1104/pp.15.01460